REPORT UAG-97

WORLD DATA CENTER A
for
Solar-Terrestrial Physics

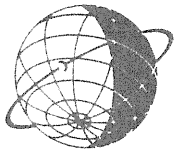

NUMERICAL MODELING OF POLAR IONOSPHERIC ELECTRODYNAMICS FOR JULY 23-24, 1983 UTILIZING IONOSPHERIC CONDUCTANCES DEDUCED FROM DMSP X-RAY IMAGES

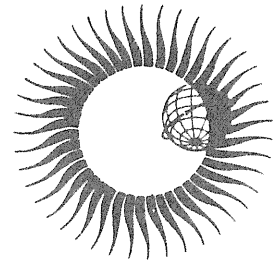

APRIL 1988

NATIONAL GEOPHYSICAL DATA CENTER

WORLD DATA CENTER A
for
Solar-Terrestrial Physics

REPORT UAG-97

NUMERICAL MODELING OF POLAR IONOSPHERIC ELECTRODYNAMICS FOR JULY 23-24, 1983 UTILIZING IONOSPHERIC CONDUCTANCES DEDUCED FROM DMSP X-RAY IMAGES

by

B.-H. Ahn,[1,2] E. Friis-Christensen,[3] D.J. Gorney,[4] Y. Kamide,[5] H.W. Kroehl,[6]
P.F. Mizera,[4] A.D. Richmond,[7] C.G. Sucksdorf,[8] and C.D. Wells[6]

1. Cooperative Institute for Research in Environmental Sciences (CIRES), University of Colorado/NOAA, Boulder, CO 80309-0449 USA
2. On leave of absence from Kyungpook National University, Taegu, Korea
3. Division of Geophysics, Danish Meteorological Institute, Copenhagen, Denmark
4. Space Sciences Laboratory, The Aerospace Corporation, P.O. Box 92957, M2-260, Los Angeles, CA 90009 USA
5. Kyoto Sangyo University, Kyoto 603, Japan
6. National Geophysical Data Center, NOAA, 325 Broadway, Boulder, CO 80303 USA
7. High Altitude Observatory, National Center for Atmospheric Research, Boulder, CO 80307 (which is sponsored by the National Science Foundation) USA
8. Finnish Meteorological Institute, 00101 Helsinki 10, Finland

APRIL 1988

Published by World Data Center A for
Solar-Terrestrial Physics, NOAA
National Geophysical Data Center
Boulder, Colorado

and printed by
U.S. Department Of Commerce
National Oceanic and Atmospheric Administration
National Environmental Satellite, Data, and Information Service
National Geophysical Data Center
Boulder, CO 80303 USA

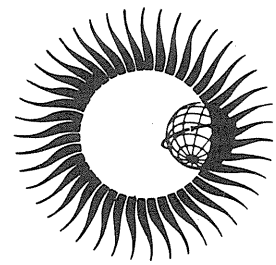

Table of Contents

PART I

1. INTRODUCTION

During the International Magnetospheric Study (1977-1979) and the subsequent data analysis phase, it was demonstrated that ground-based magnetometer data incorporated with advanced computer algorithms proposed by Fayermark (1977), Kisabeth (1979), Mishin et al. (1980), Kamide et al. (1981), and Richmond and Kamide (1987) are a powerful remote sensing tool for investigating the global distribution of polar ionospheric electrodynamic parameters, such as, ionospheric currents, field-aligned currents, ionospheric electric potentials, Joule heating, etc. Furthermore, these magnetometer methods have a great advantage in spatial and temporal coverage as compared to either satellite data or ground-based radar data, both of which require the construction of statistical, empirical models to define instantaneous and global distributions.

In order to estimate the ionospheric electrodynamics from those methods, ionospheric conductances must be provided as an input. As discussed extensively by Kamide and Richmond (1982), the electric potential distribution and the Joule heating rate are highly sensitive to the choice of ionospheric conductance. To date, the results of these methods have been limited by the accuracy of statistical models of ionospheric conductance resulting from precipitating particles and constructed from satellite-recorded data organized by an index of geomagnetic activity, cf., Wallis and Budzinski (1981), Spiro et al. (1982), or Fuller-Rowell and Evans (1987).

Owing to the introduction of a method for estimating the ionospheric conductance based on bremsstrahlung X-ray spectral imagery acquired from satellites (Gorney et al., 1985), it is now possible to determine pertinent ionospheric quantities on an individual basis through the magnetogram-inversion technique combined with such a more realistic conductance distribution. The purpose of this report is to show the results of our modeling efforts by calculating the distribution of ionospheric electrodynamic parameters for July 23 - 24, 1983 from the ground magnetic data from 88 northern hemispheric stations. This report differs from the previous UAG Reports (Kamide et al., 1982, 1983) in that the calculation employs, for the first time, a realistic ionospheric conductance distribution computed from "images" of precipitating electron spectra inferred from images of bremsstrahlung X-ray spectra.

In Part I of this report, the numerical modeling method and the characteristics of the interval are briefly described. The procedure for deducing the ionospheric conductance distribution from the limited view of the satellite instrument and data processing methods is described in Part II. In Part III we show the instantaneous distribution of equivalent ionospheric current, "true" ionospheric current, electrostatic potential, field-aligned current and Joule heating for each satellite crossing of the polar ionosphere. These data products, based on a realistic conductance distribution, are provided to the scientific community to improve our understanding of magnetospheric and ionospheric processes associated with magnetospheric substorms and convection.

2. PROCEDURE

Figure 1 outlines the important steps required to compute ionospheric quantities from the ground magnetic perturbations. The practical procedures of each step are summarized as follows:

(a) The magnetic variations used in this study were recorded every 5 minutes in magnetic coordinates (H or D) or geographic coordinates (X and Y). A total of 88 stations in the northern hemisphere are used. Those stations are listed in Table 1 and their distribution in the corrected geomagnetic coordinate system is shown in Figure 2. Approximately 60% of the data were received in digital form from the Space Environment Laboratory, the U.S. Geological Survey, the Canadian Department of Mines and Natural Resources, the Danish Meteorological Institute (for Greenland) and the Finnish Meteorological Institute while the remaining 40% were digitized from analog records. A quiet day variation was removed to eliminate the magnetic signature of Sq currents. In this case we used July 11, 1983 as the quiet day, since the 8 Kp values were 1-, 1-, 1-, 2-, 1o, 1o, 1- and 2o and ΣKp = 8+. The resulting values were then transformed to the corrected geomagnetic coordinate (c.g.) system of Gustafsson (1969) and labeled ΔXm and ΔYm referring to the northward and eastward components, respectively in Figure 1.

Since the DMSP satellite takes approximately 101 minutes to orbit the earth, the ionospheric conductance distribution can be computed only every 50 minutes if one assumes hemispheric conjugacy. Furthermore, the time required for the satellite to complete a polar crossing and image the polar region is about 17 minutes. Thus, as is shown in Table 2 in Part III, we averaged the four 5-minute values of the magnetic variations which were closest to each imaging interval.

(b) For the purpose of comparison with the standard AE(12) indices, we computed the auroral electrojet indices, AE, AU and AL, from the ΔXm values recorded at stations between 55° and 75° in corrected geomagnetic latitude. Forty four stations met this requirement. Magnetic activity during the two day interval is briefly discussed by these indices.

(c) The equivalent current function is calculated from a fitted magnetic potential function represented by a spherical harmonic series to the observed ground magnetic perturbation data and estimating the portion of this potential which results from overhead currents.

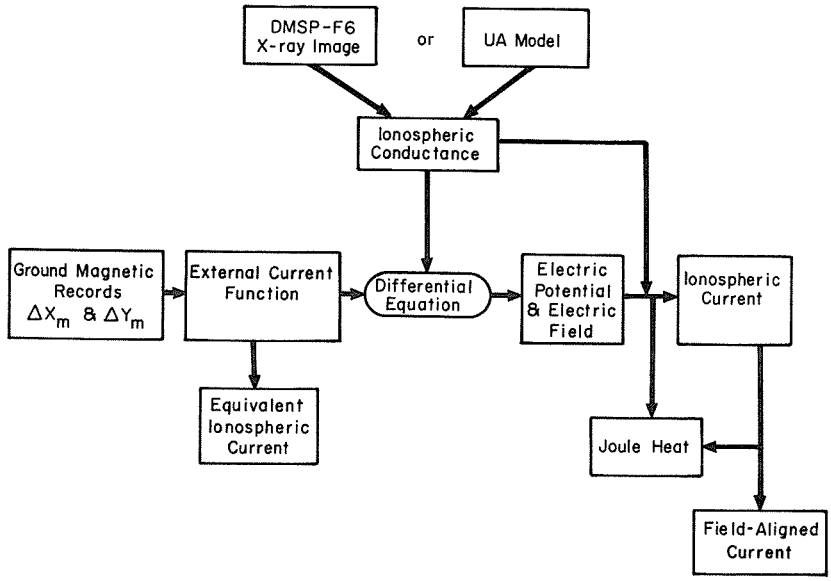

Figure 1. Flow chart describing the important steps in the present project.

(d) The computation of the ionospheric electrical potential is made for every 1° in latitude and 1 hour of local time from the equivalent current function and the ionospheric conductance following the method of Kamide et al. (1981). This process requires extensive computer computation to numerically solve a two-dimensional, second-order, partial differential equation. The electric field at each grid point is obtained simply by taking negative gradient of the electric potential. The ionospheric conductance distribution estimated from the X-ray image is used when the image includes a significant part of the auroral zone, otherwise a statistical model is used. The statistical model is described in Ahn et al. (1983) and as UA model in Figure 1.

(e) Once the electric field and the ionospheric conductance are given, the ionospheric current vectors are computed through Ohm's law.

(f) The field-aligned current distribution is computed as the divergence of the horizontal ionospheric current.

(g) The scalar product of the ionospheric current vector and the electric field vector gives the Joule heating rate.

3. METHOD

Computational details of the important steps in the flow chart of Figure 1 are summarized as follows:

(1) Equivalent Current Function

At a given time, the observed magnetic data were fitted to a magnetic potential function, V, which is represented by a spherical harmonic series,

$$V(\theta,\lambda) = \sum_{m=0}^{6} \sum_{n=m}^{56} (a_n^m \cos m\lambda + b_n^m \sin m\lambda) P_n^m(\cos\theta) \qquad (1)$$

where θ and λ are colatitude and east longitude, respectively. In this process, a total of 358 coefficients, a_n^m and b_n^m, are determined. The criteria of choosing n and m values and mathematical details of fitting procedure including the smoothing technique are intensively discussed elsewhere (Kroehl and Richmond, 1979; Kamide et al., 1982; 1983). The root-mean-square difference between computed and observed magnetic perturbations is typically 15%. However, at certain times the discrepancy rises above 20%.

Table 1. List of Magnetic Stations Supplying Data.

	STATION NAME	GEOGRAPHIC LAT	GEOGRAPHIC LONG	CORRECTED GEOMAGNETIC LAT	CORRECTED GEOMAGNETIC LONG
1	Abisko	68.36	18.82	65.04	103.55
2	Alert	82.50	297.50	86.77	124.34
3	Alma Ata	43.25	76.92	37.97	148.71
4	Alta	68.86	22.96	66.23	107.61
5	Arkhangelsk	64.60	40.50	60.18	118.02
6	Baker Lake	64.33	263.97	75.15	319.99
7	Barrow	71.32	203.38	69.67	248.14
8	Bear Island	74.50	19.20	71.04	110.18
9	Borok	58.03	38.97	53.56	114.21
10	Boulder	40.14	254.76	49.50	315.70
11	Cambridge Bay	69.20	255.00	77.84	299.70
12	Cape Chelyuskin	77.72	104.28	71.58	174.19
13	Cape Parry	70.17	241.70	74.61	273.58
14	Cape Wellen	66.16	190.17	62.50	242.59
15	College	64.86	211.90	64.84	259.65
16	Daneborg	74.30	339.18	75.90	84.30
17	Danmarkshavn	76.80	341.40	77.60	91.70
18	Del Rio	29.49	259.08	38.70	325.00
19	Dixon Island	73.54	80.56	68.31	154.69
20	Fort Churchill	58.77	265.90	70.27	326.01
21	Fort Simpson	61.75	238.77	67.69	289.42
22	Fort Smith	60.00	248.00	68.20	299.30
23	Fort Yukon	66.57	214.73	66.98	260.10
24	Frederikshab	62.00	310.30	70.50	39.30
25	Furstenfeldbruck	48.17	11.28	45.00	87.61
26	Godthab	64.18	308.28	72.90	38.40
27	Godhavn	69.25	306.47	77.62	41.58
28	Great Whale River	55.27	282.22	67.96	353.76
29	Guam	13.58	144.87	6.90	213.70
30	Heiss Island	80.62	58.05	74.80	144.40
31	Honolulu	21.32	202.00	21.73	267.56
32	Inuvik	68.25	226.70	71.13	268.20
33	Kanoya	31.42	130.88	25.70	200.80
34	Karaganda	49.82	73.08	44.87	145.04
35	Kautokeino	69.02	23.05	65.42	107.03
36	Kazan	55.83	48.85	51.23	122.43
37	Kevo	69.80	27.00	66.30	110.60
38	Kilpisjarvi	69.05	207.00	65.56	105.28
39	Kiruna	67.83	20.42	64.80	104.20
40	Kuvdlorssuaq	74.57	302.82	81.80	47.57
41	Leirvogur	64.18	338.30	66.82	69.60
42	Leningrad	59.95	30.71	55.82	107.77
43	Lynn Lake	56.85	258.93	66.95	319.08
44	M'Bour	14.39	343.04	10.70	57.70
45	Magadan	60.12	151.02	53.90	217.40
46	Meanook	54.62	246.67	62.61	300.90
47	Memambetsu	43.91	144.19	37.40	213.70
48	Minsk	54.10	26.50	50.35	101.88
49	Moscow	55.48	37.31	50.97	112.01
50	Mould Bay	76.20	240.60	80.56	263.54
51	Muonionalusta	68.02	23.53	64.39	106.60
52	Narssarssuaq	61.10	314.60	68.90	44.00
53	New Aalesund	78.92	11.93	75.90	114.70
54	Niemegk	52.07	12.68	47.97	90.01
55	Nord	81.60	343.24	80.80	111.70
56	Norman Wells	64.90	234.50	69.69	282.02
57	Novosibirsk	55.03	82.90	50.07	155.02
58	Nurmijarvi	60.51	24.66	56.62	103.05
59	Odessa	46.78	30.88	42.30	103.66
60	Ottawa	45.40	284.45	58.50	356.21
61	Pello	68.53	270.48	63.25	106.25
62	P. Tunguska	61.60	90.00	56.50	162.46
63	Resolute Bay	74.70	265.10	84.14	304.33
64	Sachs Harbor	72.00	235.00	76.25	272.94
65	Saint Johns	47.60	307.32	57.60	29.12
66	San Juan	18.11	293.85	31.47	5.54
67	Scoresbysund	70.48	338.03	71.98	75.39
68	Sitka	57.06	224.68	59.82	277.77
69	Sodankyla	67.37	26.63	63.56	108.54
70	Sondre Strom	67.02	309.28	75.20	42.60
71	Soroya	70.54	22.22	66.97	107.74
72	Sverdlovsk	56.73	61.07	52.70	132.50
73	Talkeetna	63.30	209.90	61.90	259.80
74	Tashkent	41.33	69.62	37.19	139.62
75	Tbilisi	42.09	44.71	37.40	115.30
76	Thule	77.48	290.83	86.77	39.20
77	Tixie Bay	71.58	129.00	65.82	195.48
78	Toledo*	39.88	355.95	33.91	73.17
79	Tromso	69.66	18.95	66.75	104.78
80	Tucson	32.25	249.17	39.88	311.36
81	Umanak	70.70	307.80	78.60	46.00
82	Upernavik	72.80	303.80	81.00	44.80
83	Valentia	51.93	349.75	50.06	71.77
84	Victoria*	48.52	236.58	54.12	292.40
85	Wingst	53.74	9.07	50.08	87.67
86	Witteveen	52.81	6.67	49.21	85.42
87	Yakutsk	62.02	129.72	55.71	199.83
88	Yellowknife	62.40	245.50	69.94	294.38

* Used only on July 24, 1983

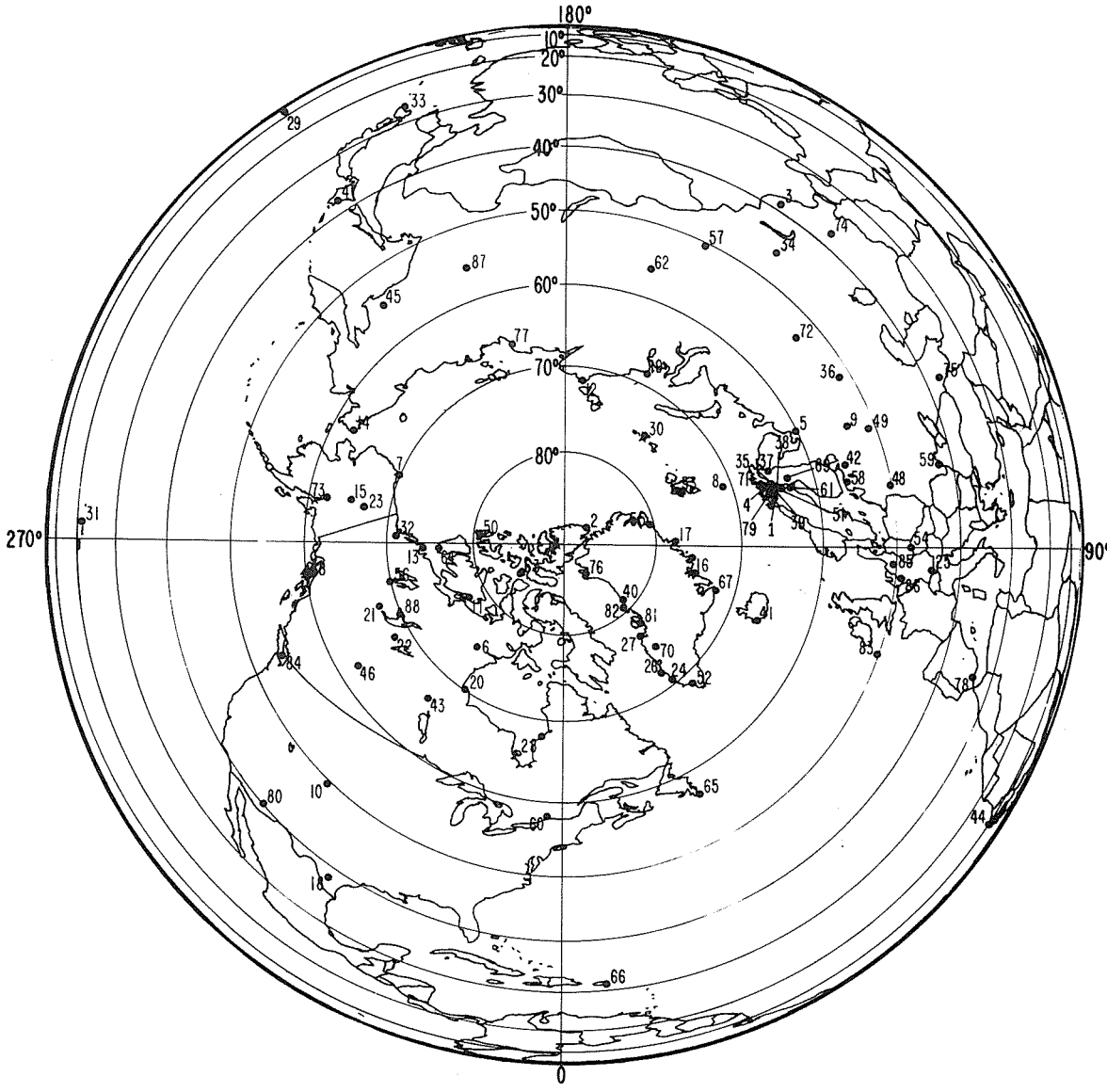

Figure 2. The locations of the magnetic stations whose data were used in this study are plotted on an orthogonic projection map, in which the plotted distance between latitude circles varies as a sine function in colatitude. For identification of station names and their coordinates both in geographic and corrected geomagnetic coordinate systems, see Table 1.

It is then assumed that there is a relatively small internal contribution to the magnetic potential caused by a perfectly conducting layer 300 km below the earth's surface. The remaining external potential $V^{(e)}$ is extrapolated to 110 km altitude and converted to an equivalent ionospheric current function by the standard procedure:

$$\Psi_n = \frac{1}{\mu_0} \frac{2n+1}{n+1} \left(\frac{a}{R_E}\right)^n V_n^{(e)} \qquad (2)$$

where

$$\Psi = \sum_n \Psi_n(\theta,\lambda)$$

$$a = R_E + 110 \text{ km}$$

$$\mu_o = 4 \times 10^{-7} \text{ H/m}$$

(2) Ionospheric Conductance

The height-integrated ionospheric conductivity, i.e., the ionospheric conductance, is assumed to have two components: one is a background conductance of solar radiation origin and the other is due to precipitating particle bombardment. For the background conductance, we employed the model originally developed by Tarpley (1970) and improved by Richmond et al. (1976). For the auroral enhancement, we use, for the first time, a realistic ionospheric conductance distribution derived from DMSP-F6 bremsstrahlung X-ray data. However, since X-ray data are not available during the entire period analyzed in this report, we employed the University of Alaska conductance model (Ahn et al., 1983) whenever an X-ray image is not available. The model was constructed by defining empirical relationships between the Pedersen and Hall conductances obtained from published Chatanika radar data and the magnitude of the horizontal component of magnetic disturbance at College, Alaska.

In Part II we discuss the basic concepts used in estimating the conductance distribution from X-ray image data and some data manipulation procedures. A comparison between the Rice University conductance model (Spiro et al., 1982) and the University of Alaska conductance model is also presented. Hereafter, we refer to the two models as Rice model and UA model, respectively.

(3) Electric Potential

According to Kamide et al. (1981), the electric potential Φ can be expressed in terms of the equivalent current function Ψ by using a two-dimensional, second-order partial differential equation,

$$A \frac{\partial^2\Phi}{\partial\theta^2} + B \frac{\partial\Phi}{\partial\theta} + C \frac{\partial^2\Phi}{\partial\lambda^2} + D \frac{\partial\Phi}{\partial\lambda} = F(\Psi,\theta,\lambda) \qquad (3)$$

where coefficients A, B, C and D are functions of the Pedersen and Hall conductances and their gradients with respect to the θ and λ directions. Using the equivalent current function and conductance distribution obtained in the previous sections as input data, the above differential equation is solved numerically with approximate boundary conditions, $\Phi(0,\lambda) = 0$ and $\partial\Phi(\pi/2,\lambda)/\partial\theta = 0$. The associated electric field is derivable from the electric potential distribution thus obtained.

(4) Ionospheric Currents and Field-Aligned Currents

The ionospheric current $\underline{J}$ is related with the electric field $\underline{E}$ and the ionospheric conductance, Σ_H and Σ_P through Ohm's law:

$$\underline{J} = \Sigma_P \underline{E} + \Sigma_H \underline{E} \times \underline{n}_r \qquad (4)$$

where $\underline{n}_r$ is a unit radial vector. From the requirement that the three-dimensional current be divergence free, the field-aligned current density $J_{\parallel}$ (positive downwards) can be calculated as

$$J_{\parallel} = \text{div } \underline{J} = \text{div } \underline{J}_p \qquad (5)$$

We also show the Pedersen and Hall components of ionospheric current and field-aligned current separately.

(5) Joule Heating Rate

The height-integrated Joule heating rate is defined by

$$u_J = \underline{J} \cdot \underline{E} \qquad (6a)$$
$$= \sum_P E^2$$

The Joule heating rate in the entire ionosphere of the northern hemisphere U_J can then be obtained by integrating u_J as

$$U_J = \iint u_J \, a^2 \sin\theta \, d\theta \, d\lambda \qquad (6b)$$

4. MAGNETIC ACTIVITY RECORDED ON JULY 23-24, 1983

On the lower panel of Figure 3 are plotted the envelope of the ΔXm values recorded at 44 stations between 55° and 75° in corrected geomagnetic latitude for July 23 and 24, 1983. The upper and lower traces are comparable to the standard AU and AL indices from 12 observatories. The difference, shown in the top panel, is similar to the standard AE (= AU-AL).

The two day interval is characterized by intense magnetic activity in the polar region including both magnetospheric substorms and enhanced magnetospheric convection. The preceding day (22 July 1983) was very quiet until a relatively strong substorm occurred late in the day. The first substorm appears to commence at 0905 UT on the 23rd as both AU and $|AL|$ rapidly increase. The interval following 1130 UT is extremely interesting as both the AU and $|AL|$ indices gradually increase until about 1800 UT while the interplanetary magnetic field (IMF) was strongly northward. Thus the magnetic activity resulted from increased, and in some cases reversed, magnetospheric convection. After 1800 UT, the IMF turned southward and a period of almost continuous substorm-like activity persisted until 0800 UT on the 24th. After this, a sequence of substorms occurred. It is also interesting to point out that indices of magnetic activity, electric fields and precipitating auroral particles during the period were not in good agreement (J.C. Foster and D.S. Evans, private communication).

5. EXAMPLES

As an example, the output plots for the epoch at 2015-30 UT on July 23, 1983 are shown in Figures 4a - 4k, during which a continuous auroral activity was observed. The AE index was 839 nT, the IMF B_Z was -11 nT and By was -23 nT.

The distribution of the equivalent ionospheric current vectors shown in Figure 4a was obtained simply by rotating the observed magnetic disturbance vectors 90° clockwise. The current vectors of the stations below 50° in corrected geomagnetic latitude are placed on the 50° latitude circle. The current pattern is characterized by an intense westward electrojet flowing in a wide local time sector and maximizing in the morning sector. Although less prominent than the westward electrojet, one can also notice that there is a well-developed eastward electrojet from noon to premidnight.

Iso-intensity contours of the calculated external current function (the so-called equivalent ionospheric current system) and the associated equivalent current vector plot are shown in Figures 4b and 4c, respectively. The current vectors are plotted at grid points every 1° in latitude and 1 hour in local time. From Figure 4b, one can see a well-developed two-cell current pattern. In interpreting the equivalent current vectors given in Figure 4c, it should be mentioned that there are uncertainties over the regions where there are absence of recordings, particularly in the large gap in the surface magnetometer data over the Arctic Ocean and eastern Siberia. However, Ahn et al. (1984) showed that such a non-uniform distribution of observatories did not seriously compromise the accuracy of the large-scale current distribution.

Smoothed isocontours of Pedersen and Hall conductances are shown in Figure 4d. A detailed discussion of the data processing procedures is presented in Part II. As expected, significant enhancements are found along the auroral region in both the Pedersen and Hall conductance distributions. Comparing these plots with statistically determined ones (for example, the Rice model), one can notice that the instantaneous distribution contains many more patch-like structures. The numerical value in the right bottom corner is the maximum value of each plot. As is the case of Figure 4d the maximum value of the Pedersen conductance during July is generally on the dayside and results from the solar UV contribution. Figure 4e shows isocontours of the electric potential calculated from the equivalent current function (Fig. 4b) and the conductance distribution (Fig. 4d). The potential distribution pattern consists of well-defined twin vortices with the highest and lowest potentials appearing in the early morning and early afternoon sectors, respectively. The negative and positive numbers in the right-bottom corner identify these two extreme values. The cross polar cap potential difference, one of the most important parameters in the magnetosphere-ionosphere coupling and magnetospheric convection, is simply the sum of the absolute value of the two extremes. For this epoch it is found to be 90 kV. During quiet periods, it is difficult to estimate the cross polar cap potential difference, because the extremes are not easily determined.

By comparing Figures 4e and 4b, one can notice that the electric potential pattern is quite similar to the equivalent current system. This seems to contradict the results of previous studies (e.g., Kamide et al., 1982 and 1983) which attributed the discrepancy in the patterns at or near auroral latitudes to result from non-uniform distribution of ionospheric conductance. As demonstrated in Part II, however, the apparent disagreement between conclusions reached in Kamide et al. (1982; 1983) and those presented here result from the use of statistical models of conductance which cannot accurately describe the conductance patterns for any given instant in time and thus do not represent the fine structure of the real situation.

Figure 4f shows the electric field vectors computed at our grid points. It is clearly seen that the dominant direction of the field in the polar cap region is dawn to dusk while the direction in the westward and eastward electrojet regions is predominantly southward and northward, respectively.

Figure 4g shows the distribution of calculated or "true" ionospheric current vectors. Although the gross distributions of the equivalent and 'true' ionospheric currents are similar, there are significant differences both in the current direction and strength. For example, the equivalent currents of the electrojet region are aligned in the pure east-west direction, but the 'true' ionospheric currents have a considerable north-south component. In Figure 4h we compare the Pedersen and Hall currents, separately. It is evident that the Hall currents are remarkably similar to the equivalent currents while the Pedersen current pattern is quite similar to that of the electric field in Figure 4f.

Figure 4i shows the distribution of the Joule heating rate. By comparing it with the ionospheric current distribution in Fig. 4g, one can notice that the major heating regions are closely associated with the auroral electrojets. It is interesting to note that no significant heating is found around local midnight sector. Such a trend has been reported from the Chatanika radar measurement (Banks, 1977). In the left-bottom corner, the total Joule heating rates integrated from the pole to 80°, 70°, 60° and 50° in latitude are listed in Watts. For this epoch they are 0.34×10^{11}, 1.62×10^{11}, 2.60×10^{11} and 2.63×10^{11} Watts, respectively, most of the heating occuring within the latitudinal zone beween 60° and 80°. The number in the bottom right corner notes the maximum heating rate calculated in Watts/m^2.

Finally, in Figure 4j, we show the isocontours of the calculated field-aligned currents where the solid and the dashed lines denote downward and upward currents, respectively. One can easily recognize the Region 1 and Region 2 currents of Iijima and Potemra (1978). The high-latitude current system on the dayside and associated with the polar cusp is also apparent. In the bottom right corner are the maximum computed upward (negative) and downward (positive) current density values. In Figure 4k we also show the Hall and Pedersen components of the field-aligned currents. As expected, the Pedersen component resembles the total field-aligned current and the Hall component is relatively small.

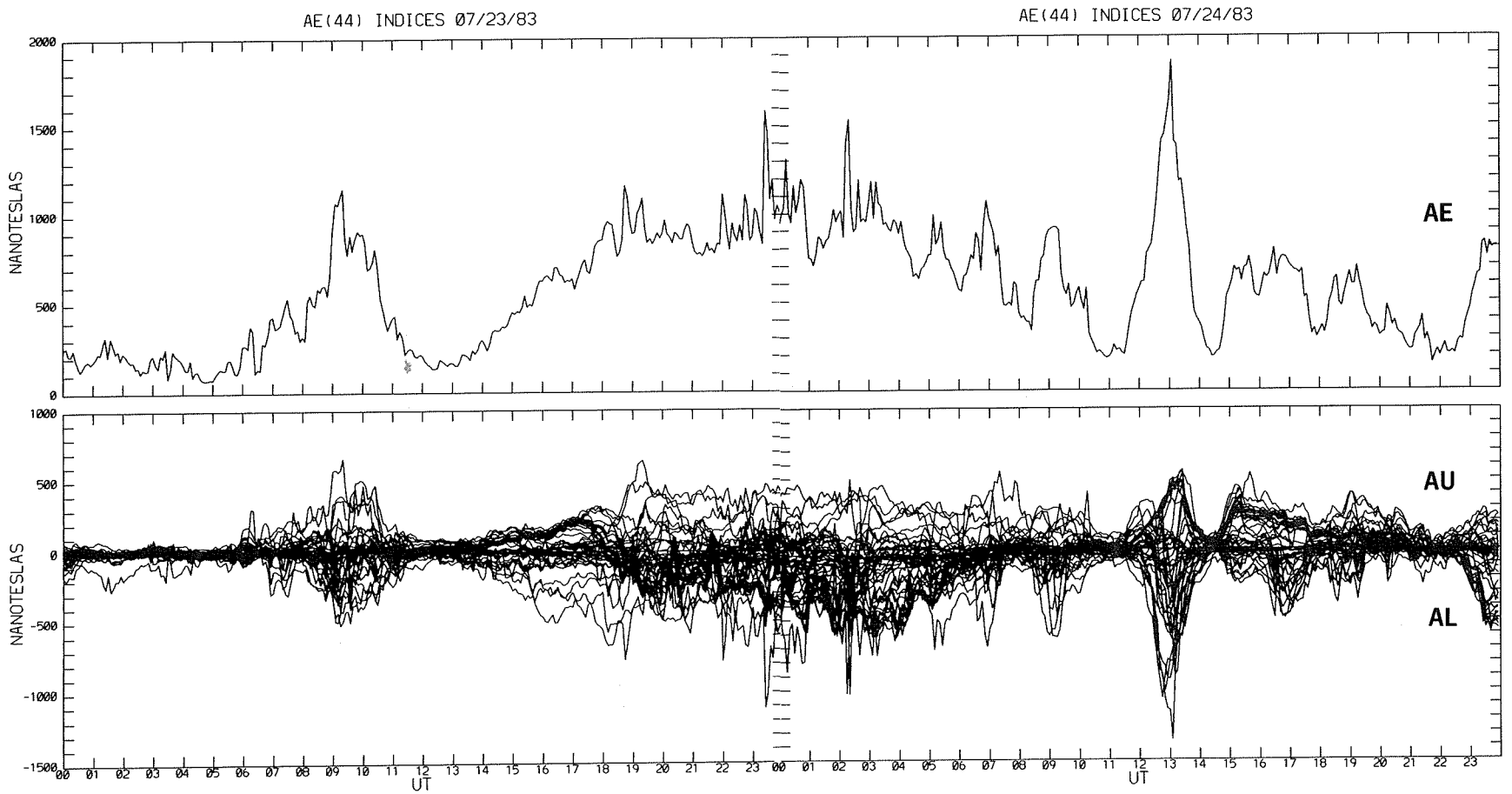

Figure 3. AE(44), AU(44) and AL(44) indices constructed from the combined Xm component from 44 stations between 55° and 75° in corrected geomagnetic latitude.

MEASURED
EQUIVALENT CURRENT VECTORS

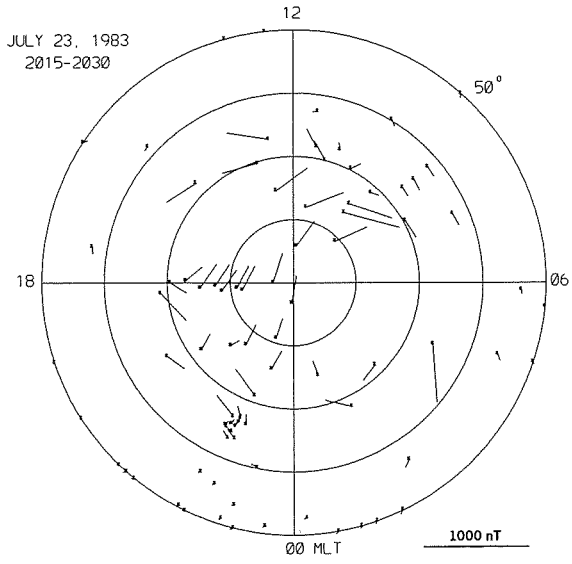

Figure 4a

EQUIVALENT CURRENT SYSTEM

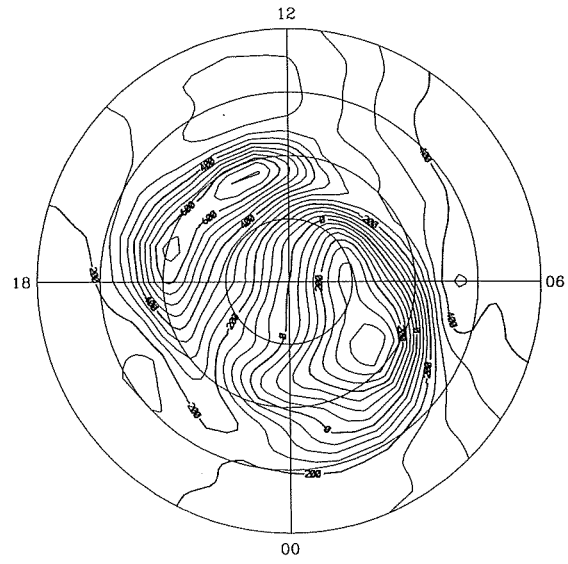

CONTOUR INTERVAL: 50,000 A

Figure 4b

EQUIVALENT CURRENT VECTORS
FROM HARMONIC ANALYSIS

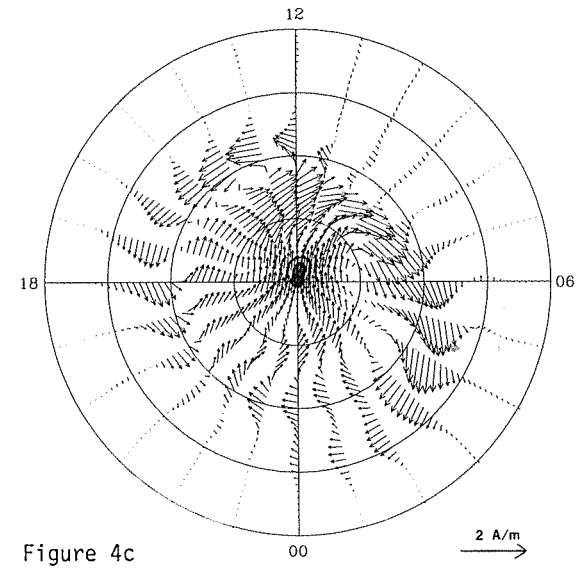

Figure 4c

ELECTRIC POTENTIAL

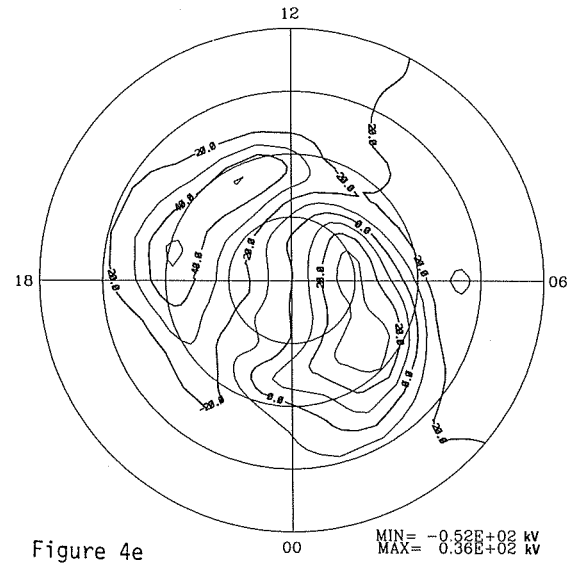

Figure 4e

CONTOUR INTERVAL: 10 kV

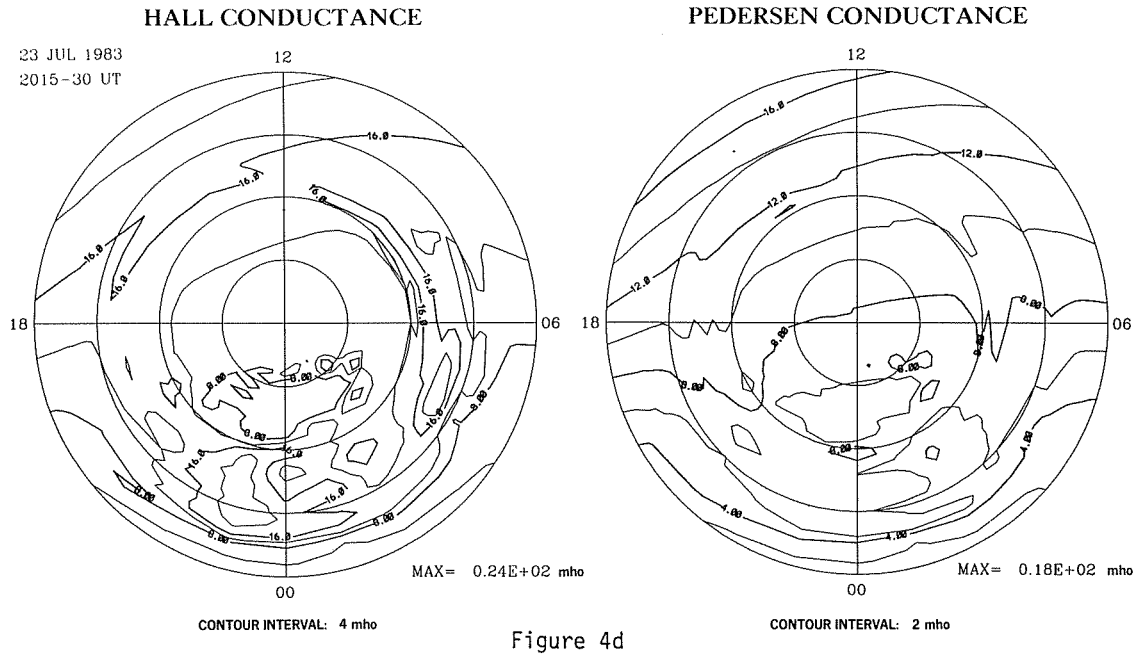

Figure 4d

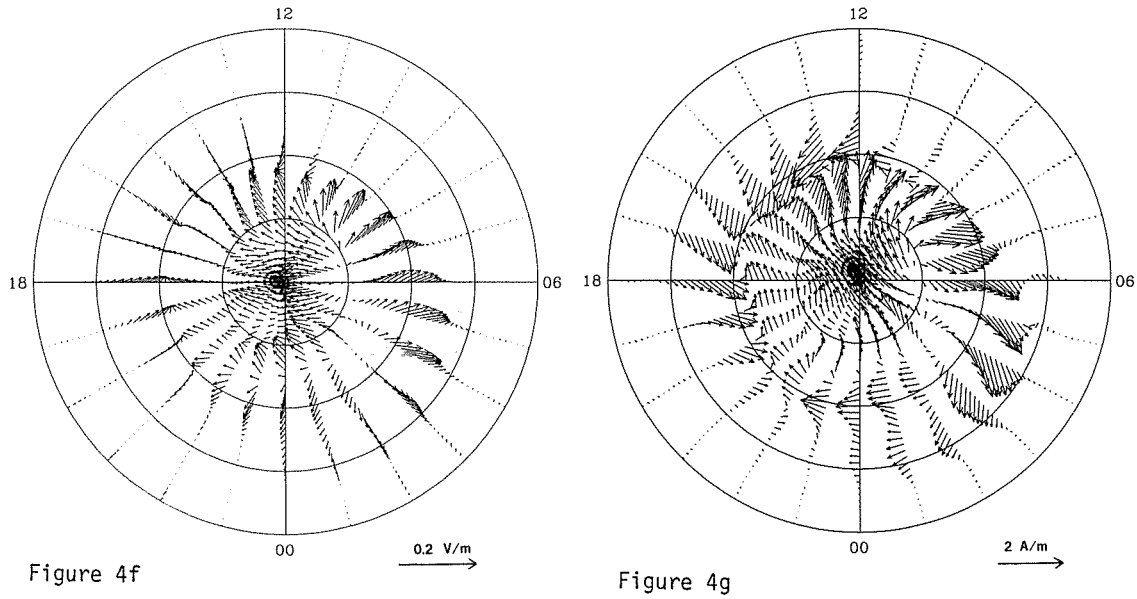

Figure 4f

Figure 4g

HALL CURRENT VECTORS

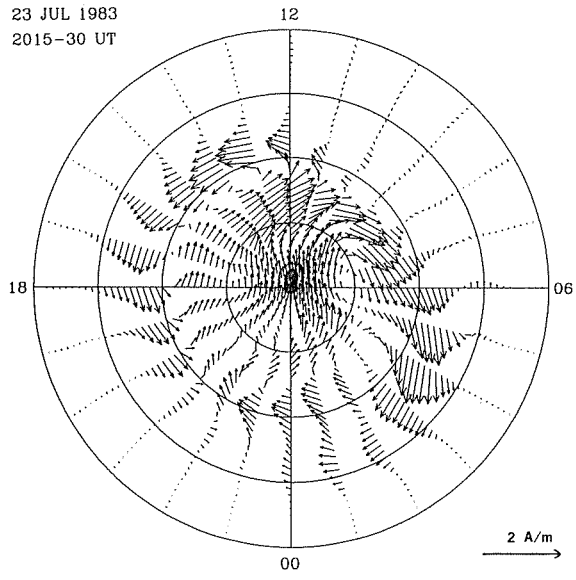

PEDERSEN CURRENT VECTORS

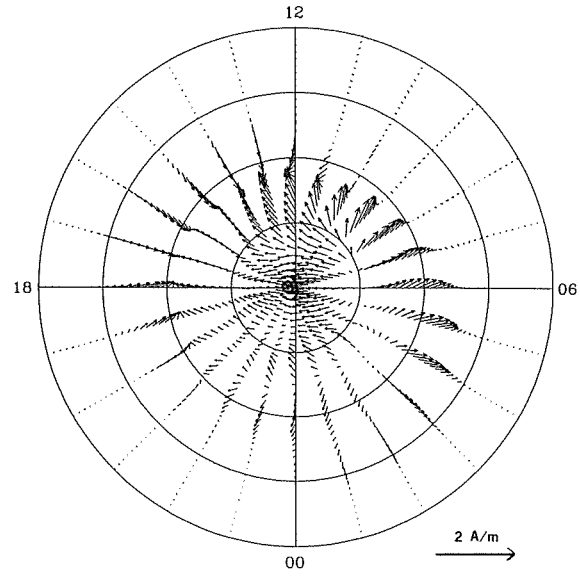

Figure 4h

JOULE HEATING RATE

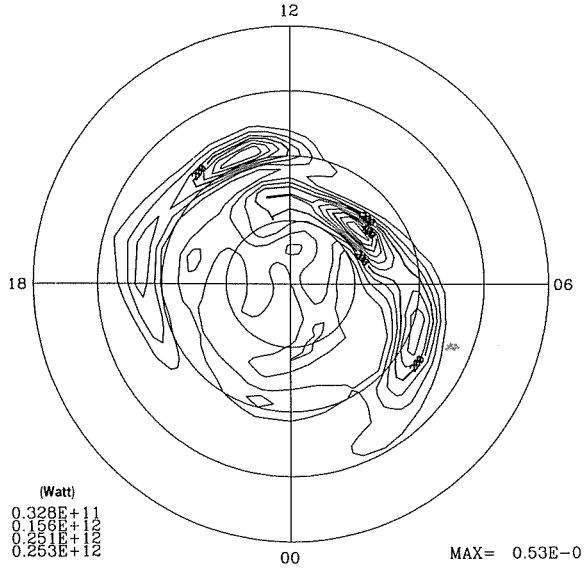

MAX= 0.53E-01 W/m²

Figure 4i CONTOUR INTERVAL: 5 mW/m²

FIELD-ALIGNED CURRENTS

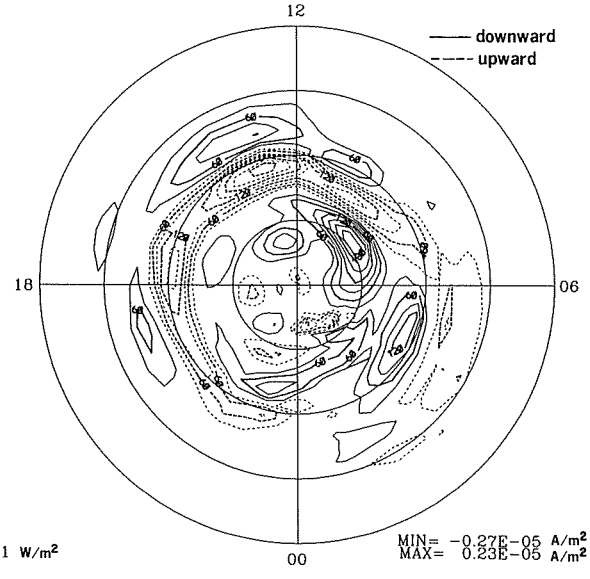

MIN= -0.27E-05 A/m²
MAX= 0.23E-05 A/m²

Figure 4j CONTOUR INTERVAL: 0.3 μA/m²

FIELD-ALIGNED CURRENT
HALL COMPONENT

FIELD-ALIGNED CURRENT
PEDERSEN COMPONENT

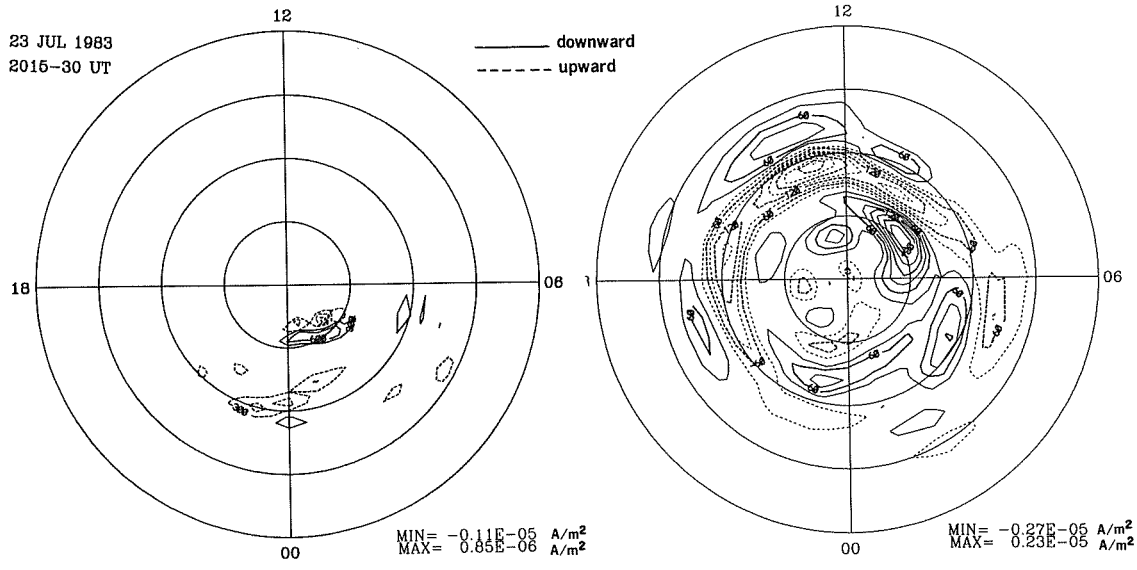

CONTOUR INTERVAL: 0.3 $\mu A/m^2$

CONTOUR INTERVAL: 0.3 $\mu A/m^2$

Figure 4k

PART II

1. IONOSPHERIC CONDUCTANCE DISTRIBUTION

Gorney et al. (1985) reported a numerical technique to provide an estimate of incident auroral electron spectra inferred from satellite observations of bremsstrahlung X-ray spectra. The technique utilizes a maximum-entropy estimate for the inferred electron spectrum based on discrete observations of bremsstrahlung spectrum. Based on the estimated auroral electron spectra, the conductivities are computed from steady state ionization profiles derived from the altitude profiles of energy deposition after Vickery et al. (1981). The X-ray technique provides a reasonable representation of the important incident electron spectral parameters and enables one to estimate the ionospheric conductance. Further, a scanning X-ray detector like the one flown on the DMSP-F6 satellite is able to image a large portion of the electron precipitation in both sunlit and not sunlit conditions while the particle detector can only provide data along the satellite orbit. We applied this method to the bremsstrahlung X-ray measurement from the Aerospace X-ray spectrometer on DMSP-F6 satellite for July 23-24, 1983.

In spite of the great advantages of an X-ray imager in estimating large-scale ionospheric conductances over other methods, there are several shortcomings inherited from the orbital characteristics of the satellite and the limitations of the instrument on board. Firstly, in its dawn-dusk low-altitude polar orbit, the instrument field of view is limited to about 3,000 km from one limb of the earth to the other, covering the major portion of aurora only at the best viewing situation. Secondly, since the geomagnetic axis is tilted 11° away from the rotational axis and the inclination of the satellite is 99°, the satellite ground-tract footprint may miss the magnetic dawn-dusk meridian point by as much as 20°, leaving a significant portion of nightside or dayside aurora out of the field of view. Thirdly, the DMSP X-ray spectrometer uses satellite motion to image the polar region, thus, one image takes 17 minutes and consecutive X-ray images of a hemisphere are acquired once an orbit or about 100 minutes apart. However, since remarkable auroral conjugacy has been established (Akasofu, 1977 and references therein, Mizera et al., 1987), the images taken over the southern polar region have also been utilized in this study as though they were taken over the northern hemisphere. Thus we have a 17 minute image every 50 minutes. Fourthly, it is difficult to apply the X-ray remote sensing technique at energies less than 1.5 kV. However, the exclusion of the low energy portion of the spectrum does not significantly affect the estimate of Hall and Pedersen conductance since such particles do not penetrate deep enough in altitude to contribute more than 10% to the E region conductance. Low signal-to-noise ratios limit the X-ray technique to measurements of conductance values greater than 5 mhos for Hall and 2.5 mhos for Pedersen conductance.

2. DATA PROCESSING TECHNIQUES

To construct a global ionospheric conductance distribution, we used all the information available from the image whether above the instrument threshold or below it. Then we employed the following techniques to fill gaps in coverage of the instrument. We completed the polar region distribution which was not imaged by the DMSP instrument. Sometimes the data gap appeared in the midnight portion and sometimes in the dayside portion of the auroral oval. The gaps in the midnight sector were filled by interpolating the data recorded in dawn and dusk sectors for that image. The dayside gaps were filled by extrapolating (or stretching) the available data in the dawn and/or dusk sectors, recognizing that a minimum in conductance occurs near 1400 MLT (Fuller-Rowell and Evans, 1987). Values below the threshold have been filled with special care to keep either extrapolated or interpolated values below that threshold. Figure 5 shows an example of the ionospheric Hall conductance distribution based solely on the recorded X-ray image (a), after the data gaps have been filled (b), and after the solar UV contribution is added (c).

Occasionally the X-ray image is not available or all pixel values are significantly below the threshold values or the instrument views only a small portion of the dayside oval. In such cases we substitute the entire conductance distribution of that time with one from an empirical model. To decide which model is suitable for this purpose, the cross-polar cap potential differences, Φ , based on different conductivity models are compared with those based on the realistic distribution from the available X-ray images because the electric potential distribution is most sensitive to the choice of the conductivity model. For this purpose we used the models reported by Spiro et al. (1982) and Ahn et al. (1983).

The Rice University conductance model described in Spiro et al. (1982) was adjusted, as suggested by Kamide et al. (1982), by shifting the latitude of the maximum Hall conductance to the latitude of the equivalent current maximum when necessary. The search for the difference between the two maxima has been further restricted to the latitude zone between 55° and 75° since the auroral enhancement is usually found in that region. Figures 6 and 7 show the ionospheric Pedersen conductance distributions and the calculated electrical potential distributions for 0355-0410 UT on March 24, 1983. One can notice that all three distribution patterns of the electrical potential consist basically of a well-defined, two-cell convection pattern. The estimated cross-polar cap potential differences are 95, 96 and 79 kV for the DMSP X-ray image, UA and Rice University conductance distributions, respectively. The unusually high positive potential cell of 90 kV in the evening sector below 60° latitude of the potential distribution based on the Rice model results from an unrealistically low conductance value of the model in that region. In determining the cross-polar cap potential difference of the potential distribution based on the Rice model, we took the positive cell value in the dawn sector of 35 kV instead of the lower latitude value. Such a modification is quite often needed in the potential distribution based on the Rice model. Due to the underestimation of the potential difference and the ambiguity encountered frequently in determining the extreme value of the electric potential distribution for the Rice model, we have used the UA model in this report to substitute for the realistic conductance distribution whenever the images are not available.

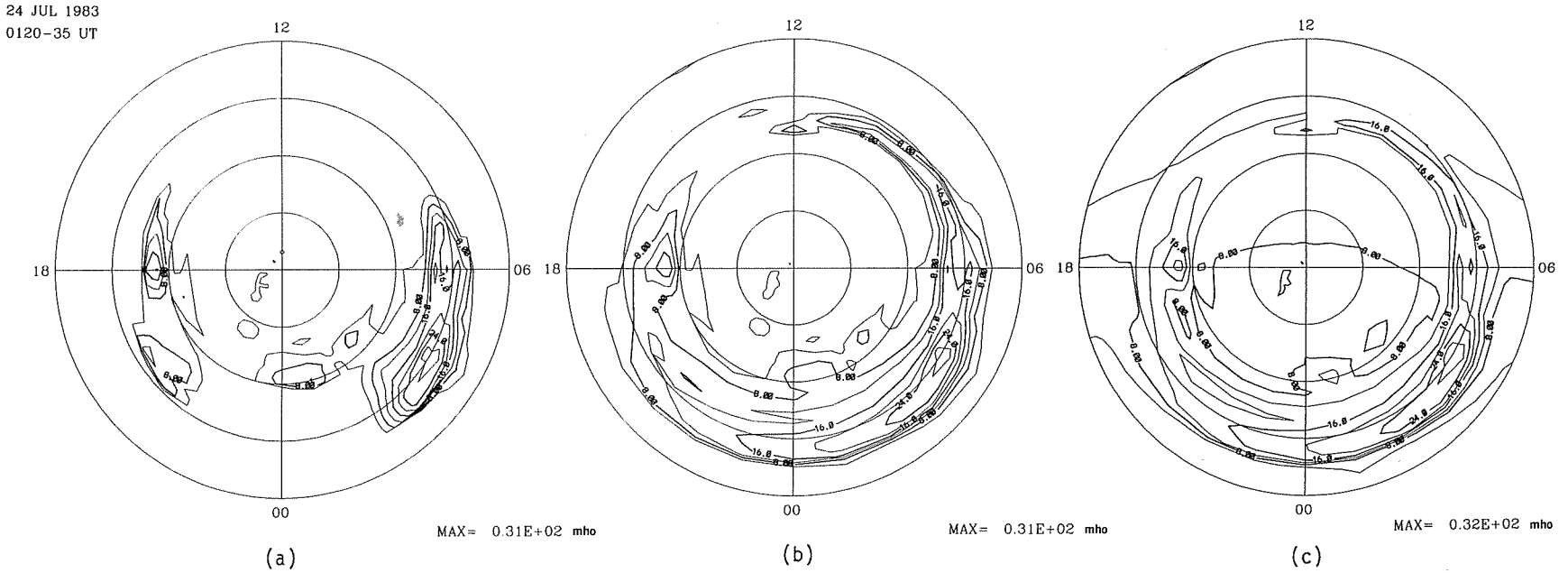

Figure 5. The Hall conductance distributions at 0120-35 UT on July 24, 1983
(a) based on the original X-ray image with data gaps in the midnight and noon sectors;
(b) after filling up the gaps;
and (c) including the solar UV contribution.

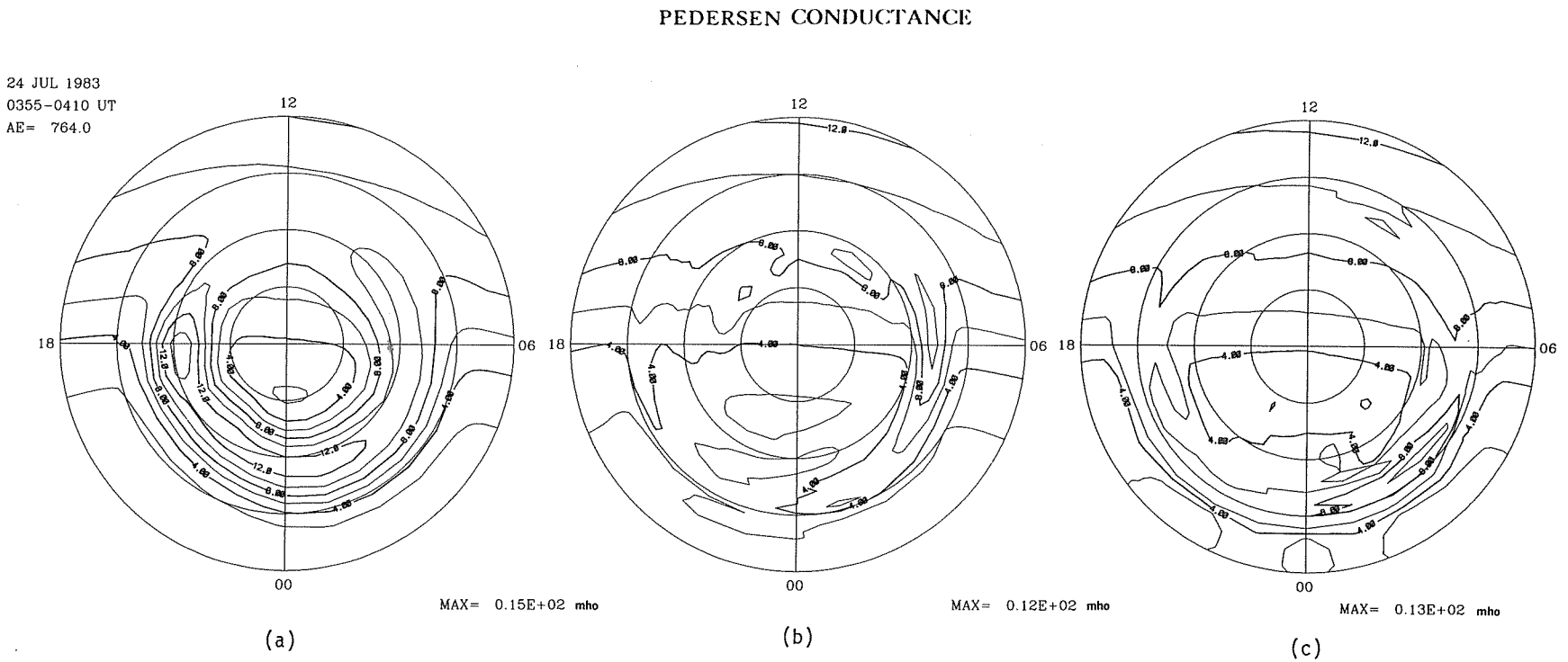

Figure 6. The ionospheric Pedersen conductance distributions at 0355-0410 UT on July 24, 1983 based on the
(a) Rice model;
(b) UA model; and
(c) DMSP X-ray image data
and used in generating the electric potential distributions in Figure 7.

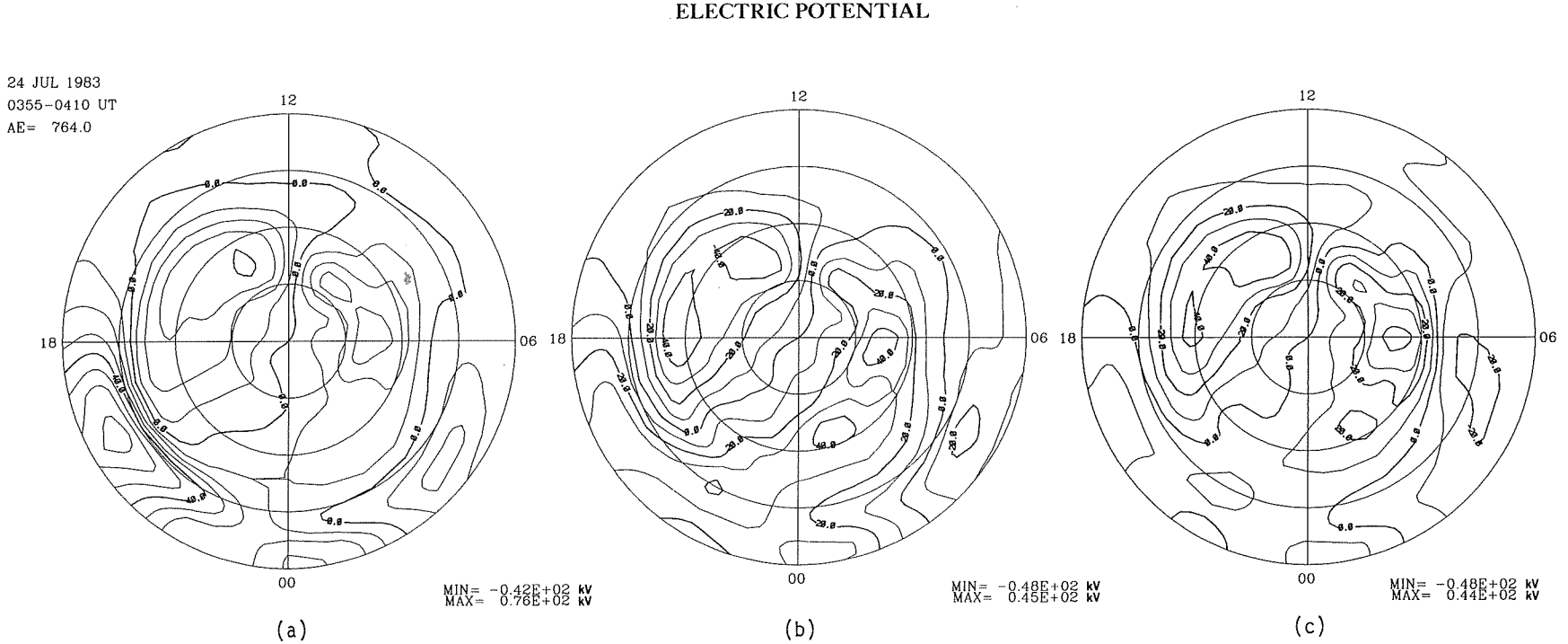

Figure 7. The electric potential distribution patterns at 0355-0410 UT on July 24, 1983 based on the
(a) Rice model;
(b) UA model, and
(c) DMSP X-ray image data.

REFERENCES

AHN, B.-H., Y. KAMIDE, and S.-I. AKASOFU 1984 Global ionospheric current distributions during substorms, J. Geophys. Res., 89, 1613.

AHN, B.-H., R.M. ROBINSON, Y. KAMIDE and S.-I. AKASOFU 1983 Electric conductivities, electric fields and auroral particle energy injection rate in the auroral ionosphere and their empirical relations to the horizontal magnetic disturbances, Planet. Space Sci., 31, 641.

AKASOFU, S.-I. 1977 Physics of Magnetospheric Substorms, p. 81, D. Reidel, Hingham, Mass.

AKASOFU, S.-I., Y. KAMIDE and J.L. KISABETH 1981 Comparison of two modeling methods for three dimensional current systems, J. Geophys. Res., 86, 3389.

BANKS, P.M. 1977 Observations of Joule and particle heating in the auroral zone, J. Atmos. Terr. Phys., 39, 179.

FAYERMARK, D.S. 1977 Reconstruction of the three-dimensional current system of the high-latitude region from ground-based geomagnetic measurements, Geomagn. Aeron., Engl. Transl., 17, 114.

FULLER-ROWELL, T.J., and D.S. EVANS 1987 Height-integrated Pedersen and Hall conductivity patterns inferred from the TIROS-NOAA satellite data, J. Geophys. Res., 92, 7606.

GORNEY, D.J., P.F. MIZERA, and J.L. ROEDER 1985 A maximum-entropy technique for deconvolution of atmospheric bremsstrahlung spectra, Space Sciences Lab. Report No. SSL-86(6940-06)-6, Aerospace Corporation, Los Angeles.

GUSTAFSSON, G. 1969 A revised corrected geomagnetic coordinate system, Kiruna Geophysical Observatory, Report No. 694, Royal Swedish Academy of Science.

IIJIMA, T., and T.A. POTEMRA 1978 Large-scale characteristics of field-aligned currents associated with substorms, J. Geophys. Res., 83, 599.

KAMIDE, Y., H.W. KROEHL, B.A. HAUSMAN, R.L. MCPHERRON, S.-I. AKASOFU, A.D. RICHMOND, P.H. REIFF, and S. MATSUSHITA 1983 Numerical modeling of ionospheric parameters from global IMS magnetometer data for the CDAW-6 intervals, WDC-A Report UAG-88.

KAMIDE, Y., H.W. KROEHL, A.D. RICHMOND, B.-H AHN, S.-I AKASOFU, W. BAUMJOHANN, J.K. WALKER, and A.N. ZAITZEV 1982 Changes in the global electric fields and currents for March 17-19, 1978 from six IMS meridian chains of magnetometers, WDC-A Report UAG-87

KAMIDE, Y., and A.D. RICHMOND 1982 Ionospheric conductivity dependence of electric fields and currents estimated from ground magnetic observations, J. Geophys. Res., 87, 8331.

KAMIDE, Y., A.D. RICHMOND, and S. MATSUSHITA 1981 Estimation of ionospheric electric fields, ionospheric currents and field-aligned currents from ground magnetic records, J. Geophys. Res., 86, 801.

KISABETH, J.L. 1979 On calculating magnetic and vector potential fields due to large-scale magnetospheric current systems and induced currents in an infinitely conducting earth, in Quantitative Modeling of Magnetospheric Processes, ed. by W.P. Olson, Amer. Geophys. Union, pp. 473-498.

KROEHL, H.W., and A.D. RICHMOND 1979 Magnetic substorm characteristics described by magnetic potential maps for 26-28 March, 1976, in Dynamics of the Magnetosphere, ed. by S.-I. Akasofu, D. Reidel, pp. 269-286, Hingham, Mass.

MISHIN, V.M., A.D. BAZARZHAPOV, and G.V. SHPYNEV 1980 Electric fields and currents in the earth's magnetosphere, in Dynamics of the Magnetosphere, ed. by S.-I. Akasofu, D. Reidel, pp. 249-268, Hingham, Mass.

REFERENCES continued

MIZERA, P.F., D.J. GORNEY, and D.S. EVANS — 1987 — On the conjugacy of the aurora: High and low latitudes, Geophys. Res. Lett., 14, 190.

RICHMOND, A.D., and Y. KAMIDE — 1987 — Mapping electrodynamic features of the high-latitude ionosphere from localized observations: Technique, J. Geophys. Res., submitted.

RICHMOND, A.D., S. MATSUSHITA, and J.D. TARPLEY — 1976 — On the production mechanism of electric currents and fields in the ionosphere, J. Geophys. Res., 81, 547.

SPIRO, R.W., P.H. REIFF, and L.G. MAHER, JR. — 1982 — Precipitating electron energy flux and auroral zone conductances--An empirical model, J. Geophys. Res., 87, 8215.

TARPLEY, J.D. — 1970 — The ionospheric wind dynamo, 1, Lunar Tide, Planet. Space Sci., 18, 1075.

VICKREY, J.F., R.R. VONDRAK, and S.J. MATTHEWS — 1981 — The diurnal and latitudinal variation of auroral zone ionospheric conductivity, J. Geophys. Res., 86, 65.

WALLIS, D.D., and E.E. BUDZINSKI — 1981 — Empirical models of height-integrated conductivities, J. Geophys. Res., 86, 125.

PART III

Table 2 lists the time periods for processing the magnetometer data, i.e., within 5 minutes of a polar crossing of the DMSP-F6 Satellite and presented in this report and the availability of the X-ray imagery. The second column of the table shows the scanning time of the instrument and the third column lists the four 5-minute data values of geomagnetic variations used in the calculation. All plots in this report are based on the average magnetic variation during the four 5-minute intervals rather than the time of each individual scan or within the scan period. The fourth column indicates the X-ray data availability, with 'N' and 'S' showing the hemispheric location of the satellite. A question mark is added when an image is available but does not contain enough information to use. Whenever the X-ray data are not usable, the UA conductance model is employed.

Except for the distributions of equivalent ionospheric current vectors and electric field vectors shown in Figures 4a-k, we show all the other outputs for the 57 events in this Part. Thirty of the events are based on the realistic conductance distribution and are captioned with "DMSP." The outermost circle is 50°N in corrected geomagnetic coordinates, with other latitude circles spaced every 10°. Date and UT are marked on each diagram.

Table 2. The time period processed in this report and the X-ray image availability.

	July 23, 1983			July 24, 1983		
No.	Scanning Period (UT)	Processed Period (UT)	Hemisphere	No.	Scanning Period (UT)	Processed Period (UT)	Hemisphere
1	0001-0017	0000-0015	N	30	0031-0048	0030-0045	S
2	0052-0108	0055-0110	S	31	0119-0136	0120-0135	N
3		0145-0200		32	0211-0228	0210-0225	S
4	0232-0248	0235-0250	S	33	0302-0319	0305-0320	N
5	0322-0338	0325-0340	N	34	0352-0408	0355-0410	S
				35	0442-0459	0445-0500	N
6		0415-0430		36	0531-0548	0530-0545	S
7		0505-0520		37	0622-0638	0620-0635	N
8		0555-0610		38	0711-0727	0710-0725	S
9		0645-0700		39	0802-0818	0800-0815	N
10	0732-0748	0735-0750	S				
				40	0852-0908	0850-0905	S
11	0824-0840	0825-0840	N	41	0941-0958	0940-0955	N
12	0913-0929	0915-0930	S	42	1031-1047	1030-1045	S
13	1004-1020	1005-1020	N	43	1126-1143	1125-1140	N
14	1054-1110	1055-1110	S ?	44	1215-1232	1215-1230	S ?
15	1146-1202	1145-1200	N				
				45	1305-1322	1305-1320	N
16		1240-1255		46	1358-1415	1400-1415	S ?
17		1330-1345		47		1450-1505	
18		1420-1435		48		1540-1555	
19		1510-1525		49		1630-1645	
20		1600-1615					
				50		1720-1735	
21	1652-1708	1650-1705	N	51		1810-1825	
22		1745-1800		52		1900-1915	
23	1834-1851	1835-1850	N	53		1950-2005	
24	1925-1942	1925-1940	S ?	54		2040-2055	
25	2015-2032	2015-2030	N				
				55		2130-2145	
26	2109-2126	2110-2125	S ?	56		2220-2235	
27	2157-2214	2200-2215	N	57		2310-2325	
28	2251-2307	2250-2305	S				
29	2339-2356	2340-2355	N				

ACKNOWLEDGEMENTS

The authors are grateful to the many individuals and institutes who assisted in obtaining the original magnetometer data. This research was supported by USAF Geophysics Laboratory (GLH7-6022) and USAF Office of Scientific Research (AFOSR-ISSA-87-0049). The work at The Aerospace Corporation was supported by USAF System Command's Space Division under Contract No. F04701-85-C-0086. B.-H. Ahn acknowledges the generous hospitality of NOAA's National Geophysical Data Center and partial support from the Korea Science and Engineering Foundation. (B.-H. Ahn, x6280)

EQUIVALENT CURRENT VECTORS

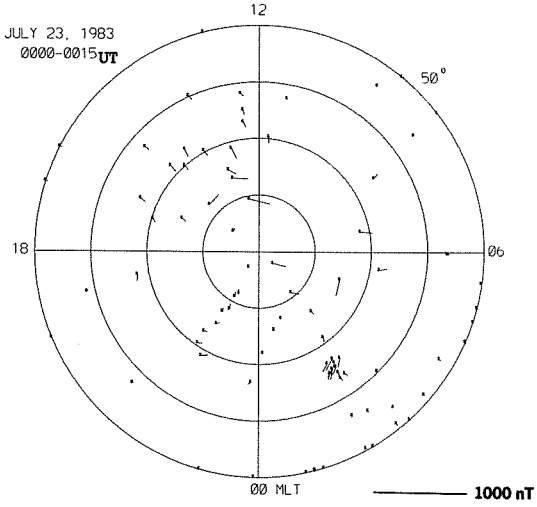

EQUIVALENT CURRENT SYSTEM

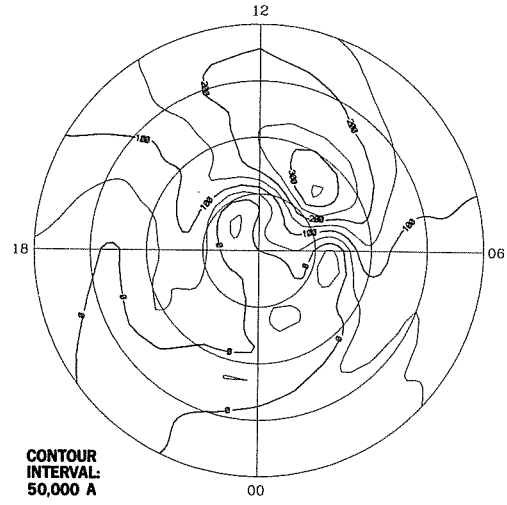

HALL CONDUCTANCE

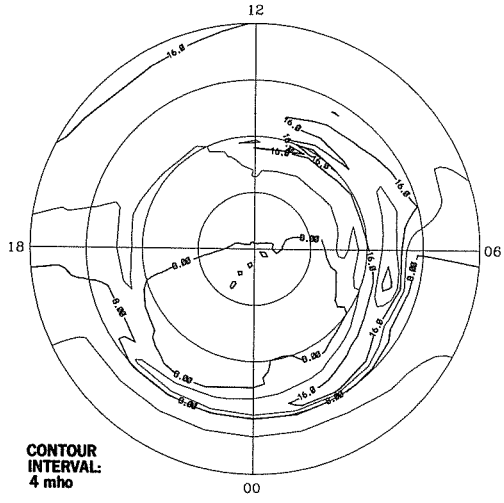

MAX= 0.25E+02 mho

DMSP

PEDERSEN CONDUCTANCE

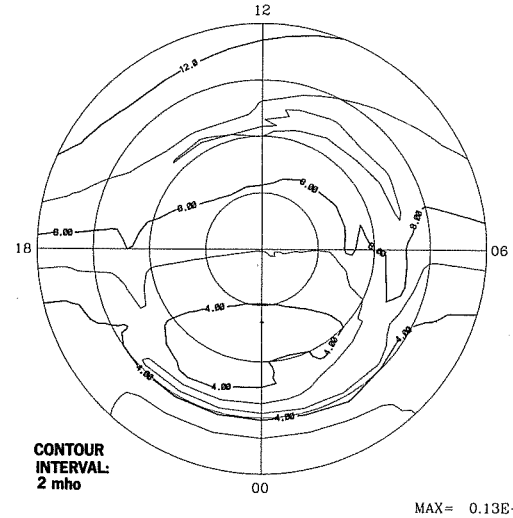

MAX= 0.13E+02 mho

ELECTRIC POTENTIAL

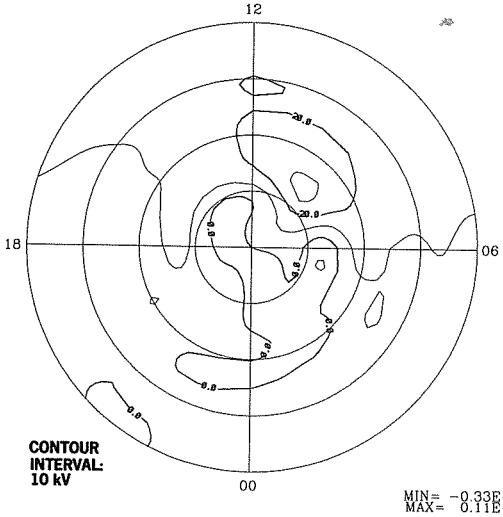

MIN= -0.33E+02 kV
MAX= 0.11E+02 kV

IONOSPHERIC CURRENT VECTORS

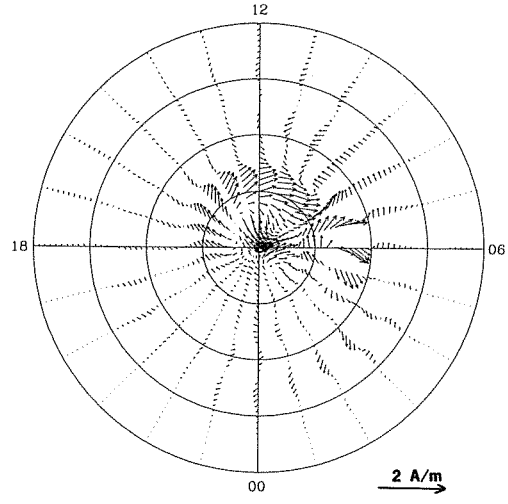

FIELD-ALIGNED CURRENT

23 JUL 1983
0000-15 UT

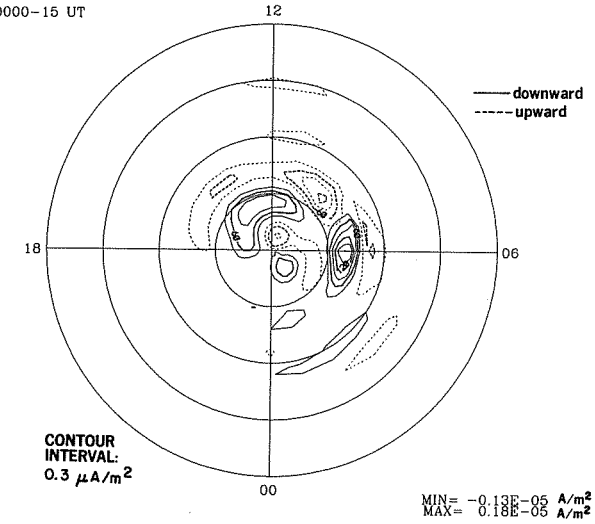

MIN= -0.13E-05 A/m²
MAX= 0.18E-05 A/m²

JOULE HEATING RATE

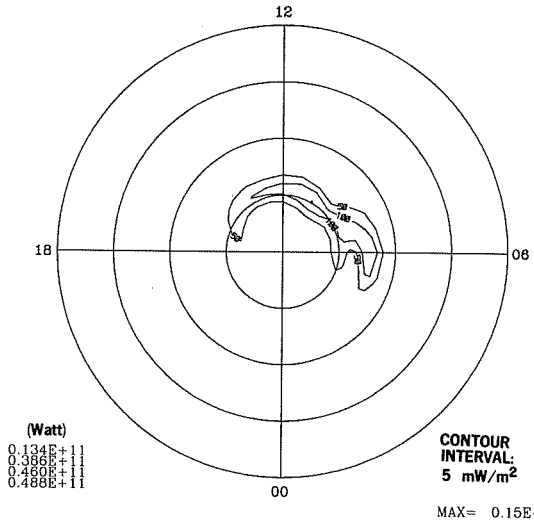

MAX= 0.15E-01 W/m²

HALL CURRENT VECTORS

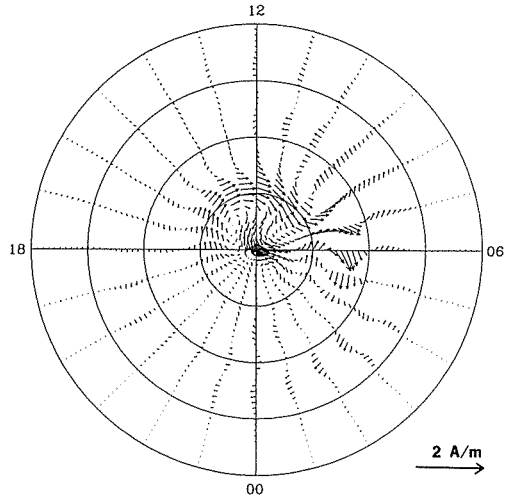

PEDERSEN CURRENT VECTORS

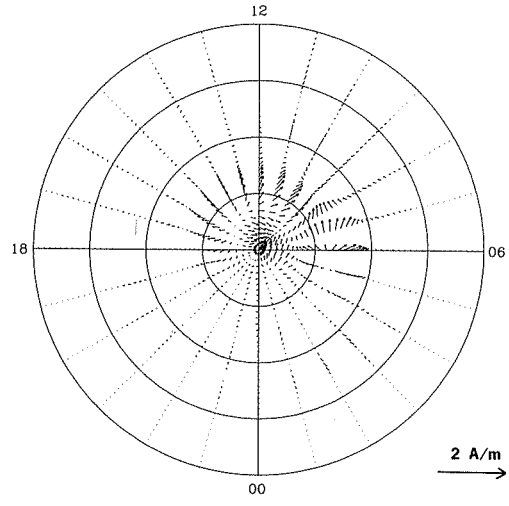

FIELD-ALIGNED HALL CURRENT

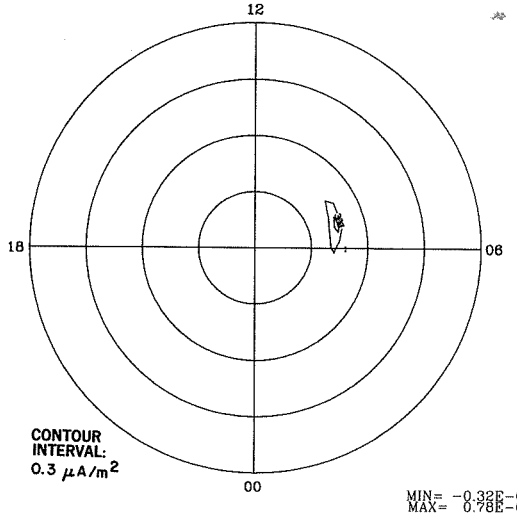

MIN= -0.32E-06 A/m²
MAX= 0.78E-06 A/m²

FIELD-ALIGNED PEDERSEN CURRENT

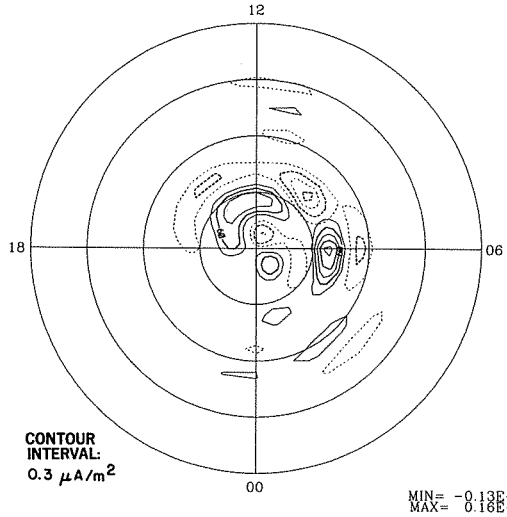

MIN= -0.13E-05 A/m²
MAX= 0.16E-05 A/m²

EQUIVALENT CURRENT VECTORS

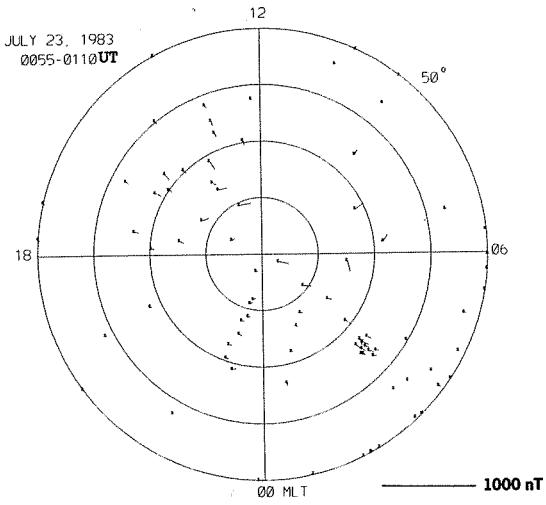

EQUIVALENT CURRENT SYSTEM

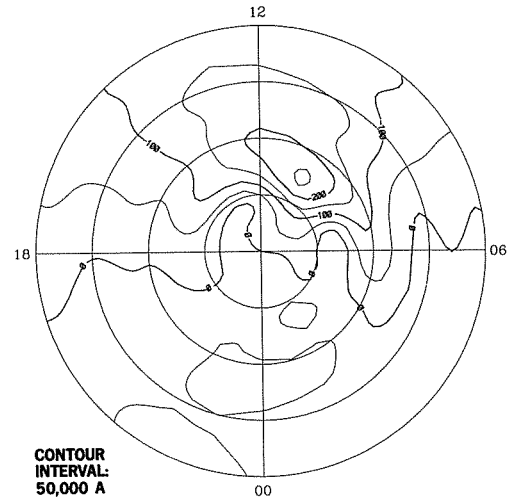

HALL CONDUCTANCE

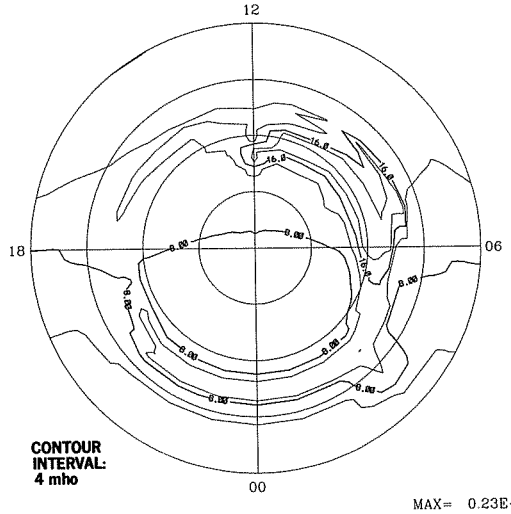

MAX= 0.23E+02 **mho**

DMSP

PEDERSEN CONDUCTANCE

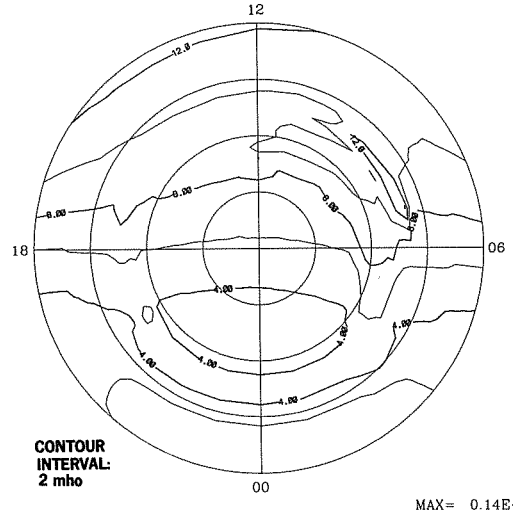

MAX= 0.14E+02 **mho**

ELECTRIC POTENTIAL

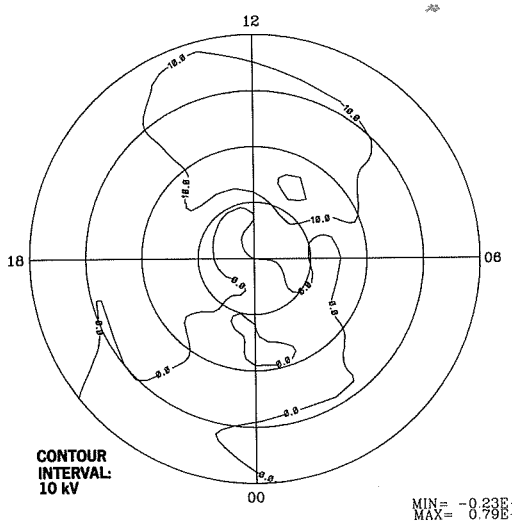

MIN= -0.23E+02 **kV**
MAX= 0.79E+01 **kV**

IONOSPHERIC CURRENT VECTORS

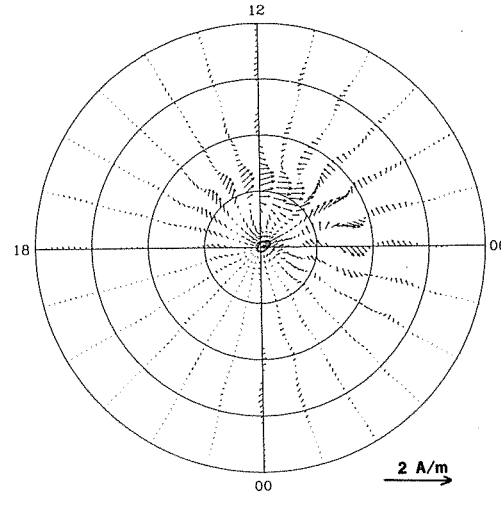

FIELD-ALIGNED CURRENT

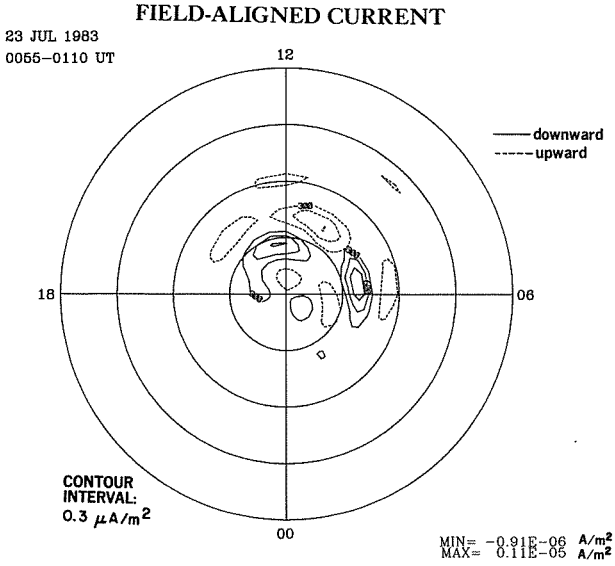

JOULE HEATING RATE

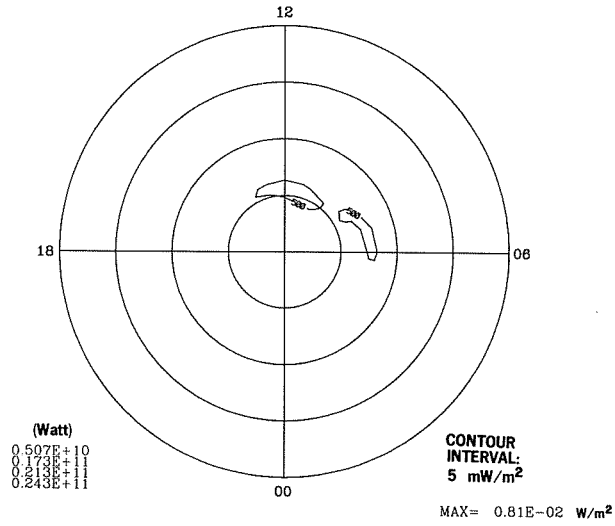

HALL CURRENT VECTORS

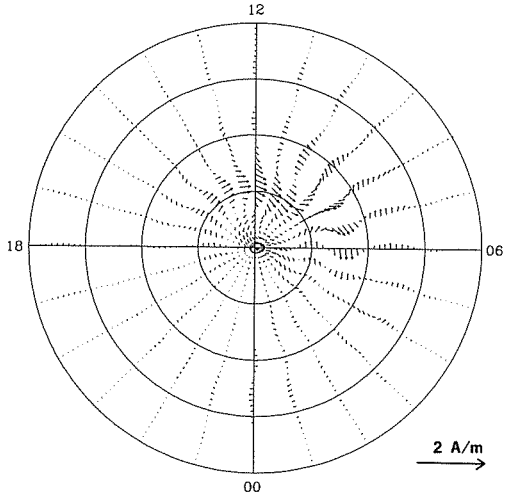

PEDERSEN CURRENT VECTORS

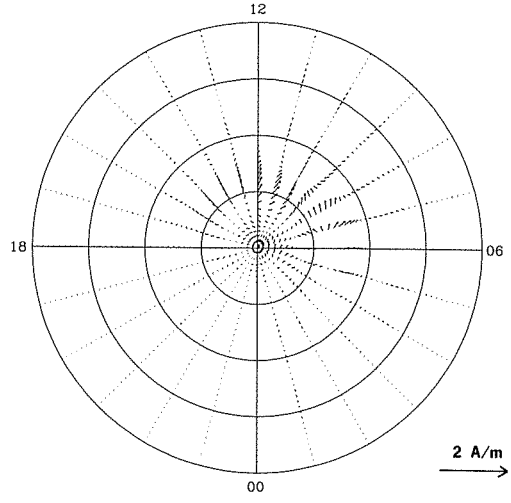

FIELD-ALIGNED HALL CURRENT

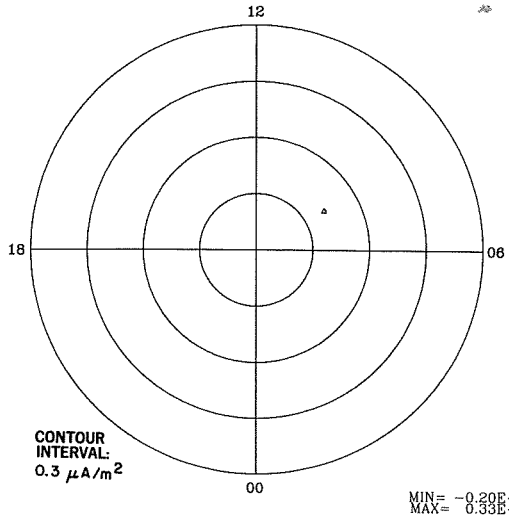

FIELD-ALIGNED PEDERSEN CURRENT

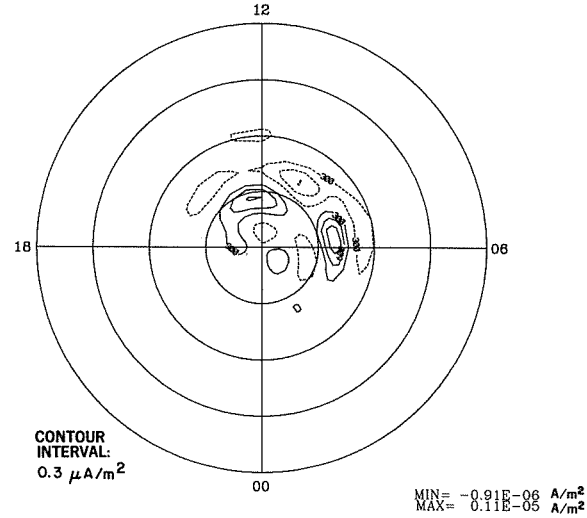

EQUIVALENT CURRENT VECTORS

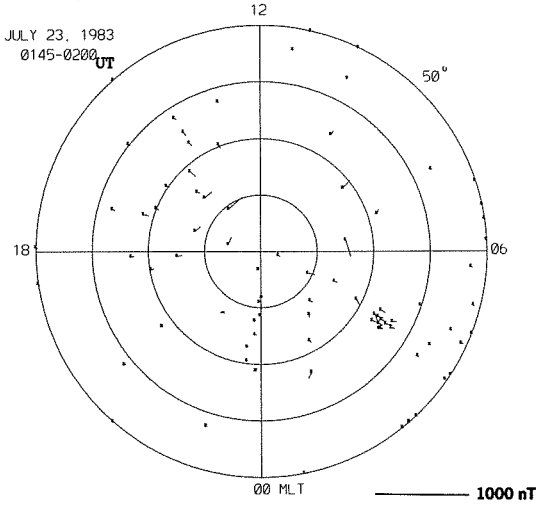

EQUIVALENT CURRENT SYSTEM

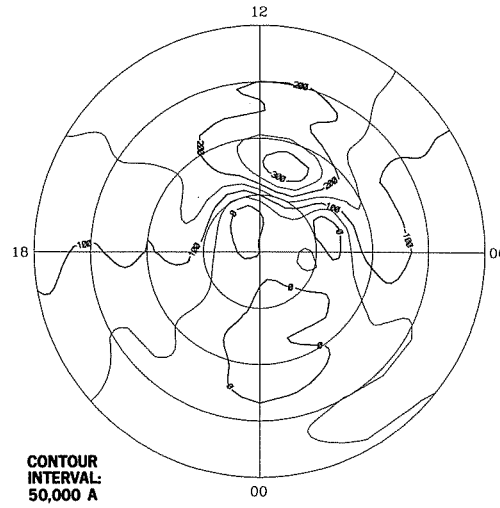

HALL CONDUCTANCE

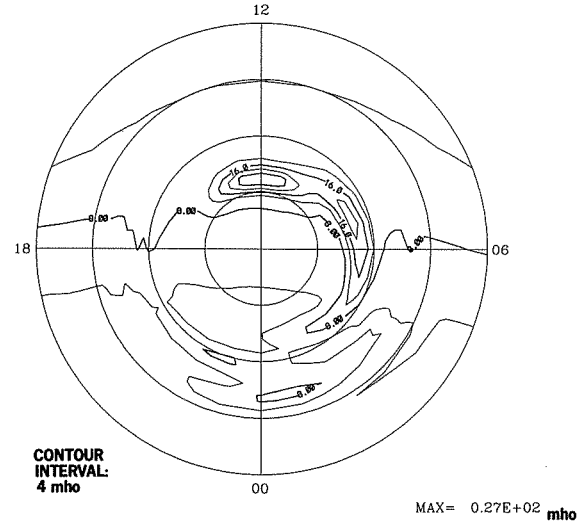

MAX= 0.27E+02 mho

PEDERSEN CONDUCTANCE

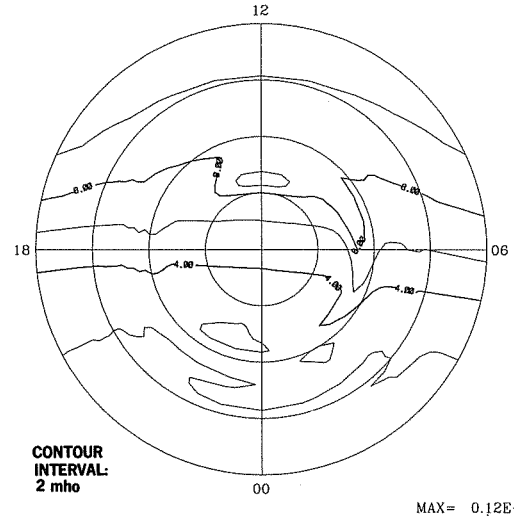

MAX= 0.12E+02 mho

ELECTRIC POTENTIAL

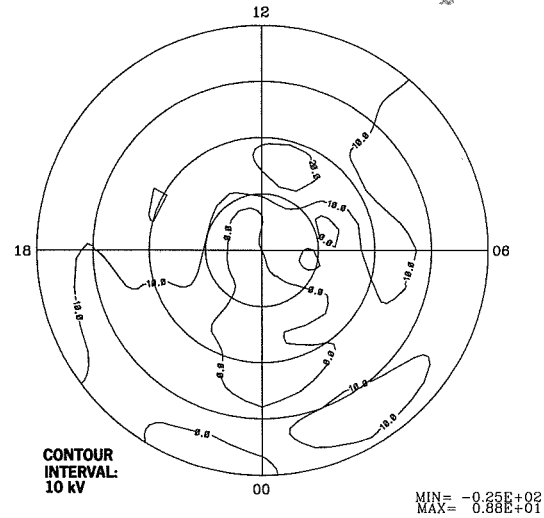

MIN= -0.25E+02 kV
MAX= 0.88E+01 kV

IONOSPHERIC CURRENT VECTORS

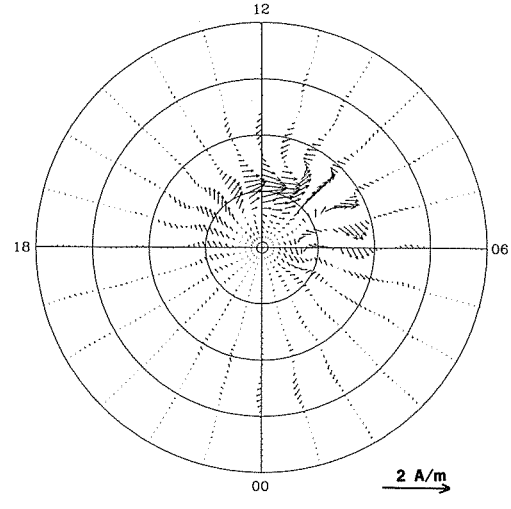

FIELD-ALIGNED CURRENT

23 JUL 1983
0145–0200 UT

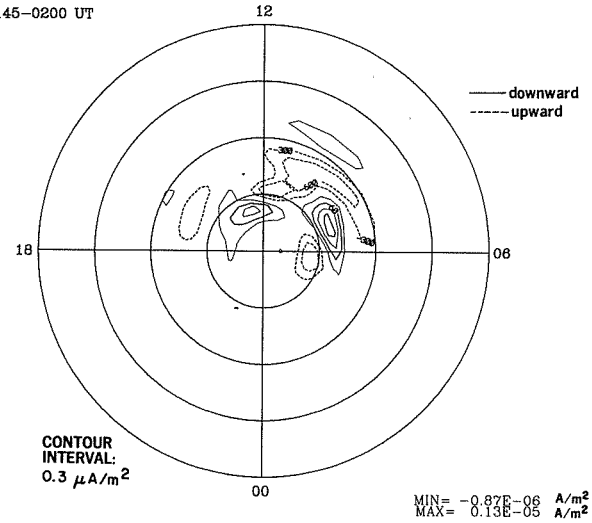

MIN= −0.87E−06 A/m²
MAX= 0.13E−05 A/m²

JOULE HEATING RATE

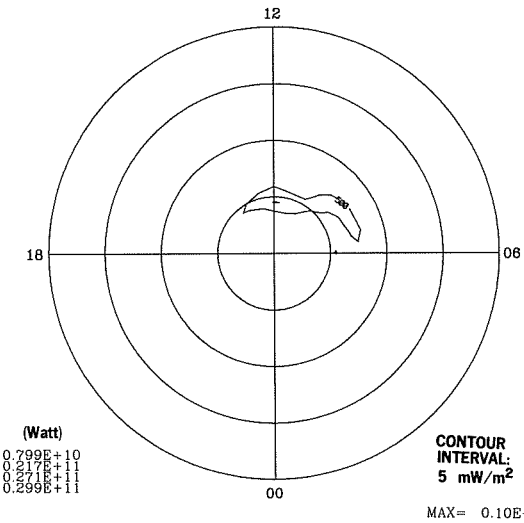

MAX= 0.10E−01 W/m²

HALL CURRENT VECTORS

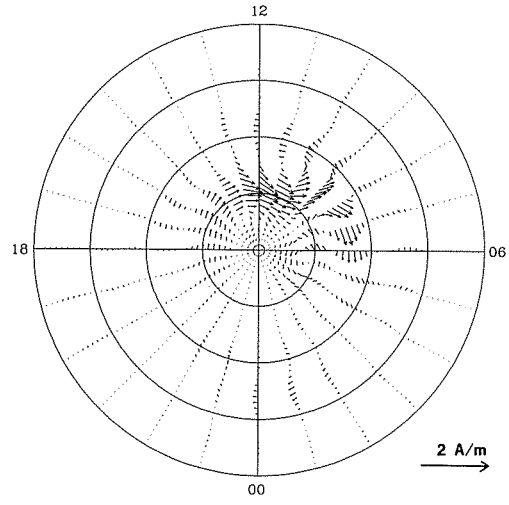

PEDERSEN CURRENT VECTORS

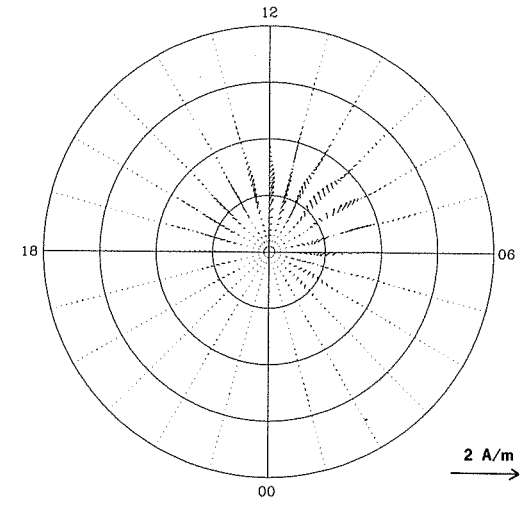

FIELD-ALIGNED HALL CURRENT

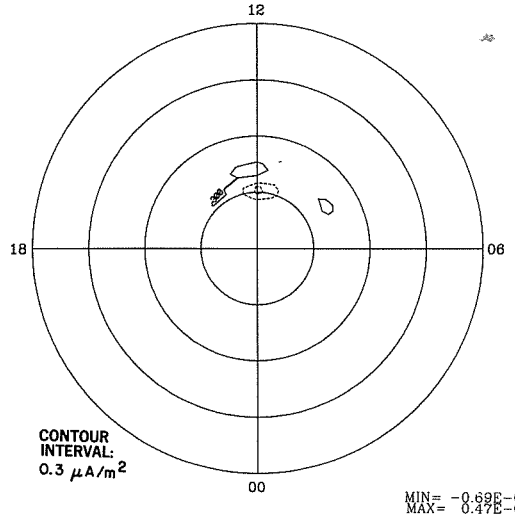

MIN= −0.69E−06 A/m²
MAX= 0.47E−06 A/m²

FIELD-ALIGNED PEDERSEN CURRENT

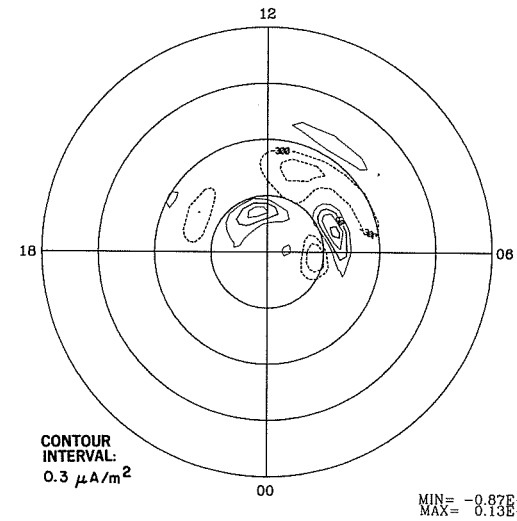

MIN= −0.87E−06 A/m²
MAX= 0.13E−05 A/m²

EQUIVALENT CURRENT VECTORS

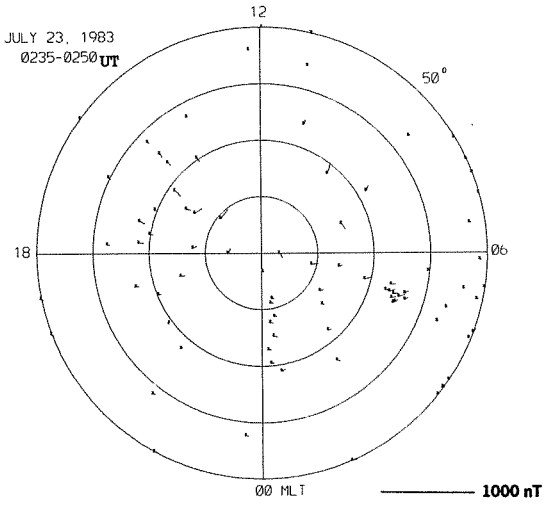

EQUIVALENT CURRENT SYSTEM

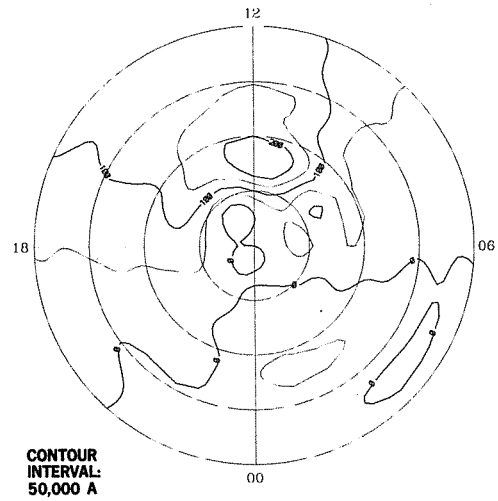

HALL CONDUCTANCE

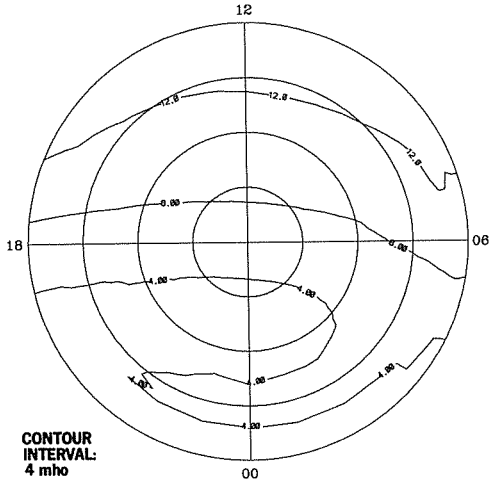

MAX= 0.15E+02 **mho**

DMSP

PEDERSEN CONDUCTANCE

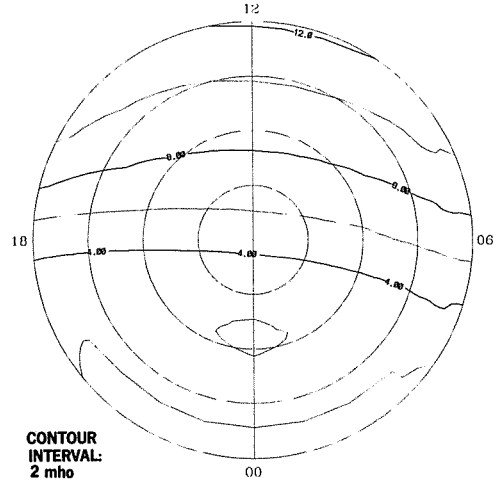

MAX= 0.12E+02 **mho**

ELECTRIC POTENTIAL

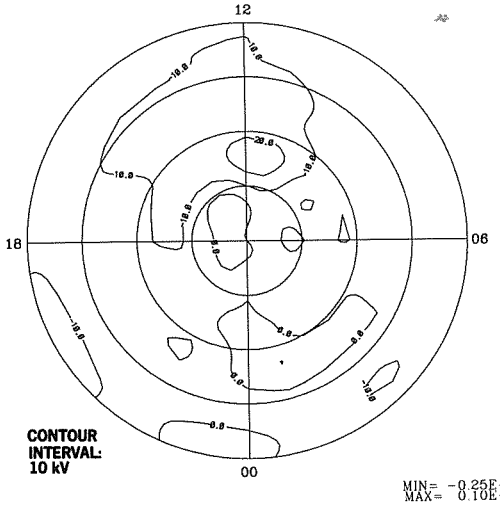

MIN= -0.25E+02 **kV**
MAX= 0.10E+02 **kV**

IONOSPHERIC CURRENT VECTORS

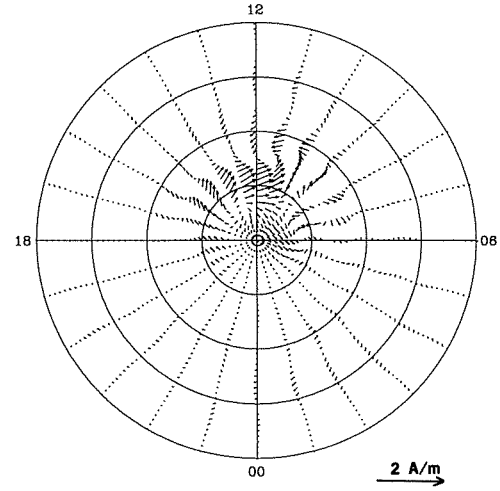

FIELD-ALIGNED CURRENT

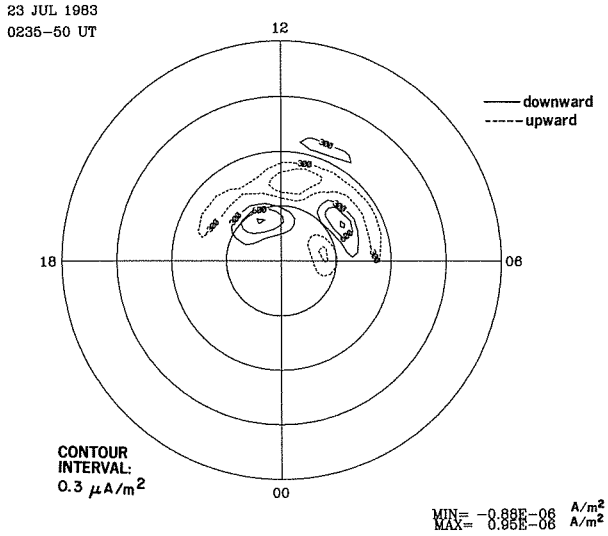

JOULE HEATING RATE

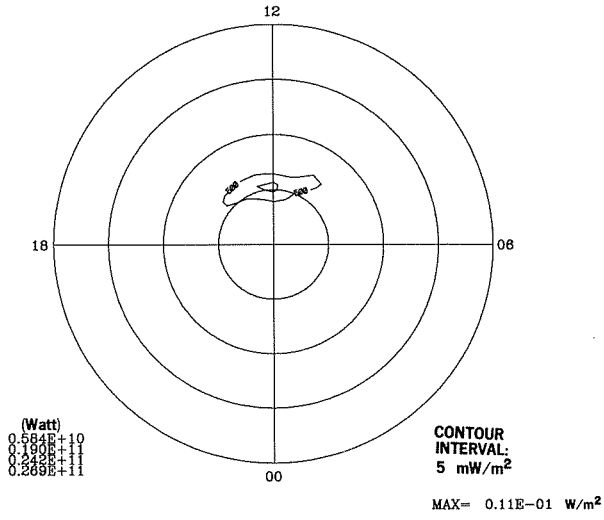

HALL CURRENT VECTORS

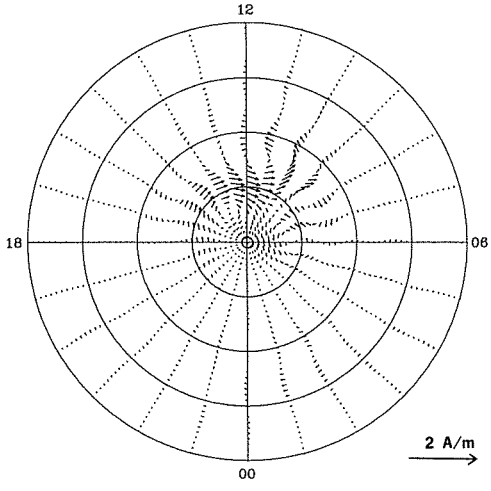

PEDERSEN CURRENT VECTORS

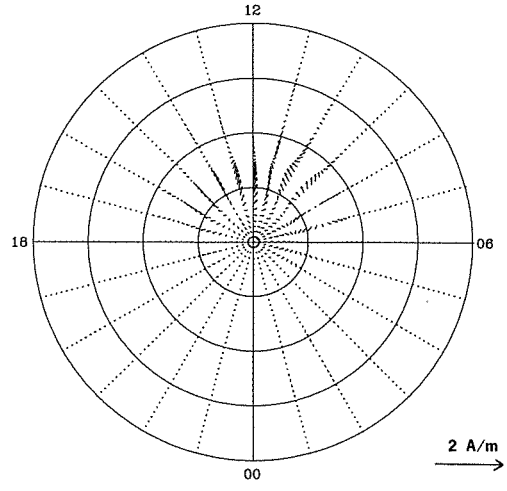

FIELD-ALIGNED HALL CURRENT

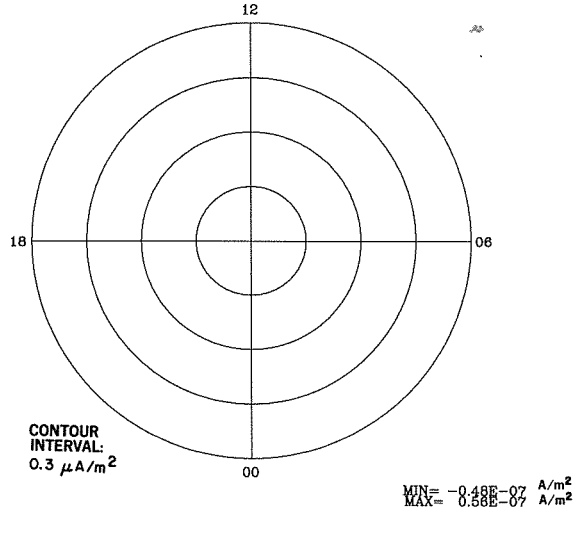

FIELD-ALIGNED PEDERSEN CURRENT

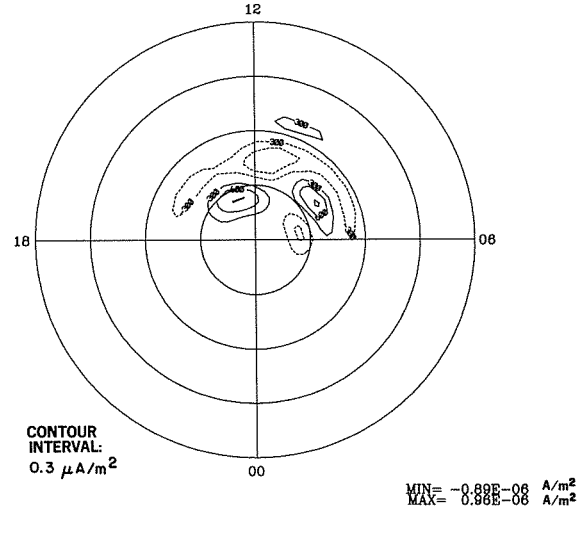

EQUIVALENT CURRENT VECTORS

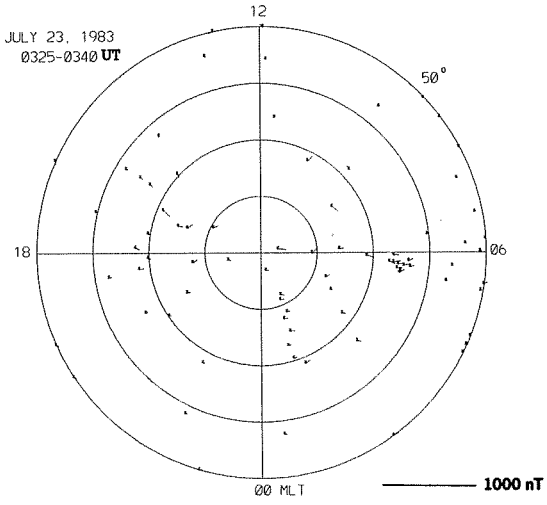

EQUIVALENT CURRENT SYSTEM

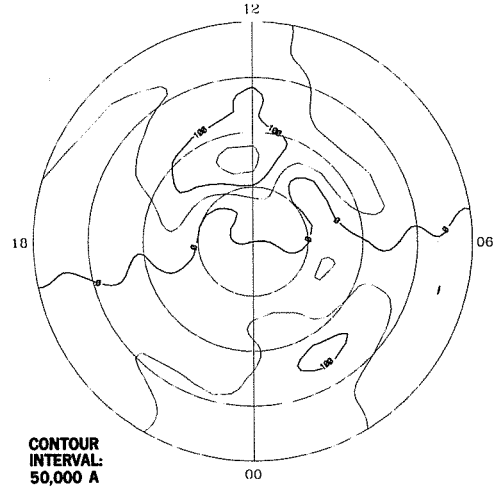

HALL CONDUCTANCE

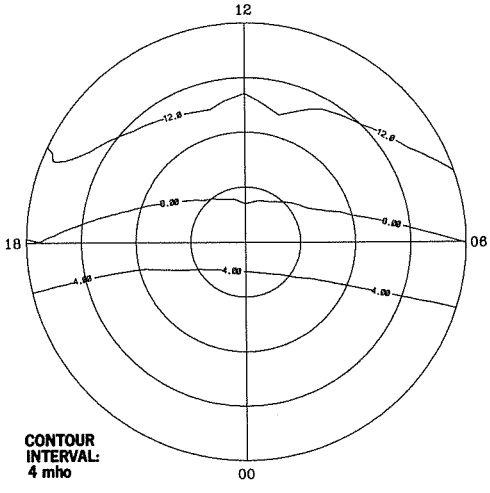

MAX= 0.16E+02 **mho**

DMSP

PEDERSEN CONDUCTANCE

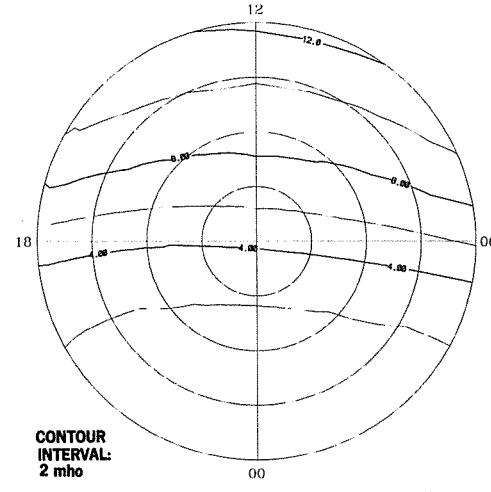

MAX= 0.12E+02 **mho**

ELECTRIC POTENTIAL

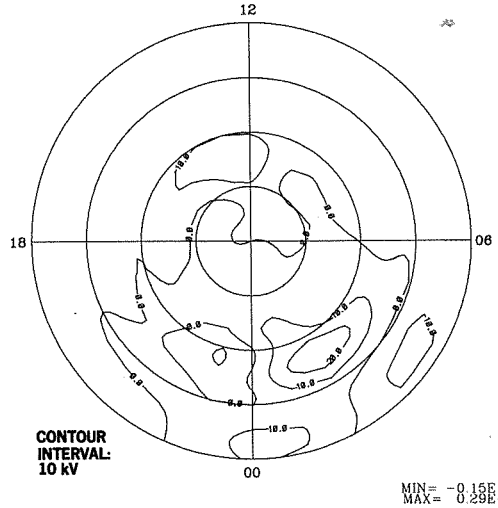

MIN= -0.15E+02 **kV**
MAX= 0.29E+02 **kV**

IONOSPHERIC CURRENT VECTORS

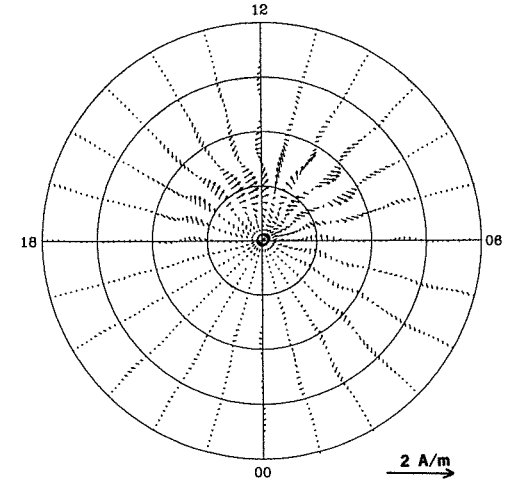

FIELD-ALIGNED CURRENT

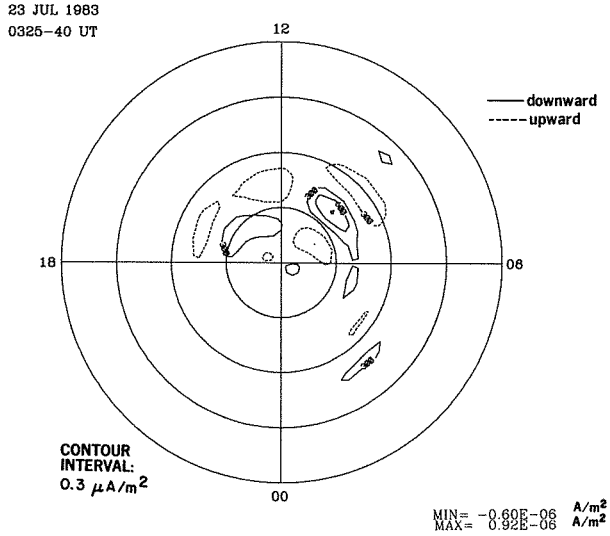

JOULE HEATING RATE

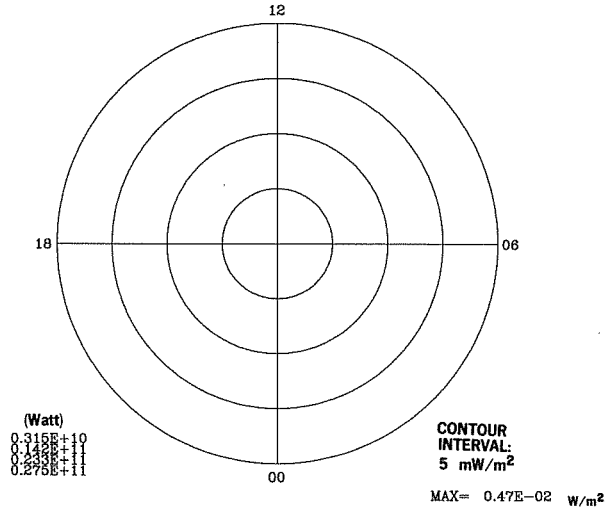

HALL CURRENT VECTORS

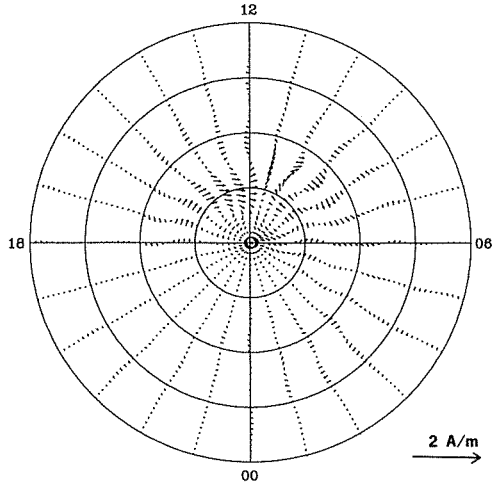

PEDERSEN CURRENT VECTORS

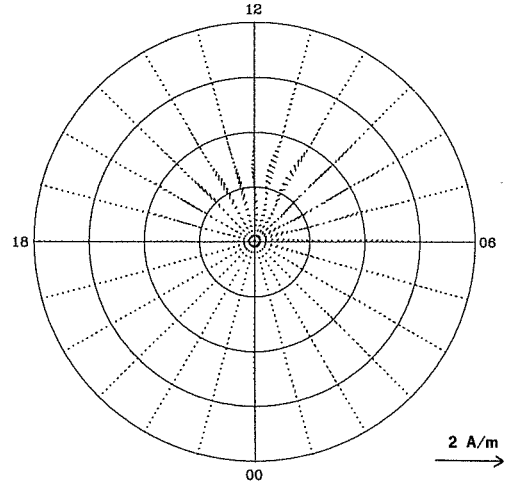

FIELD-ALIGNED HALL CURRENT

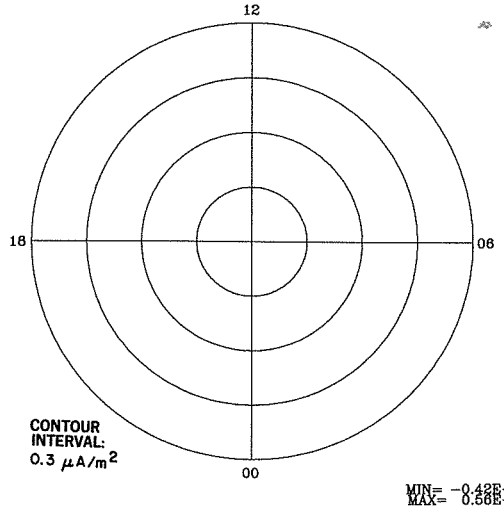

FIELD-ALIGNED PEDERSEN CURRENT

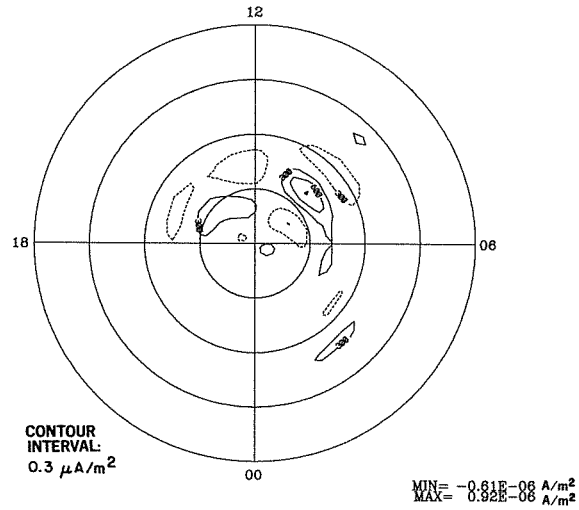

EQUIVALENT CURRENT VECTORS

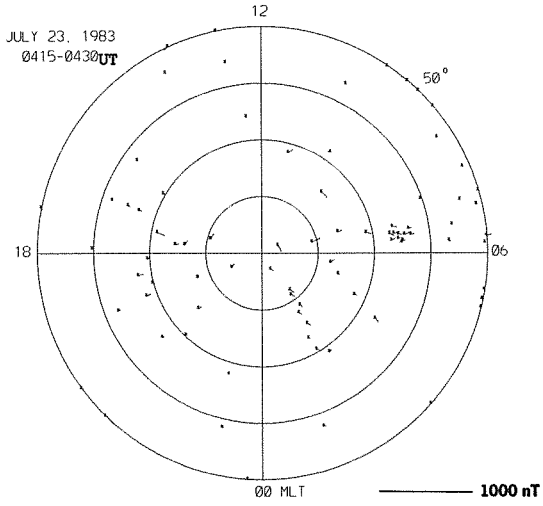

EQUIVALENT CURRENT SYSTEM

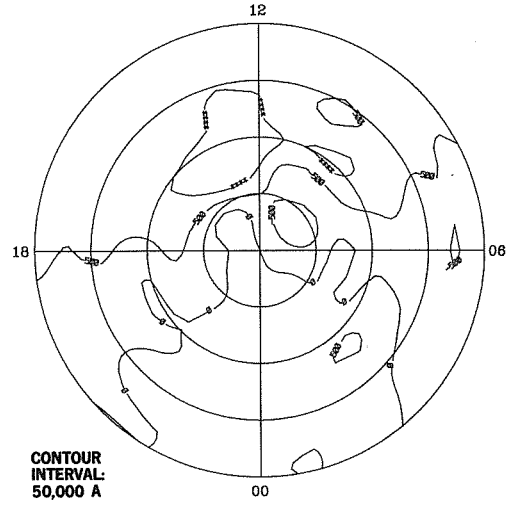

HALL CONDUCTANCE

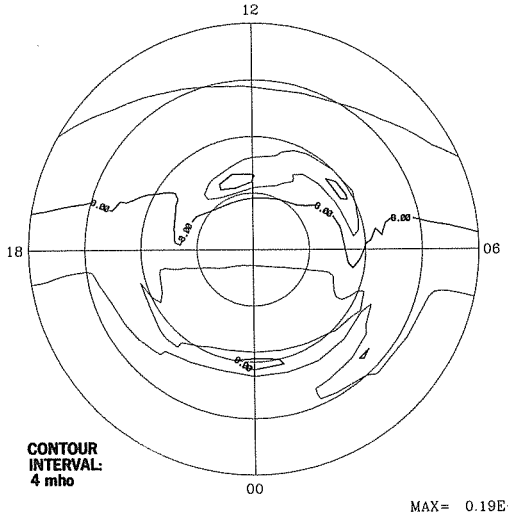

MAX= 0.19E+02 **mho**

PEDERSEN CONDUCTANCE

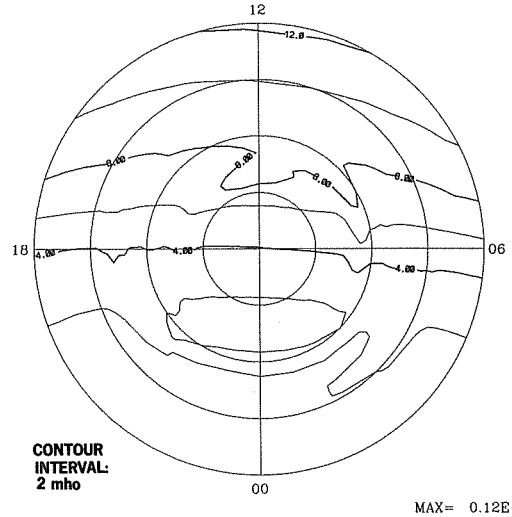

MAX= 0.12E+02 **mho**

ELECTRIC POTENTIAL

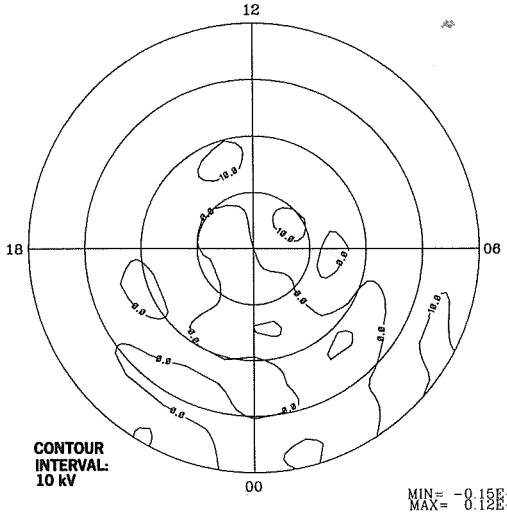

MIN= -0.15E+02 **kV**
MAX= 0.12E+02 **kV**

IONOSPHERIC CURRENT VECTORS

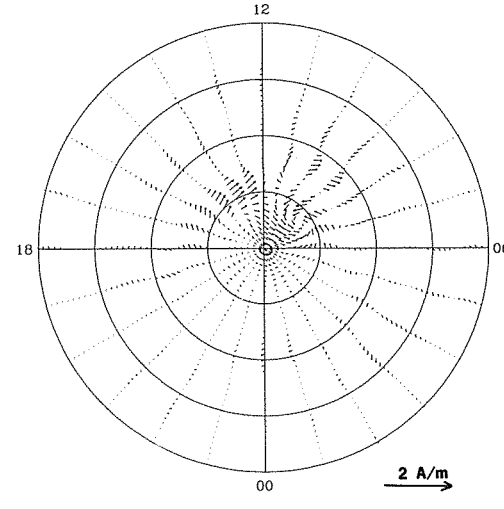

FIELD-ALIGNED CURRENT

23 JUL 1983
0415–30 UT

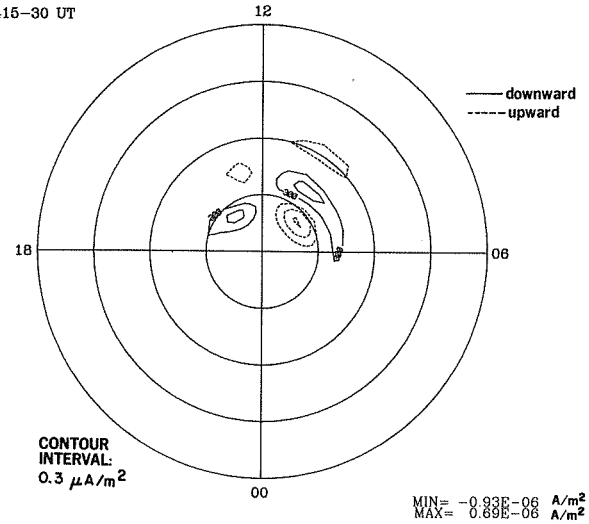

MIN= -0.93E-06 A/m²
MAX= 0.69E-06 A/m²

JOULE HEATING RATE

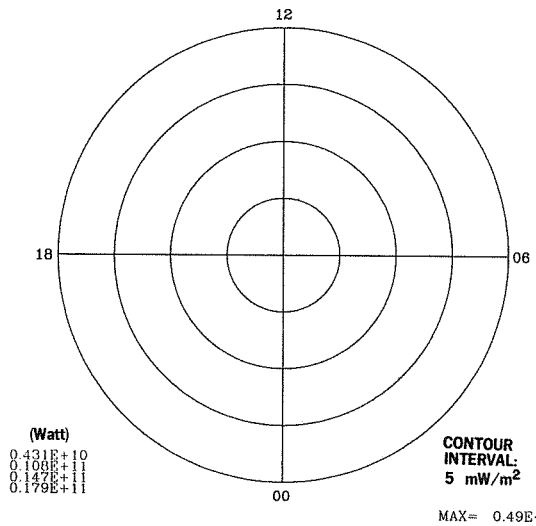

MAX= 0.49E-02 W/m²

HALL CURRENT VECTORS

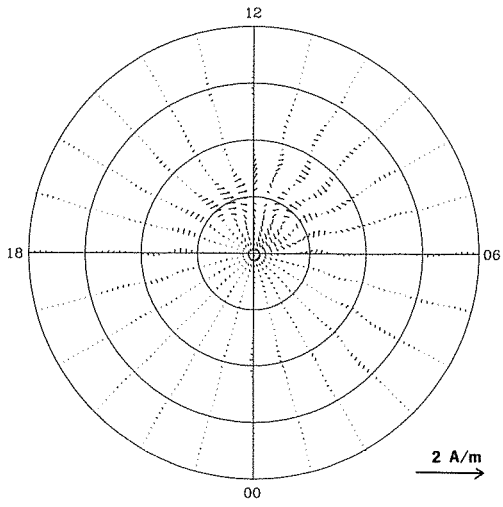

PEDERSEN CURRENT VECTORS

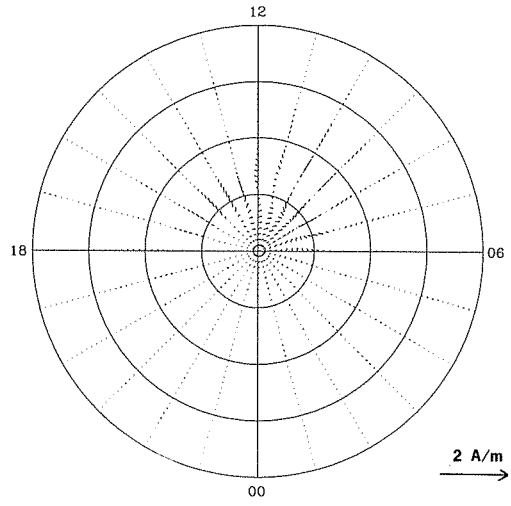

FIELD-ALIGNED HALL CURRENT

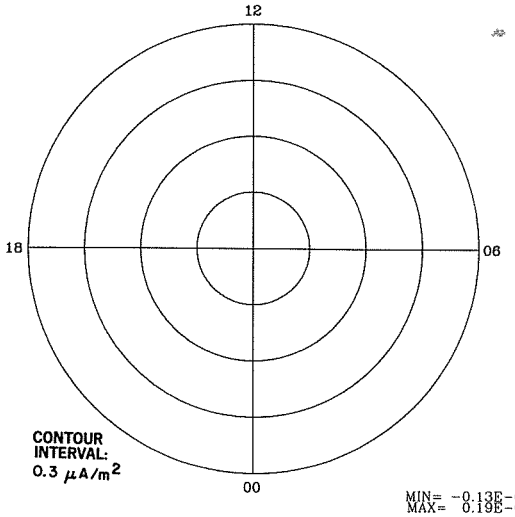

MIN= -0.13E-06 A/m²
MAX= 0.19E-06 A/m²

FIELD-ALIGNED PEDERSEN CURRENT

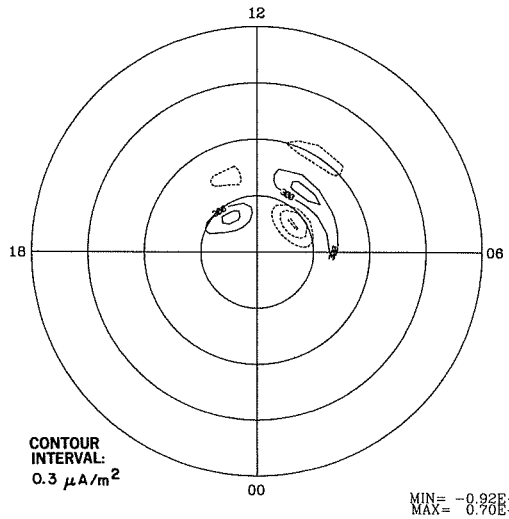

MIN= -0.92E-06 A/m²
MAX= 0.70E-06 A/m²

EQUIVALENT CURRENT VECTORS

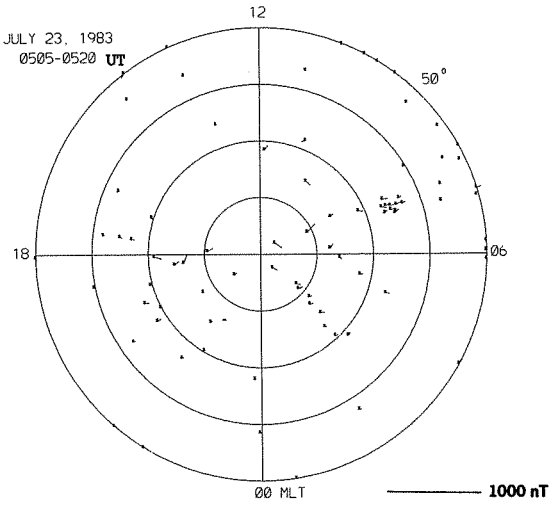

EQUIVALENT CURRENT SYSTEM

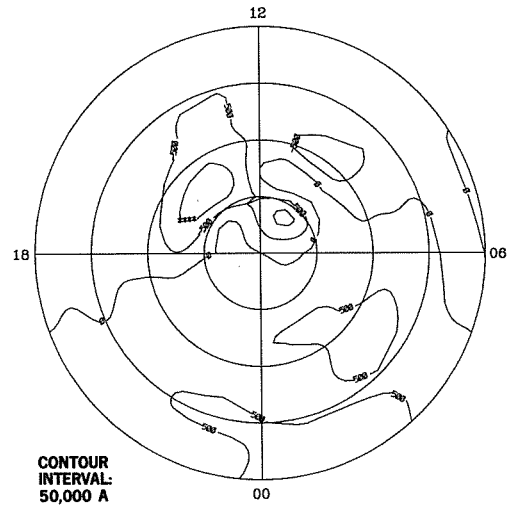

HALL CONDUCTANCE

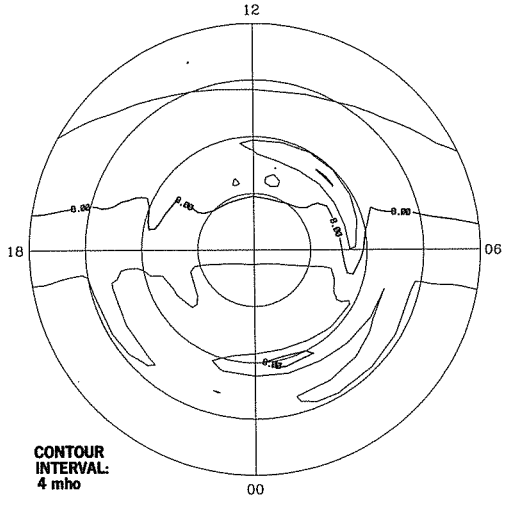

MAX= 0.16E+02 **mho**

PEDERSEN CONDUCTANCE

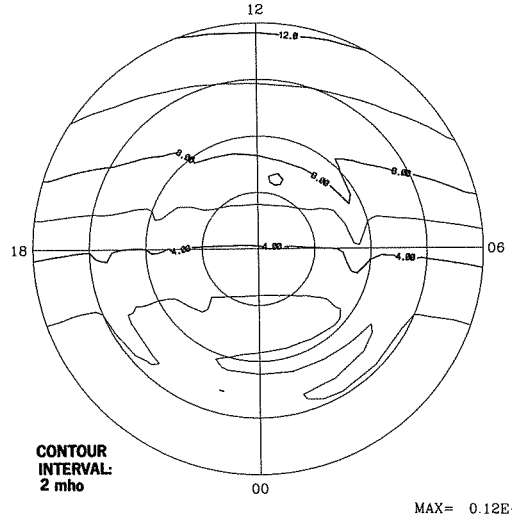

MAX= 0.12E+02 **mho**

ELECTRIC POTENTIAL

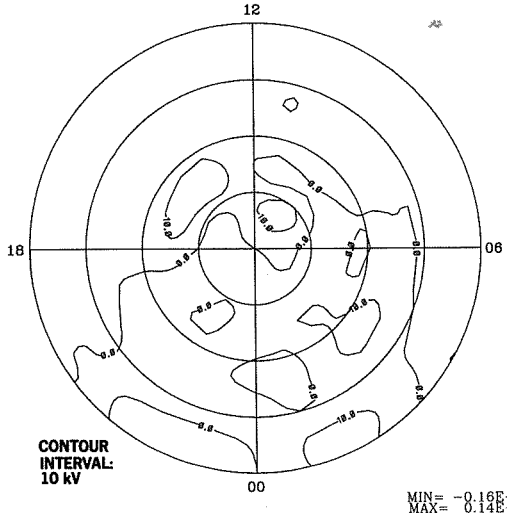

MIN= -0.16E+02 **kV**
MAX= 0.14E+02 **kV**

IONOSPHERIC CURRENT VECTORS

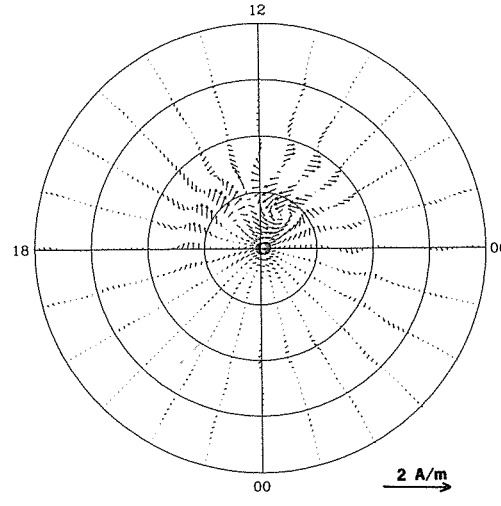

FIELD-ALIGNED CURRENT

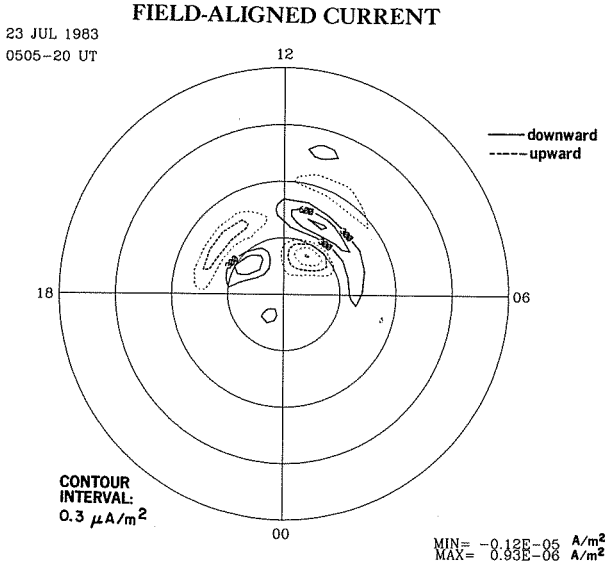

JOULE HEATING RATE

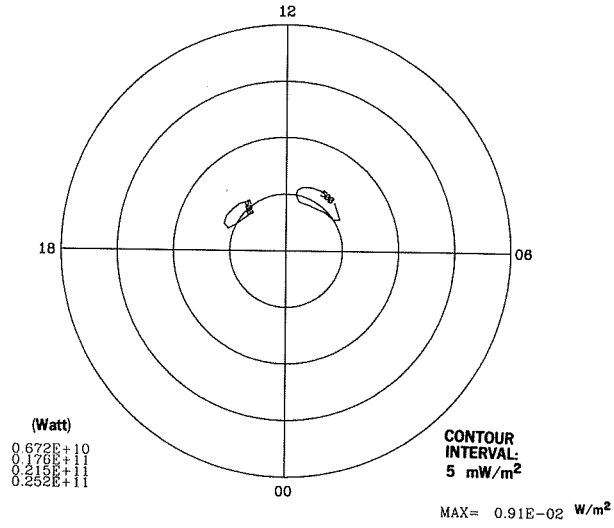

HALL CURRENT VECTORS

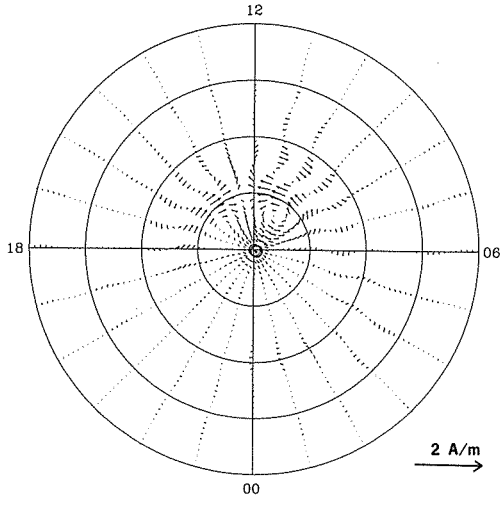

PEDERSEN CURRENT VECTORS

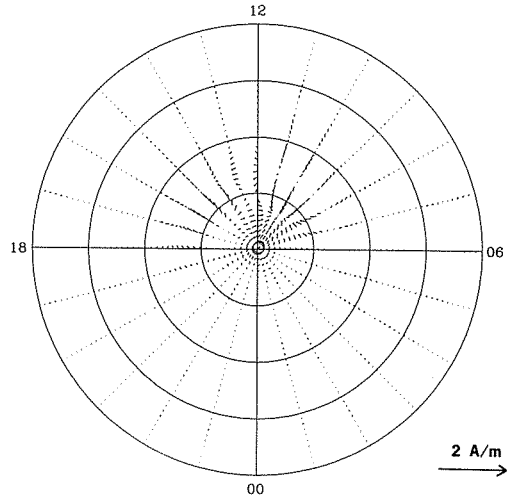

FIELD-ALIGNED HALL CURRENT

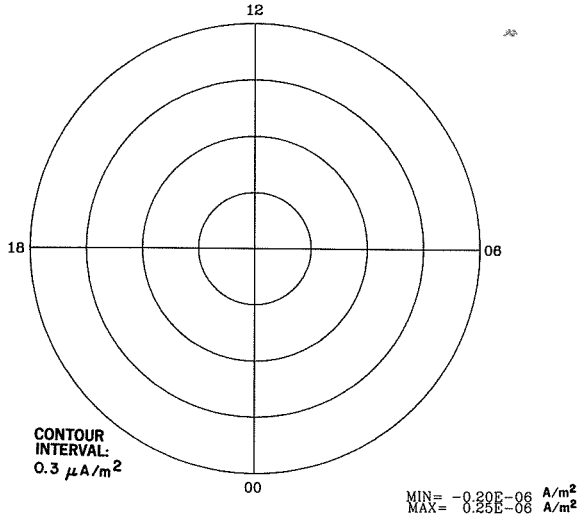

FIELD-ALIGNED PEDERSEN CURRENT

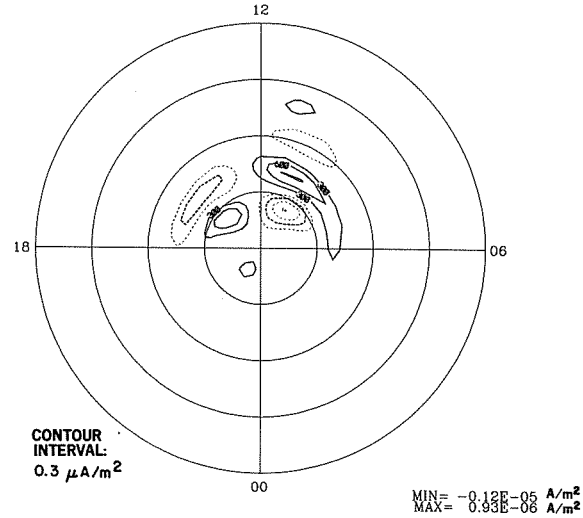

EQUIVALENT CURRENT VECTORS

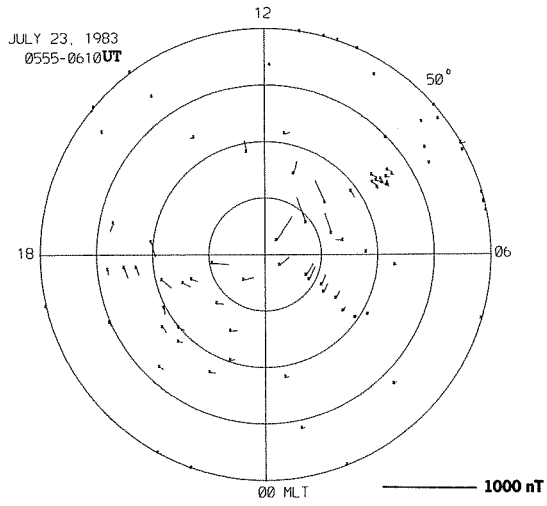

EQUIVALENT CURRENT SYSTEM

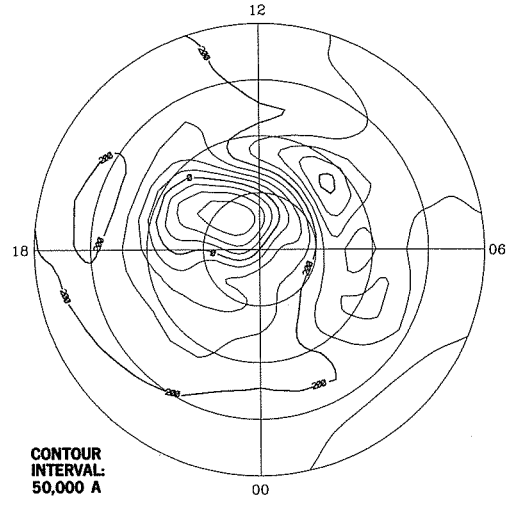

HALL CONDUCTANCE

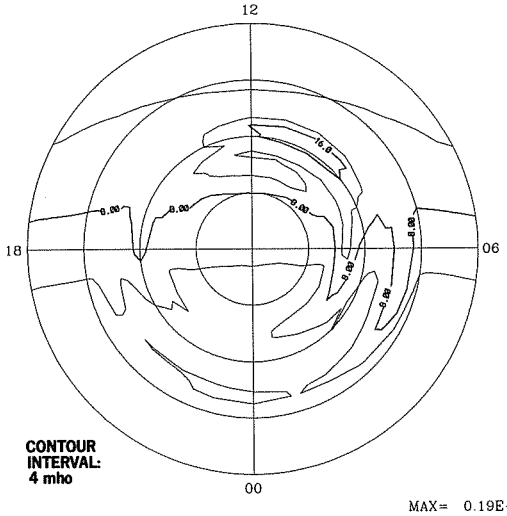

MAX= 0.19E+02 **mho**

PEDERSEN CONDUCTANCE

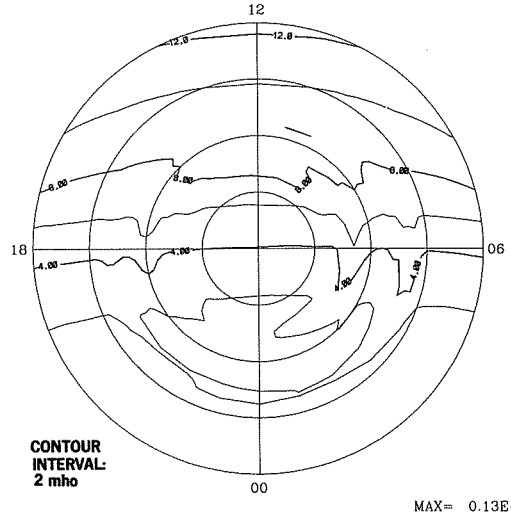

MAX= 0.13E+02 **mho**

ELECTRIC POTENTIAL

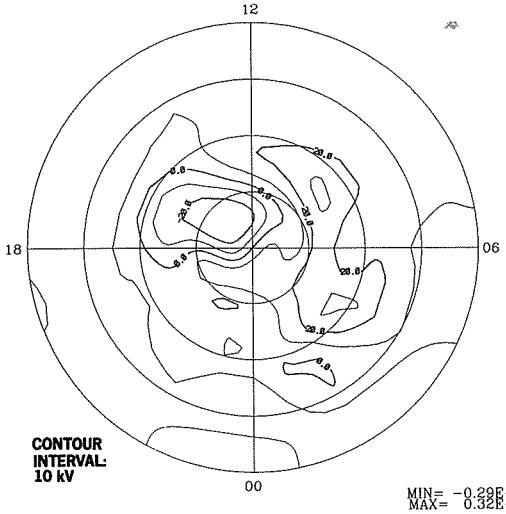

MIN= -0.29E+02 **kV**
MAX= 0.32E+02 **kV**

IONOSPHERIC CURRENT VECTORS

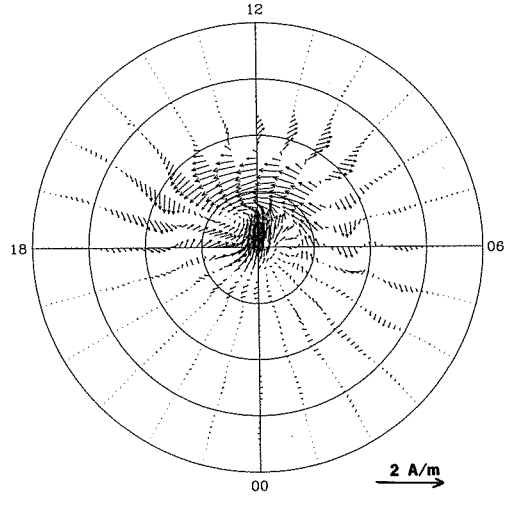

FIELD-ALIGNED CURRENT

23 JUL 1983
0555-0610 UT

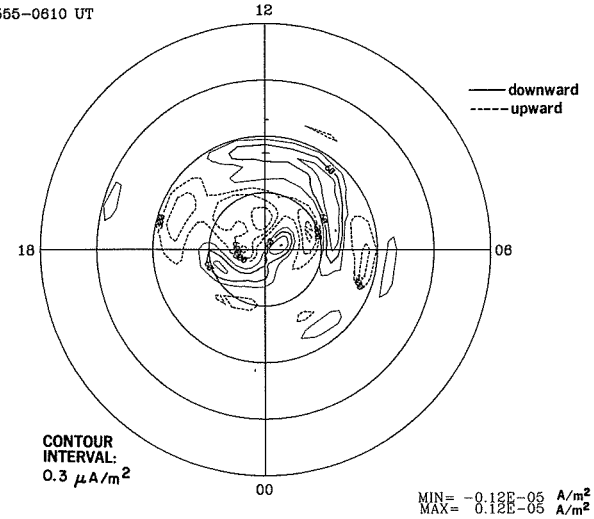

MIN= -0.12E-05 A/m²
MAX= 0.12E-05 A/m²

JOULE HEATING RATE

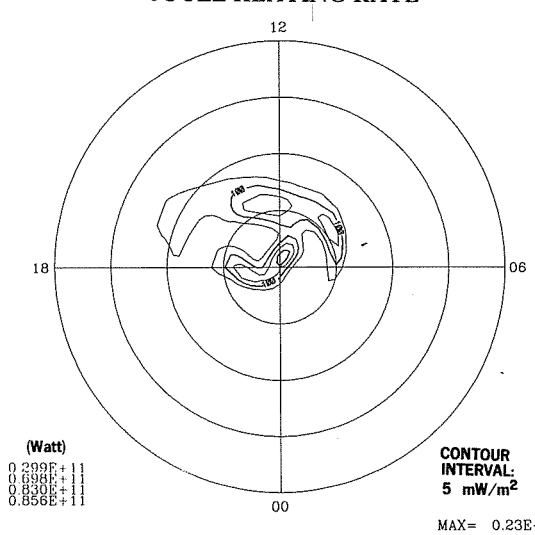

MAX= 0.23E-01 W/m²

HALL CURRENT VECTORS

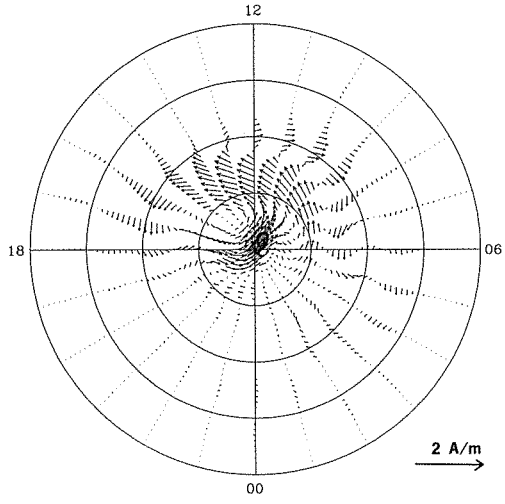

PEDERSEN CURRENT VECTORS

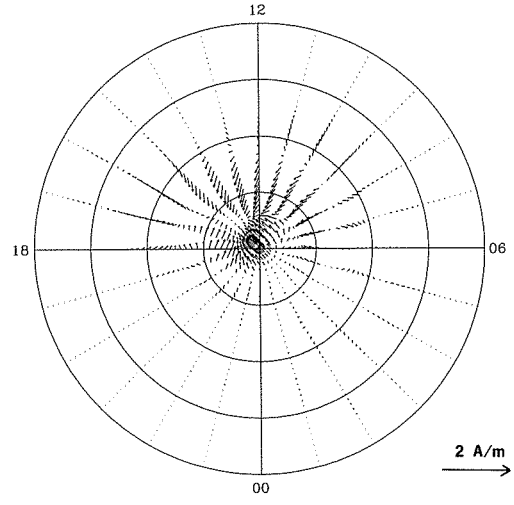

FIELD-ALIGNED HALL CURRENT

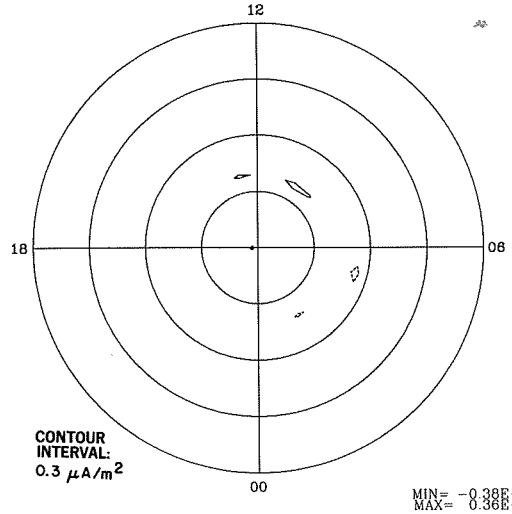

MIN= -0.38E-06 A/m²
MAX= 0.36E-06 A/m²

FIELD-ALIGNED PEDERSEN CURRENT

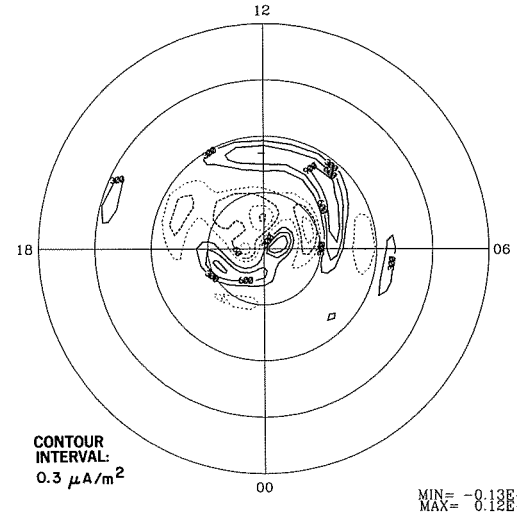

MIN= -0.13E-05 A/m²
MAX= 0.12E-05 A/m²

EQUIVALENT CURRENT VECTORS

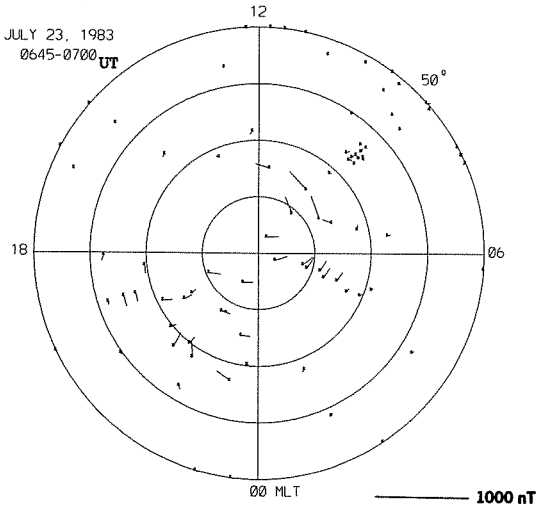

EQUIVALENT CURRENT SYSTEM

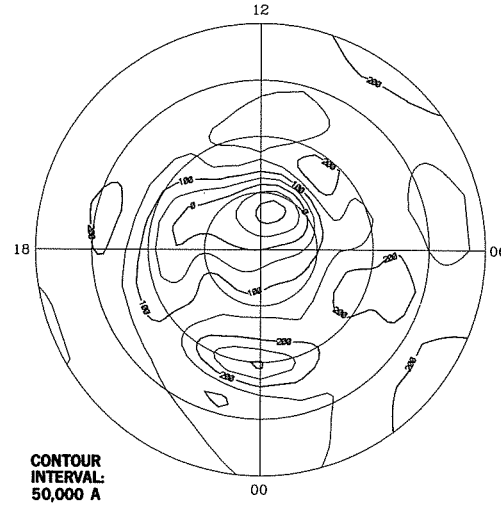

HALL CONDUCTANCE

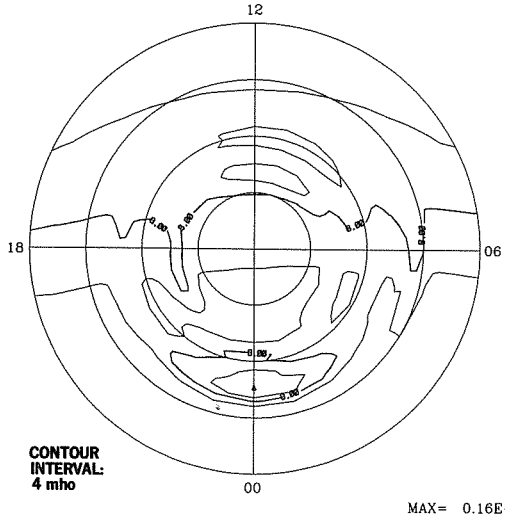

MAX= 0.16E+02 mho

PEDERSEN CONDUCTANCE

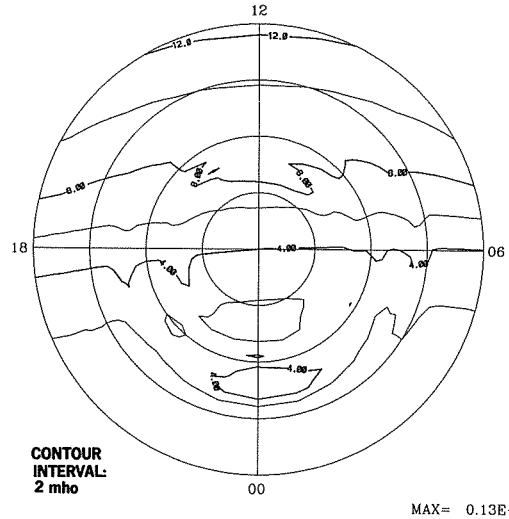

MAX= 0.13E+02 mho

ELECTRIC POTENTIAL

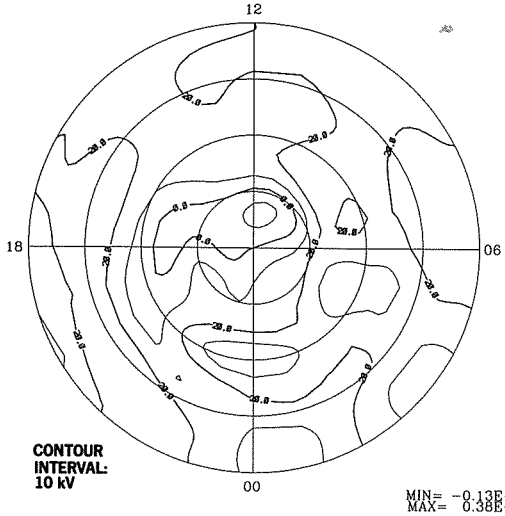

MIN= -0.13E+02 kV
MAX= 0.38E+02 kV

IONOSPHERIC CURRENT VECTORS

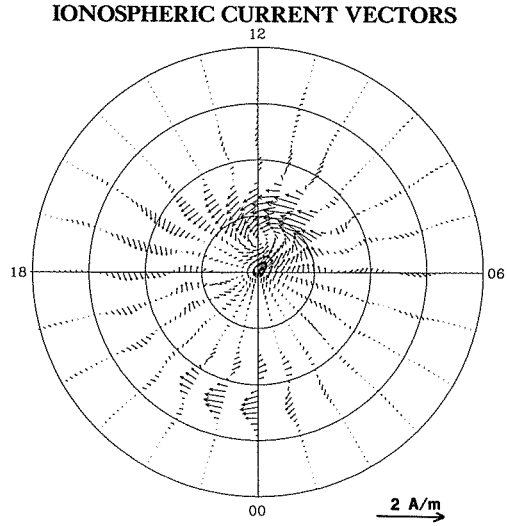

FIELD-ALIGNED CURRENT

23 JUL 1983
0645-0700 UT

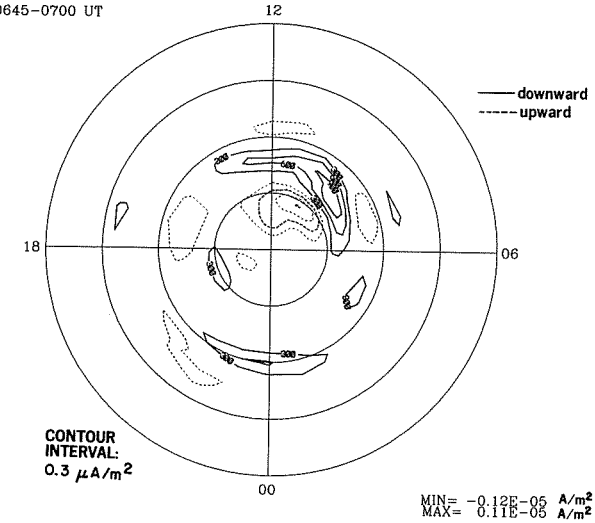

MIN= -0.12E-05 A/m2
MAX= 0.11E-05 A/m2

JOULE HEATING RATE

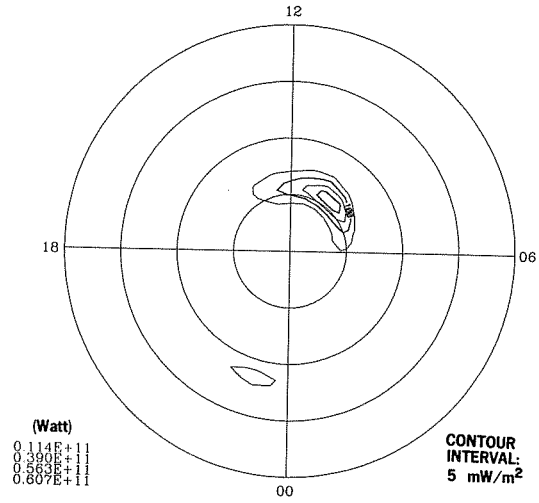

MAX= 0.23E-01 W/m2

HALL CURRENT VECTORS

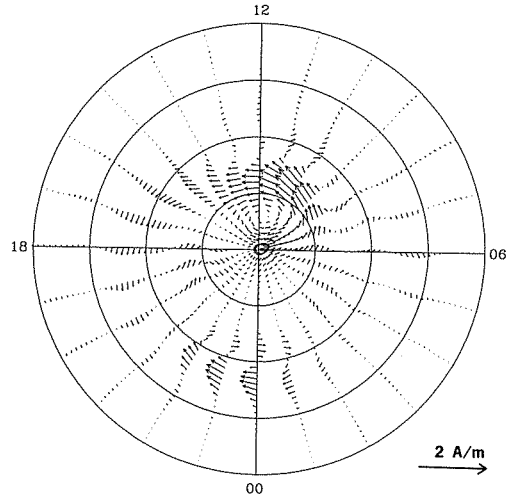

PEDERSEN CURRENT VECTORS

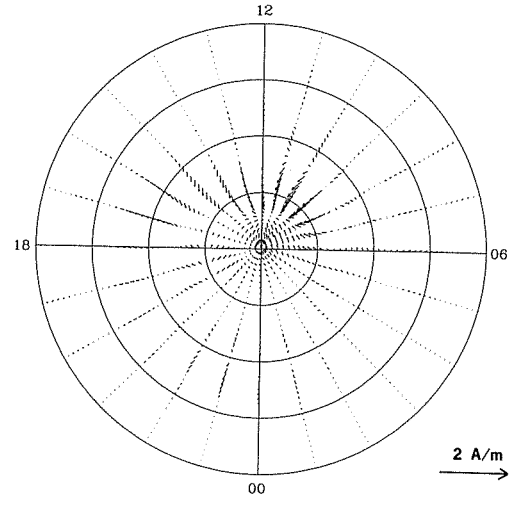

FIELD-ALIGNED HALL CURRENT

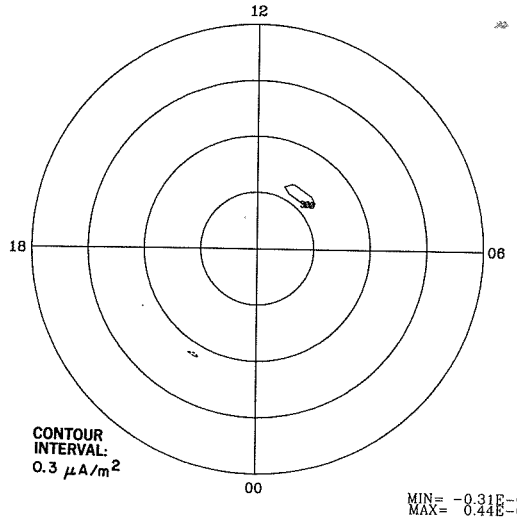

MIN= -0.31E-06 A/m2
MAX= 0.44E-06 A/m2

FIELD-ALIGNED PEDERSEN CURRENT

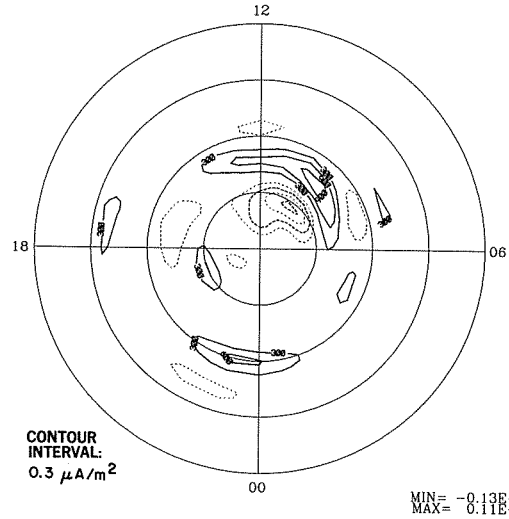

MIN= -0.13E-05 A/m2
MAX= 0.11E-05 A/m2

EQUIVALENT CURRENT VECTORS

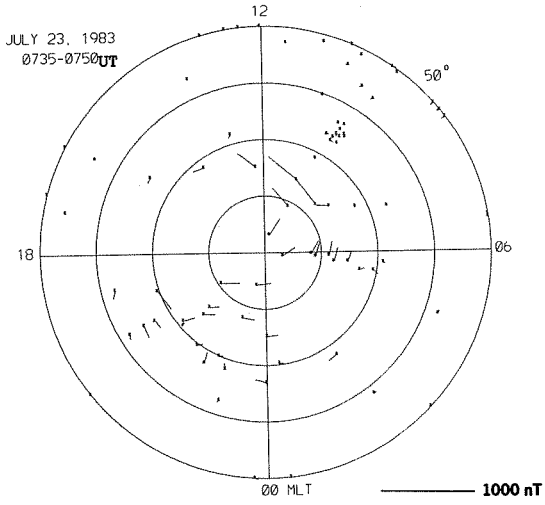

EQUIVALENT CURRENT SYSTEM

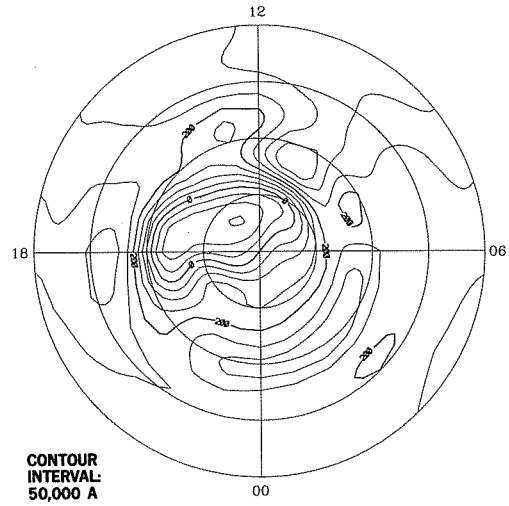

HALL CONDUCTANCE

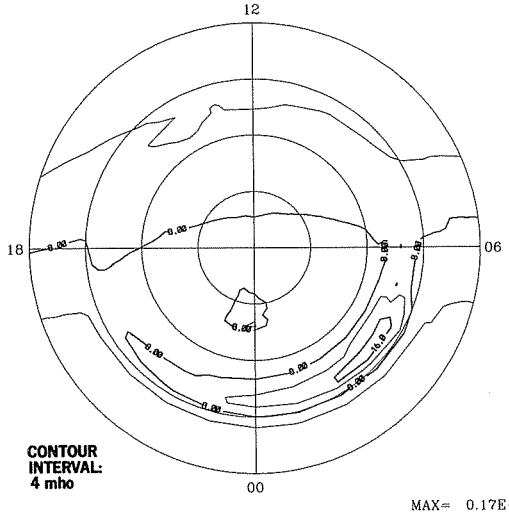

MAX= 0.17E+02 mho

DMSP

PEDERSEN CONDUCTANCE

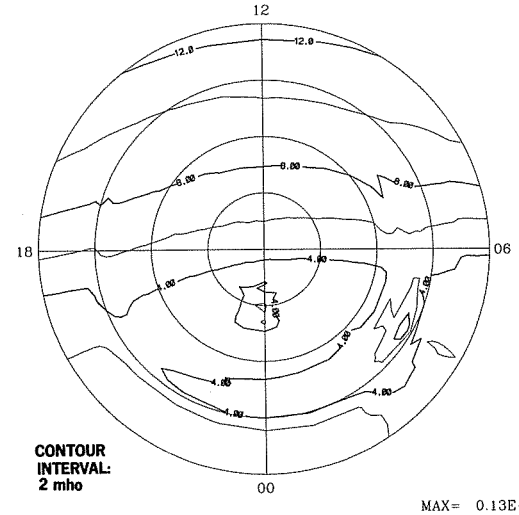

MAX= 0.13E+02 mho

ELECTRIC POTENTIAL

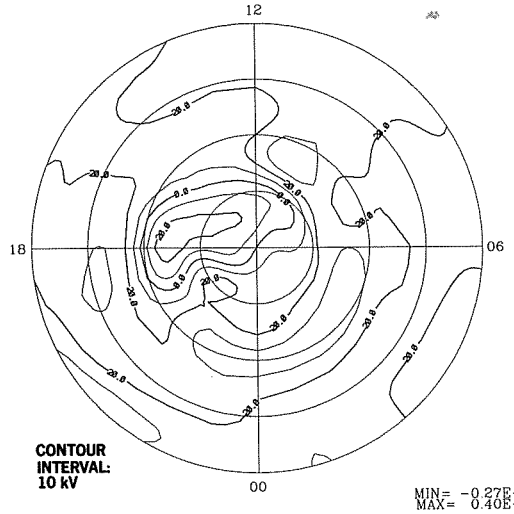

MIN= -0.27E+02 kV
MAX= 0.40E+02 kV

IONOSPHERIC CURRENT VECTORS

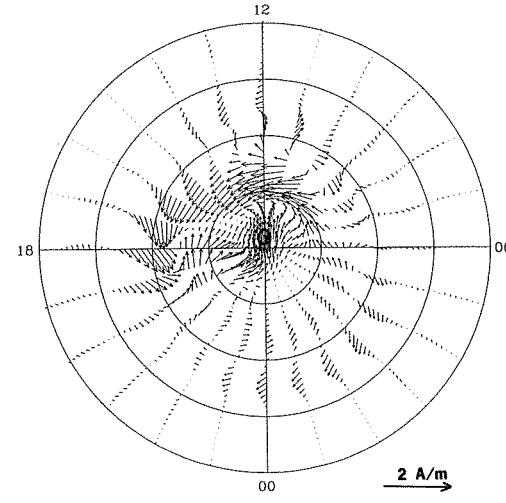

FIELD-ALIGNED CURRENT

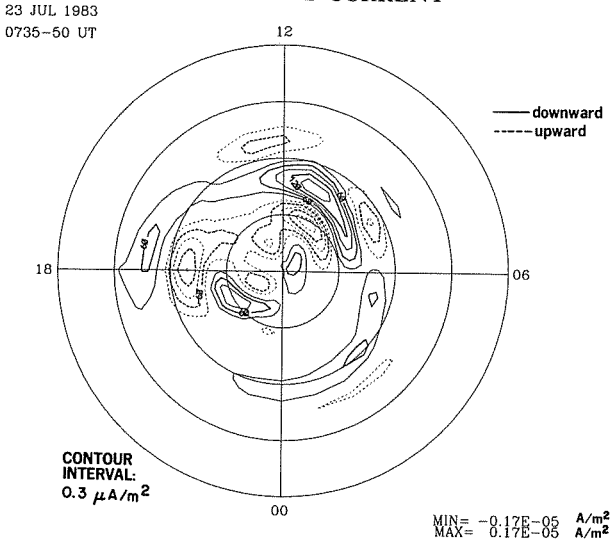

JOULE HEATING RATE

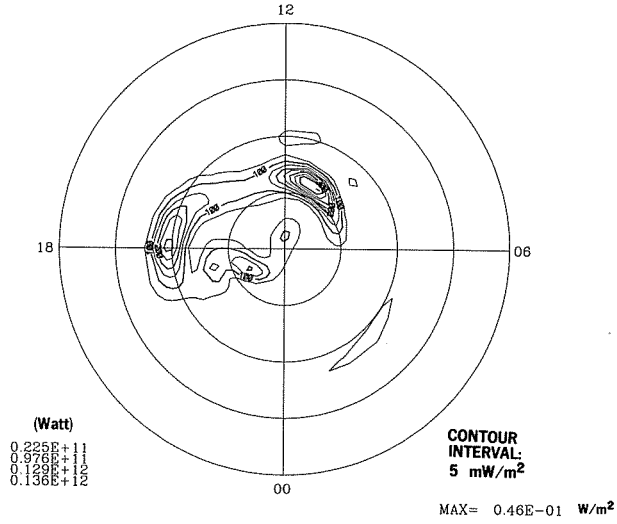

HALL CURRENT VECTORS

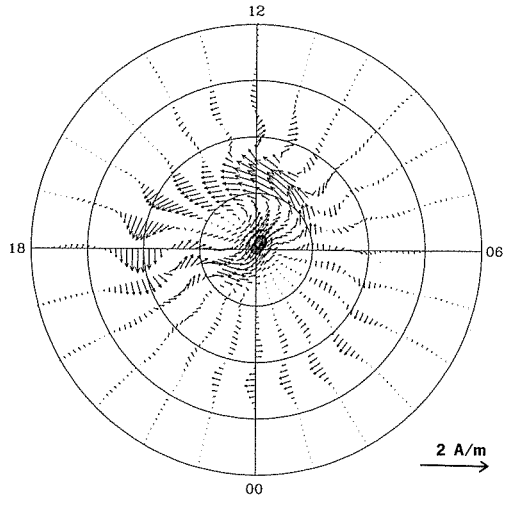

PEDERSEN CURRENT VECTORS

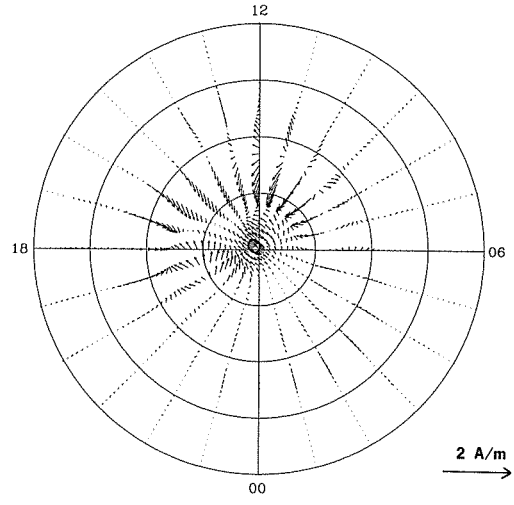

FIELD-ALIGNED HALL CURRENT

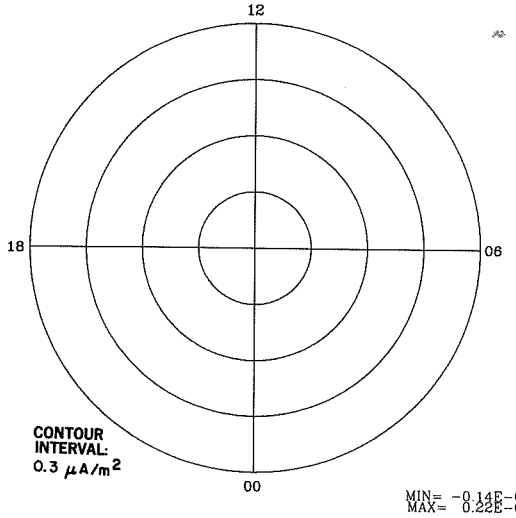

FIELD-ALIGNED PEDERSEN CURRENT

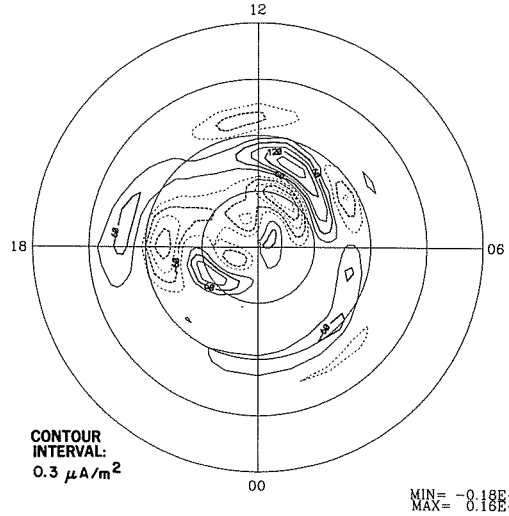

EQUIVALENT CURRENT VECTORS

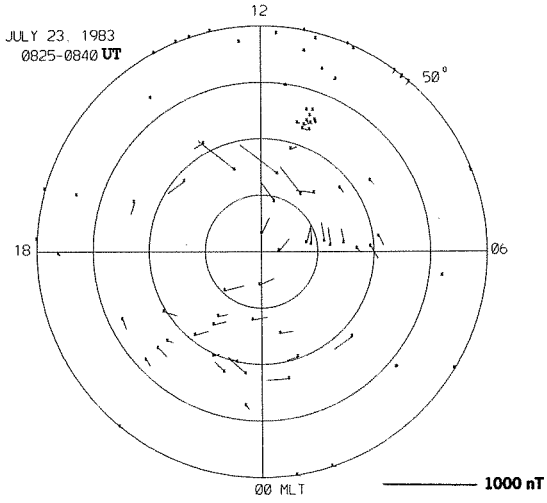

EQUIVALENT CURRENT SYSTEM

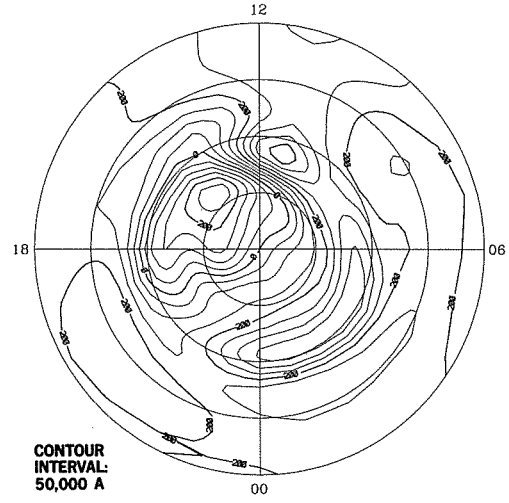

HALL CONDUCTANCE

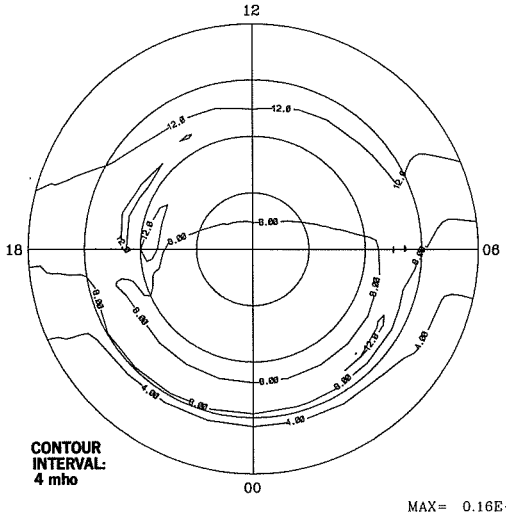

MAX= 0.16E+02 **mho**

DMSP

PEDERSEN CONDUCTANCE

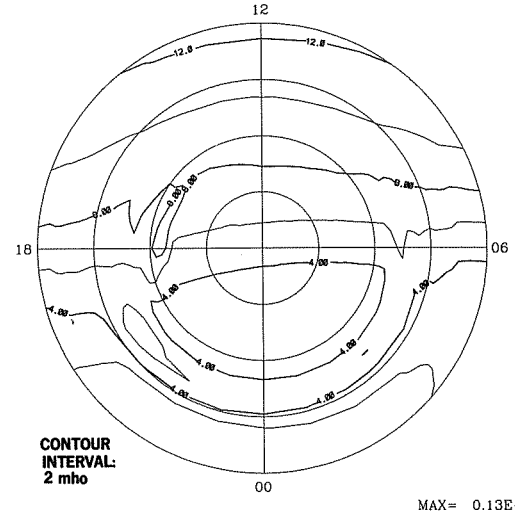

MAX= 0.13E+02 **mho**

ELECTRIC POTENTIAL

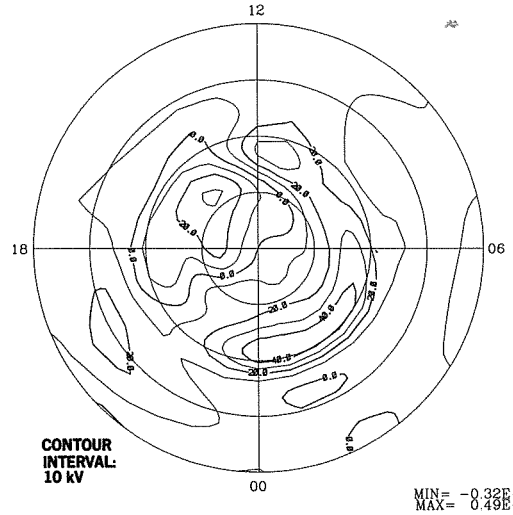

MIN= -0.32E+02 **kV**
MAX= 0.49E+02 **kV**

IONOSPHERIC CURRENT VECTORS

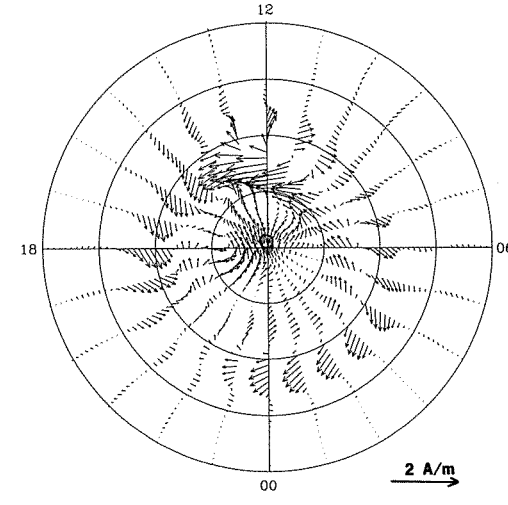

FIELD-ALIGNED CURRENT

23 JUL 1983
0825-40 UT

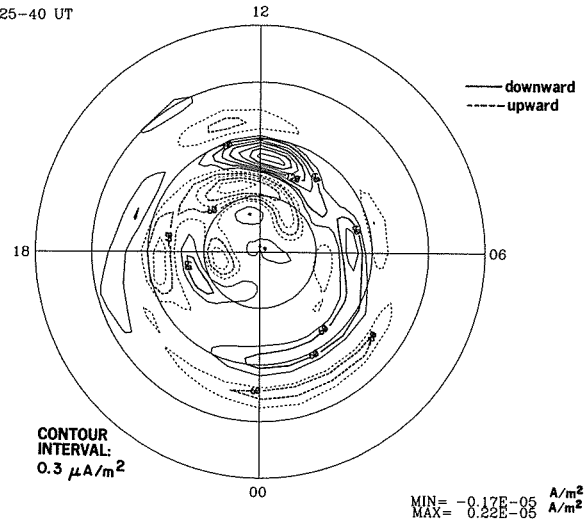

MIN= -0.17E-05 A/m²
MAX= 0.22E-05 A/m²

JOULE HEATING RATE

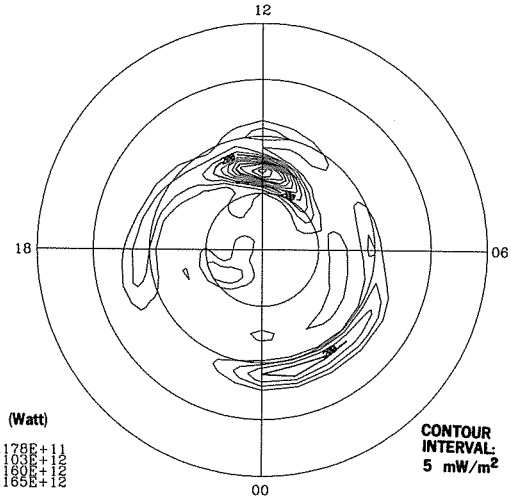

MAX= 0.59E-01 W/m²

HALL CURRENT VECTORS

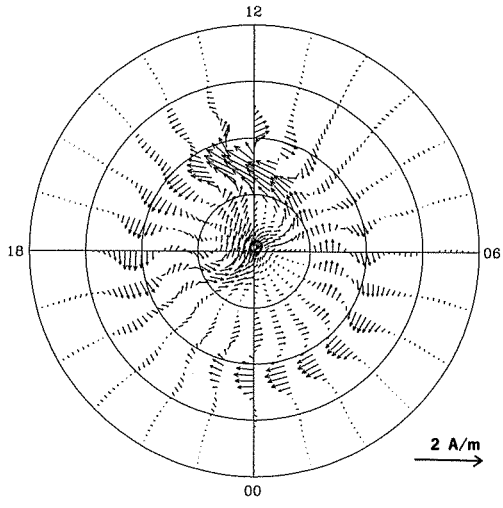

PEDERSEN CURRENT VECTORS

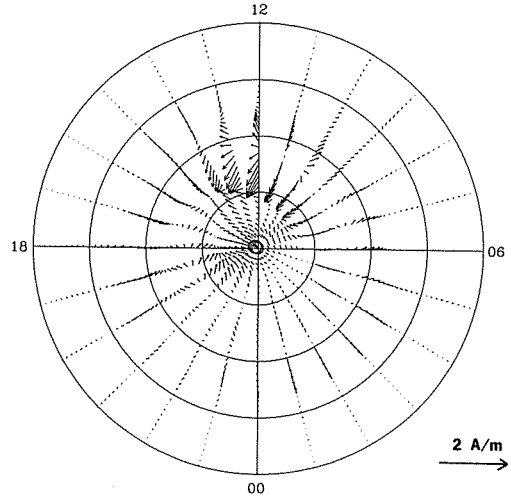

FIELD-ALIGNED HALL CURRENT

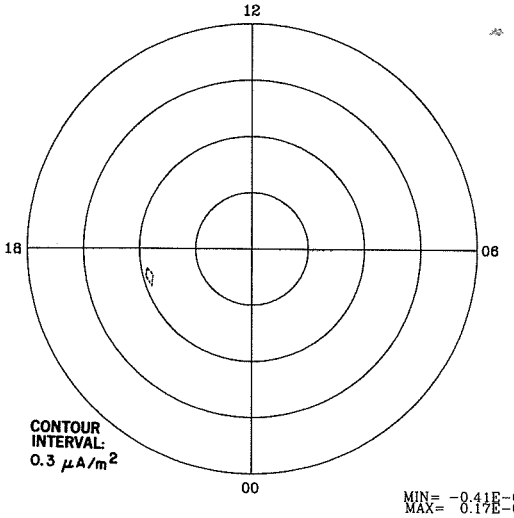

MIN= -0.41E-06 A/m²
MAX= 0.17E-06 A/m²

FIELD-ALIGNED PEDERSEN CURRENT

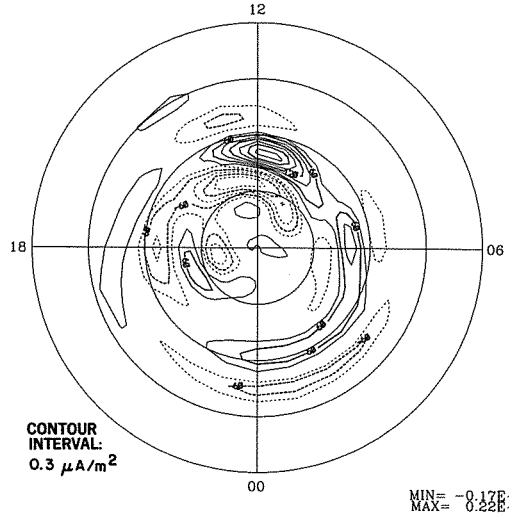

MIN= -0.17E-05 A/m²
MAX= 0.22E-05 A/m²

EQUIVALENT CURRENT VECTORS

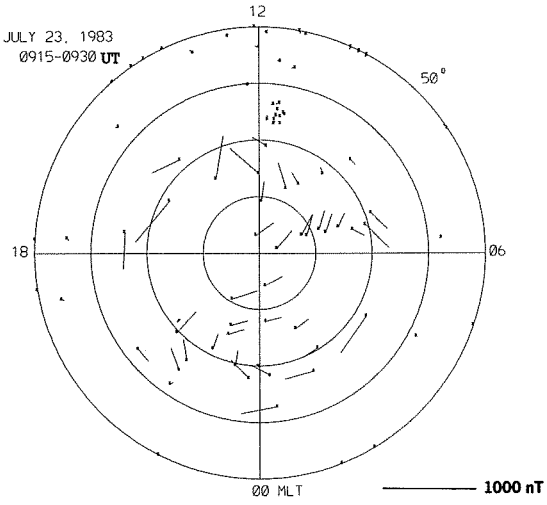

EQUIVALENT CURRENT SYSTEM

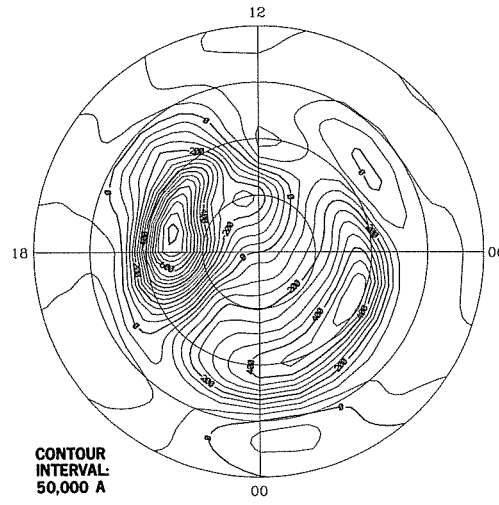

HALL CONDUCTANCE

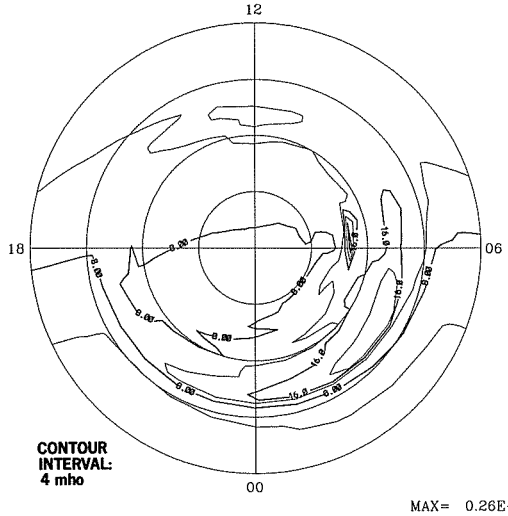

MAX= 0.26E+02 **mho**

DMSP

PEDERSEN CONDUCTANCE

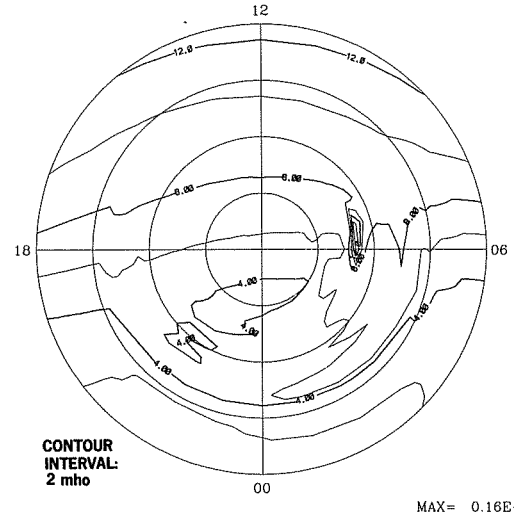

MAX= 0.16E+02 **mho**

ELECTRIC POTENTIAL

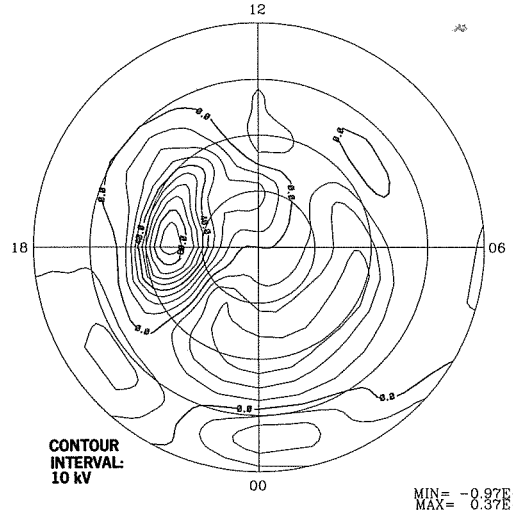

MIN= -0.97E+02 **kV**
MAX= 0.37E+02 **kV**

IONOSPHERIC CURRENT VECTORS

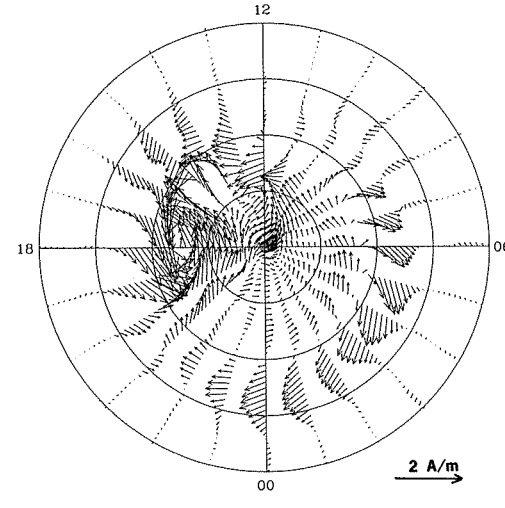

FIELD-ALIGNED CURRENT

23 JUL 1983
0915-30 UT

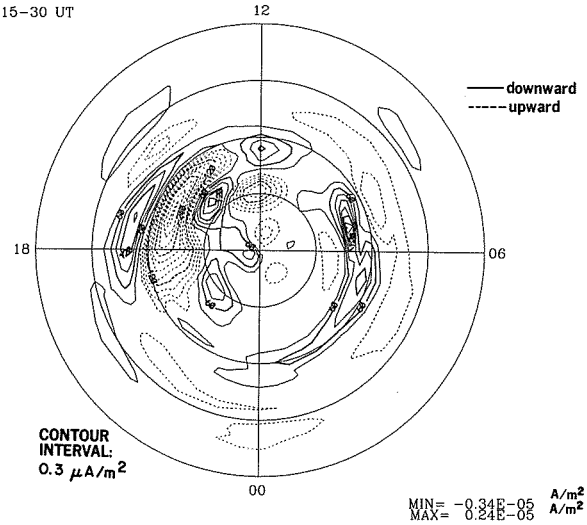

MIN= −0.34E-05 A/m²
MAX= 0.24E-05 A/m²

JOULE HEATING RATE

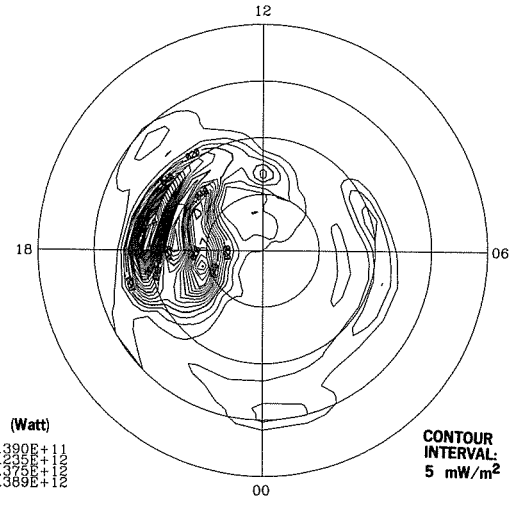

MAX= 0.13E+00 W/m²

HALL CURRENT VECTORS

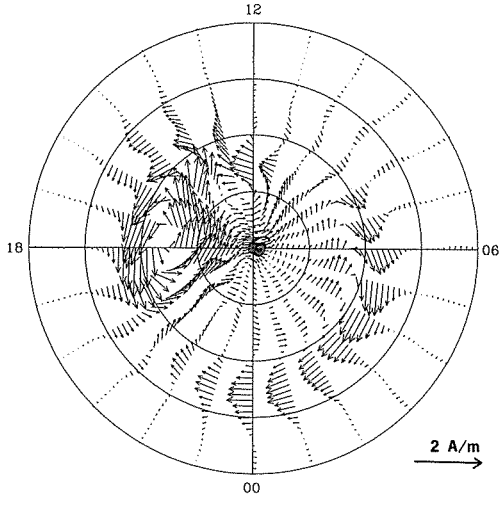

PEDERSEN CURRENT VECTORS

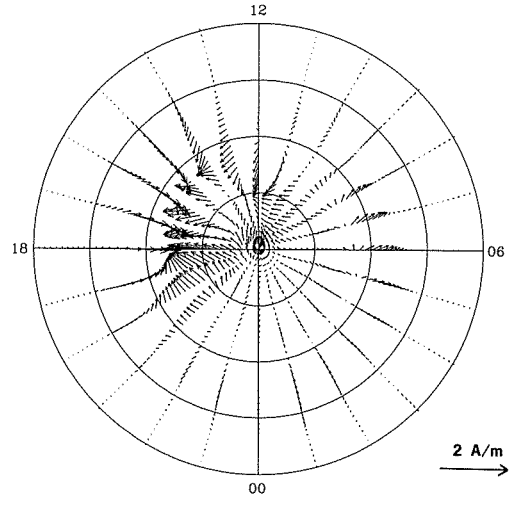

FIELD-ALIGNED HALL CURRENT

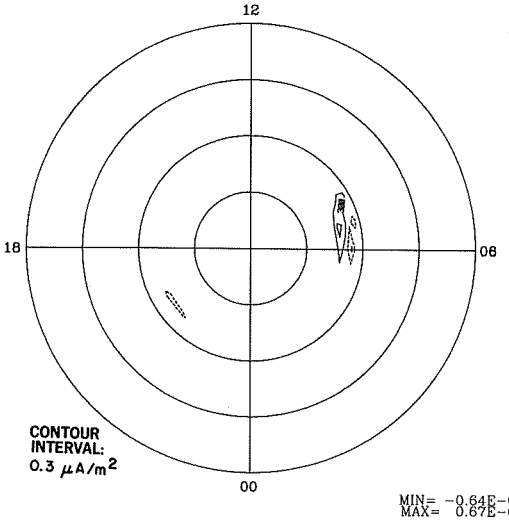

MIN= −0.64E-06 A/m²
MAX= 0.67E-06 A/m²

FIELD-ALIGNED PEDERSEN CURRENT

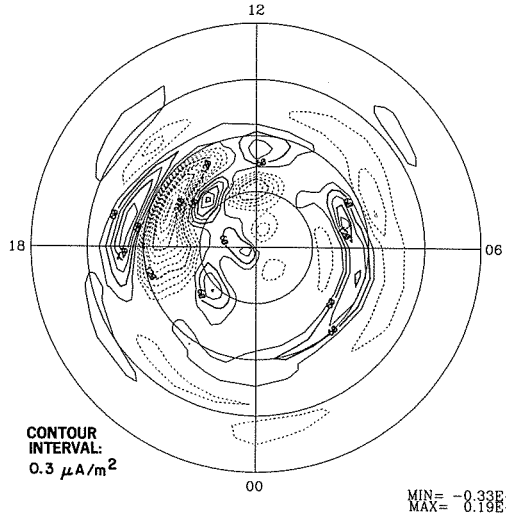

MIN= −0.33E-05 A/m²
MAX= 0.19E-05 A/m²

EQUIVALENT CURRENT VECTORS

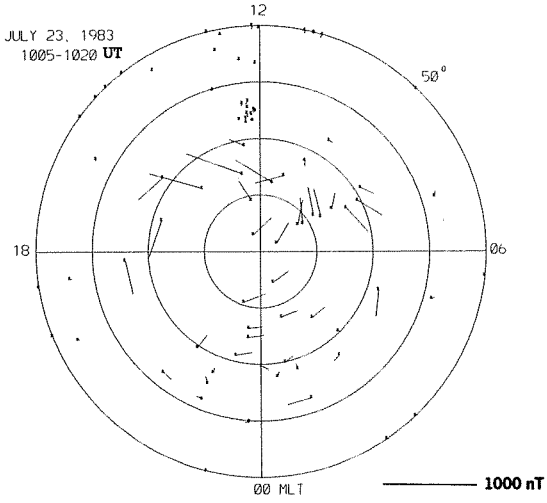

EQUIVALENT CURRENT SYSTEM

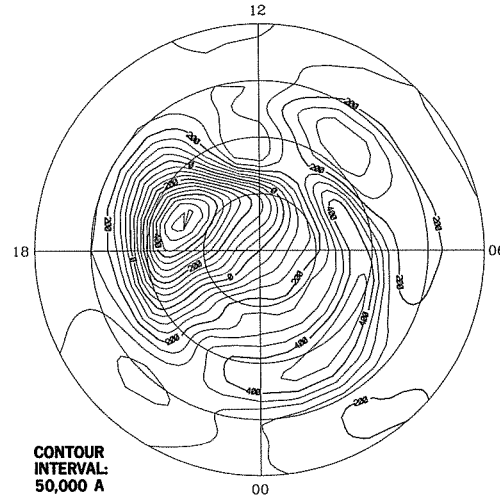

HALL CONDUCTANCE

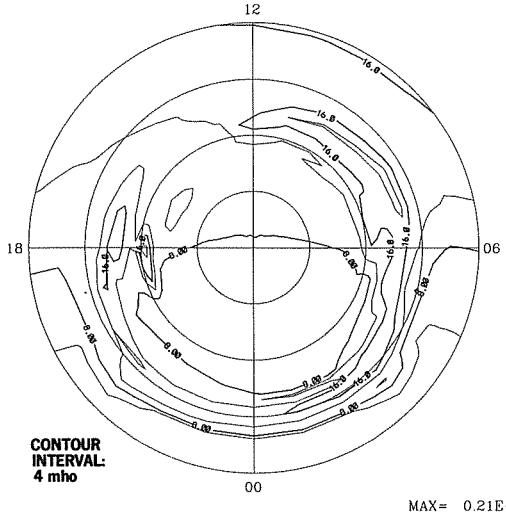

MAX= 0.21E+02 **mho**

DMSP

PEDERSEN CONDUCTANCE

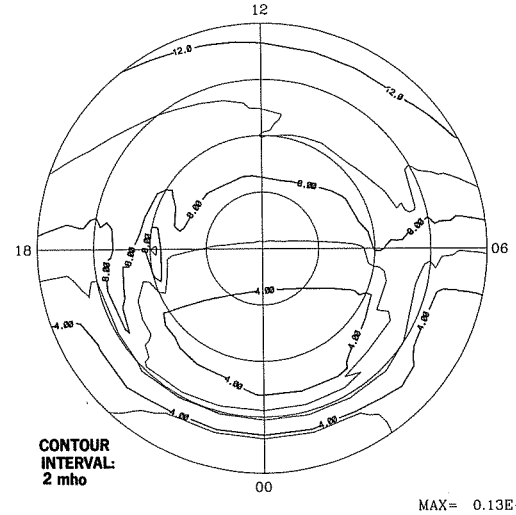

MAX= 0.13E+02 **mho**

ELECTRIC POTENTIAL

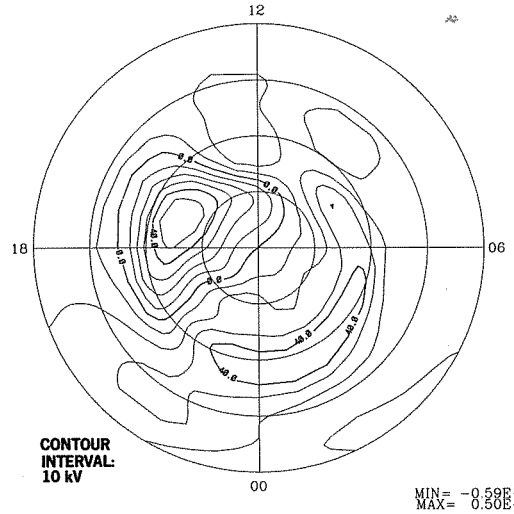

MIN= -0.59E+02 **kV**
MAX= 0.50E+02 **kV**

IONOSPHERIC CURRENT VECTORS

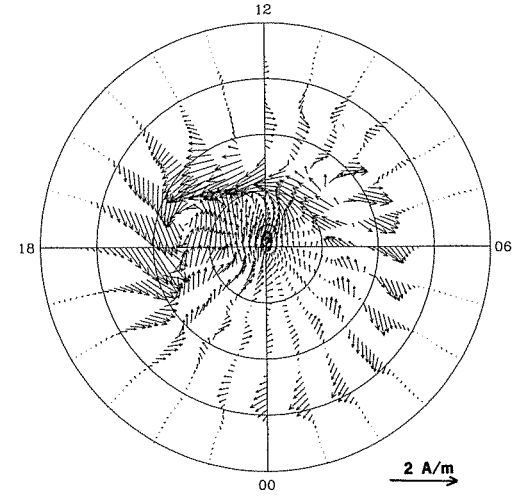

FIELD-ALIGNED CURRENT

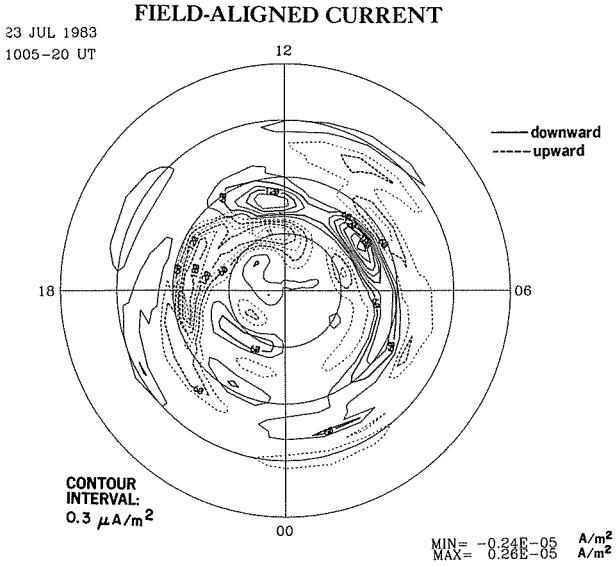

JOULE HEATING RATE

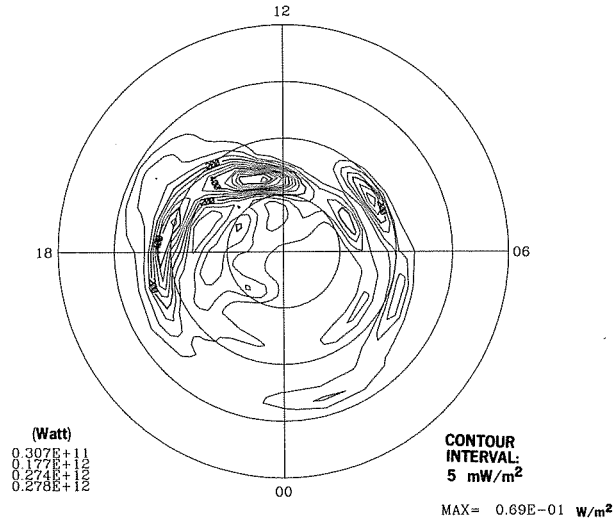

HALL CURRENT VECTORS

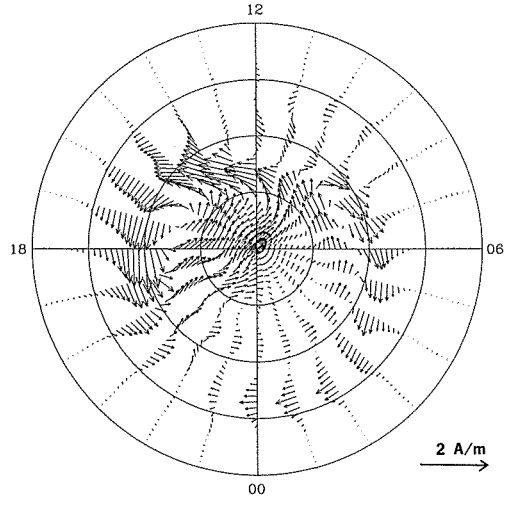

PEDERSEN CURRENT VECTORS

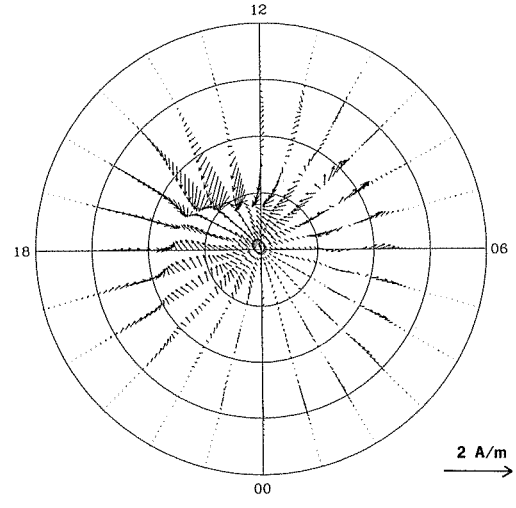

FIELD-ALIGNED HALL CURRENT

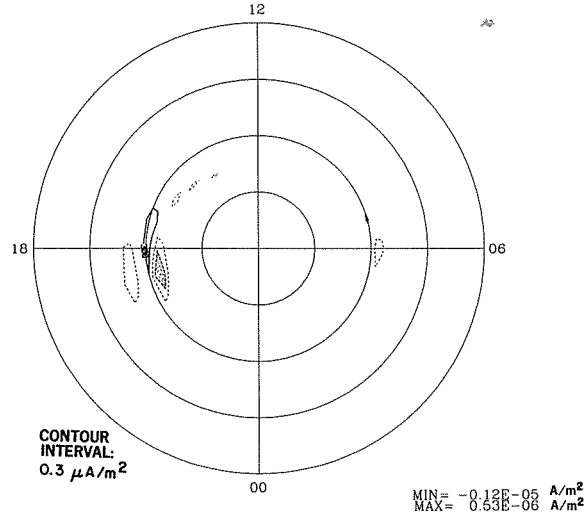

FIELD-ALIGNED PEDERSEN CURRENT

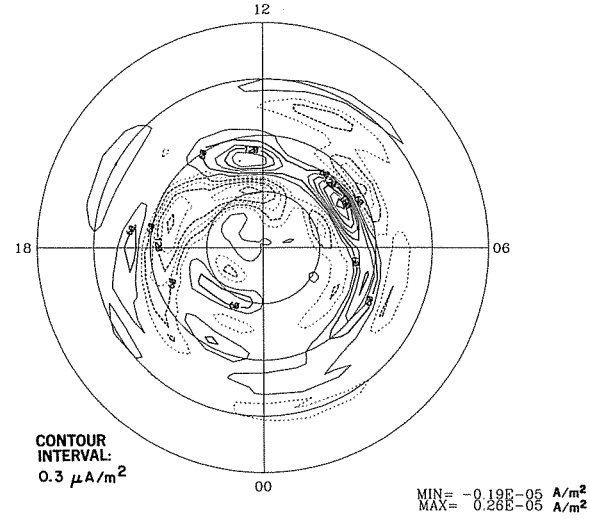

EQUIVALENT CURRENT VECTORS

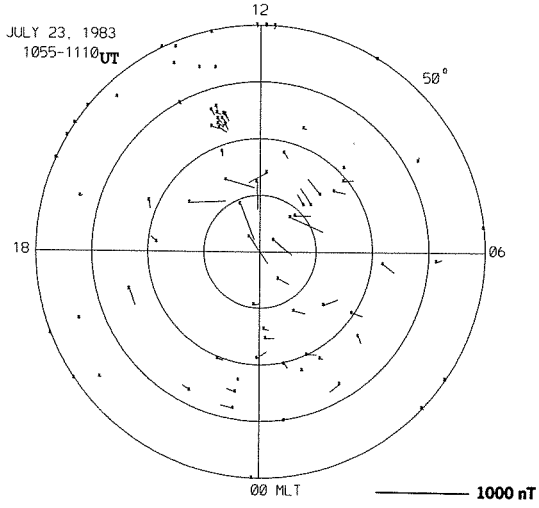

EQUIVALENT CURRENT SYSTEM

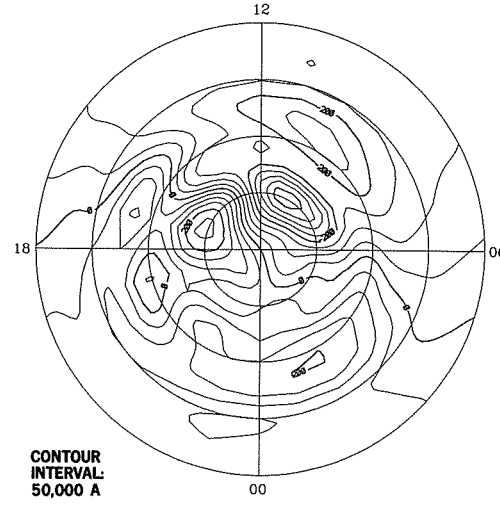

HALL CONDUCTANCE

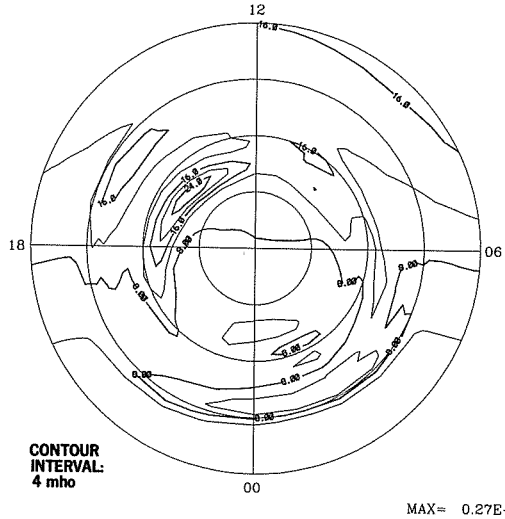

MAX= 0.27E+02 mho

PEDERSEN CONDUCTANCE

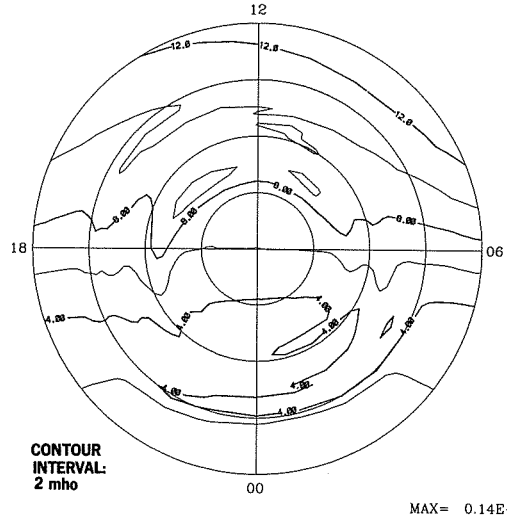

MAX= 0.14E+02 mho

ELECTRIC POTENTIAL

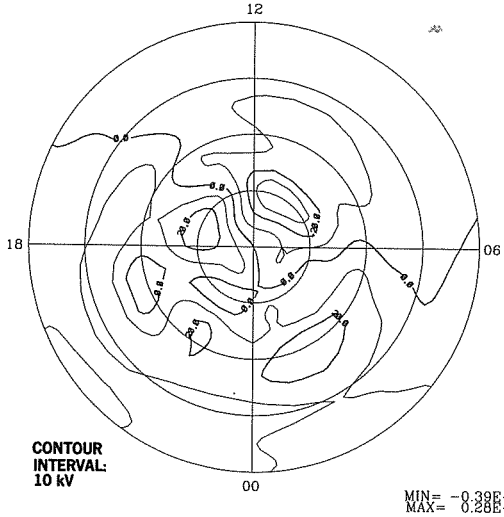

MIN= -0.39E+02 kV
MAX= 0.28E+02 kV

IONOSPHERIC CURRENT VECTORS

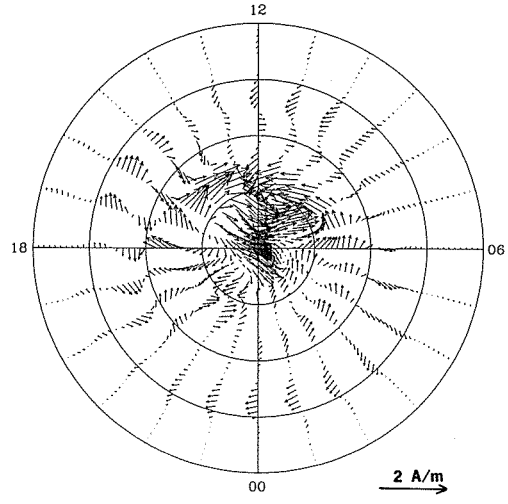

FIELD-ALIGNED CURRENT

23 JUL 1983
1055–1110 UT

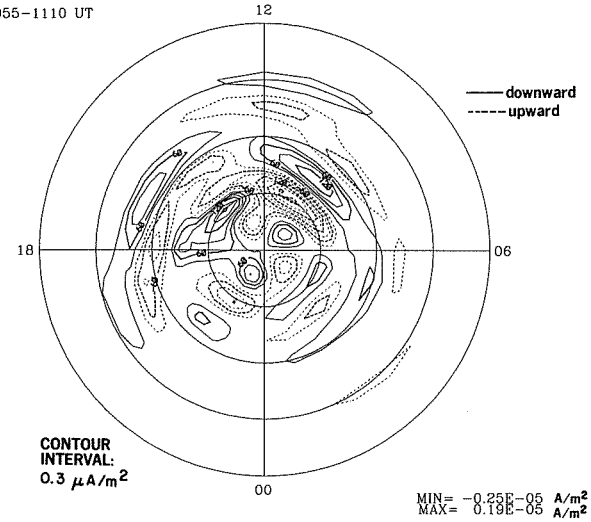

MIN= −0.25E−05 A/m²
MAX= 0.19E−05 A/m²

JOULE HEATING RATE

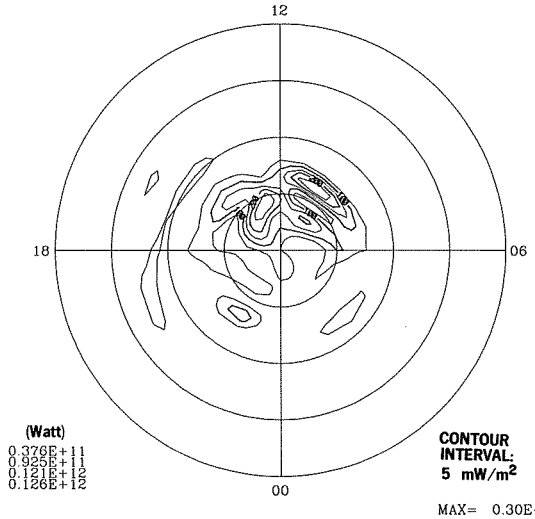

MAX= 0.30E−01 W/m²

HALL CURRENT VECTORS

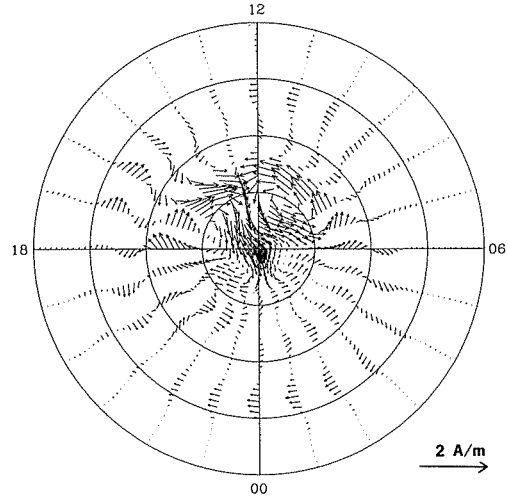

PEDERSEN CURRENT VECTORS

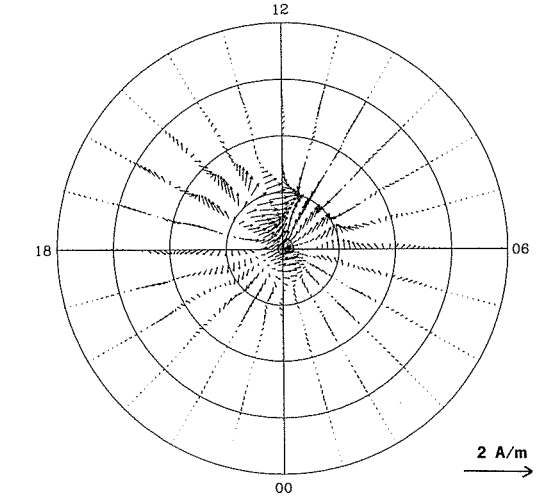

FIELD-ALIGNED HALL CURRENT

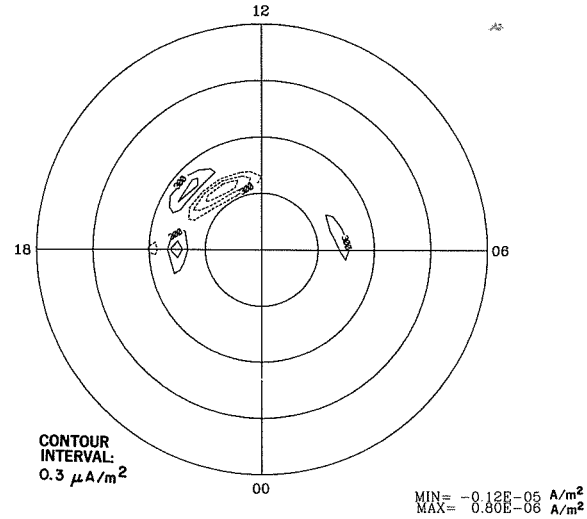

MIN= −0.12E−05 A/m²
MAX= 0.80E−06 A/m²

FIELD-ALIGNED PEDERSEN CURRENT

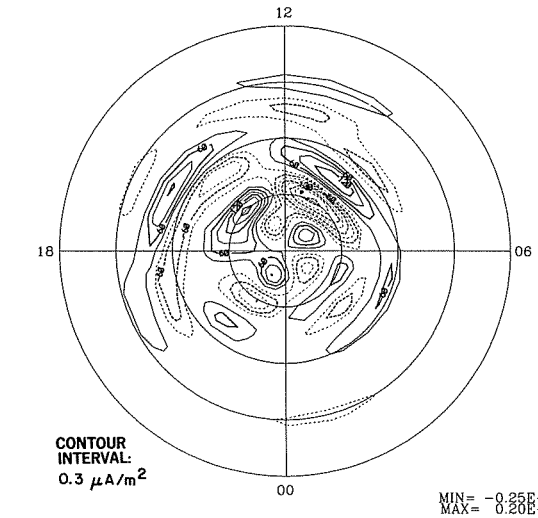

MIN= −0.25E−05 A/m²
MAX= 0.20E−05 A/m²

EQUIVALENT CURRENT VECTORS

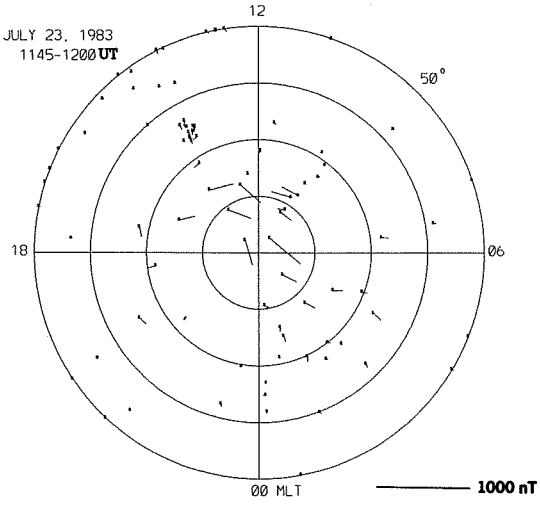

EQUIVALENT CURRENT SYSTEM

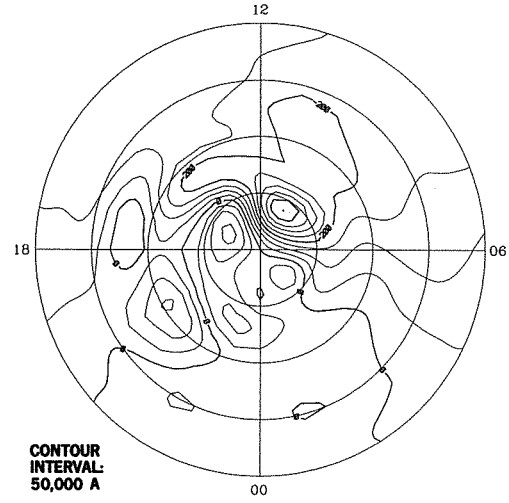

HALL CONDUCTANCE

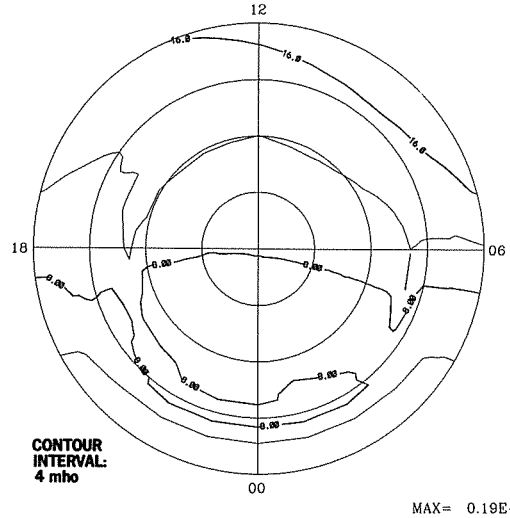

MAX= 0.19E+02 **mho**

DMSP

PEDERSEN CONDUCTANCE

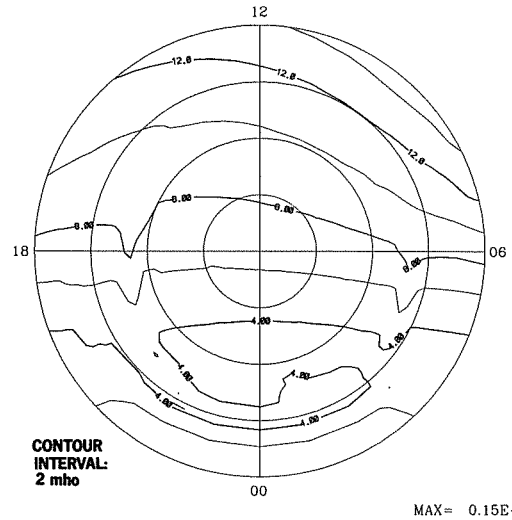

MAX= 0.15E+02 **mho**

ELECTRIC POTENTIAL

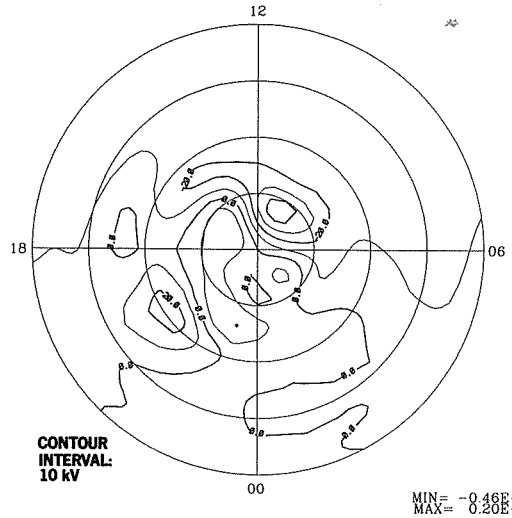

MIN= -0.46E+02 **kV**
MAX= 0.20E+02 **kV**

IONOSPHERIC CURRENT VECTORS

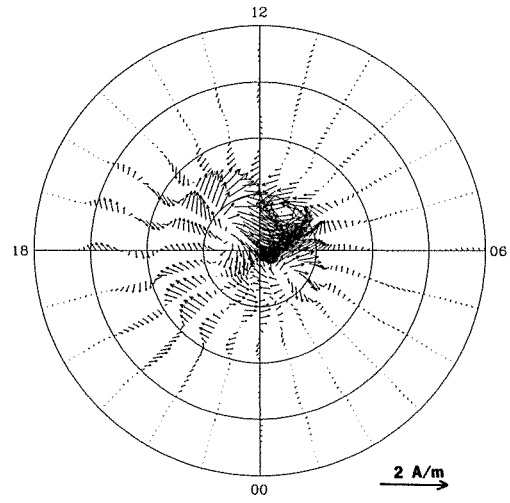

FIELD-ALIGNED CURRENT

23 JUL 1983
1145-1200 UT

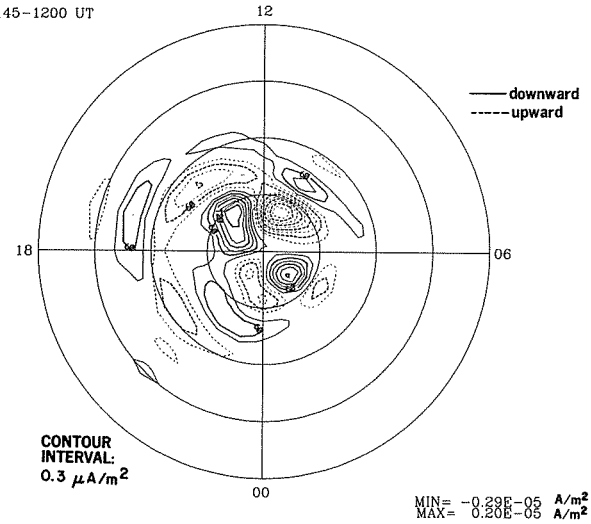

MIN= -0.29E-05 A/m²
MAX= 0.20E-05 A/m²

JOULE HEATING RATE

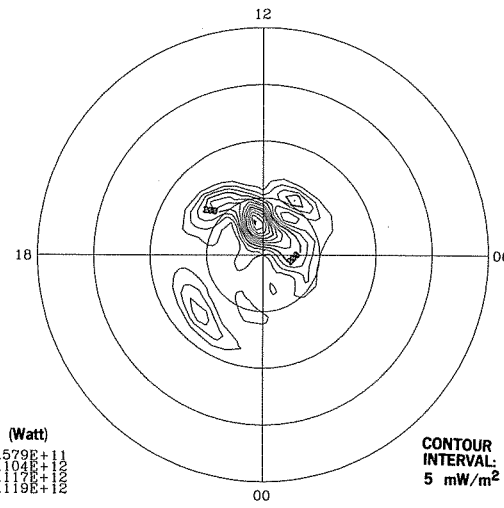

MAX= 0.61E-01 W/m²

HALL CURRENT VECTORS

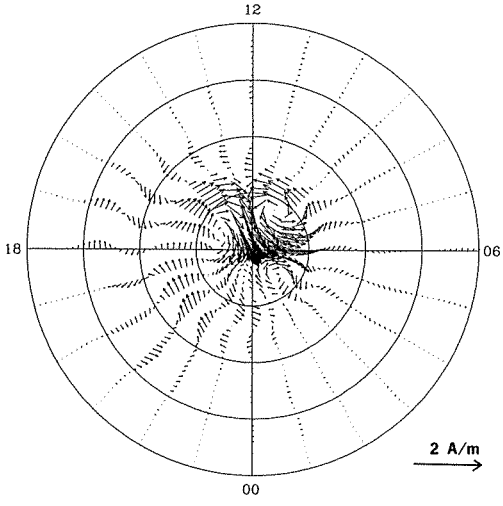

PEDERSEN CURRENT VECTORS

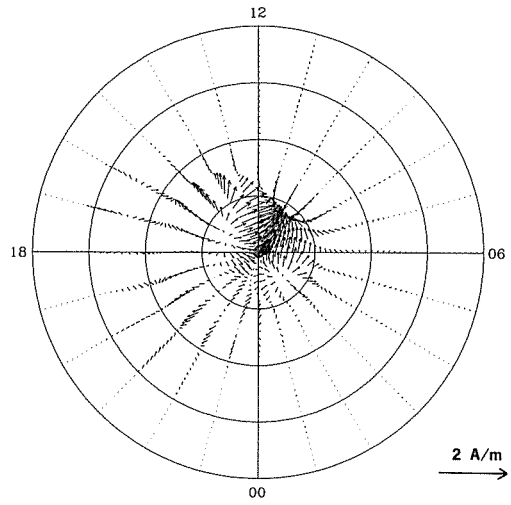

FIELD-ALIGNED HALL CURRENT

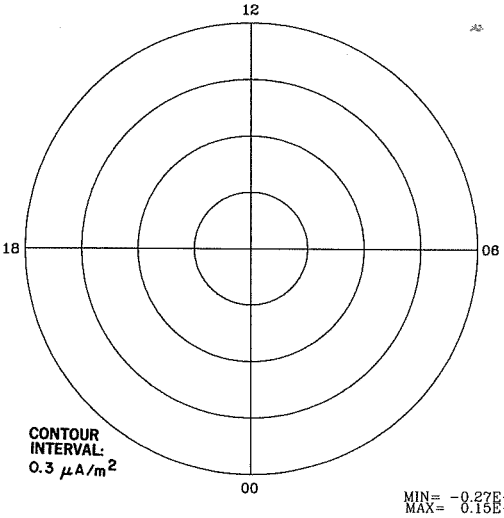

MIN= -0.27E-06 A/m²
MAX= 0.15E-06 A/m²

FIELD-ALIGNED PEDERSEN CURRENT

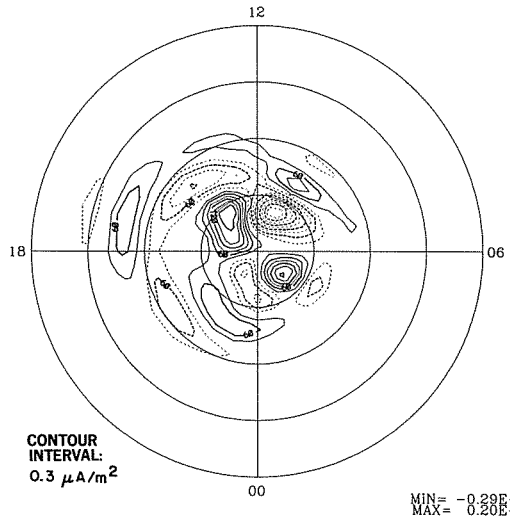

MIN= -0.29E-05 A/m²
MAX= 0.20E-05 A/m²

EQUIVALENT CURRENT VECTORS

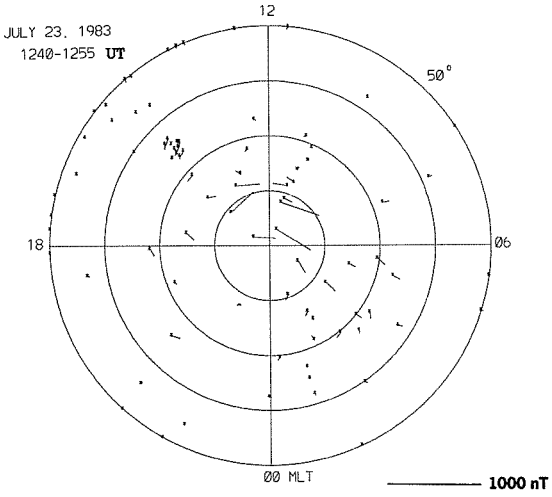

EQUIVALENT CURRENT SYSTEM

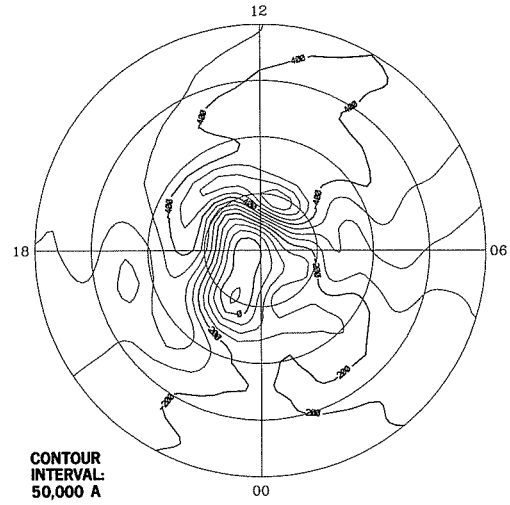

HALL CONDUCTANCE

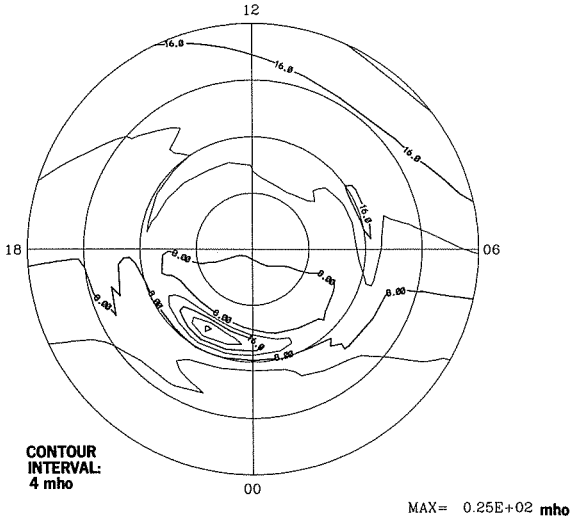

MAX= 0.25E+02 **mho**

PEDERSEN CONDUCTANCE

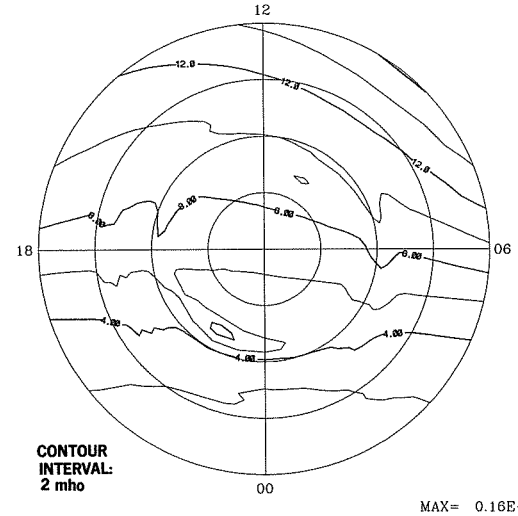

MAX= 0.16E+02 **mho**

ELECTRIC POTENTIAL

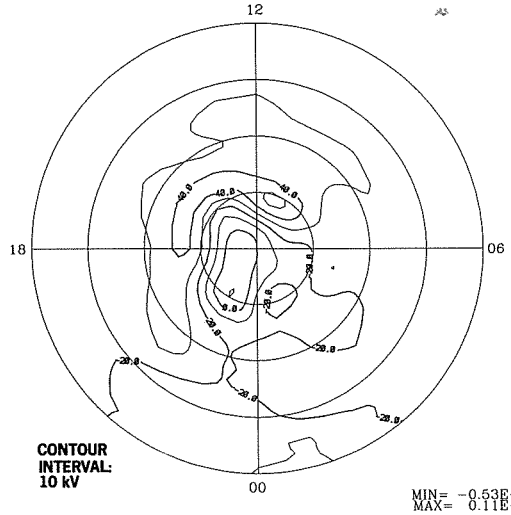

MIN= -0.53E+02 **kV**
MAX= 0.11E+02 **kV**

IONOSPHERIC CURRENT VECTORS

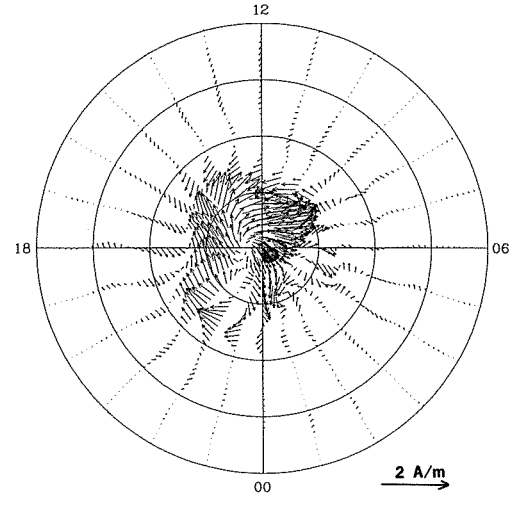

FIELD-ALIGNED CURRENT

23 JUL 1983
1240-55 UT

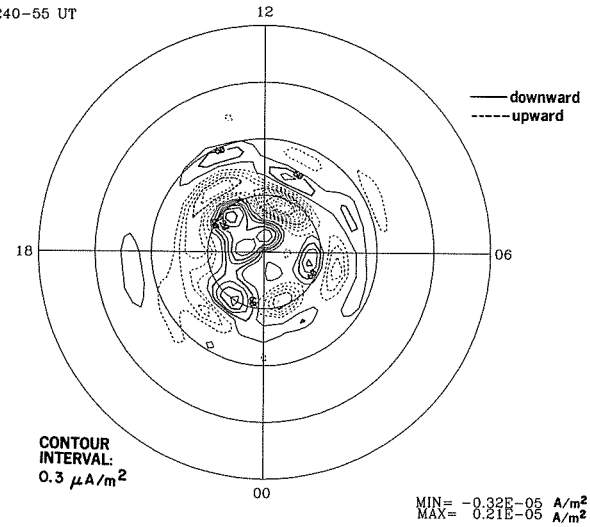

MIN= -0.32E-05 A/m²
MAX= 0.21E-05 A/m²

JOULE HEATING RATE

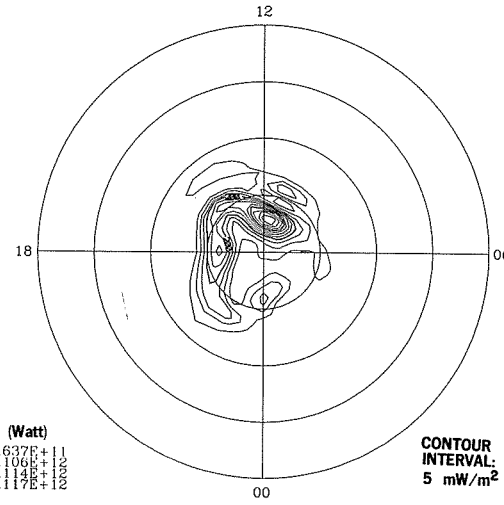

MAX= 0.59E-01 W/m²

HALL CURRENT VECTORS

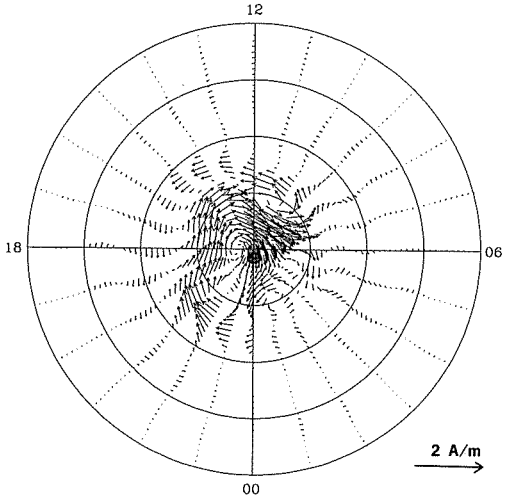

PEDERSEN CURRENT VECTORS

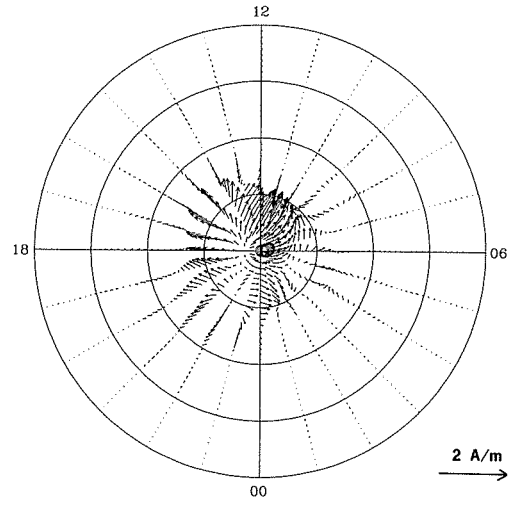

FIELD-ALIGNED HALL CURRENT

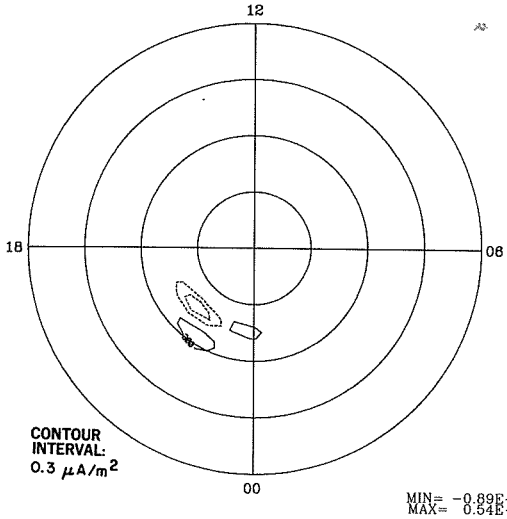

MIN= -0.89E-06 A/m²
MAX= 0.54E-06 A/m²

FIELD-ALIGNED PEDERSEN CURRENT

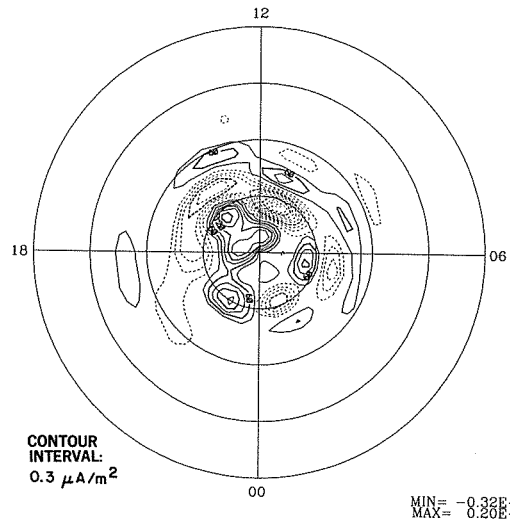

MIN= -0.32E-05 A/m²
MAX= 0.20E-05 A/m²

EQUIVALENT CURRENT VECTORS

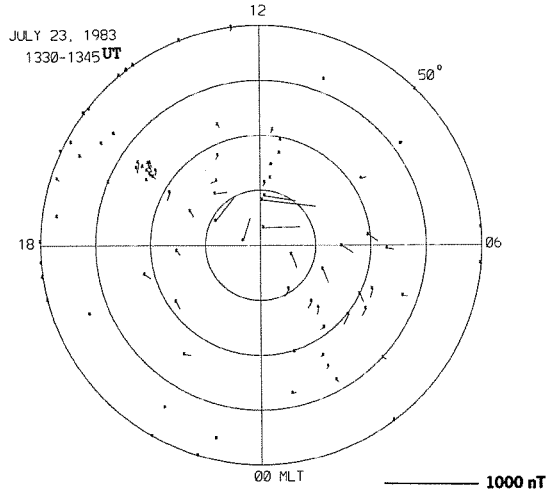

EQUIVALENT CURRENT SYSTEM

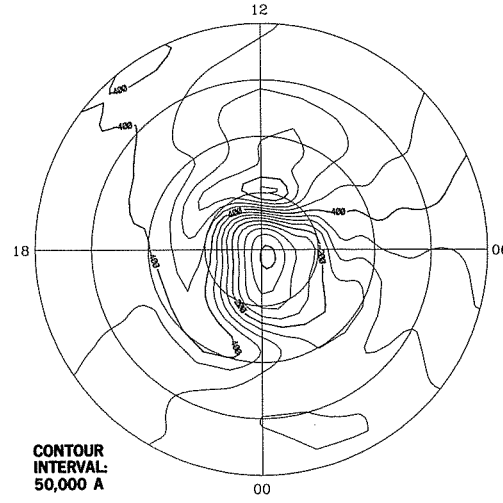

HALL CONDUCTANCE

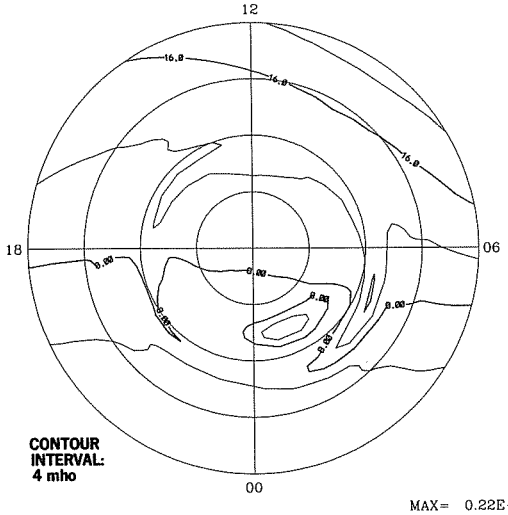

MAX= 0.22E+02 **mho**

PEDERSEN CONDUCTANCE

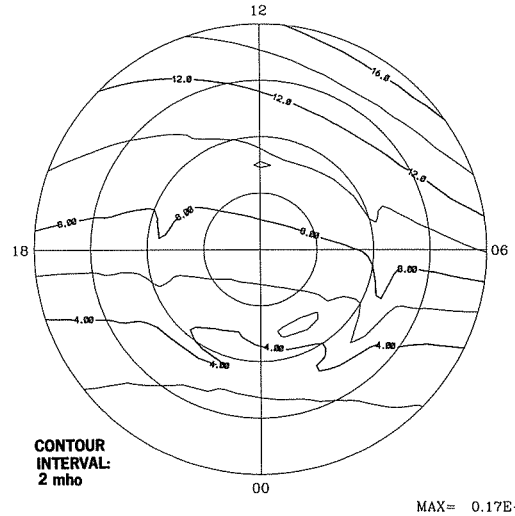

MAX= 0.17E+02 **mho**

ELECTRIC POTENTIAL

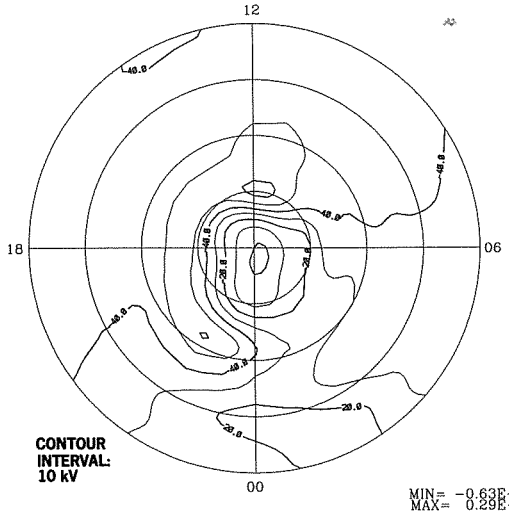

MIN= −0.63E+02 **kV**
MAX= 0.29E+01 **kV**

IONOSPHERIC CURRENT VECTORS

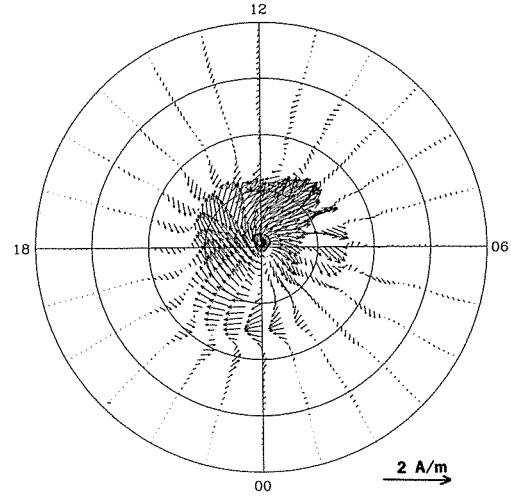

FIELD-ALIGNED CURRENT

23 JUL 1983
1330-45 UT

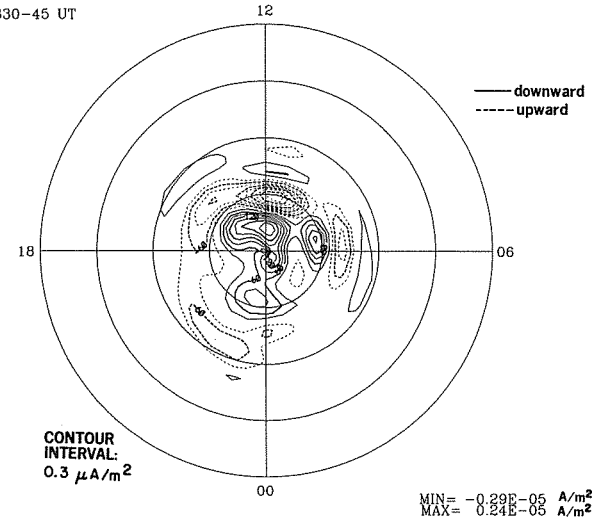

JOULE HEATING RATE

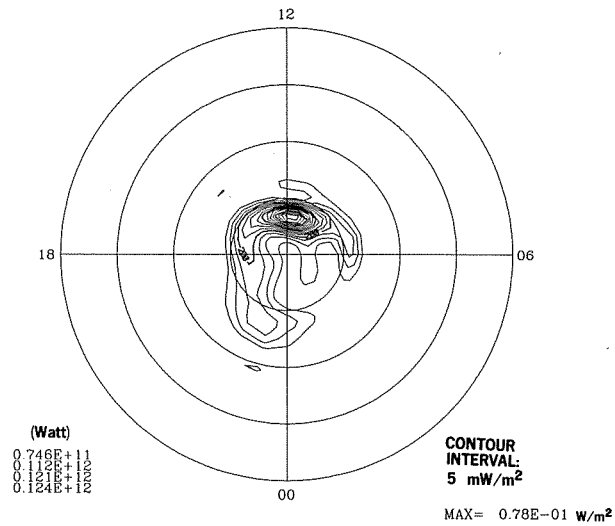

HALL CURRENT VECTORS

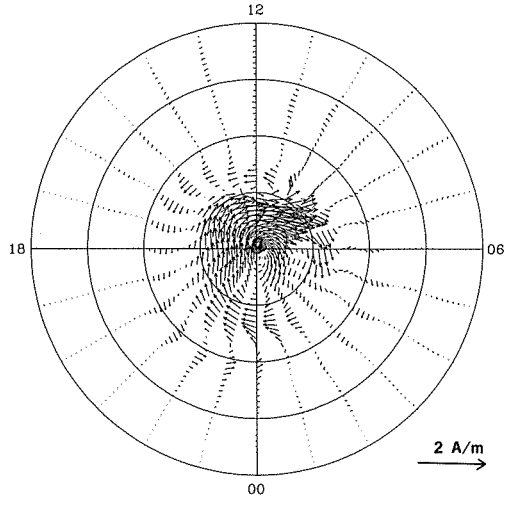

PEDERSEN CURRENT VECTORS

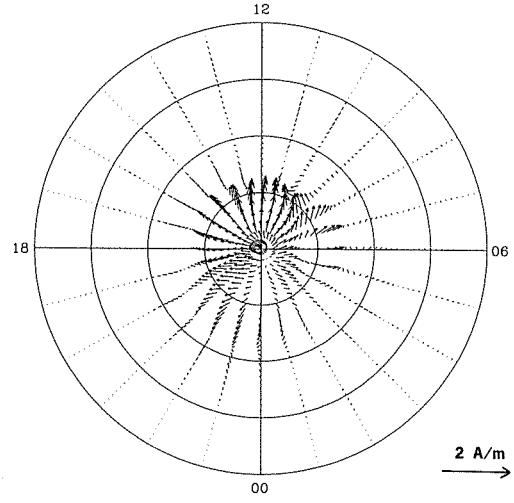

FIELD-ALIGNED HALL CURRENT

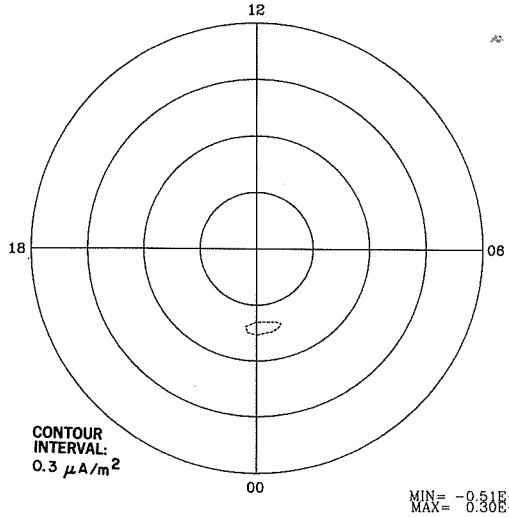

FIELD-ALIGNED PEDERSEN CURRENT

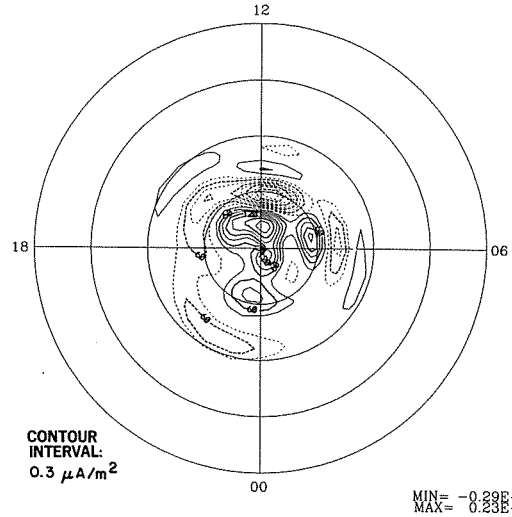

EQUIVALENT CURRENT VECTORS

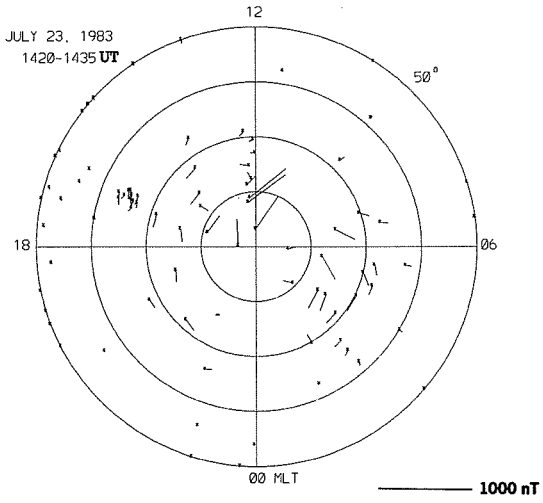

EQUIVALENT CURRENT SYSTEM

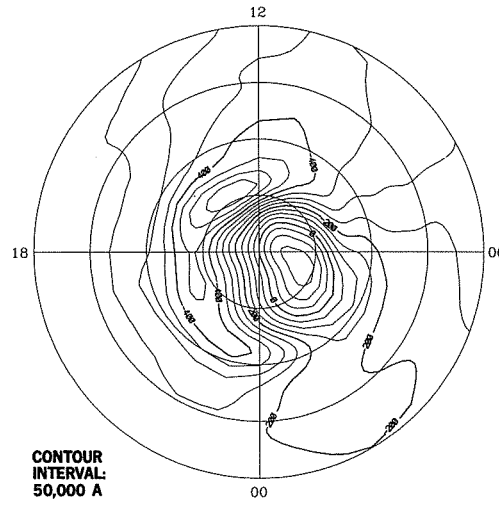

HALL CONDUCTANCE

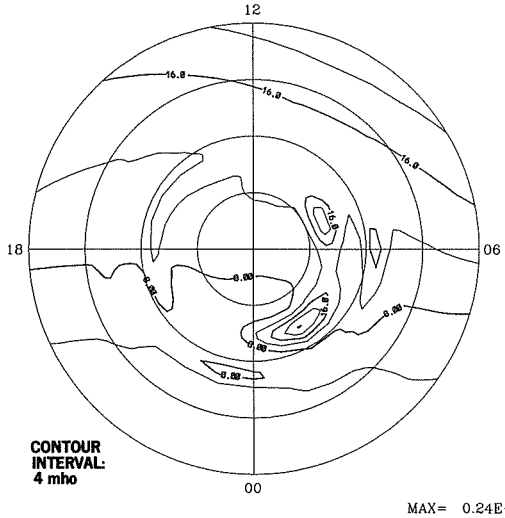

MAX= 0.24E+02 **mho**

PEDERSEN CONDUCTANCE

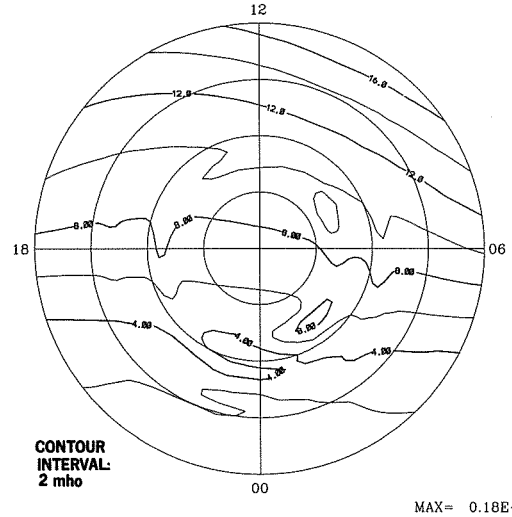

MAX= 0.18E+02 **mho**

ELECTRIC POTENTIAL

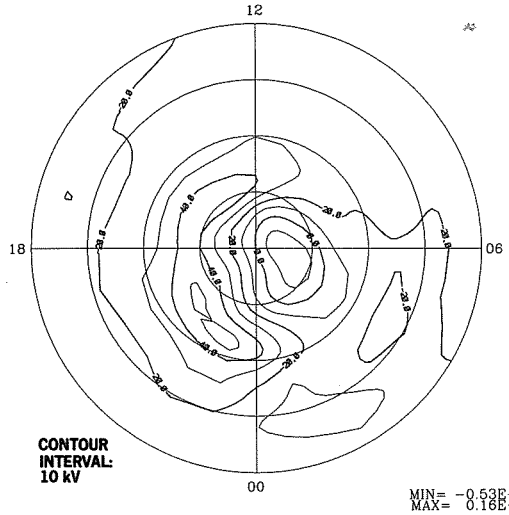

MIN= -0.53E+02 **kV**
MAX= 0.16E+02 **kV**

IONOSPHERIC CURRENT VECTORS

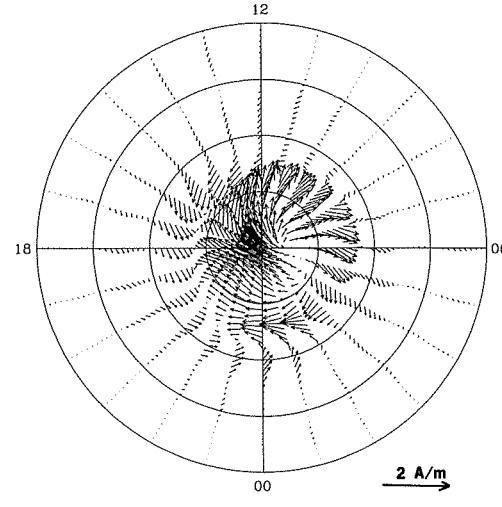

FIELD-ALIGNED CURRENT

23 JUL 1983
1420-35 UT

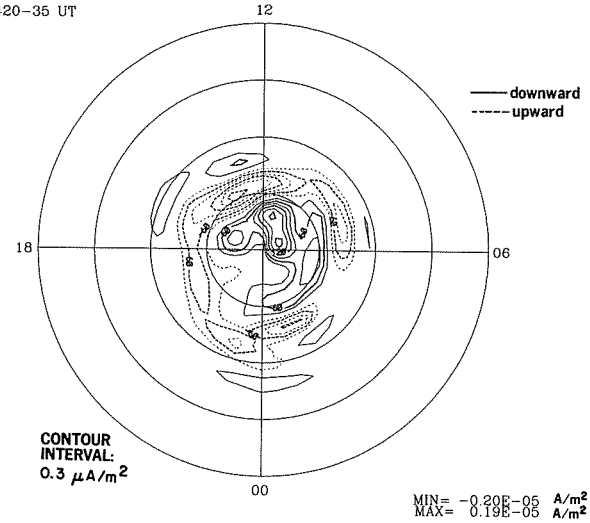

MIN= -0.20E-05 A/m²
MAX= 0.19E-05 A/m²

JOULE HEATING RATE

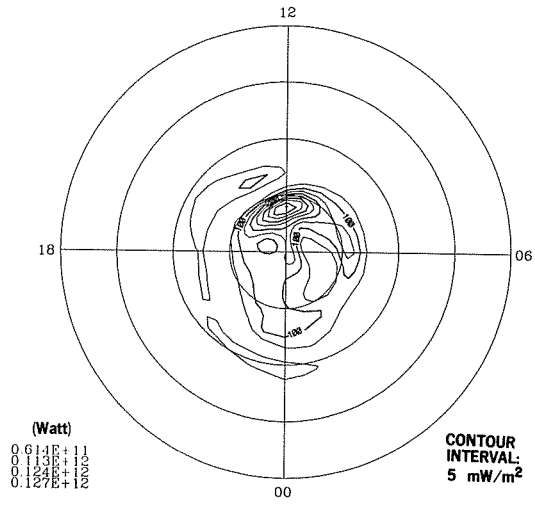

MAX= 0.46E-01 W/m²

HALL CURRENT VECTORS

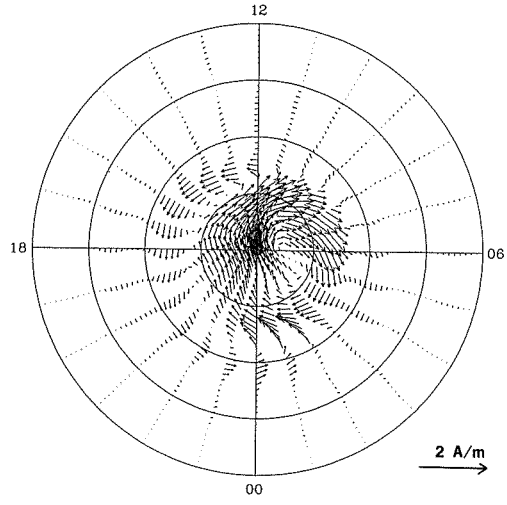

PEDERSEN CURRENT VECTORS

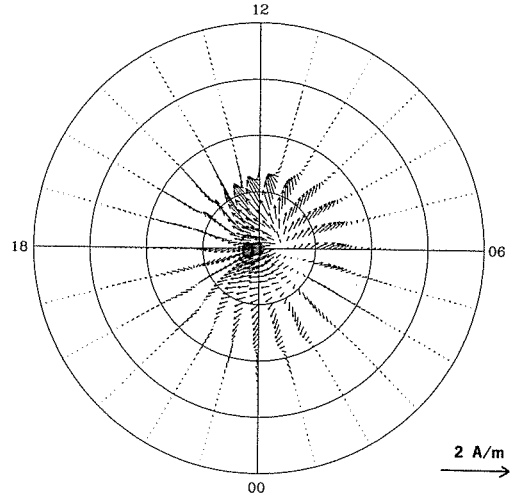

FIELD-ALIGNED HALL CURRENT

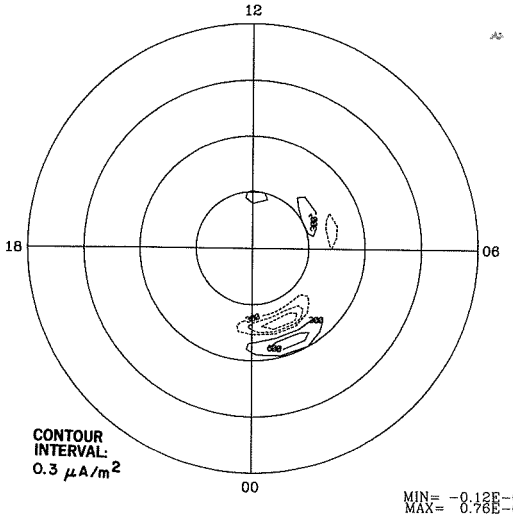

MIN= -0.12E-05 A/m²
MAX= 0.76E-06 A/m²

FIELD-ALIGNED PEDERSEN CURRENT

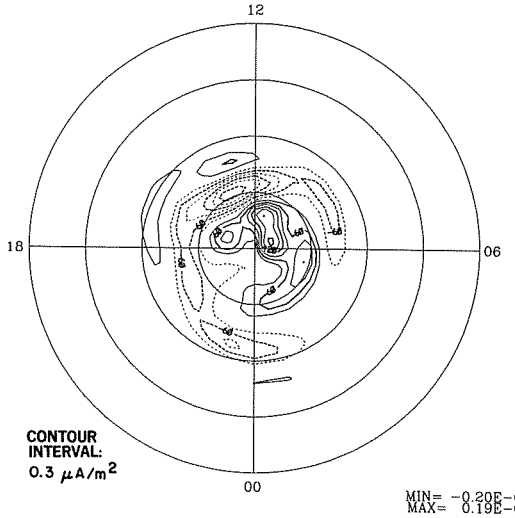

MIN= -0.20E-05 A/m²
MAX= 0.19E-05 A/m²

EQUIVALENT CURRENT VECTORS

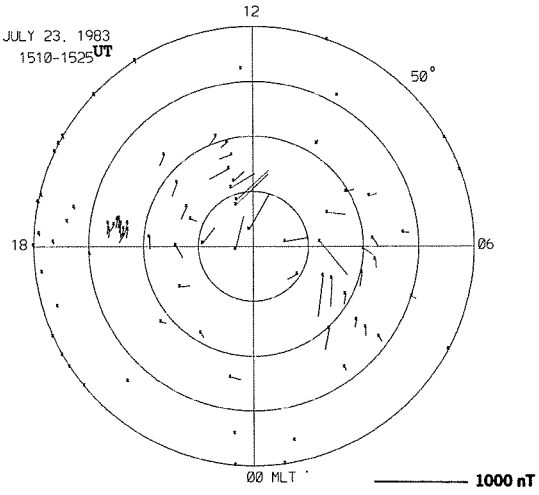

EQUIVALENT CURRENT SYSTEM

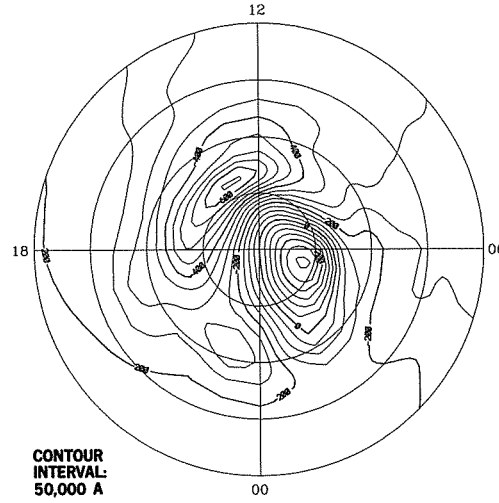

HALL CONDUCTANCE

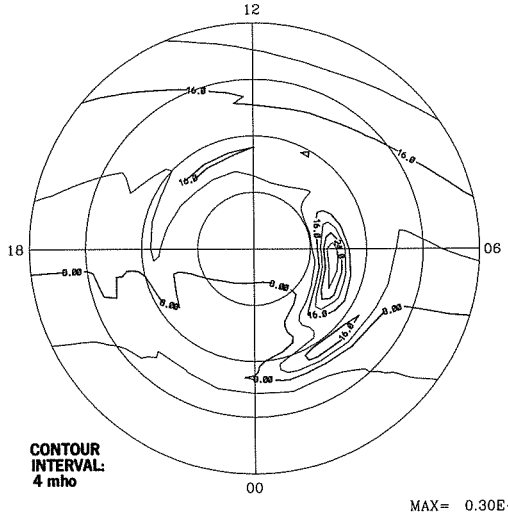

MAX= 0.30E+02 mho

PEDERSEN CONDUCTANCE

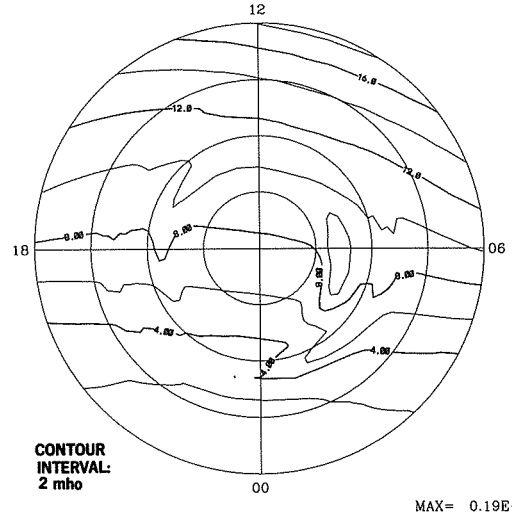

MAX= 0.19E+02 mho

ELECTRIC POTENTIAL

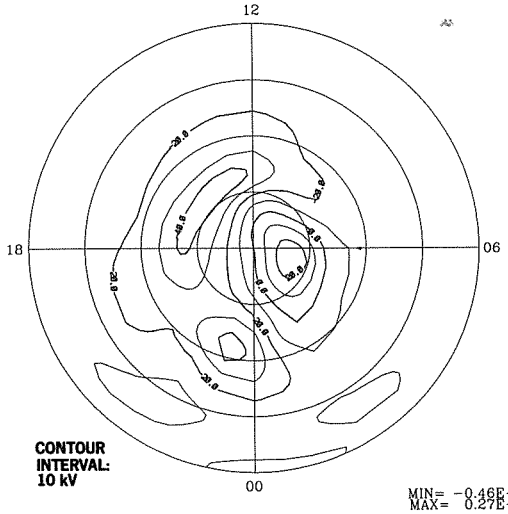

MIN= -0.46E+02 kV
MAX= 0.27E+02 kV

IONOSPHERIC CURRENT VECTORS

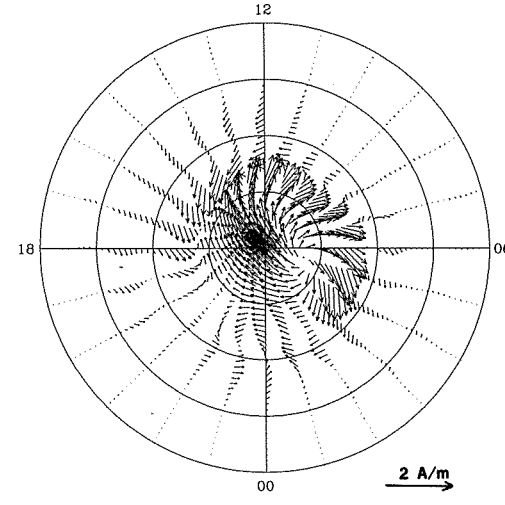

FIELD-ALIGNED CURRENT

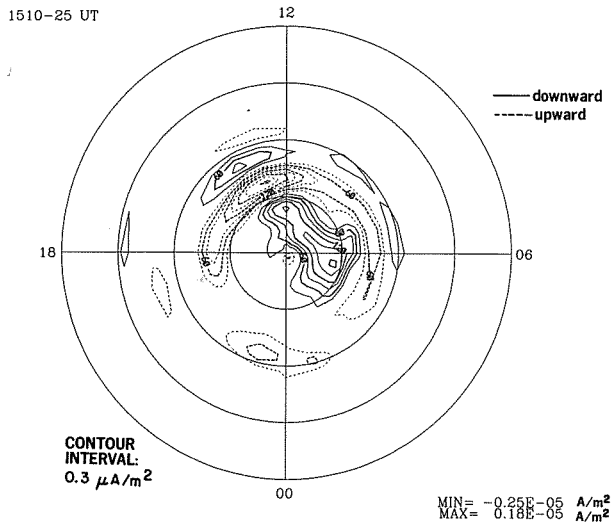

JOULE HEATING RATE

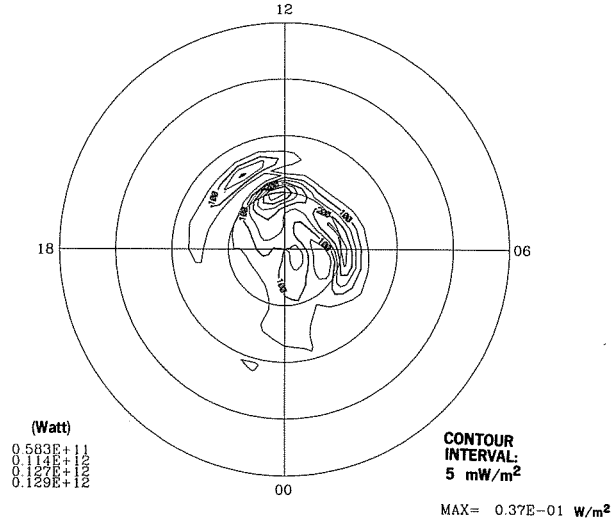

HALL CURRENT VECTORS

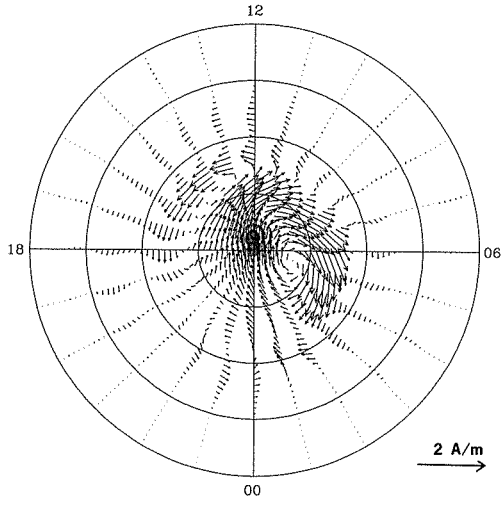

PEDERSEN CURRENT VECTORS

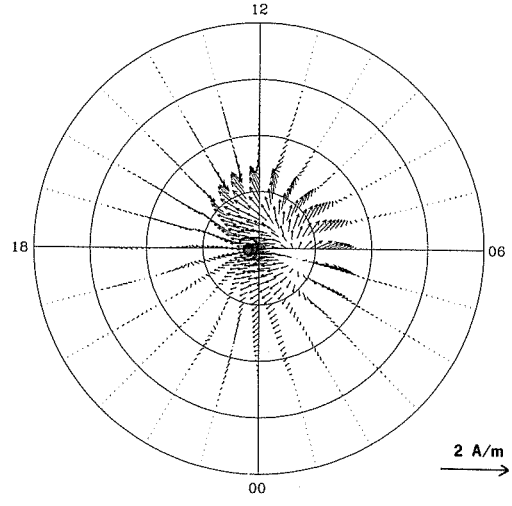

FIELD-ALIGNED HALL CURRENT

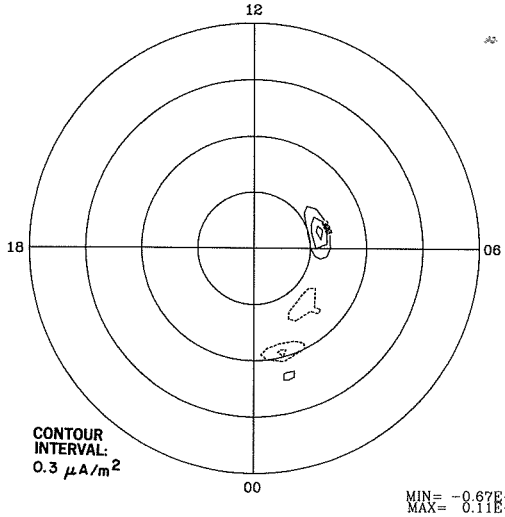

FIELD-ALIGNED PEDERSEN CURRENT

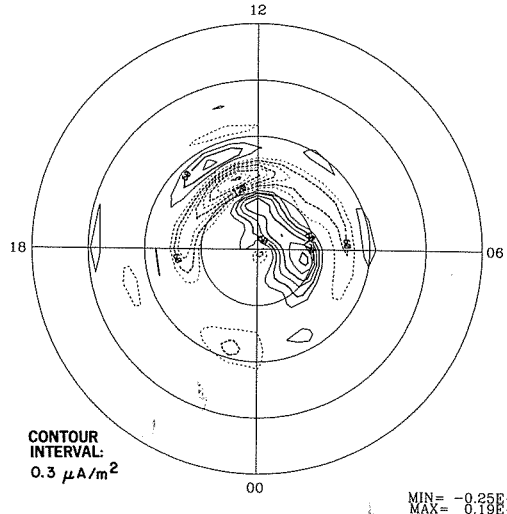

EQUIVALENT CURRENT VECTORS

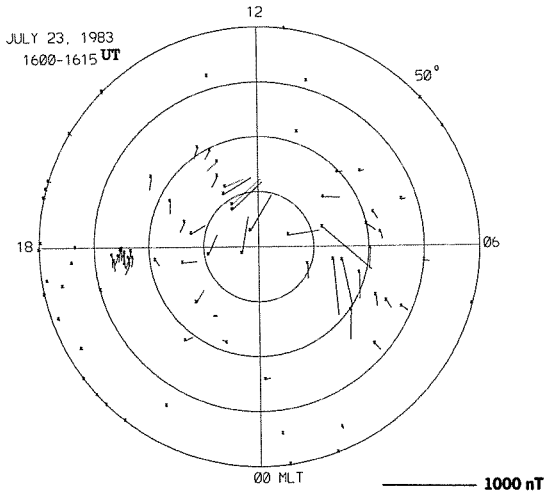

EQUIVALENT CURRENT SYSTEM

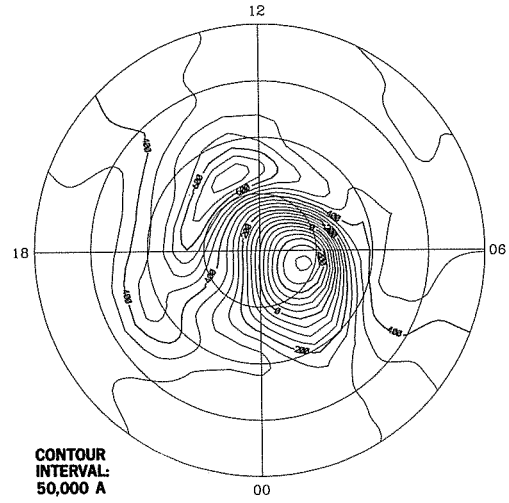

HALL CONDUCTANCE

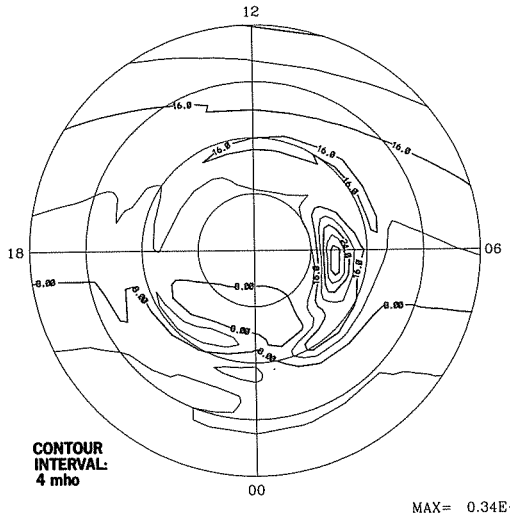

MAX= 0.34E+02 **mho**

PEDERSEN CONDUCTANCE

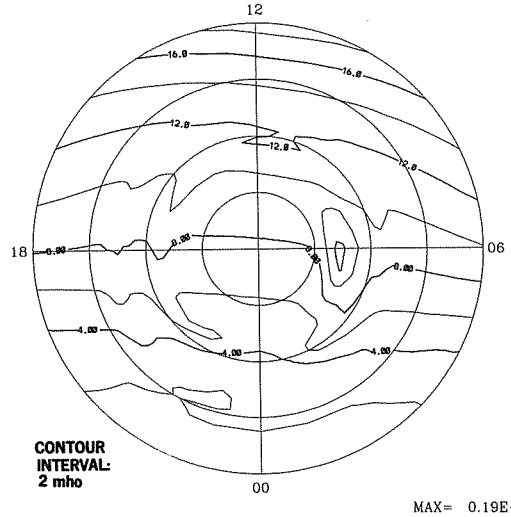

MAX= 0.19E+02 **mho**

ELECTRIC POTENTIAL

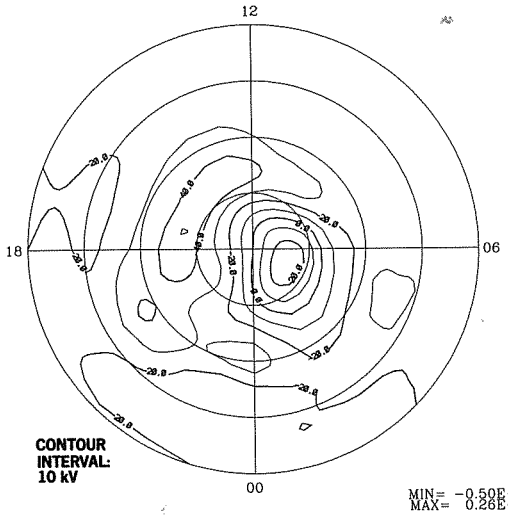

MIN= -0.50E+02 **kV**
MAX= 0.26E+02 **kV**

IONOSPHERIC CURRENT VECTORS

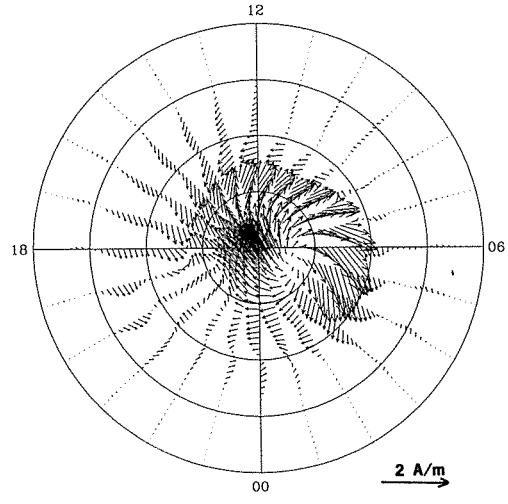

FIELD-ALIGNED CURRENT

23 JUL 1983
1600-15 UT

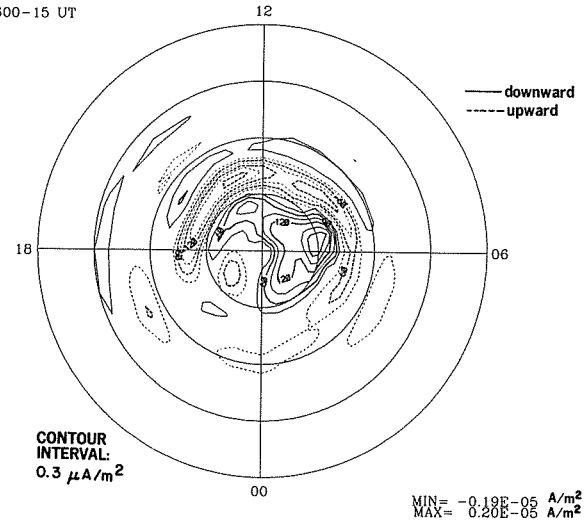

MIN= -0.19E-05 A/m²
MAX= 0.20E-05 A/m²

JOULE HEATING RATE

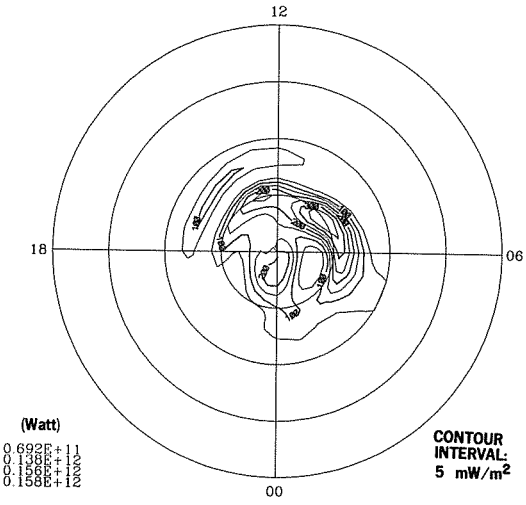

MAX= 0.40E-01 W/m²

HALL CURRENT VECTORS

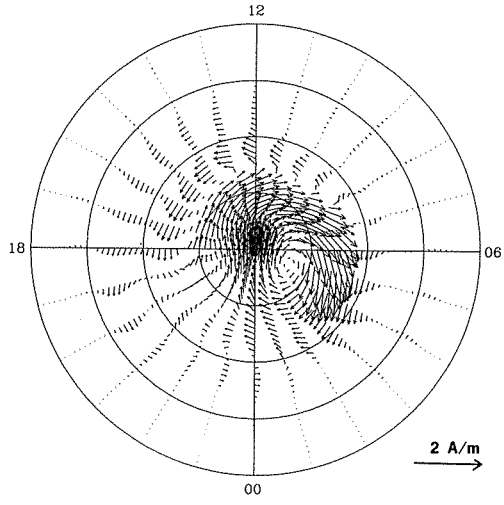

PEDERSEN CURRENT VECTORS

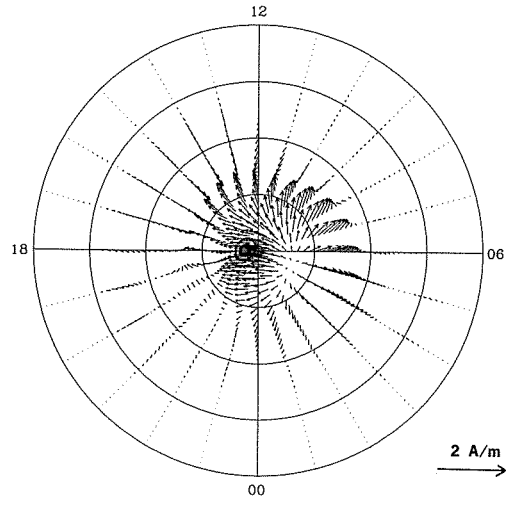

FIELD-ALIGNED HALL CURRENT

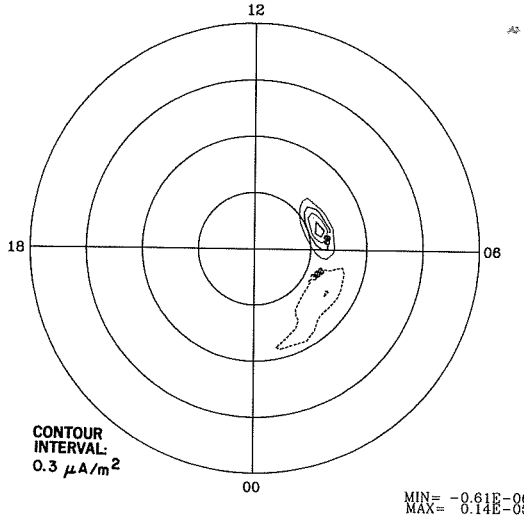

MIN= -0.61E-06 A/m²
MAX= 0.14E-05 A/m²

FIELD-ALIGNED PEDERSEN CURRENT

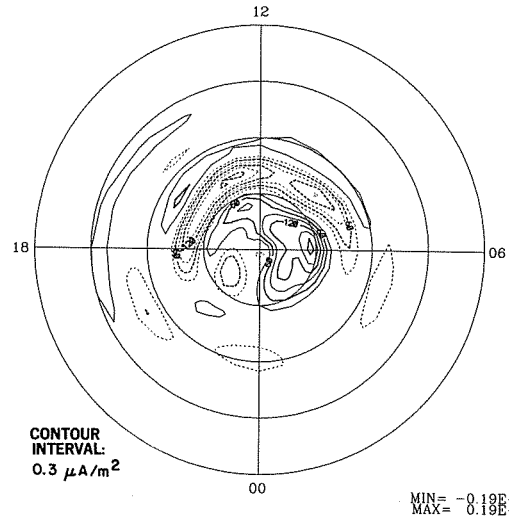

MIN= -0.19E-05 A/m²
MAX= 0.19E-05 A/m²

EQUIVALENT CURRENT VECTORS

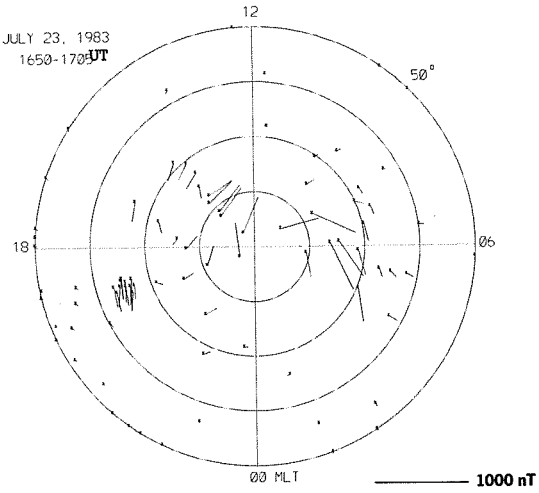

EQUIVALENT CURRENT SYSTEM

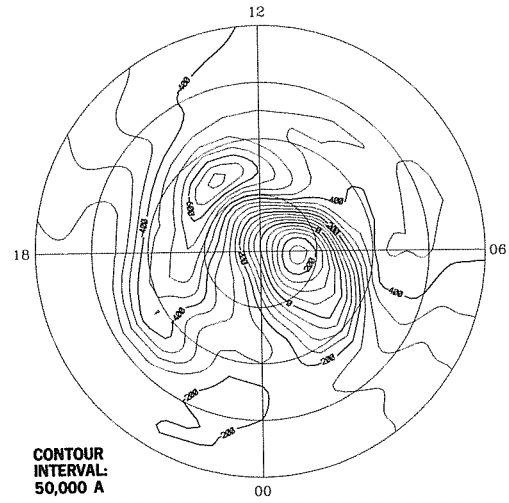

HALL CONDUCTANCE

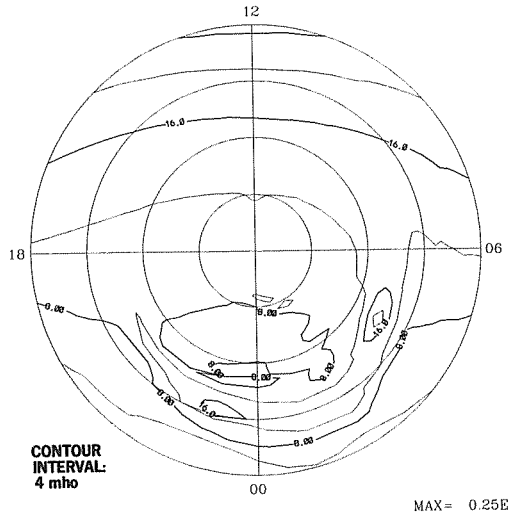

MAX= 0.25E+02 **mho**

DMSP

PEDERSEN CONDUCTANCE

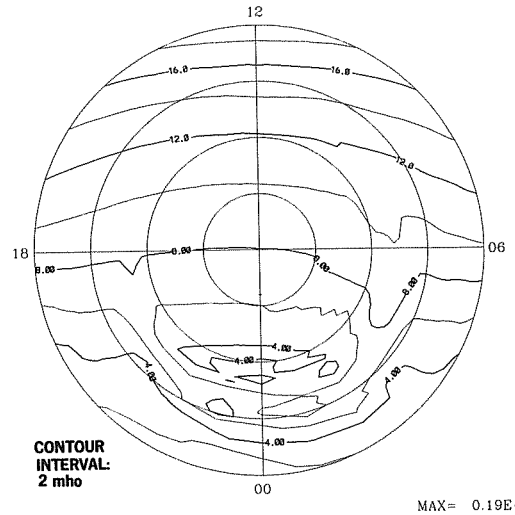

MAX= 0.19E+02 **mho**

ELECTRIC POTENTIAL

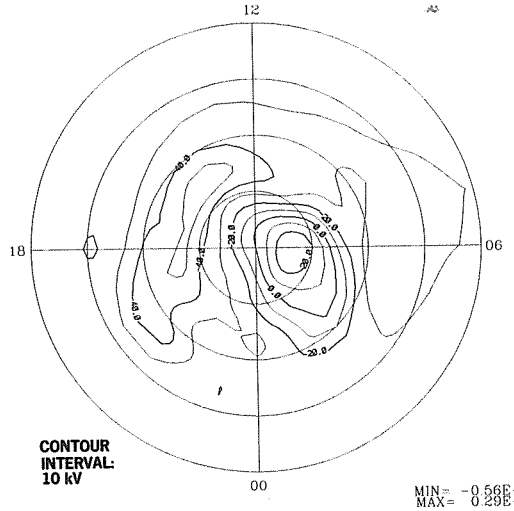

MIN= -0.56E+02 **kV**
MAX= 0.29E+02 **kV**

IONOSPHERIC CURRENT VECTORS

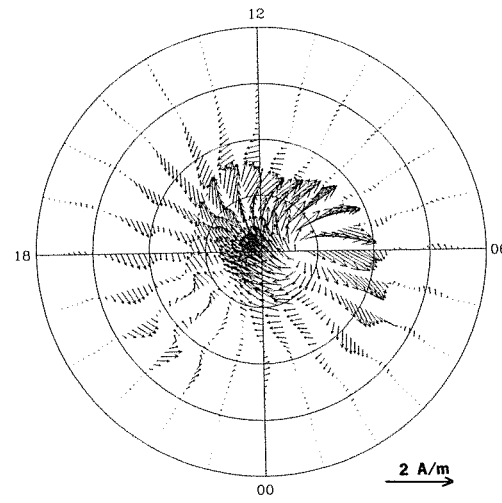

FIELD-ALIGNED CURRENT

23 JUL 1983
1650-1705 UT

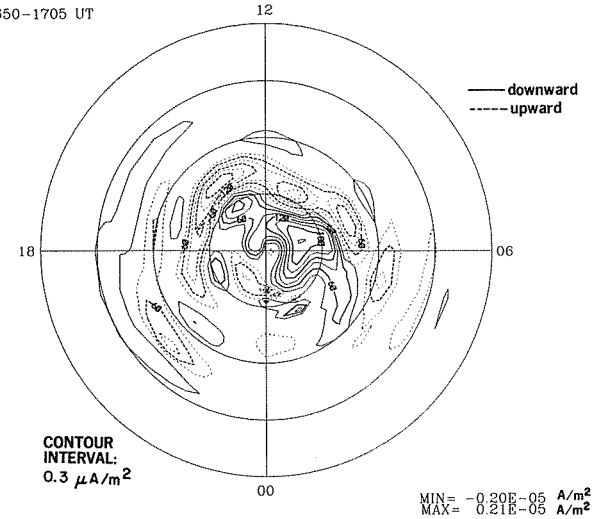

MIN= -0.20E-05 A/m²
MAX= 0.21E-05 A/m²

JOULE HEATING RATE

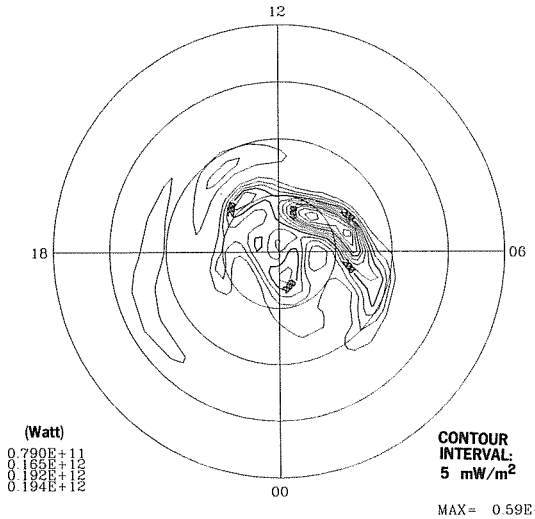

MAX= 0.59E-01 W/m²

HALL CURRENT VECTORS

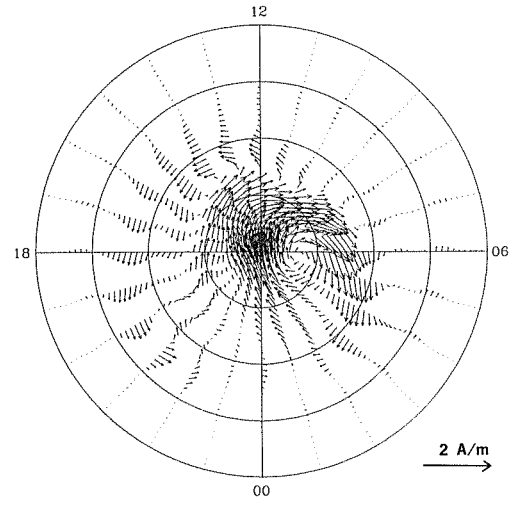

PEDERSEN CURRENT VECTORS

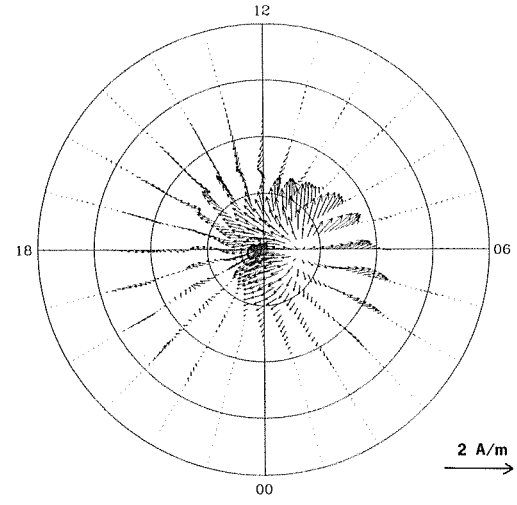

FIELD-ALIGNED HALL CURRENT

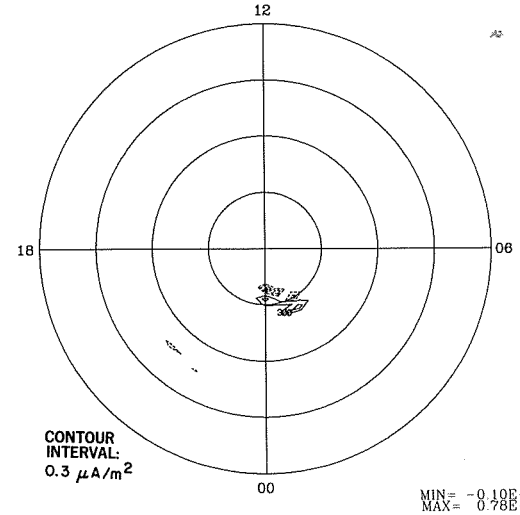

MIN= -0.10E-05 A/m²
MAX= 0.78E-06 A/m²

FIELD-ALIGNED PEDERSEN CURRENT

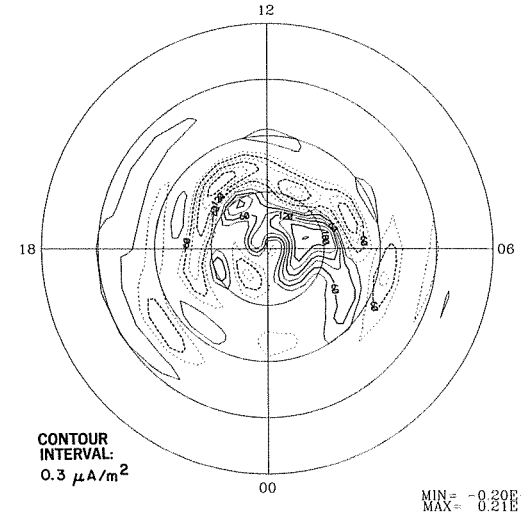

MIN= -0.20E-05 A/m²
MAX= 0.21E-05 A/m²

EQUIVALENT CURRENT VECTORS

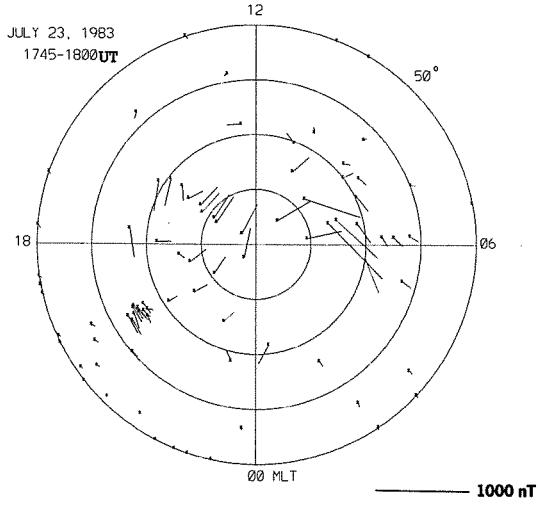

EQUIVALENT CURRENT SYSTEM

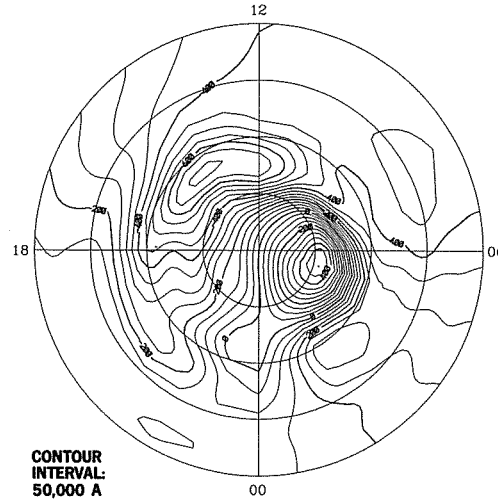

HALL CONDUCTANCE

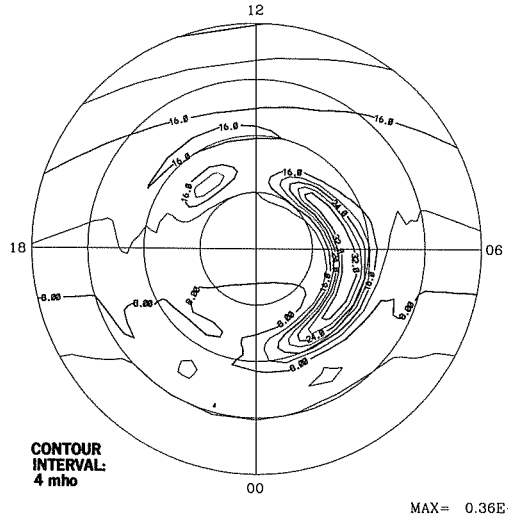

MAX= 0.36E+02 mho

PEDERSEN CONDUCTANCE

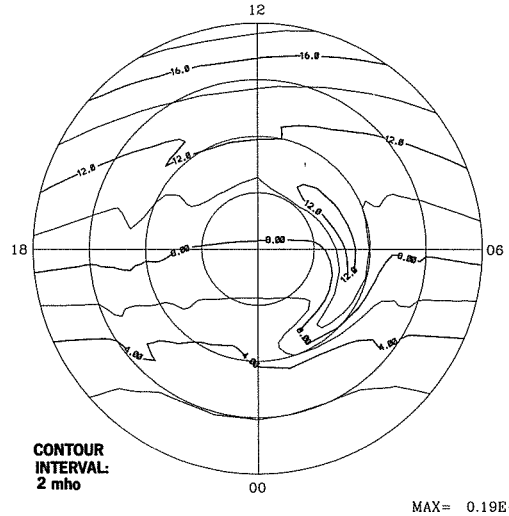

MAX= 0.19E+02 mho

ELECTRIC POTENTIAL

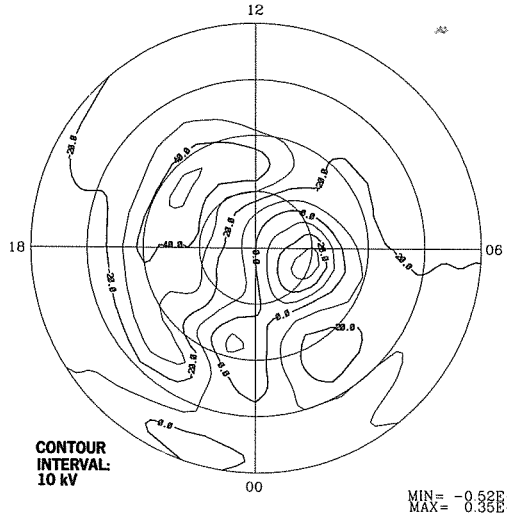

MIN= -0.52E+02 kV
MAX= 0.35E+02 kV

IONOSPHERIC CURRENT VECTORS

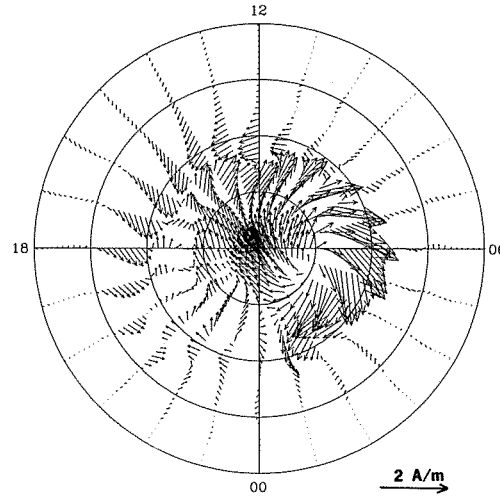

FIELD-ALIGNED CURRENT

23 JUL 1983
1745-1800 UT

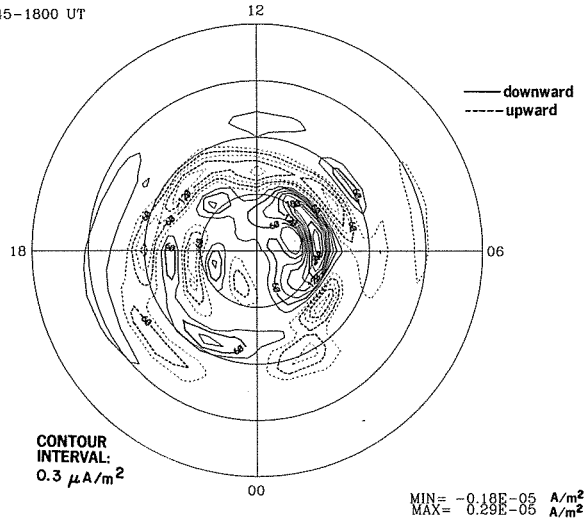

MIN= -0.18E-05 A/m²
MAX= 0.29E-05 A/m²

JOULE HEATING RATE

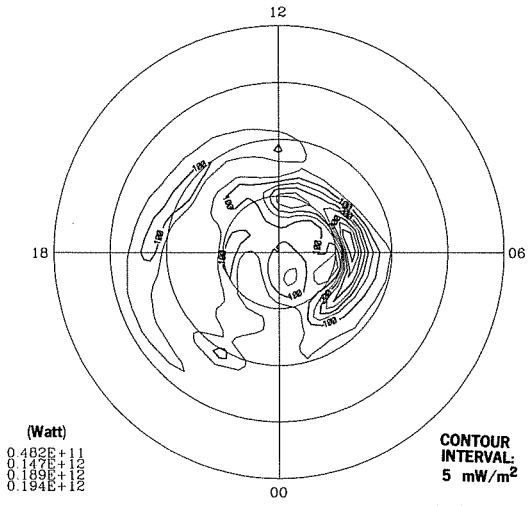

MAX= 0.44E-01 W/m²

HALL CURRENT VECTORS

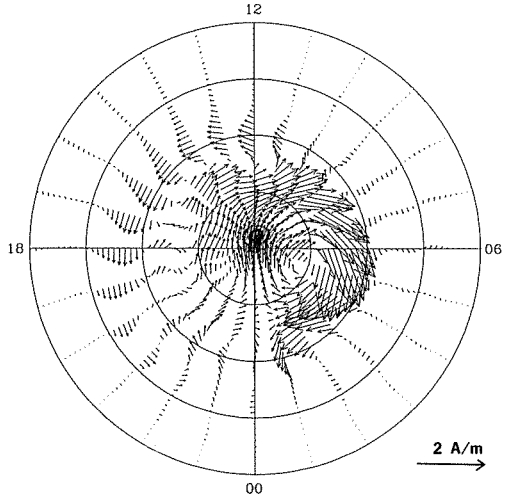

PEDERSEN CURRENT VECTORS

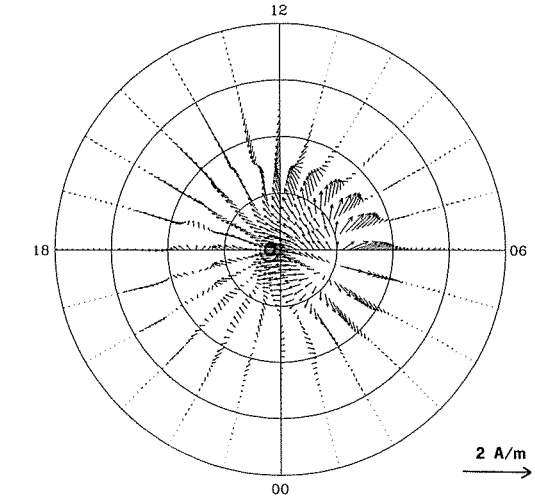

FIELD-ALIGNED HALL CURRENT

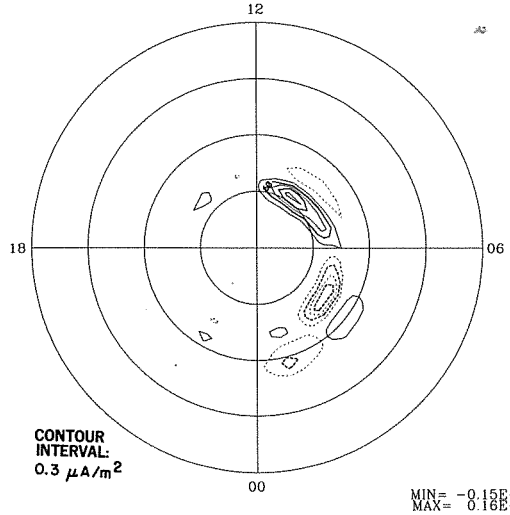

MIN= -0.15E-05 A/m²
MAX= 0.16E-05 A/m²

FIELD-ALIGNED PEDERSEN CURRENT

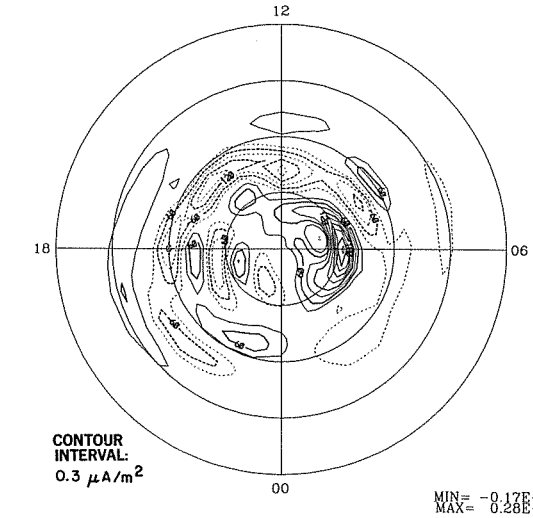

MIN= -0.17E-05 A/m²
MAX= 0.28E-05 A/m²

EQUIVALENT CURRENT VECTORS

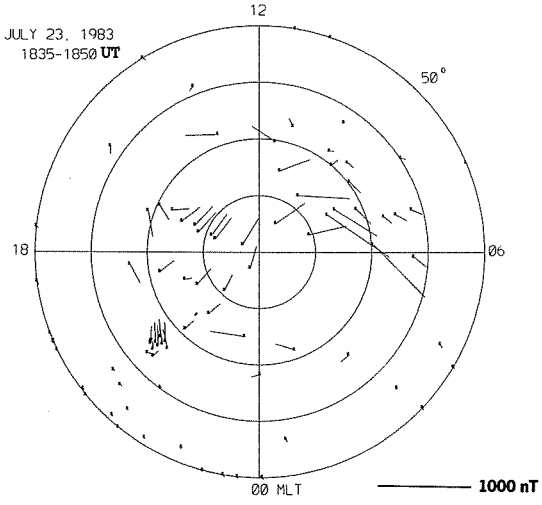

EQUIVALENT CURRENT SYSTEM

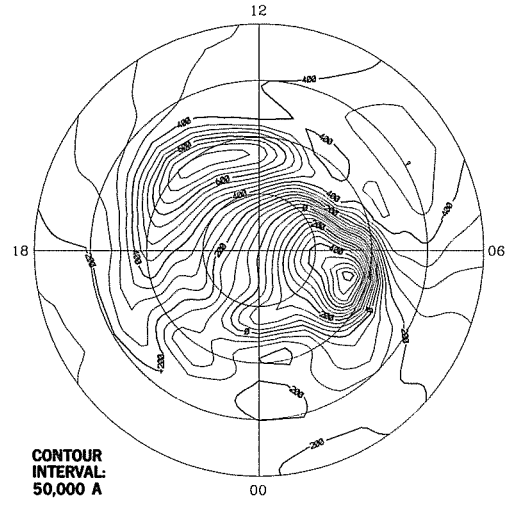

HALL CONDUCTANCE

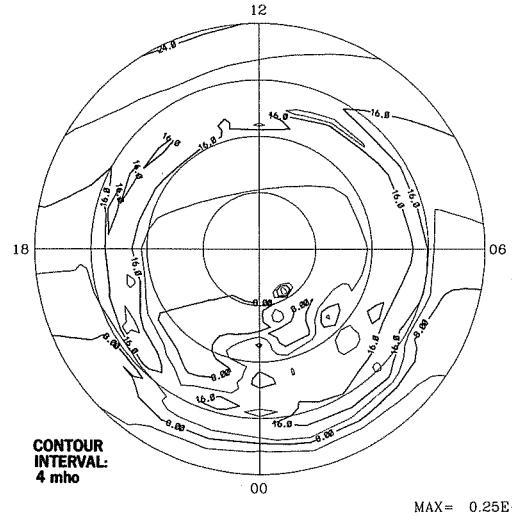

MAX= 0.25E+02 **mho**

DMSP

PEDERSEN CONDUCTANCE

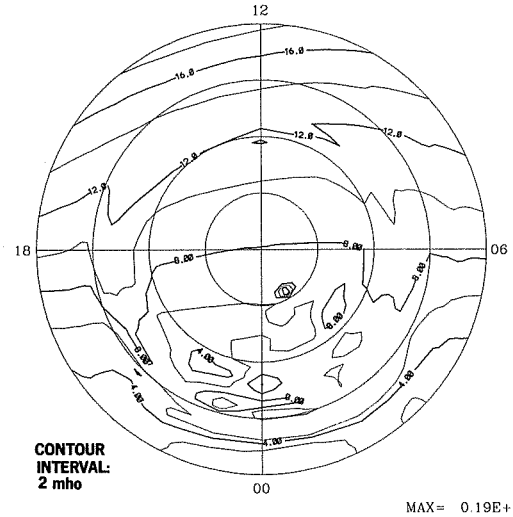

MAX= 0.19E+02 **mho**

ELECTRIC POTENTIAL

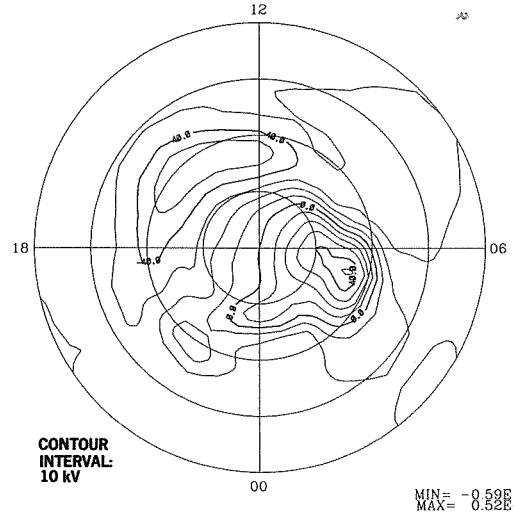

MIN= -0.59E+02 **kV**
MAX= 0.52E+02 **kV**

IONOSPHERIC CURRENT VECTORS

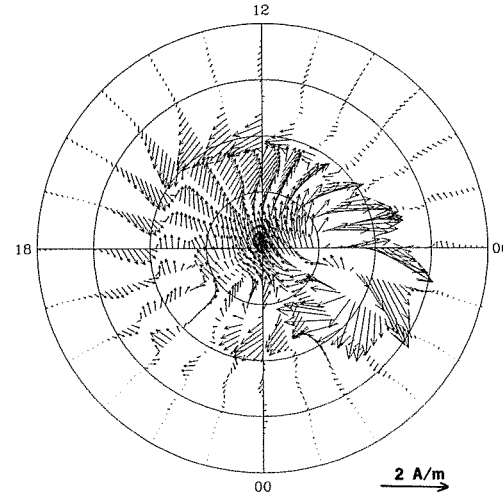

FIELD-ALIGNED CURRENT

23 JUL 1983
1835-50 UT

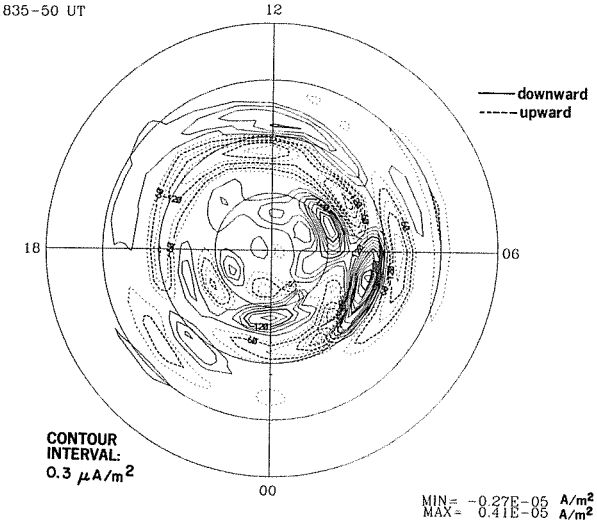

MIN= -0.27E-05 A/m²
MAX= 0.41E-05 A/m²

JOULE HEATING RATE

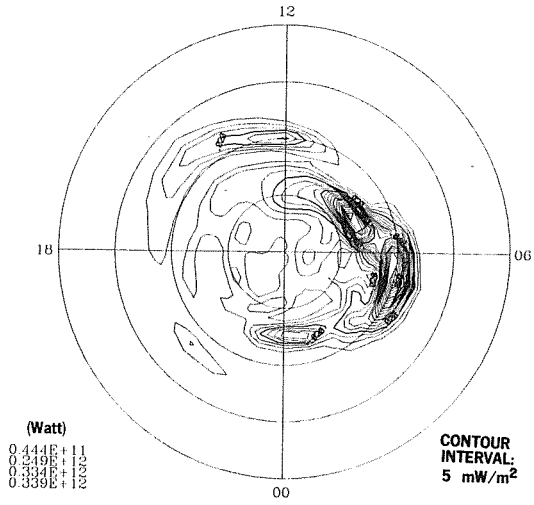

MAX= 0.11E+00 W/m²

HALL CURRENT VECTORS

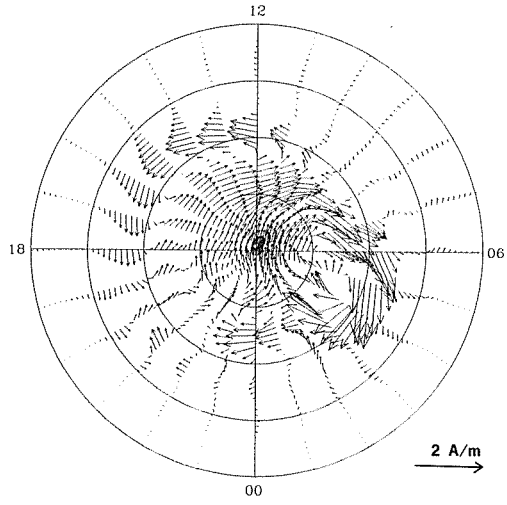

PEDERSEN CURRENT VECTORS

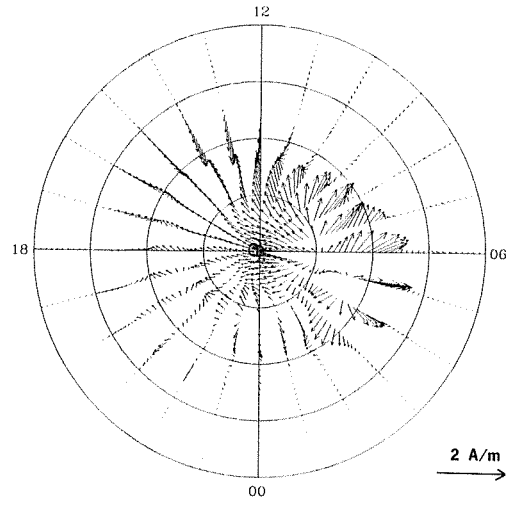

FIELD-ALIGNED HALL CURRENT

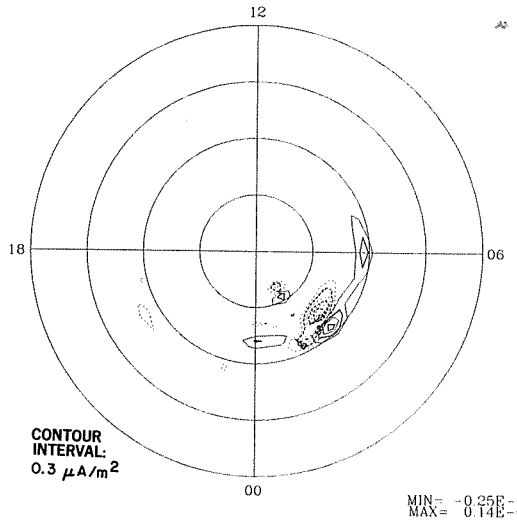

MIN= -0.25E-05 A/m²
MAX= 0.14E-05 A/m²

FIELD-ALIGNED PEDERSEN CURRENT

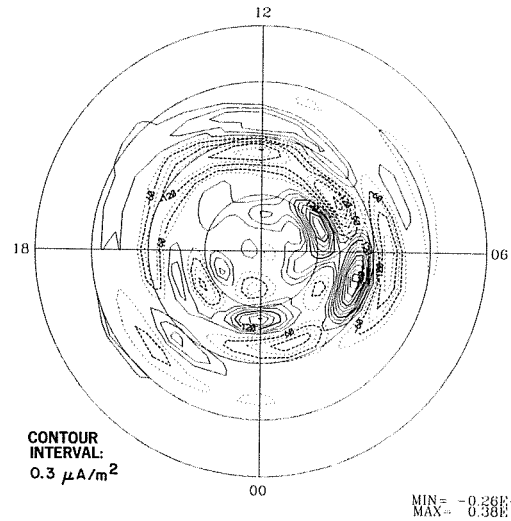

MIN= -0.26E-05 A/m²
MAX= 0.38E-05 A/m²

EQUIVALENT CURRENT VECTORS

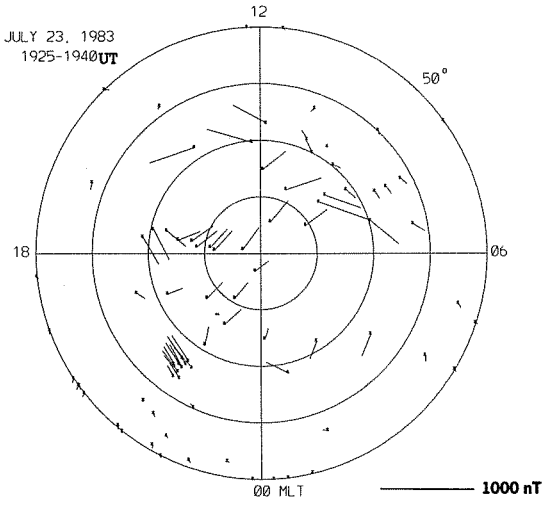

EQUIVALENT CURRENT SYSTEM

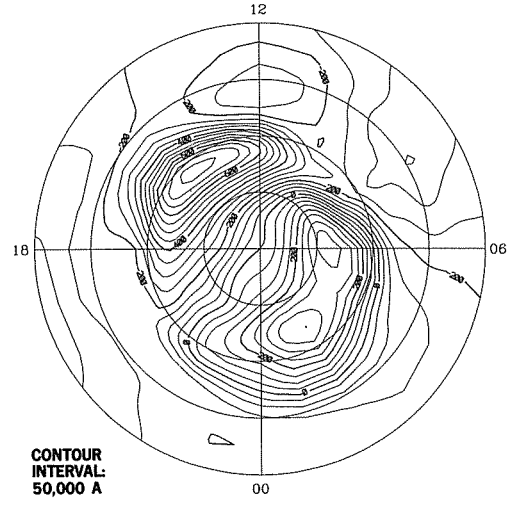

HALL CONDUCTANCE

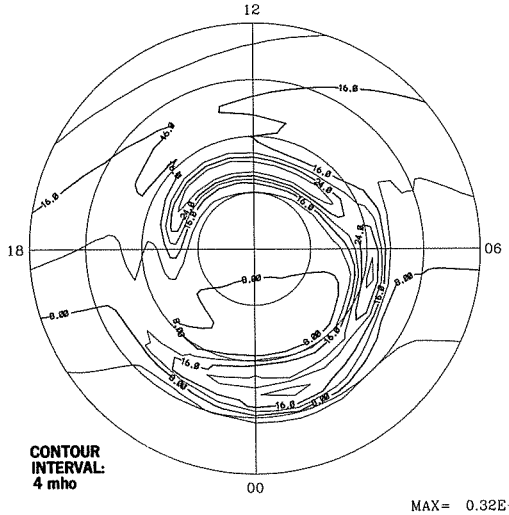

MAX= 0.32E+02 mho

PEDERSEN CONDUCTANCE

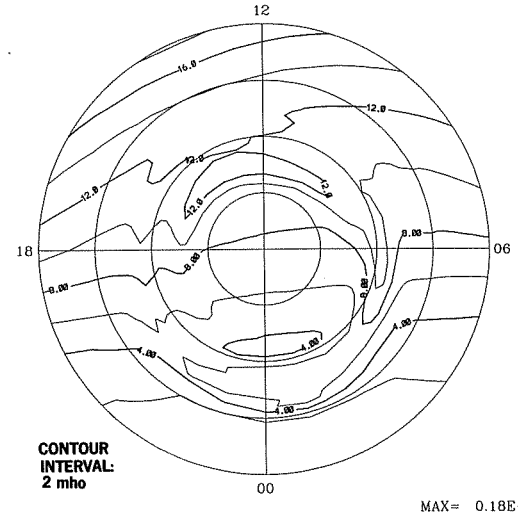

MAX= 0.18E+02 mho

ELECTRIC POTENTIAL

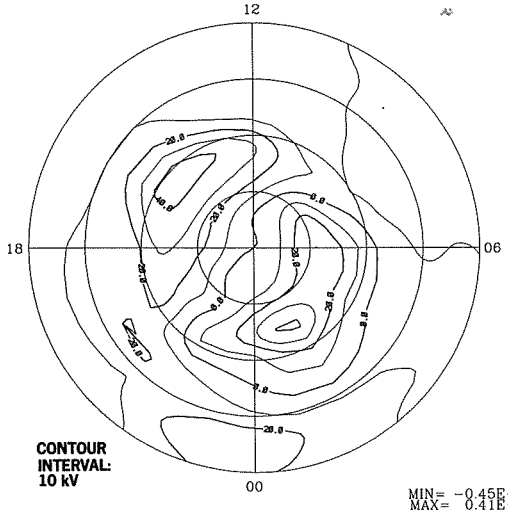

MIN= -0.45E+02 kv
MAX= 0.41E+02 kv

IONOSPHERIC CURRENT VECTORS

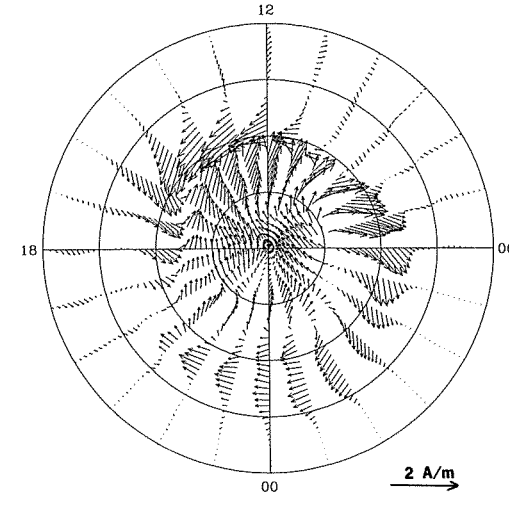

FIELD-ALIGNED CURRENT

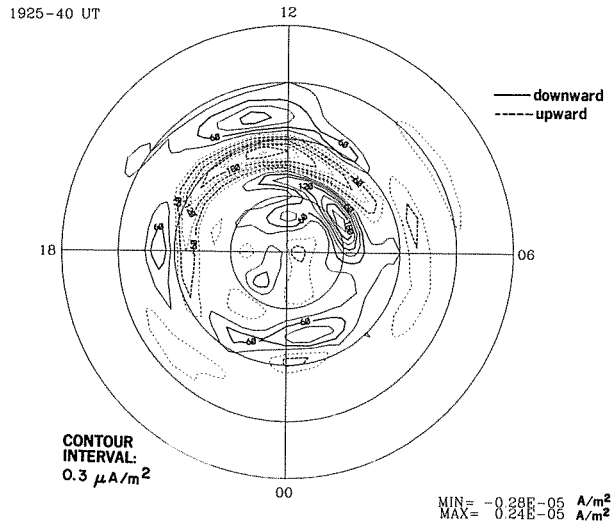

JOULE HEATING RATE

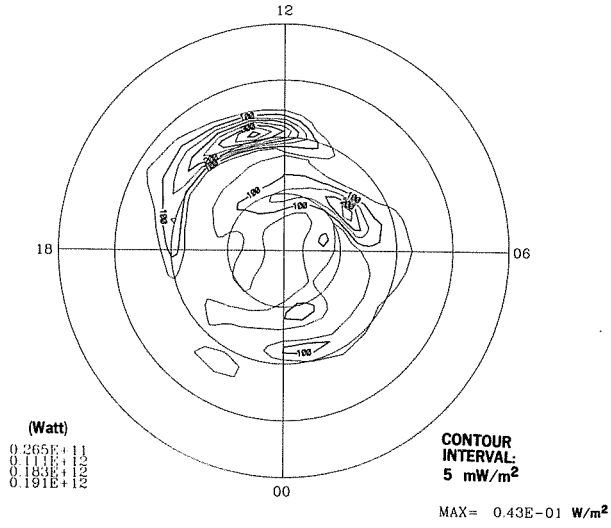

HALL CURRENT VECTORS

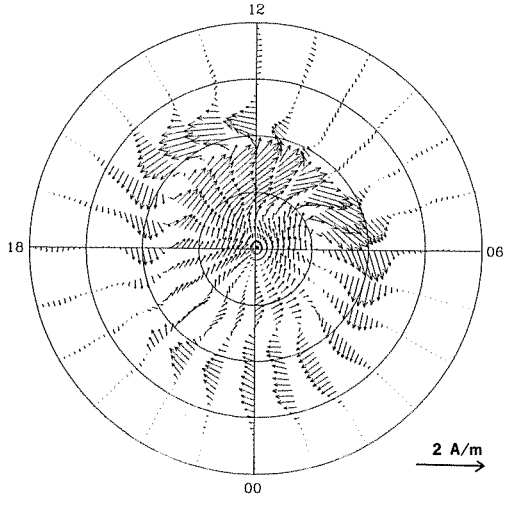

PEDERSEN CURRENT VECTORS

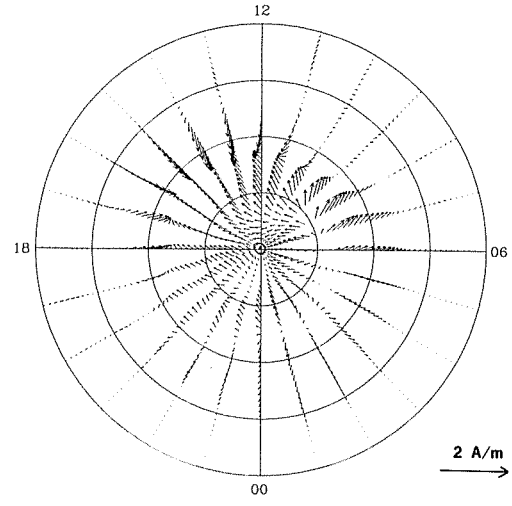

FIELD-ALIGNED HALL CURRENT

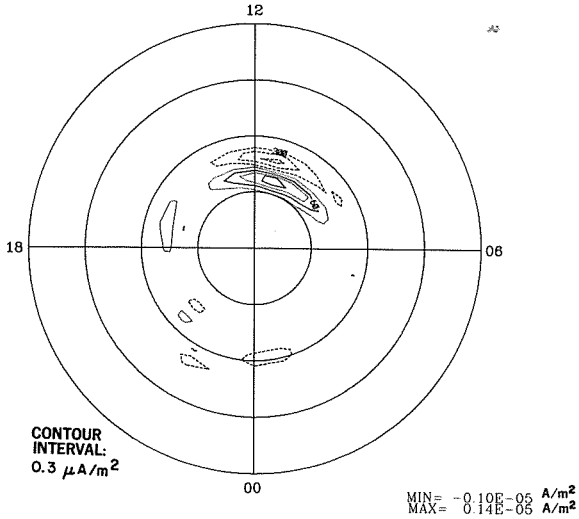

FIELD-ALIGNED PEDERSEN CURRENT

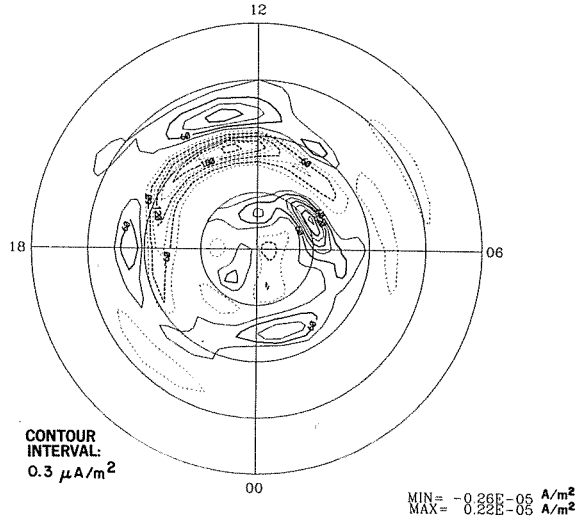

EQUIVALENT CURRENT VECTORS

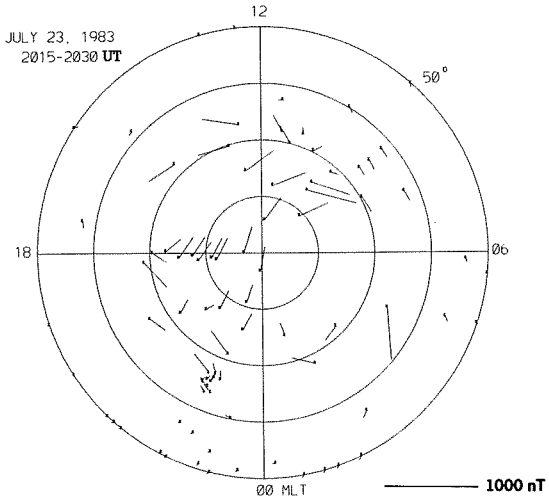

EQUIVALENT CURRENT SYSTEM

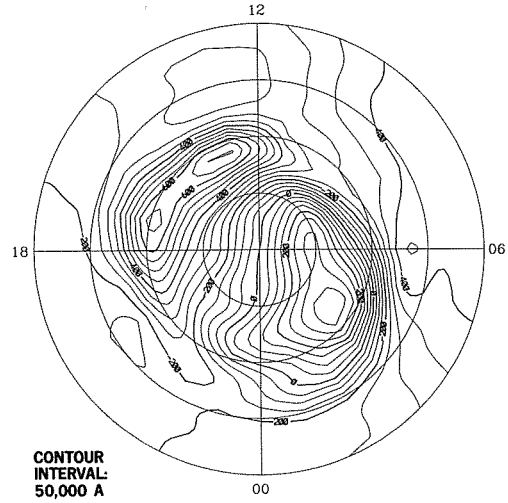

HALL CONDUCTANCE

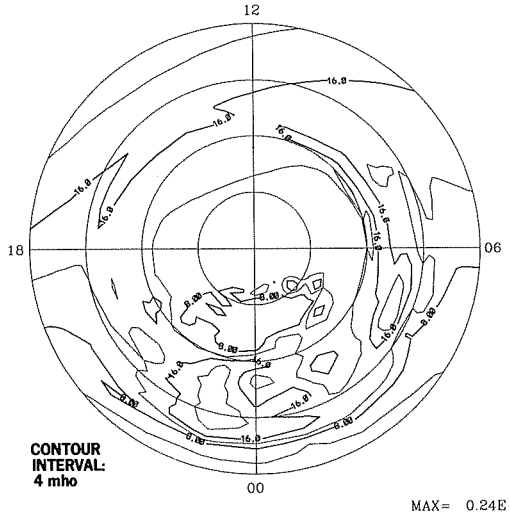

MAX= 0.24E+02 mho

DMSP

PEDERSEN CONDUCTANCE

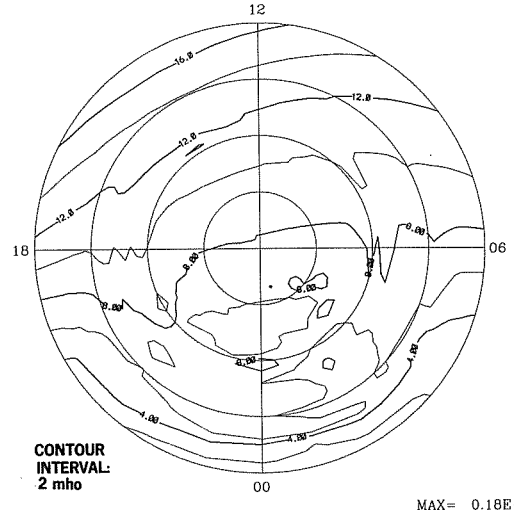

MAX= 0.18E+02 mho

ELECTRIC POTENTIAL

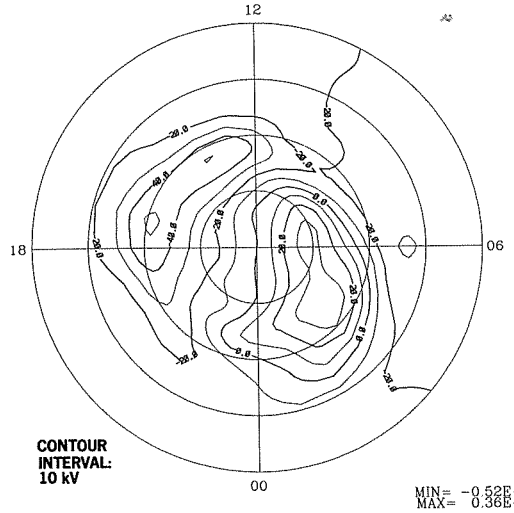

MIN= -0.52E+02 kV
MAX= 0.36E+02 kV

IONOSPHERIC CURRENT VECTORS

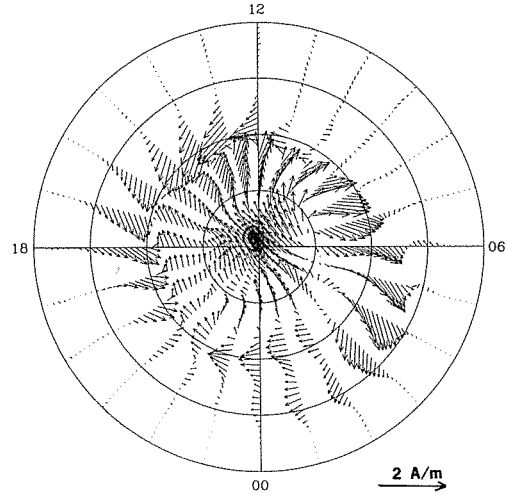

FIELD-ALIGNED CURRENT

23 JUL 1983
2015-30 UT

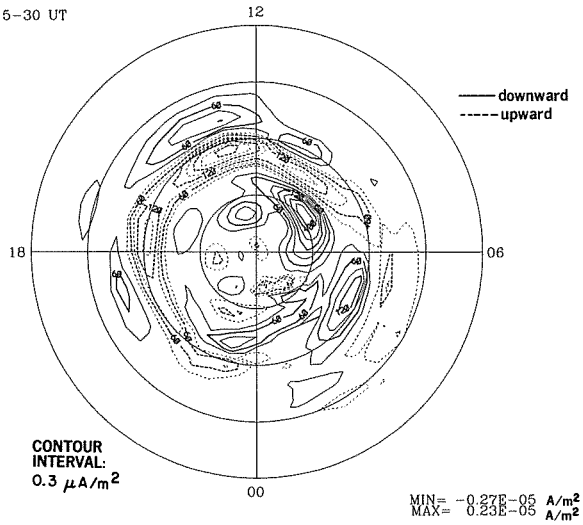

MIN= -0.27E-05 A/m²
MAX= 0.23E-05 A/m²

JOULE HEATING RATE

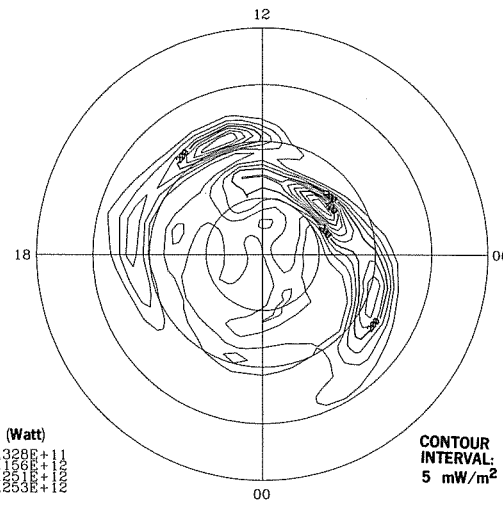

MAX= 0.53E-01 W/m²

HALL CURRENT VECTORS

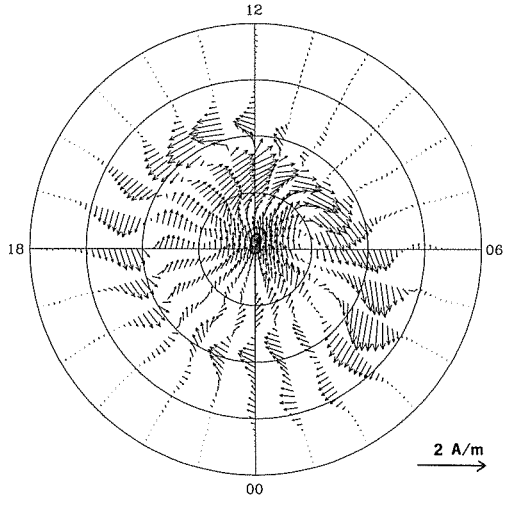

PEDERSEN CURRENT VECTORS

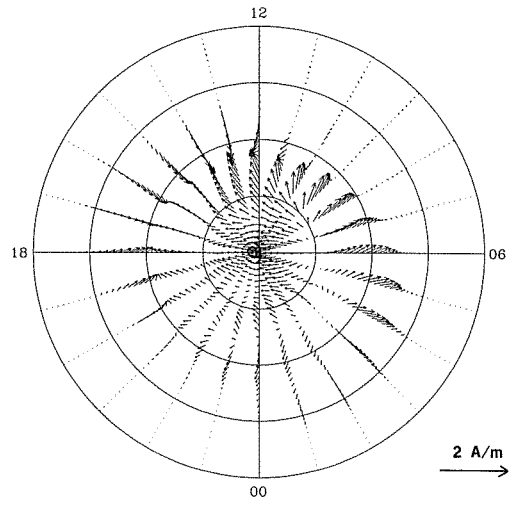

FIELD-ALIGNED HALL CURRENT

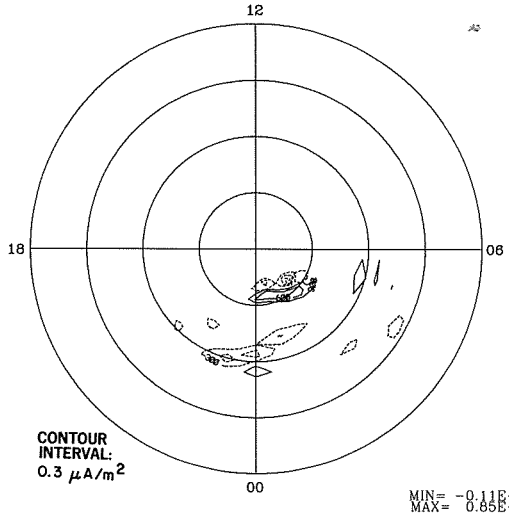

MIN= -0.11E-05 A/m²
MAX= 0.85E-06 A/m²

FIELD-ALIGNED PEDERSEN CURRENT

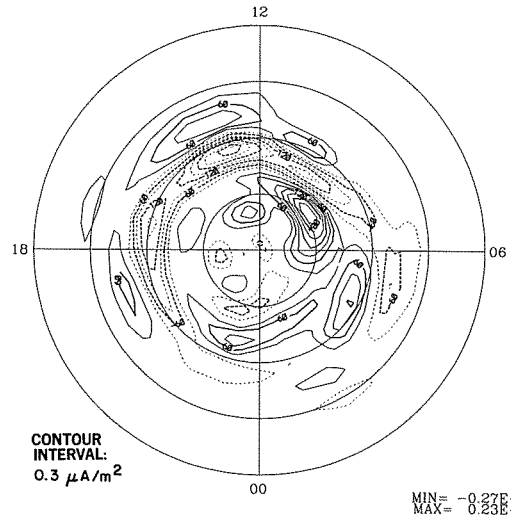

MIN= -0.27E-05 A/m²
MAX= 0.23E-05 A/m²

EQUIVALENT CURRENT VECTORS

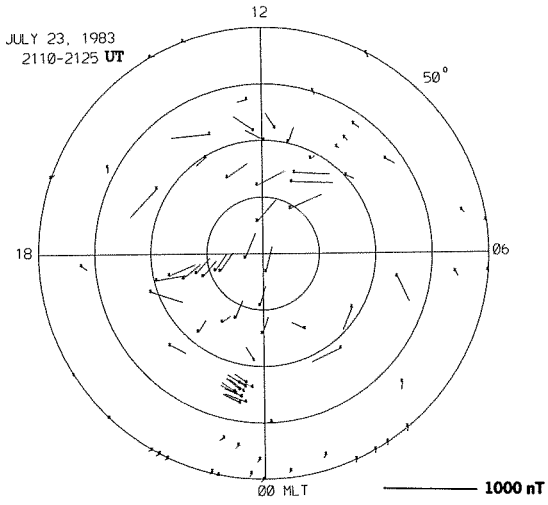

EQUIVALENT CURRENT SYSTEM

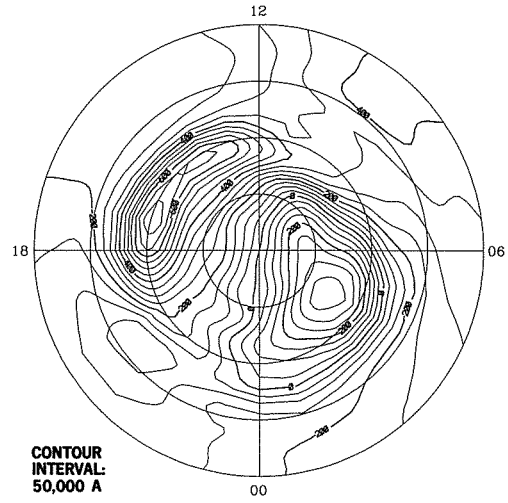

HALL CONDUCTANCE

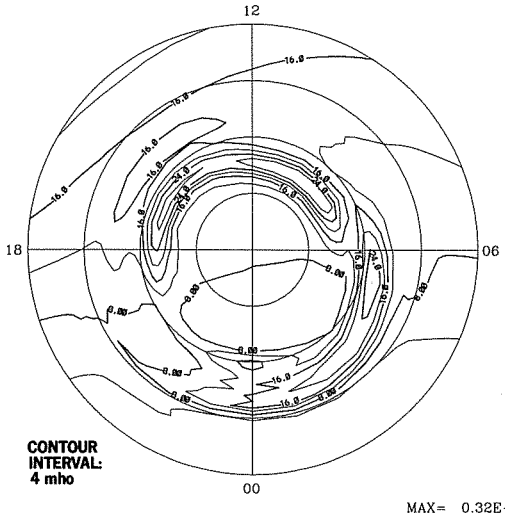

MAX= 0.32E+02 **mho**

PEDERSEN CONDUCTANCE

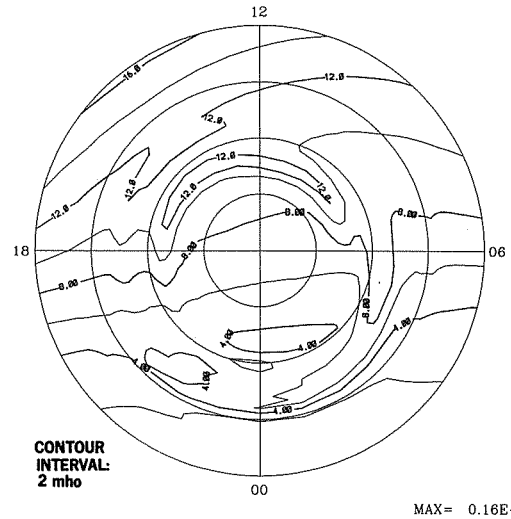

MAX= 0.16E+02 **mho**

ELECTRIC POTENTIAL

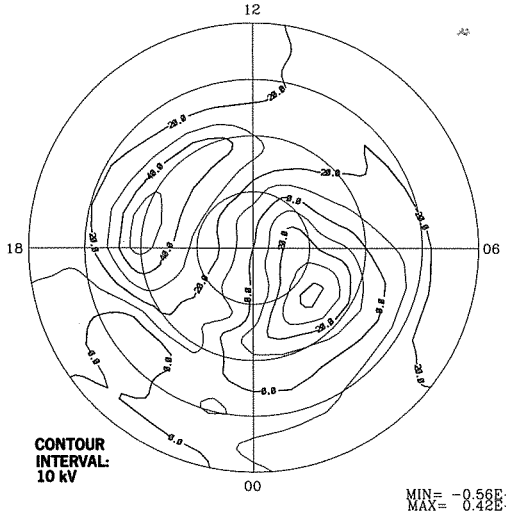

MIN= -0.56E+02 **kV**
MAX= 0.42E+02 **kV**

IONOSPHERIC CURRENT VECTORS

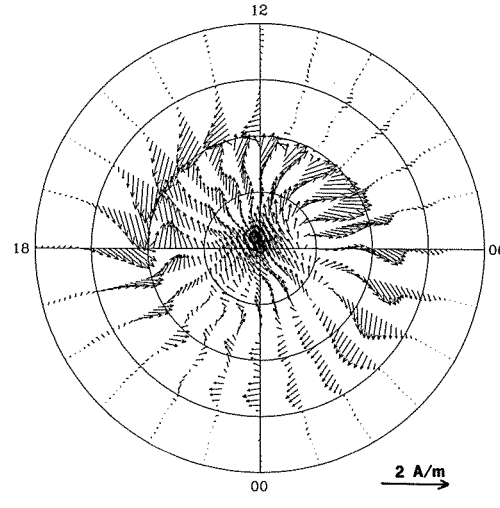

FIELD-ALIGNED CURRENT

23 JUL 1983
2110-25 UT

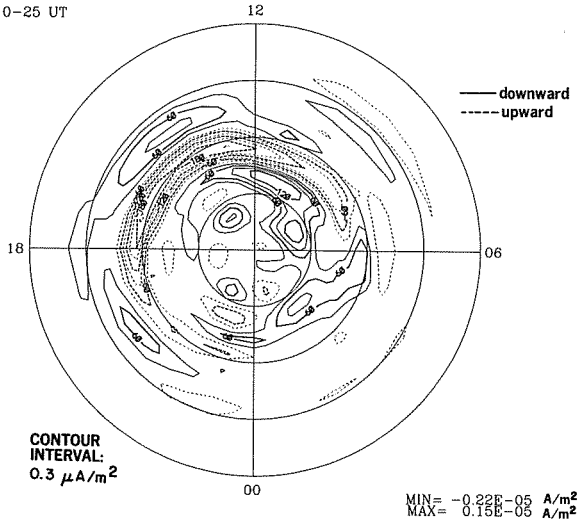

MIN= -0.22E-05 A/m²
MAX= 0.15E-05 A/m²

JOULE HEATING RATE

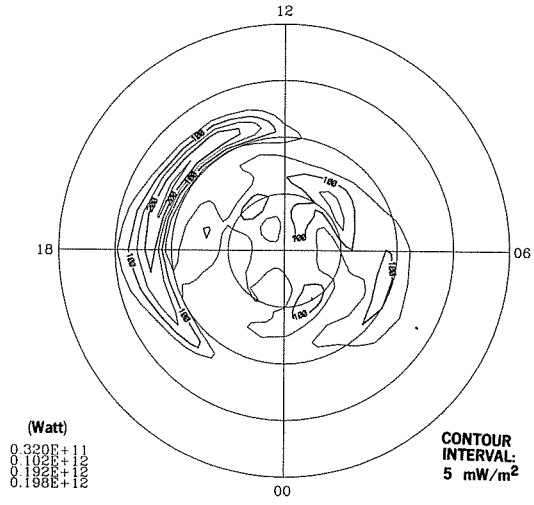

MAX= 0.26E-01 W/m²

HALL CURRENT VECTORS

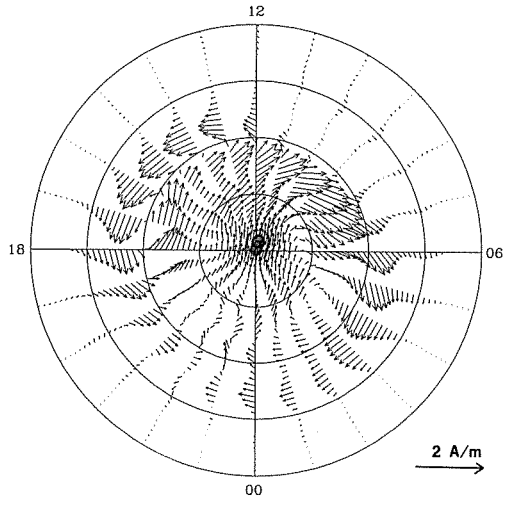

PEDERSEN CURRENT VECTORS

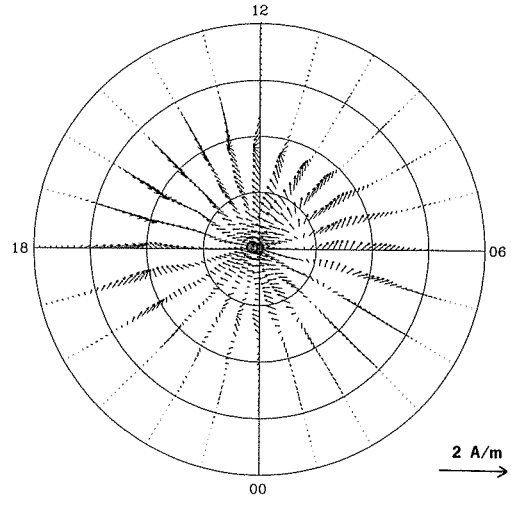

FIELD-ALIGNED HALL CURRENT

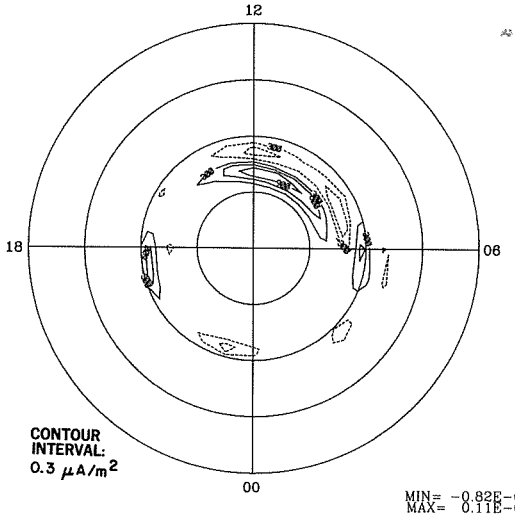

MIN= -0.82E-06 A/m²
MAX= 0.11E-05 A/m²

FIELD-ALIGNED PEDERSEN CURRENT

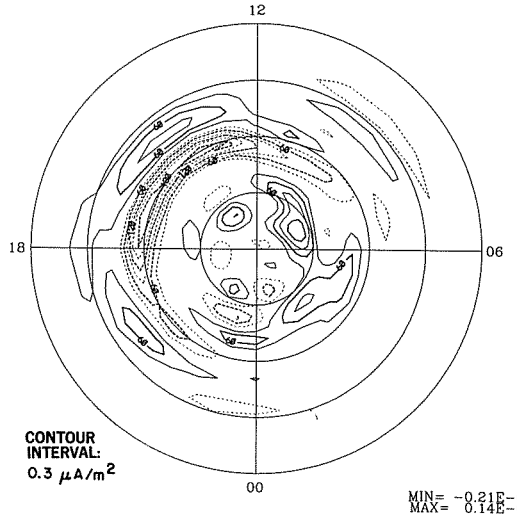

MIN= -0.21E-05 A/m²
MAX= 0.14E-05 A/m²

EQUIVALENT CURRENT VECTORS

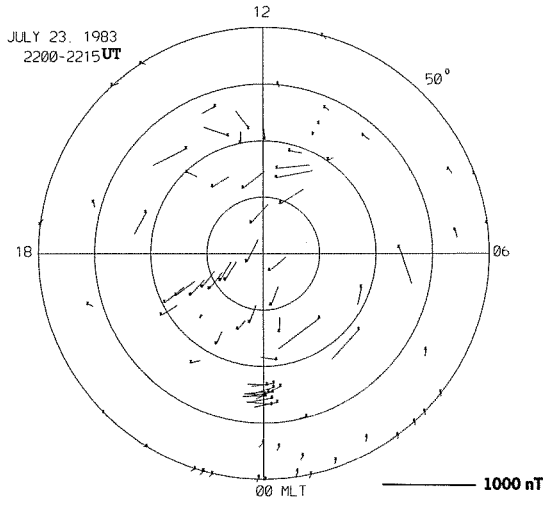

EQUIVALENT CURRENT SYSTEM

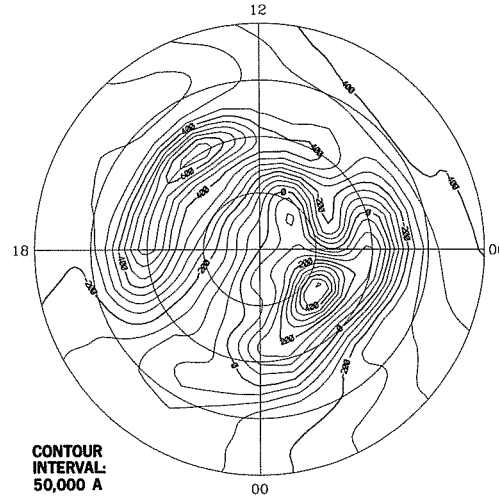

HALL CONDUCTANCE

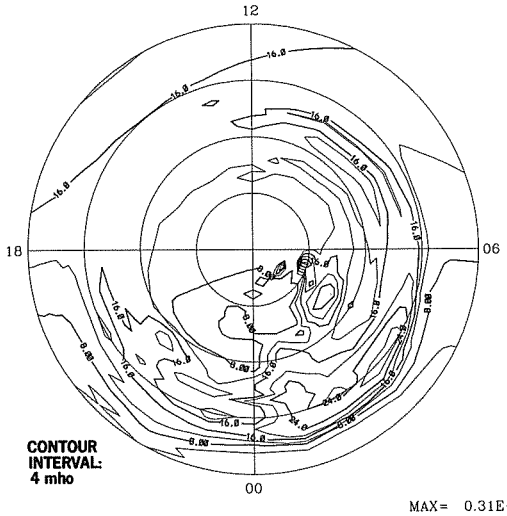

MAX= 0.31E+02 **mho**

DMSP

PEDERSEN CONDUCTANCE

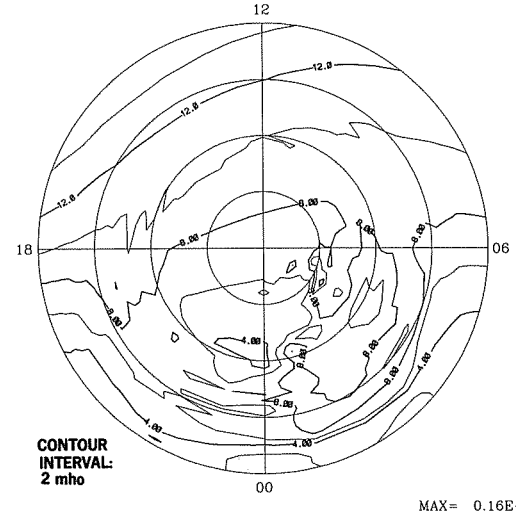

MAX= 0.16E+02 **mho**

ELECTRIC POTENTIAL

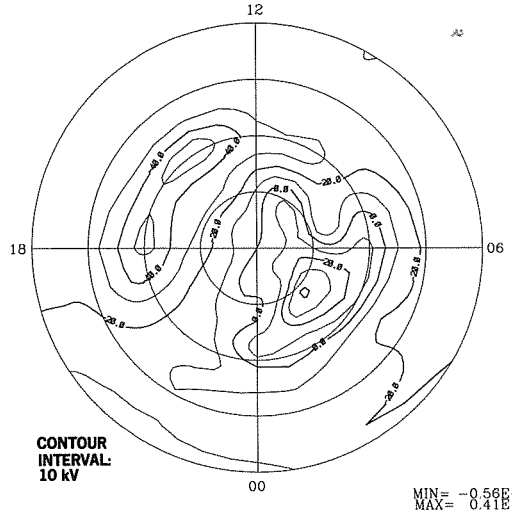

MIN= -0.56E+02 **kV**
MAX= 0.41E+02 **kV**

IONOSPHERIC CURRENT VECTORS

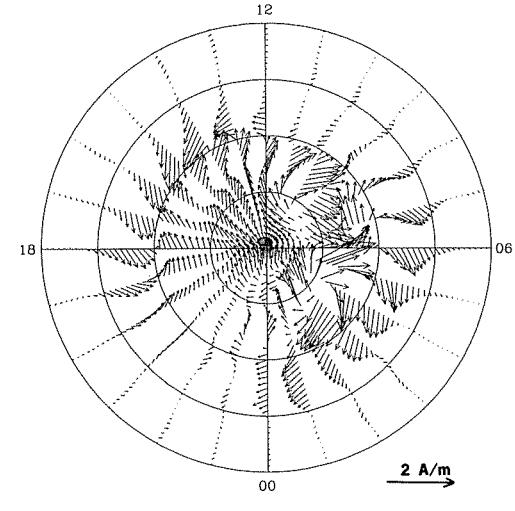

FIELD-ALIGNED CURRENT

23 JUL 1983
2200-15 UT

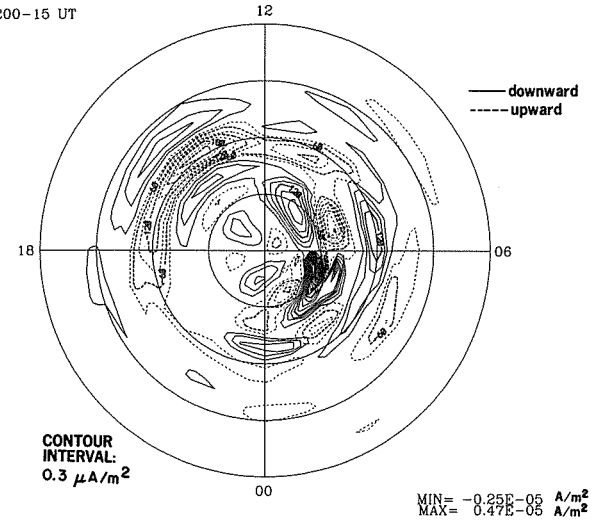

JOULE HEATING RATE

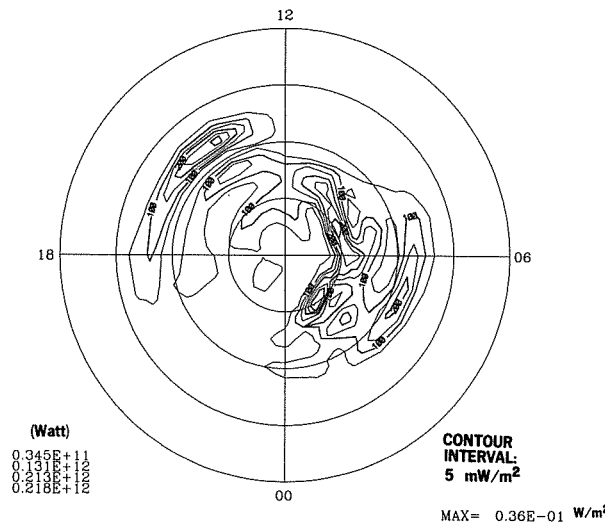

HALL CURRENT VECTORS

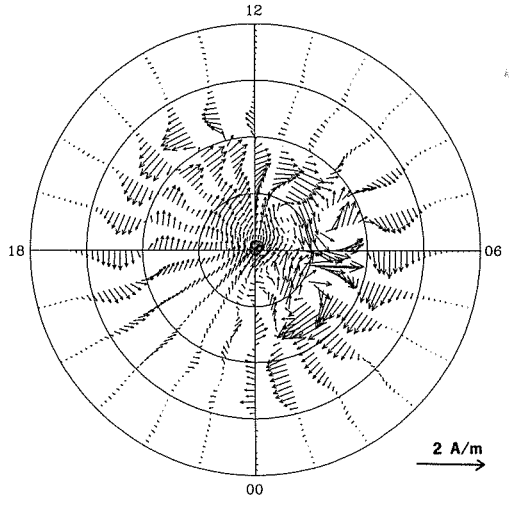

PEDERSEN CURRENT VECTORS

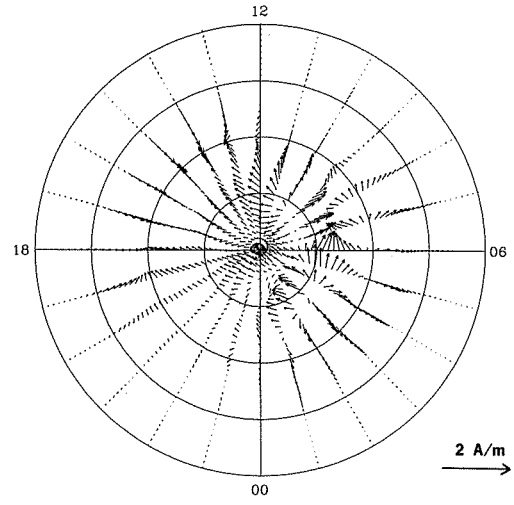

FIELD-ALIGNED HALL CURRENT

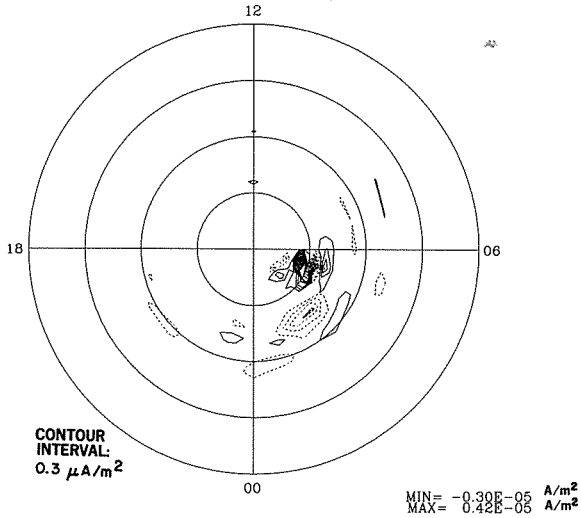

FIELD-ALIGNED PEDERSEN CURRENT

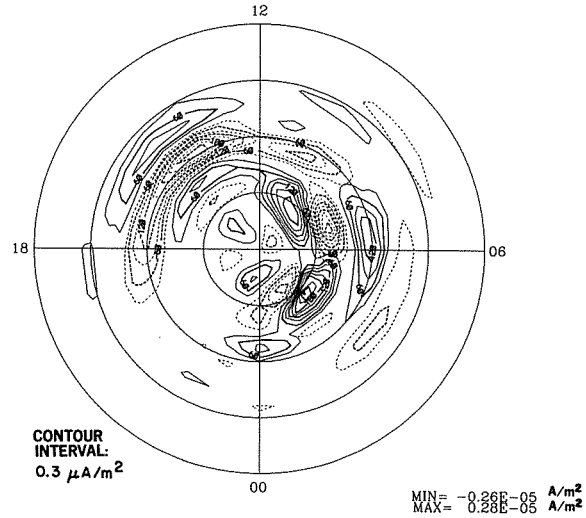

EQUIVALENT CURRENT VECTORS

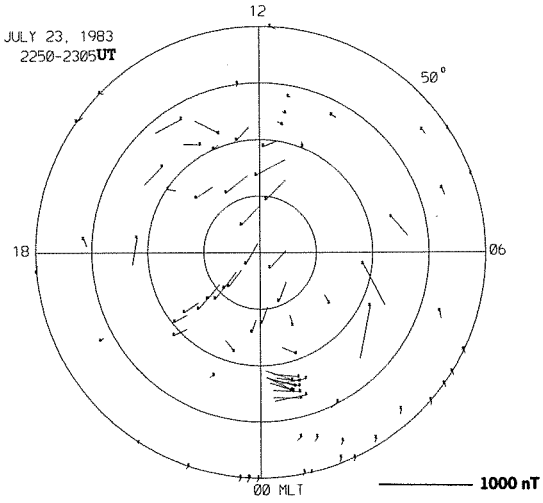

EQUIVALENT CURRENT SYSTEM

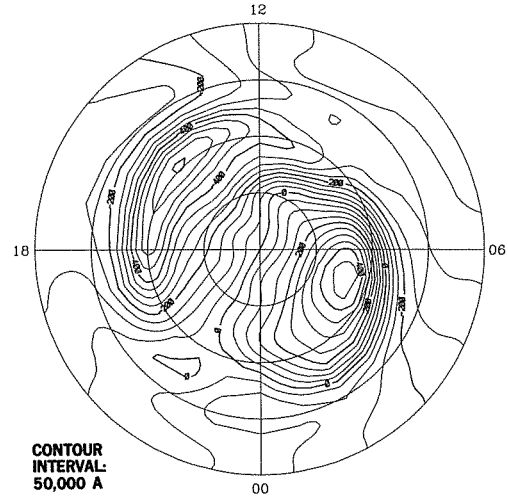

HALL CONDUCTANCE

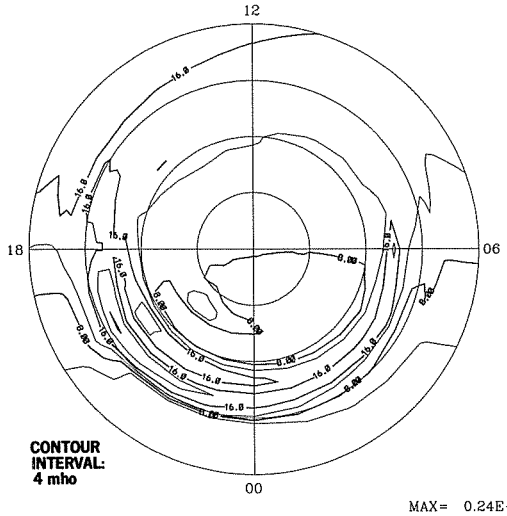

MAX= 0.24E+02 **mho**

DMSP

PEDERSEN CONDUCTANCE

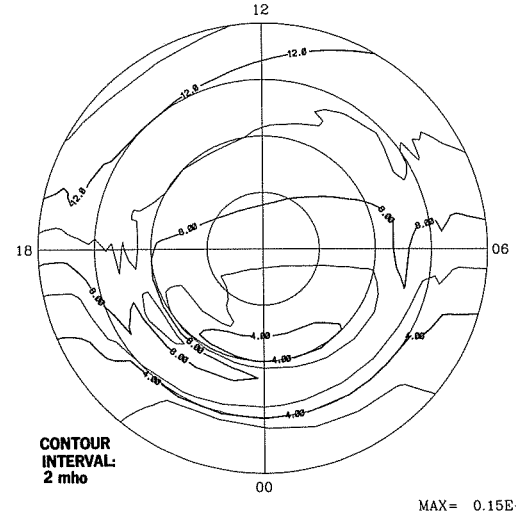

MAX= 0.15E+02 **mho**

ELECTRIC POTENTIAL

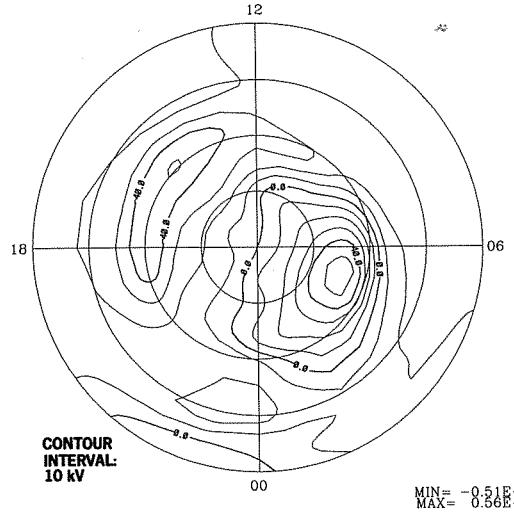

MIN= -0.51E+02 **kV**
MAX= 0.56E+02 **kV**

IONOSPHERIC CURRENT VECTORS

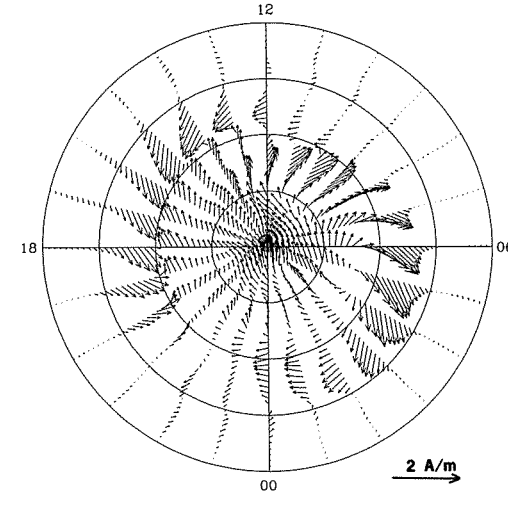

FIELD-ALIGNED CURRENT

23 JUL 1983
2250-2305 UT

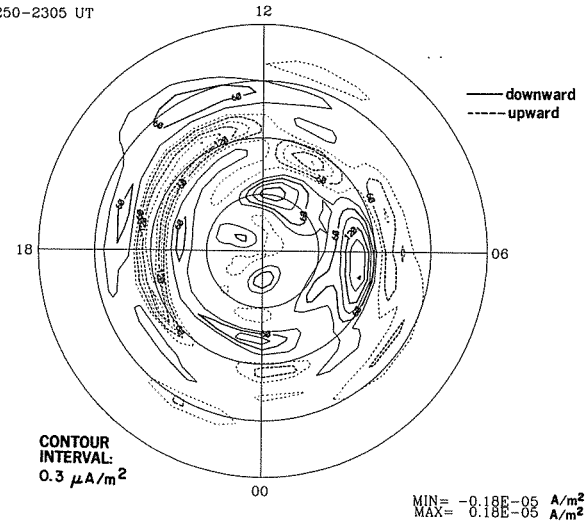

JOULE HEATING RATE

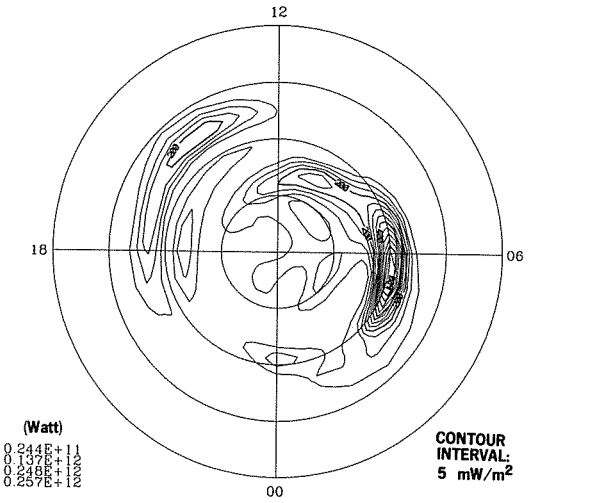

MAX= 0.70E-01 W/m²

HALL CURRENT VECTORS

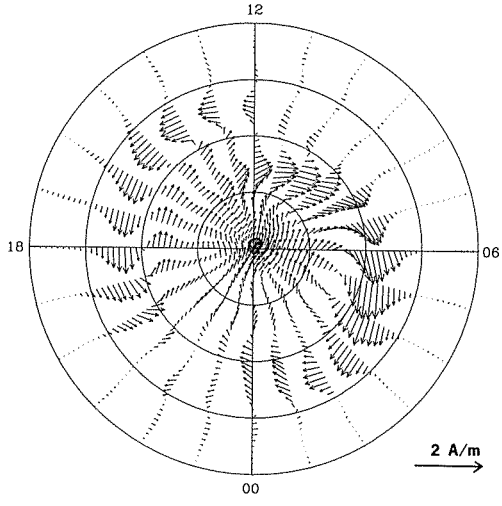

PEDERSEN CURRENT VECTORS

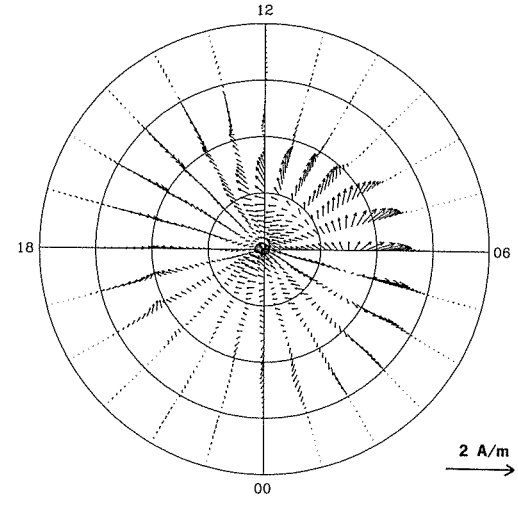

FIELD-ALIGNED HALL CURRENT

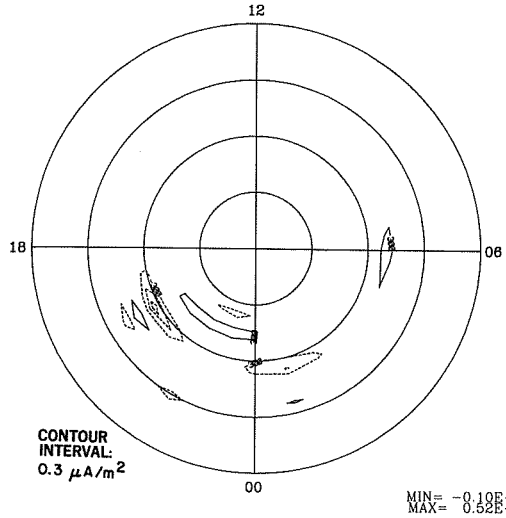

MIN= -0.10E-05 A/m²
MAX= 0.52E-06 A/m²

FIELD-ALIGNED PEDERSEN CURRENT

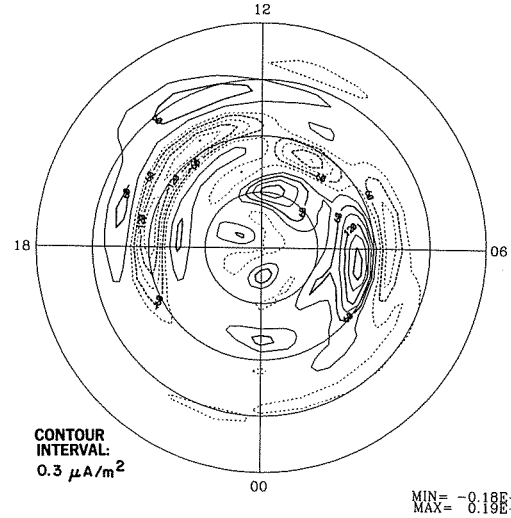

MIN= -0.18E-05 A/m²
MAX= 0.19E-05 A/m²

EQUIVALENT CURRENT VECTORS

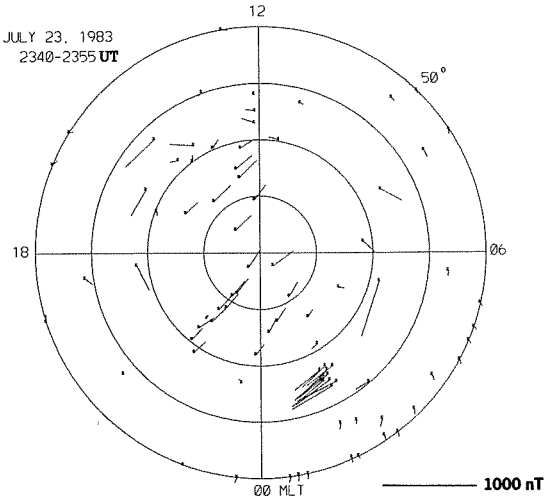

EQUIVALENT CURRENT SYSTEM

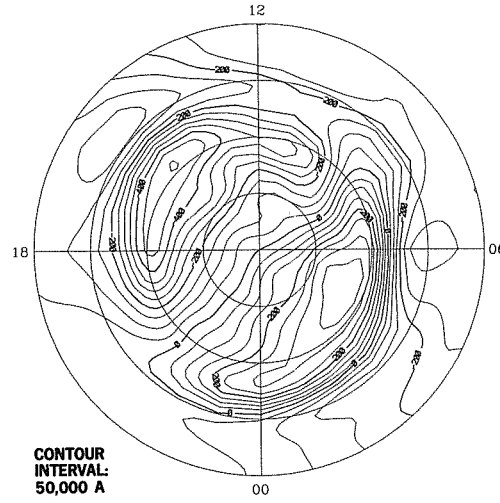

HALL CONDUCTANCE

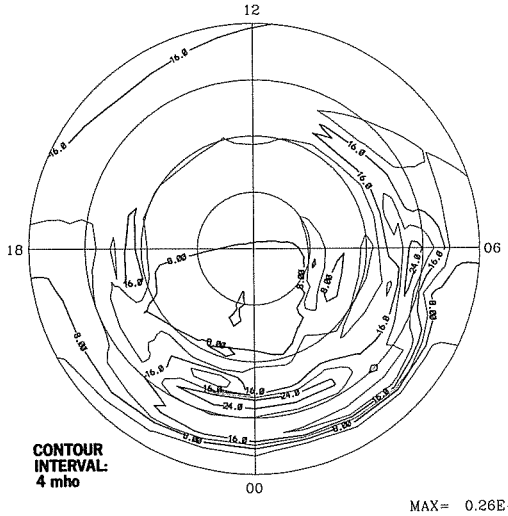

MAX= 0.26E+02 **mho**

DMSP

PEDERSEN CONDUCTANCE

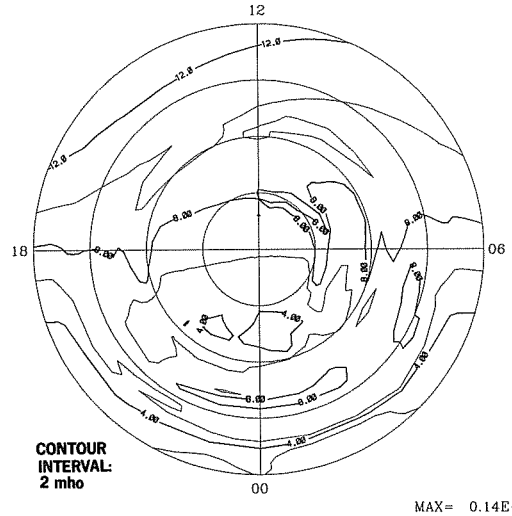

MAX= 0.14E+02 **mho**

ELECTRIC POTENTIAL

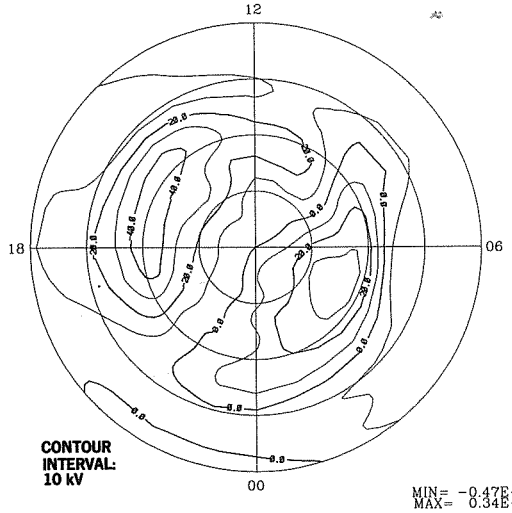

MIN= -0.47E+02 **kV**
MAX= 0.34E+02 **kV**

IONOSPHERIC CURRENT VECTORS

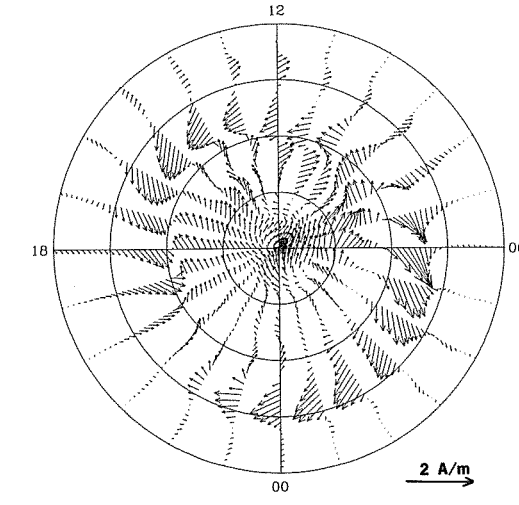

FIELD-ALIGNED CURRENT

23 JUL 1983
2340-55 UT

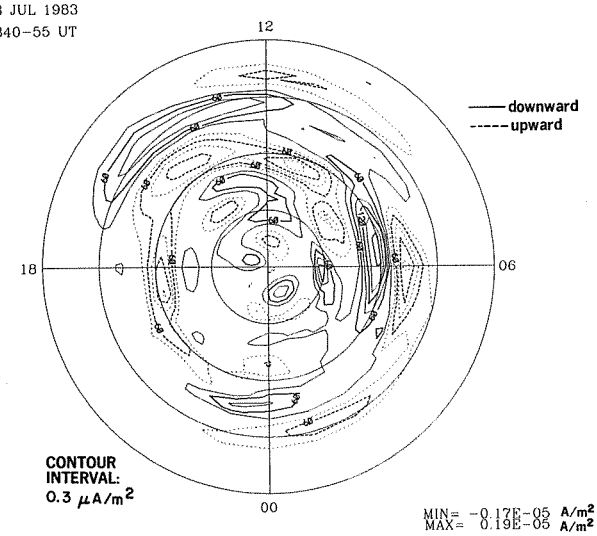

MIN= -0.17E-05 A/m²
MAX= 0.19E-05 A/m²

JOULE HEATING RATE

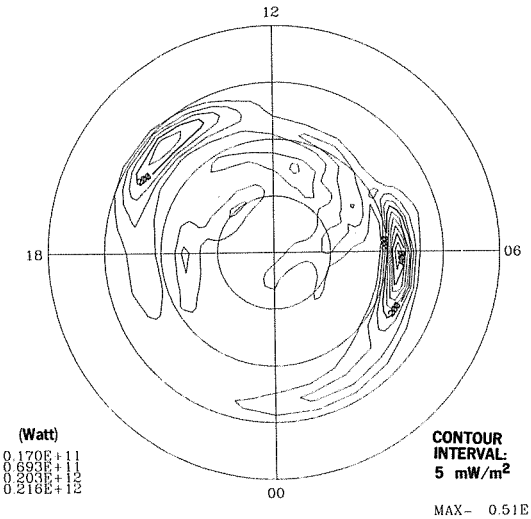

MAX- 0.51E-01 W/m²

HALL CURRENT VECTORS

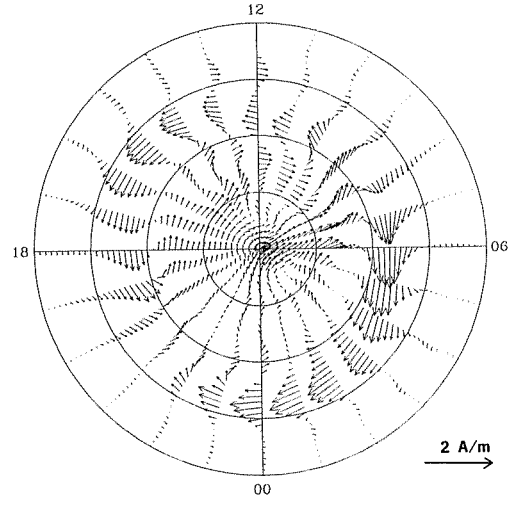

PEDERSEN CURRENT VECTORS

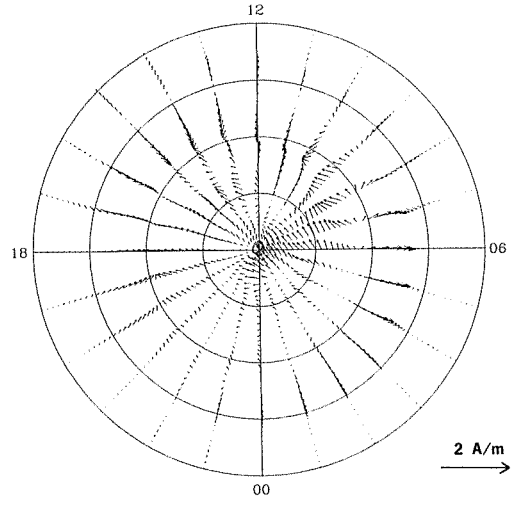

FIELD-ALIGNED HALL CURRENT

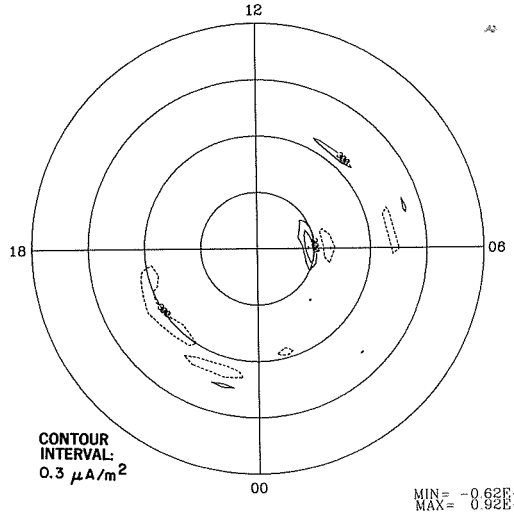

MIN= -0.62E-06 A/m²
MAX= 0.92E-06 A/m²

FIELD-ALIGNED PEDERSEN CURRENT

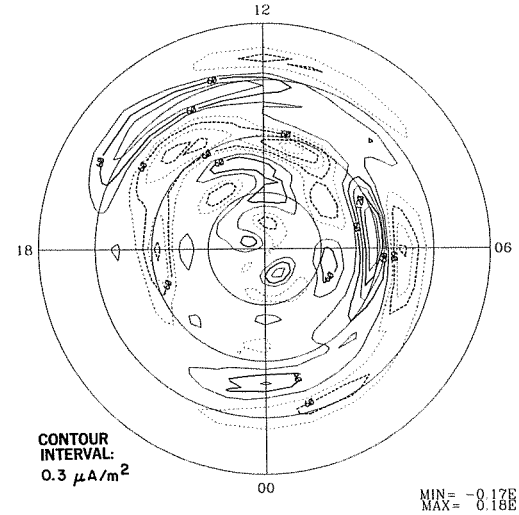

MIN= -0.17E-05 A/m²
MAX= 0.18E-05 A/m²

EQUIVALENT CURRENT VECTORS

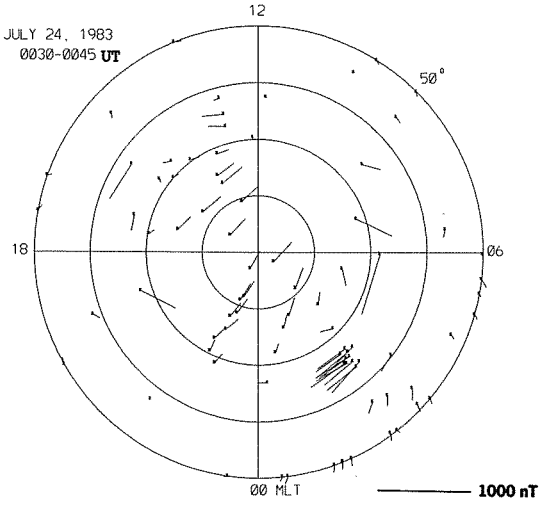

EQUIVALENT CURRENT SYSTEM

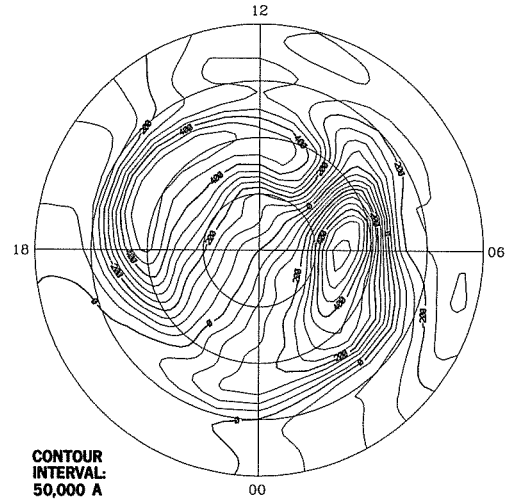

HALL CONDUCTANCE

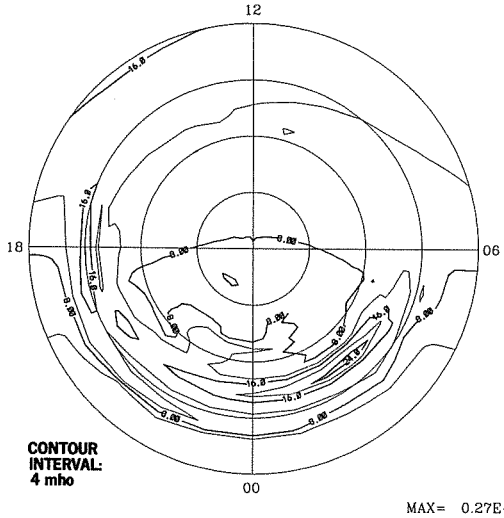

MAX= 0.27E+02 mho

DMSP

PEDERSEN CONDUCTANCE

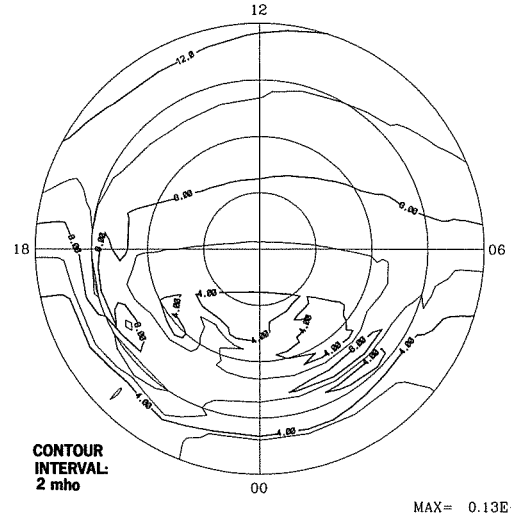

MAX= 0.13E+02 mho

ELECTRIC POTENTIAL

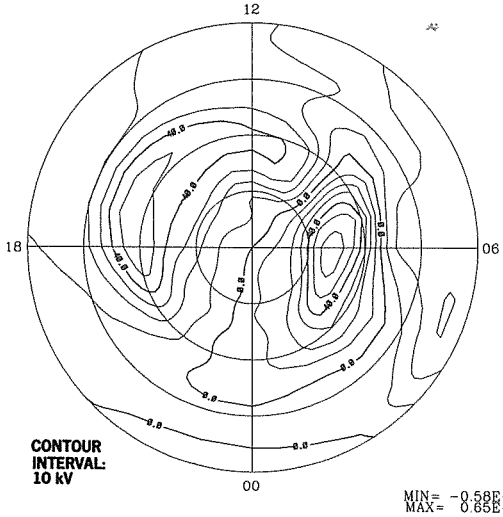

MIN= -0.58E+02 kV
MAX= 0.65E+02 kV

IONOSPHERIC CURRENT VECTORS

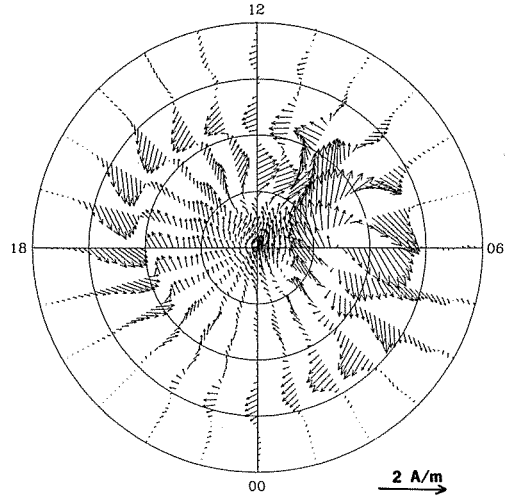

FIELD-ALIGNED CURRENT

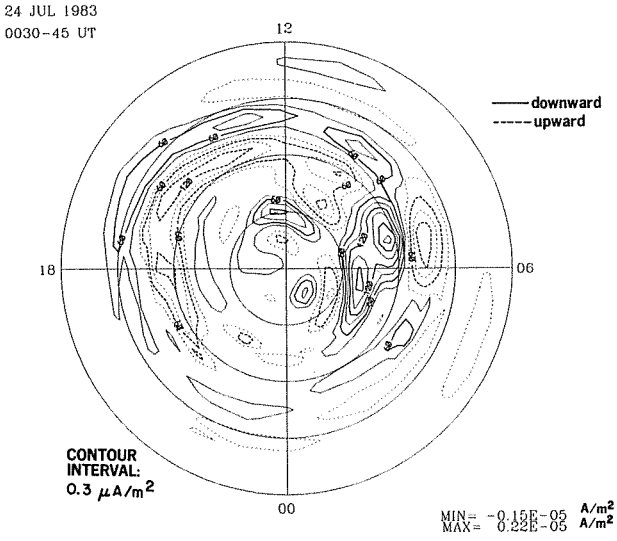

JOULE HEATING RATE

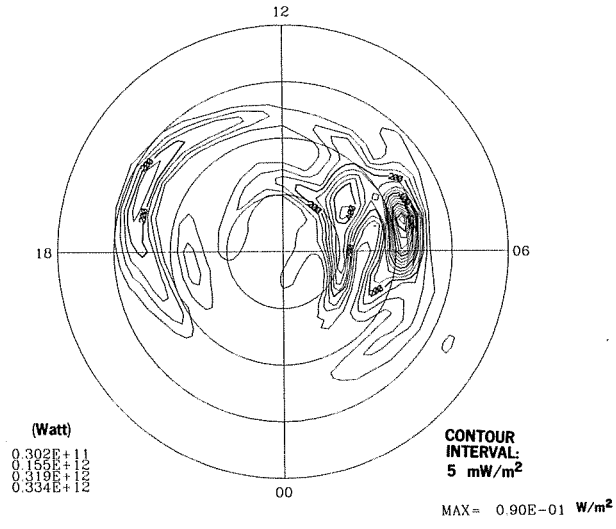

HALL CURRENT VECTORS

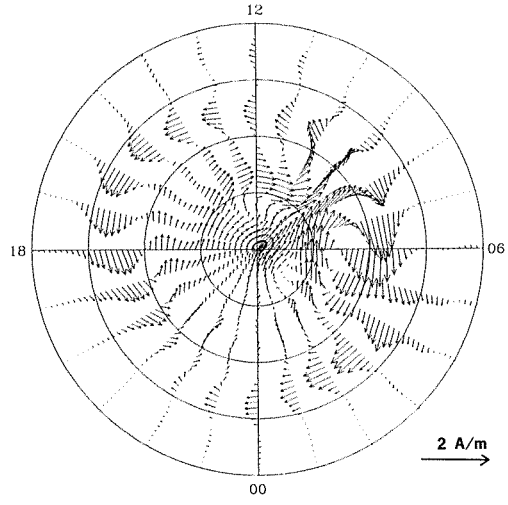

PEDERSEN CURRENT VECTORS

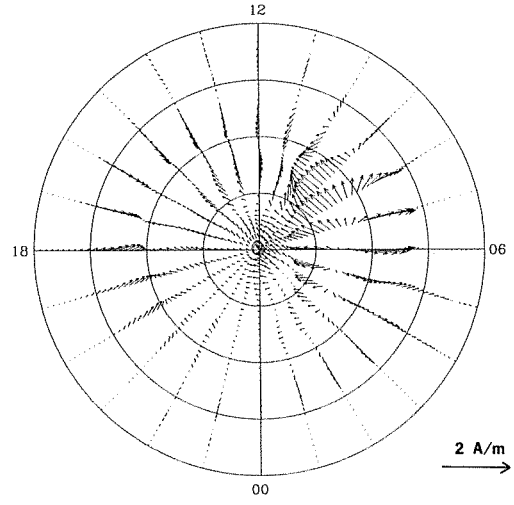

FIELD-ALIGNED HALL CURRENT

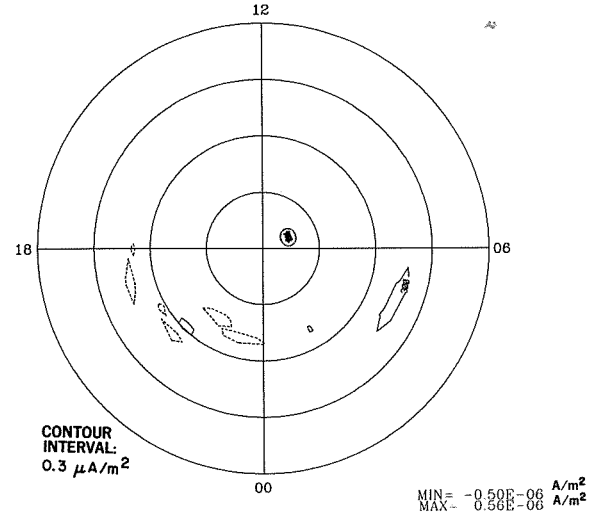

FIELD-ALIGNED PEDERSEN CURRENT

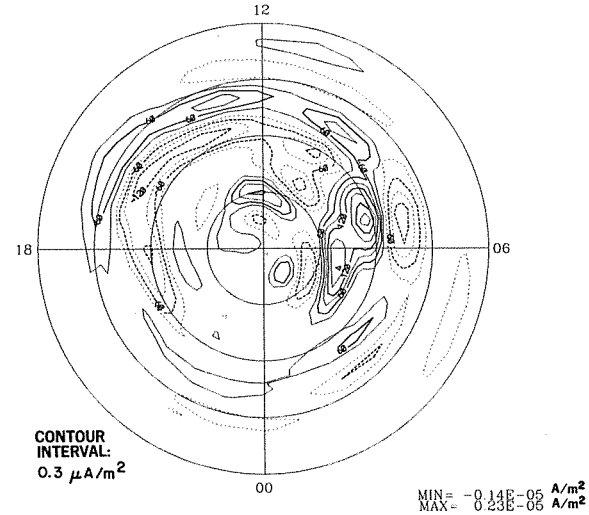

EQUIVALENT CURRENT VECTORS

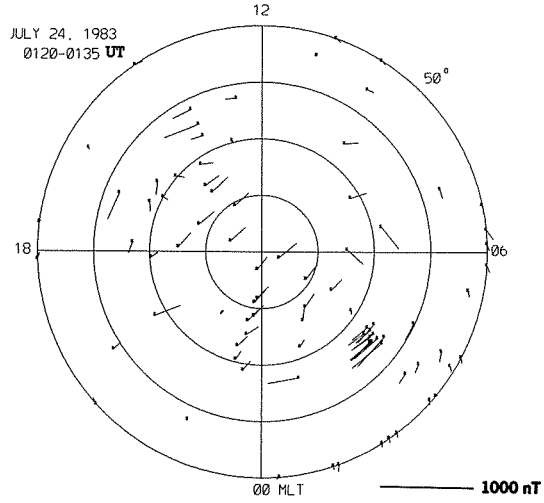

EQUIVALENT CURRENT SYSTEM

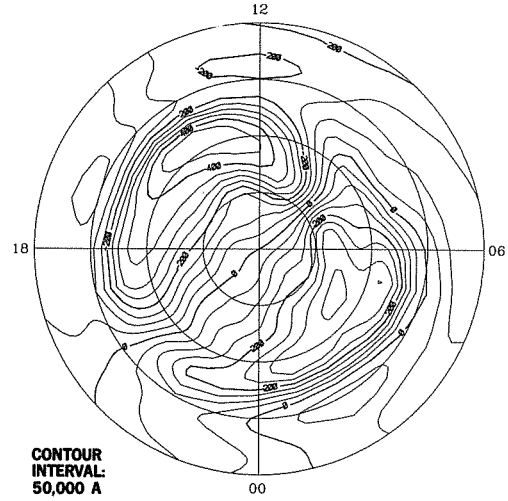

HALL CONDUCTANCE

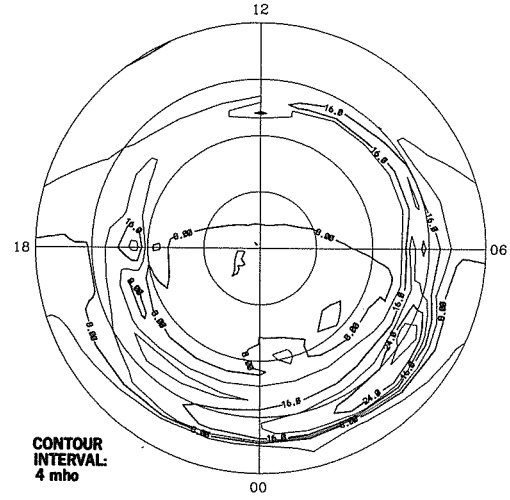

MAX= 0.32E+02 **mho**

DMSP

PEDERSEN CONDUCTANCE

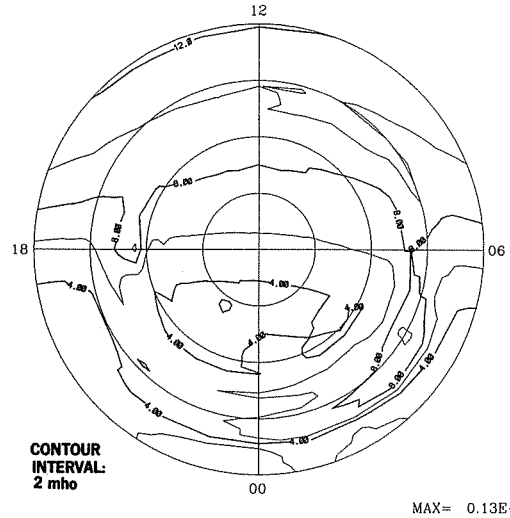

MAX= 0.13E+02 **mho**

ELECTRIC POTENTIAL

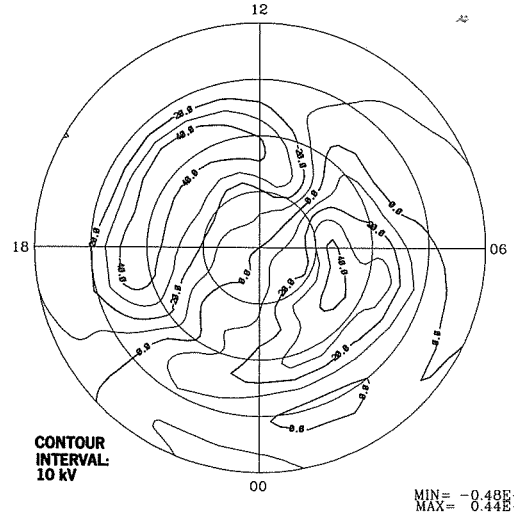

MIN= −0.48E+02 **kV**
MAX= 0.44E+02 **kV**

IONOSPHERIC CURRENT VECTORS

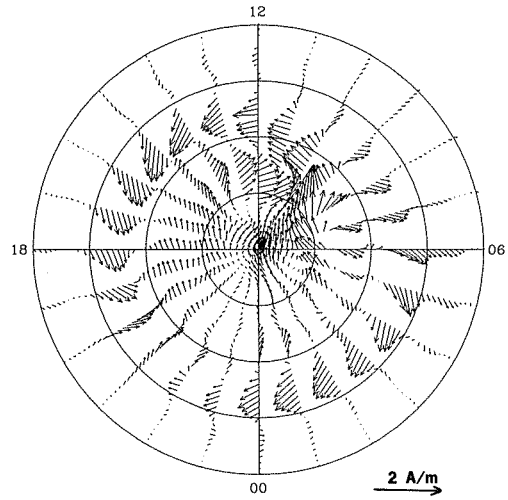

FIELD-ALIGNED CURRENT

24 JUL 1983
0120-35 UT

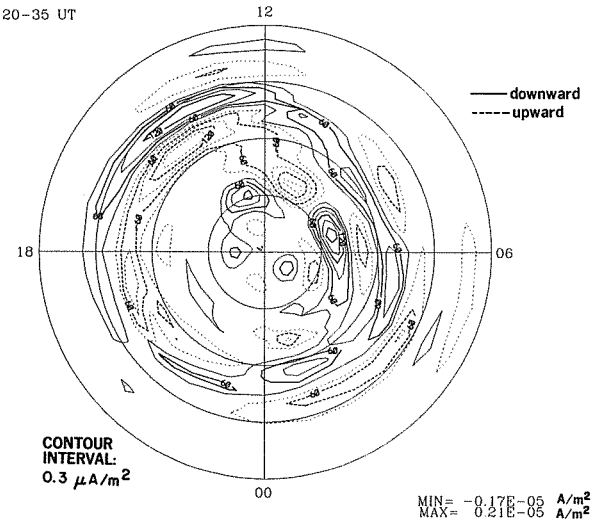

MIN= -0.17E-05 A/m²
MAX= 0.21E-05 A/m²

JOULE HEATING RATE

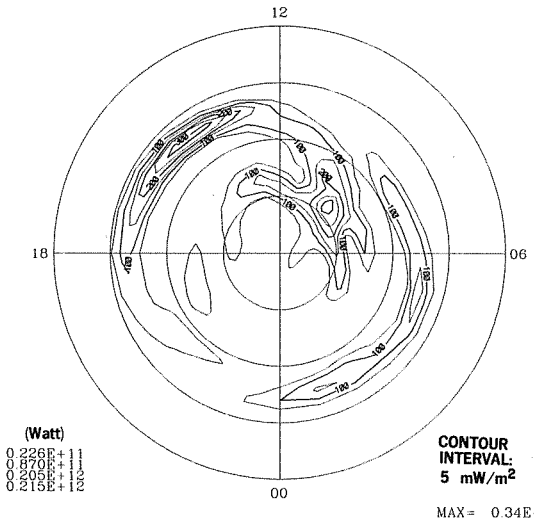

MAX= 0.34E-01 W/m²

HALL CURRENT VECTORS

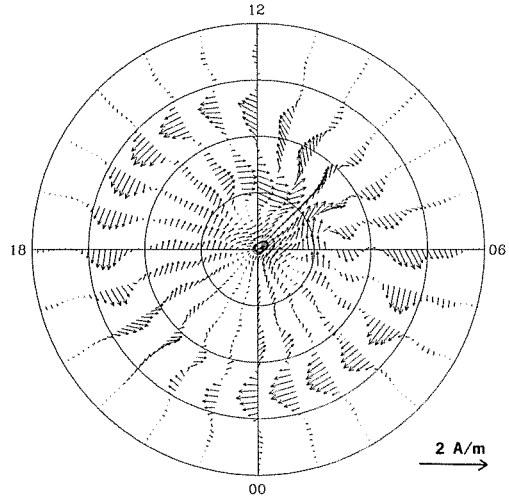

PEDERSEN CURRENT VECTORS

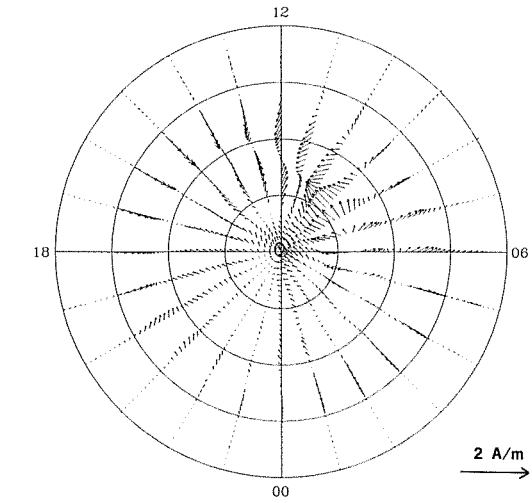

FIELD-ALIGNED HALL CURRENT

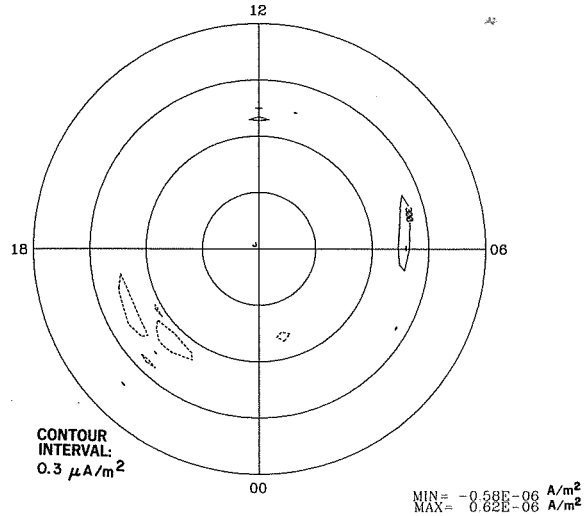

MIN= -0.58E-06 A/m²
MAX= 0.62E-06 A/m²

FIELD-ALIGNED PEDERSEN CURRENT

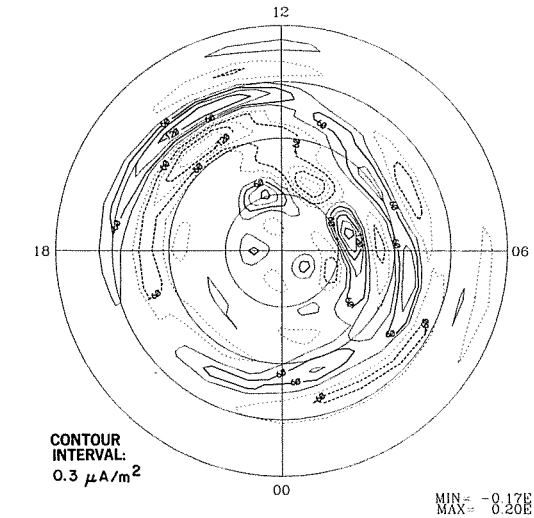

MIN= -0.17E-05 A/m²
MAX= 0.20E-05 A/m²

EQUIVALENT CURRENT VECTORS

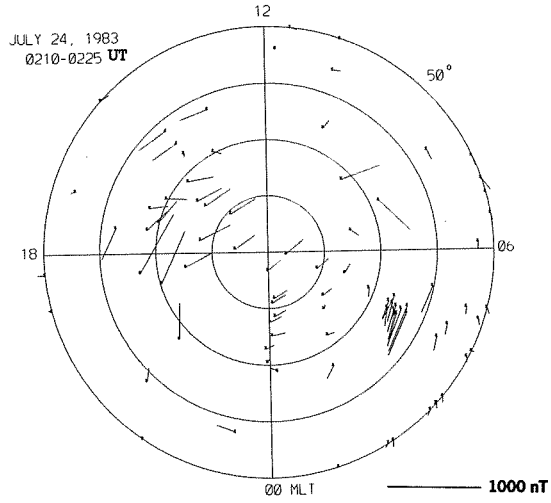

EQUIVALENT CURRENT SYSTEM

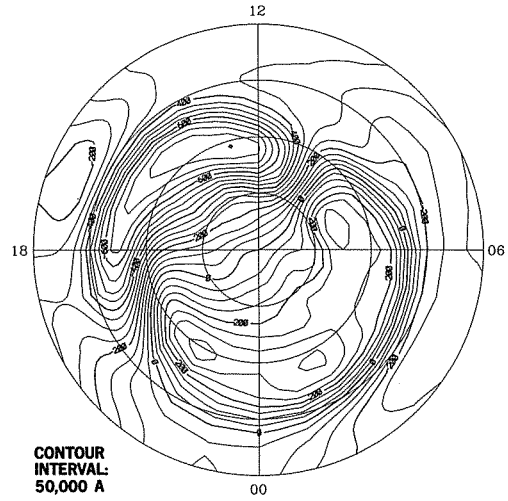

HALL CONDUCTANCE

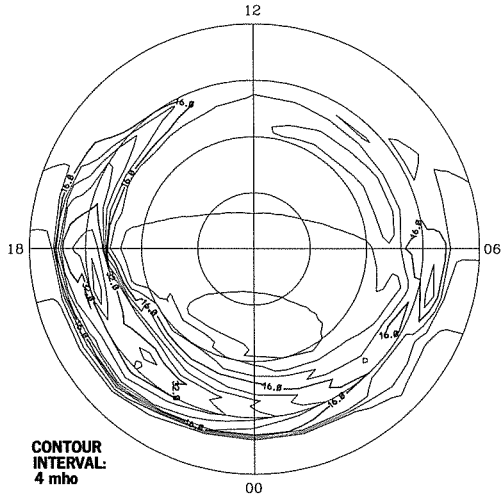

MAX= 0.44E+02 **mho**

DMSP

PEDERSEN CONDUCTANCE

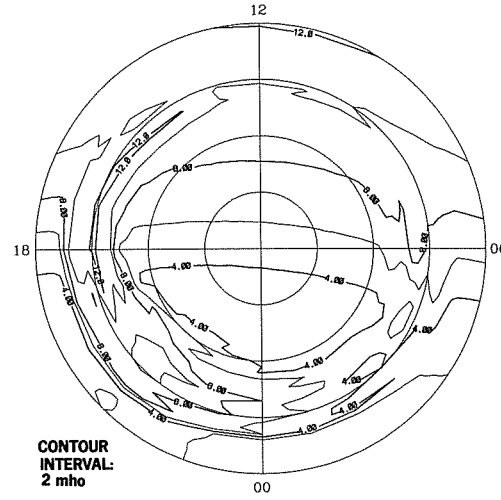

MAX= 0.13E+02 **mho**

ELECTRIC POTENTIAL

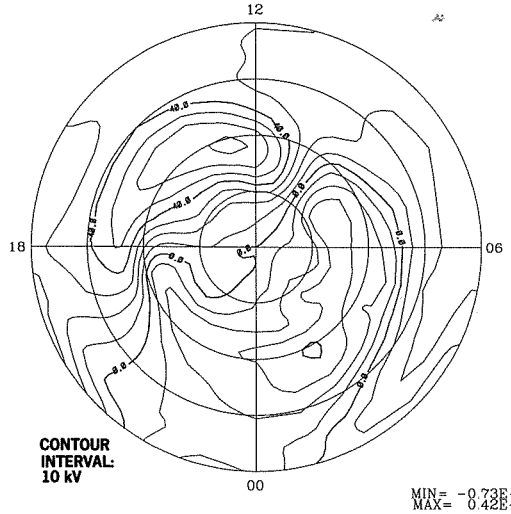

MIN= -0.73E+02 **kV**
MAX= 0.42E+02 **kV**

IONOSPHERIC CURRENT VECTORS

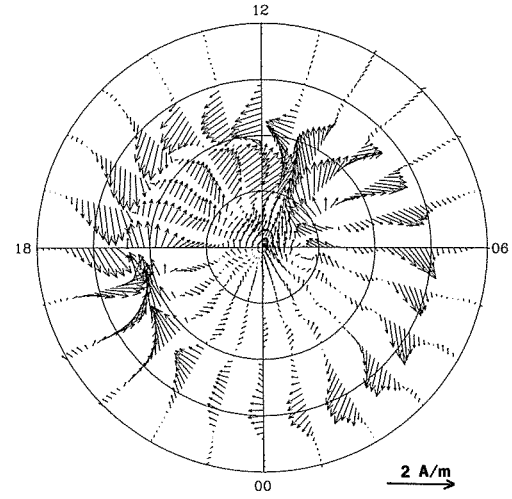

FIELD-ALIGNED CURRENT

24 JUL 1983
0210-25 UT

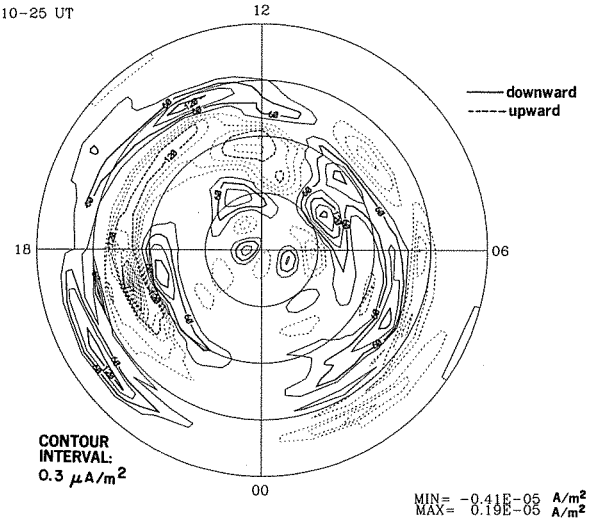

MIN= -0.41E-05 A/m²
MAX= 0.19E-05 A/m²

JOULE HEATING RATE

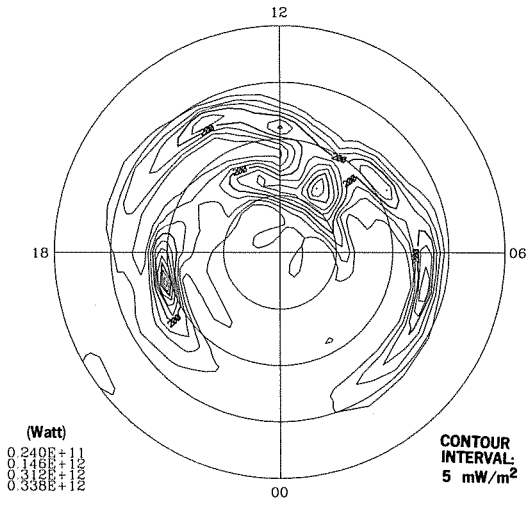

MAX= 0.55E-01 W/m²

HALL CURRENT VECTORS

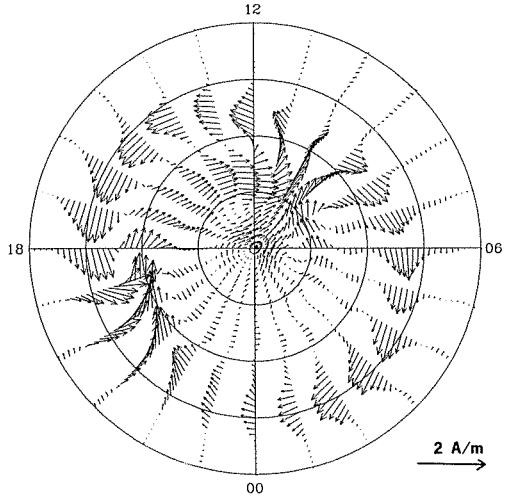

PEDERSEN CURRENT VECTORS

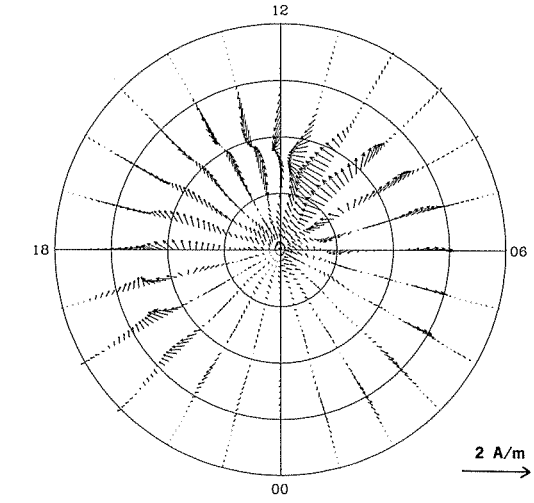

FIELD-ALIGNED HALL CURRENT

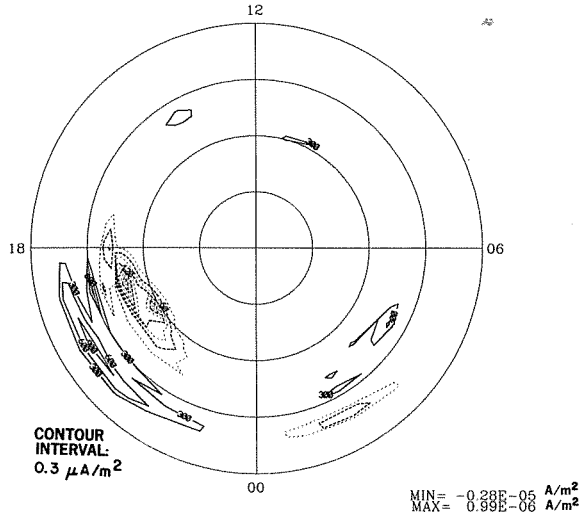

MIN= -0.28E-05 A/m²
MAX= 0.99E-06 A/m²

FIELD-ALIGNED PEDERSEN CURRENT

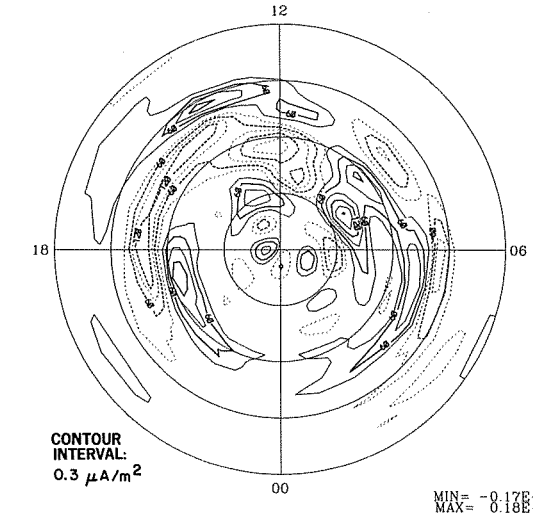

MIN= -0.17E-05 A/m²
MAX= 0.18E-05 A/m²

EQUIVALENT CURRENT VECTORS

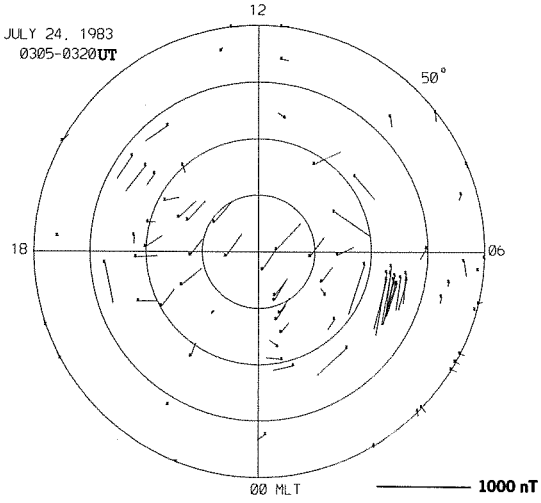

EQUIVALENT CURRENT SYSTEM

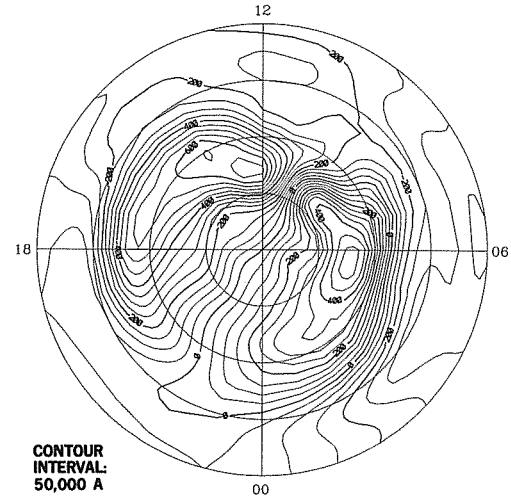

HALL CONDUCTANCE

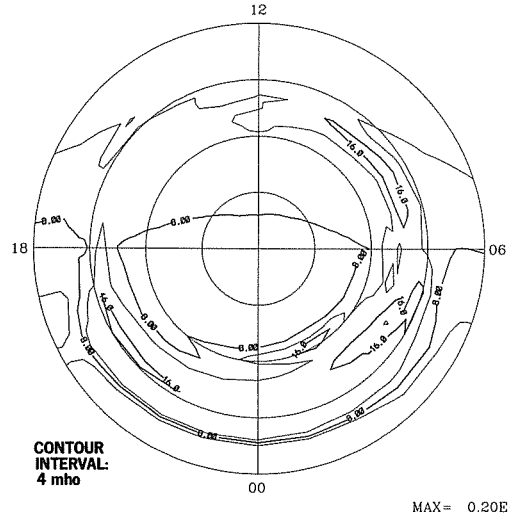

MAX= 0.20E+02 mho

DMSP

PEDERSEN CONDUCTANCE

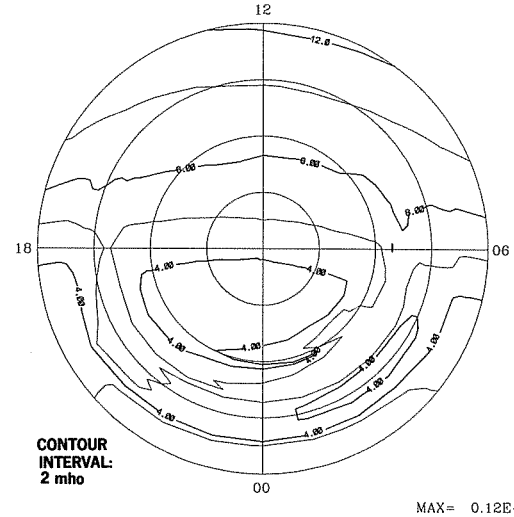

MAX= 0.12E+02 mho

ELECTRIC POTENTIAL

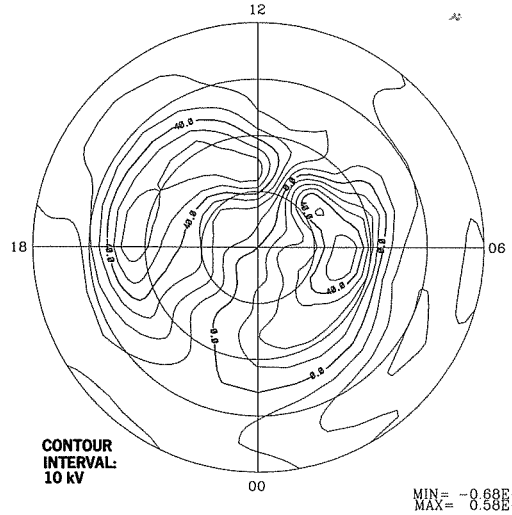

MIN= -0.68E+02 kV
MAX= 0.58E+02 kV

IONOSPHERIC CURRENT VECTORS

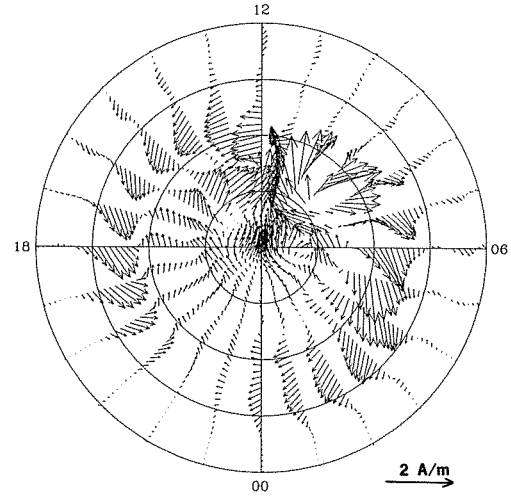

FIELD-ALIGNED CURRENT

24 JUL 1983
0305-20 UT

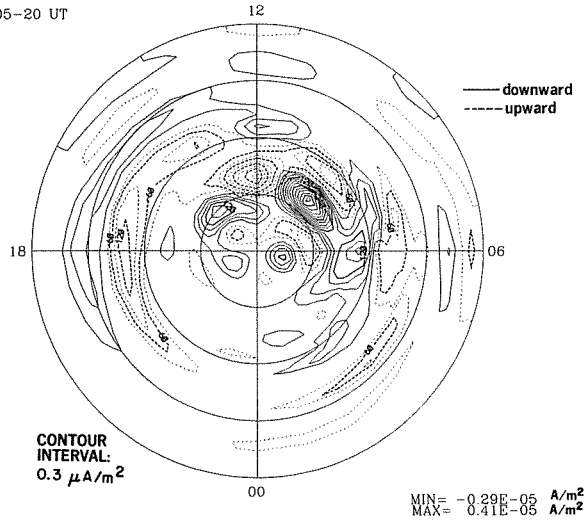

MIN= -0.29E-05 A/m²
MAX= 0.41E-05 A/m²

JOULE HEATING RATE

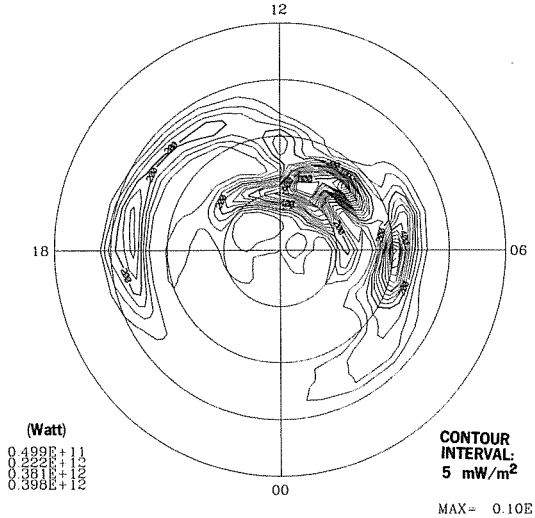

MAX= 0.10E+00 W/m²

HALL CURRENT VECTORS

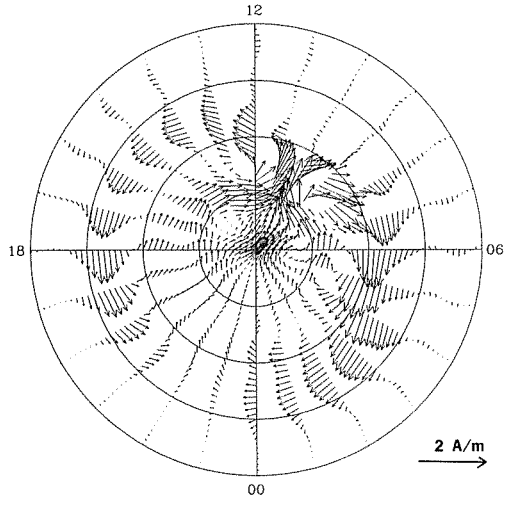

PEDERSEN CURRENT VECTORS

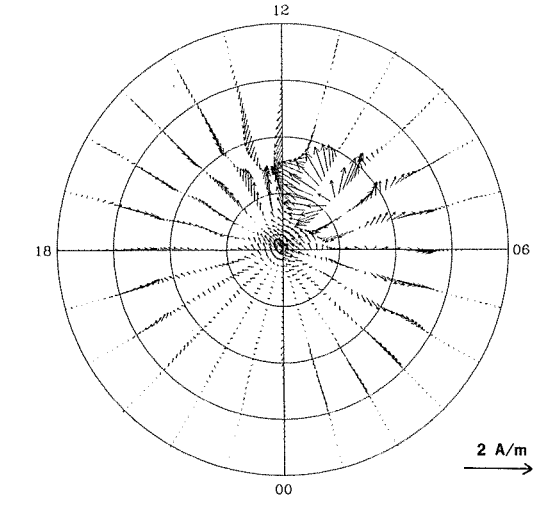

FIELD-ALIGNED HALL CURRENT

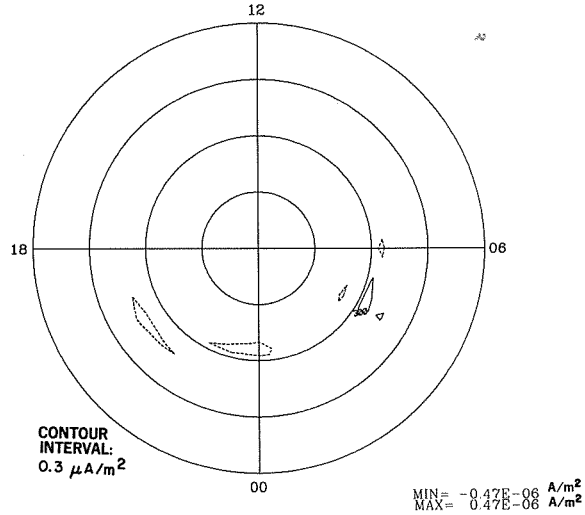

MIN= -0.47E-06 A/m²
MAX= 0.47E-06 A/m²

FIELD-ALIGNED PEDERSEN CURRENT

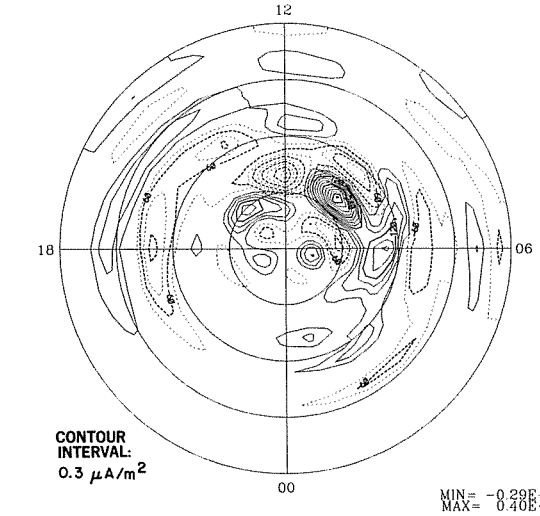

MIN= -0.29E-05 A/m²
MAX= 0.40E-05 A/m²

EQUIVALENT CURRENT VECTORS

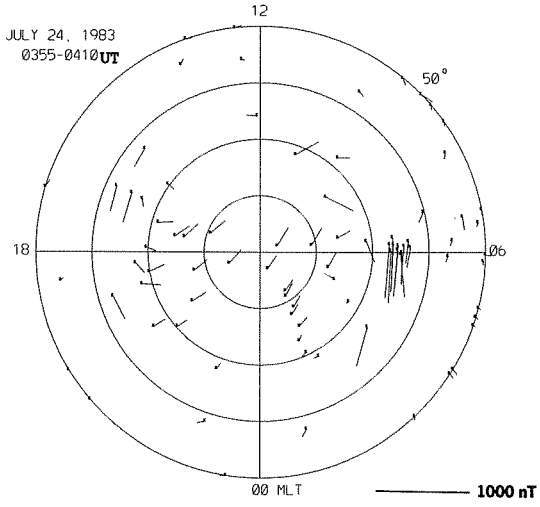

EQUIVALENT CURRENT SYSTEM

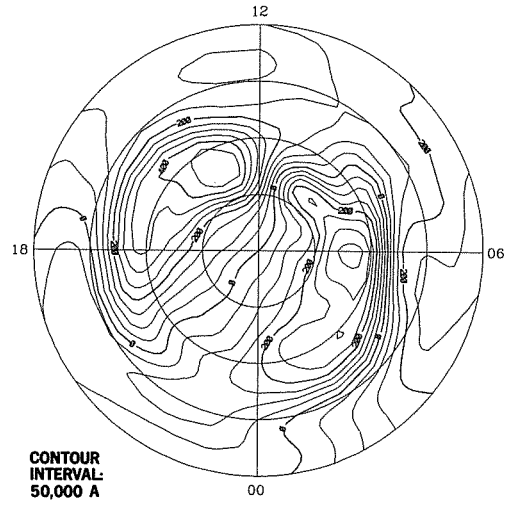

HALL CONDUCTANCE

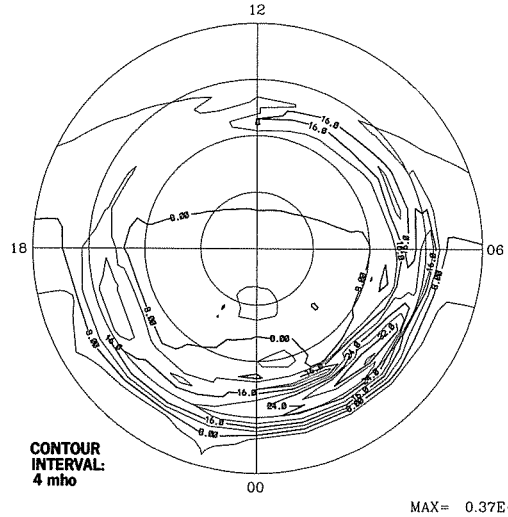

MAX= 0.37E+02 mho

DMSP

PEDERSEN CONDUCTANCE

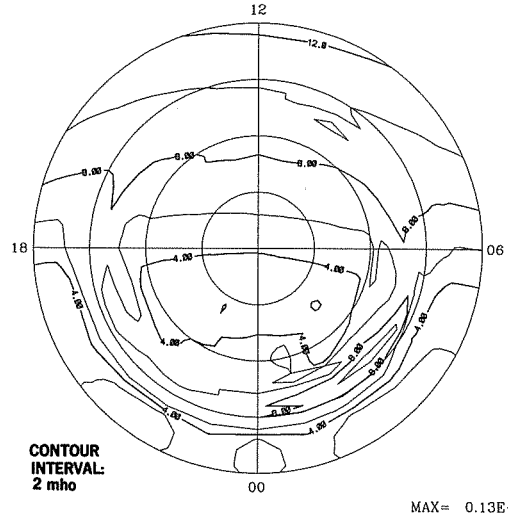

MAX= 0.13E+02 mho

ELECTRIC POTENTIAL

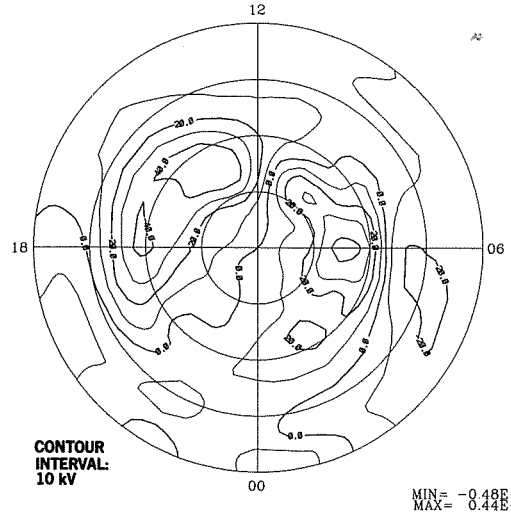

MIN= -0.48E+02 kV
MAX= 0.44E+02 kV

IONOSPHERIC CURRENT VECTORS

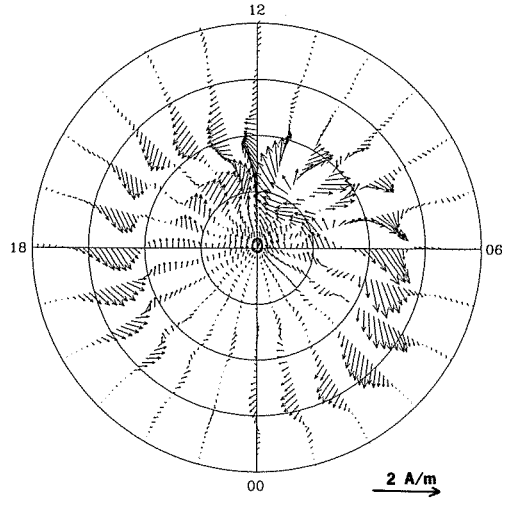

FIELD-ALIGNED CURRENT

24 JUL 1983
0355-0410 UT

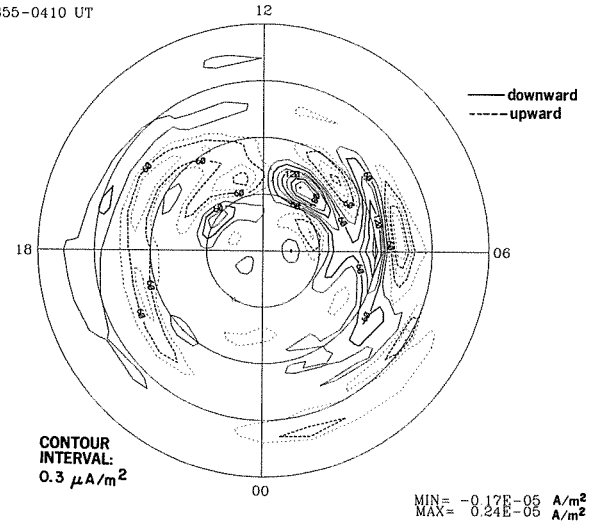

MIN= -0.17E-05 A/m²
MAX= 0.24E-05 A/m²

JOULE HEATING RATE

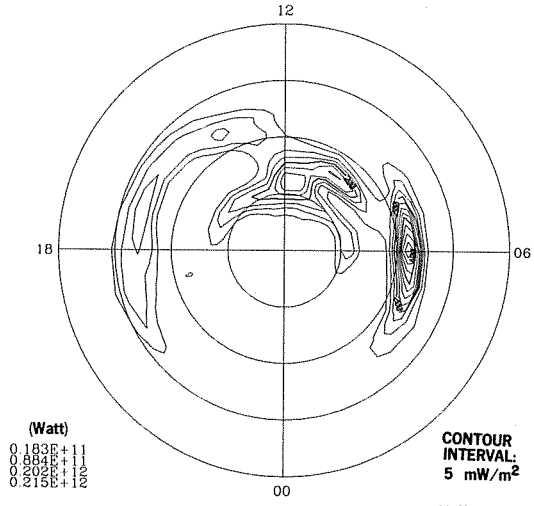

MAX= 0.60E-01 W/m²

HALL CURRENT VECTORS

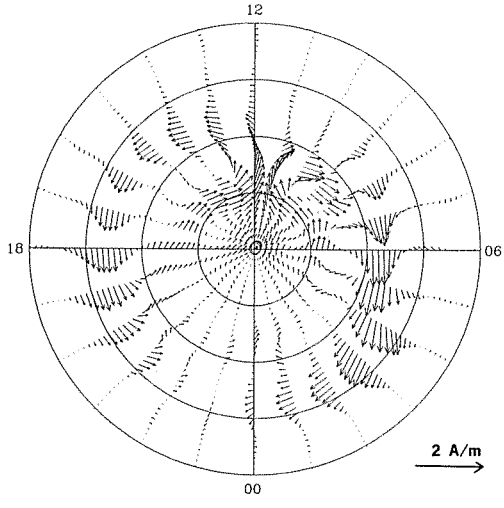

PEDERSEN CURRENT VECTORS

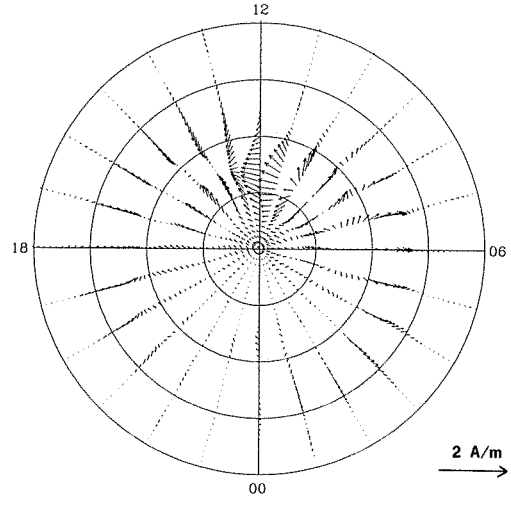

FIELD-ALIGNED HALL CURRENT

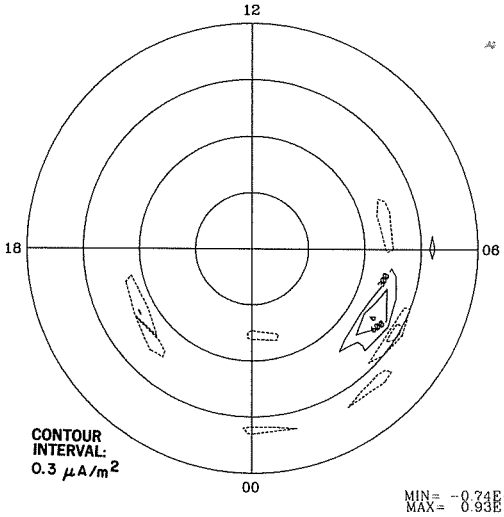

MIN= -0.74E-06 A/m²
MAX= 0.93E-06 A/m²

FIELD-ALIGNED PEDERSEN CURRENT

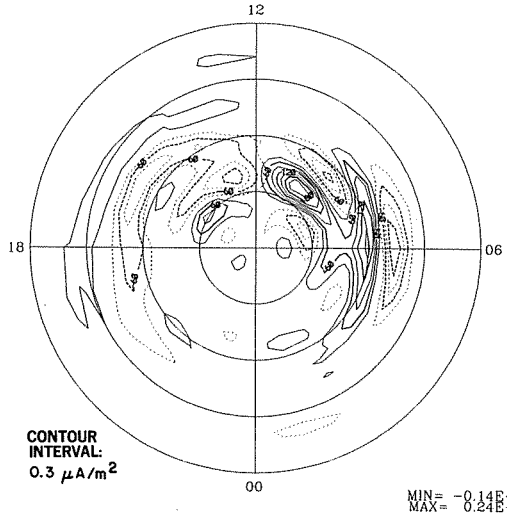

MIN= -0.14E-05 A/m²
MAX= 0.24E-05 A/m²

EQUIVALENT CURRENT VECTORS

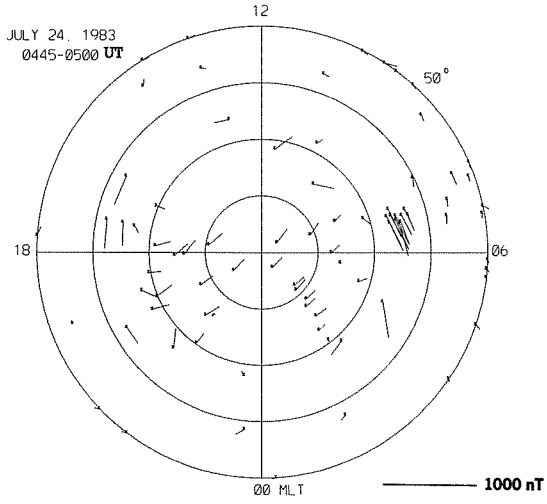

EQUIVALENT CURRENT SYSTEM

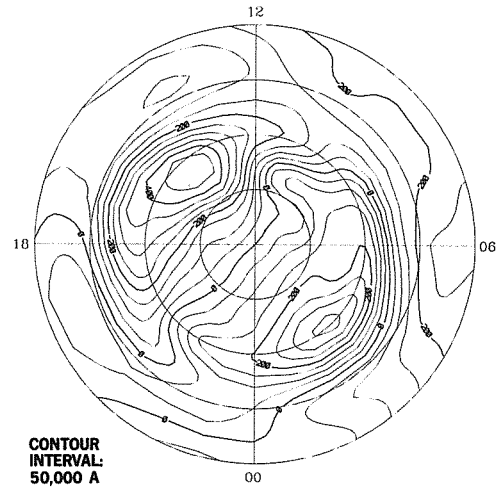

HALL CONDUCTANCE

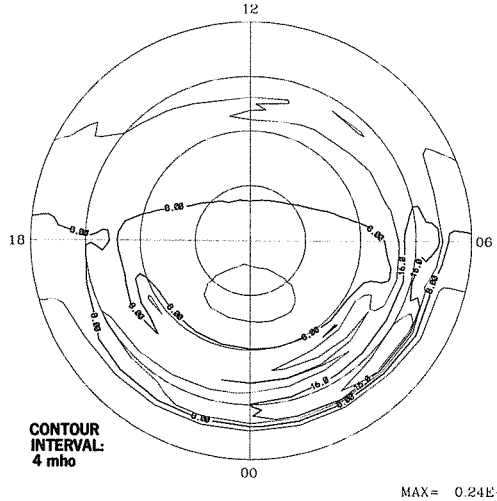

MAX= 0.24E+02 mho

DMSP

PEDERSEN CONDUCTANCE

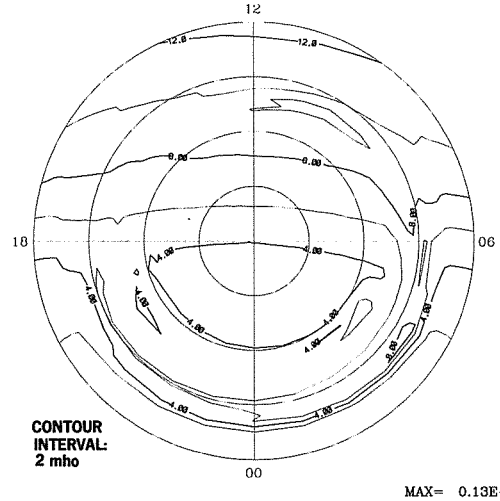

MAX= 0.13E+02 mho

ELECTRIC POTENTIAL

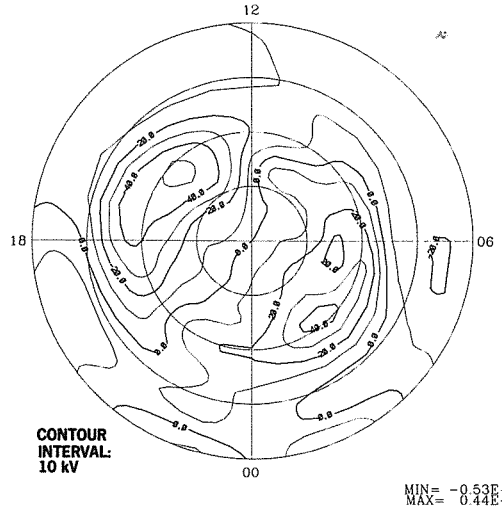

MIN= -0.53E+02 kV
MAX= 0.44E+02 kV

IONOSPHERIC CURRENT VECTORS

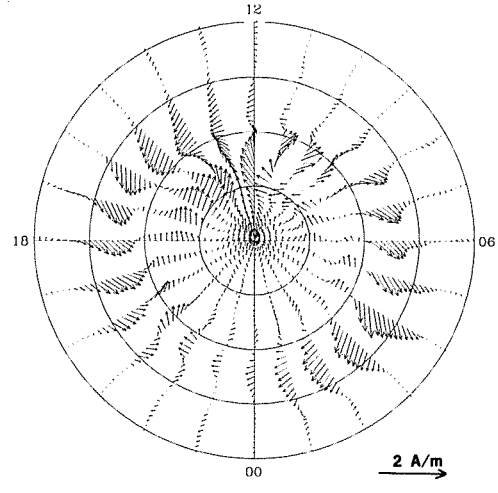

FIELD-ALIGNED CURRENT

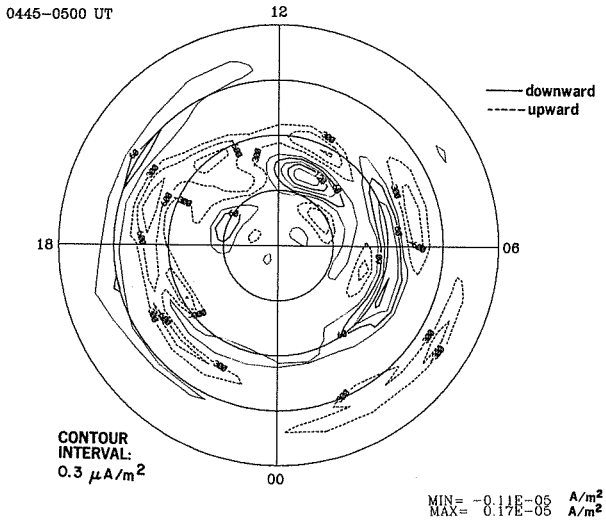

JOULE HEATING RATE

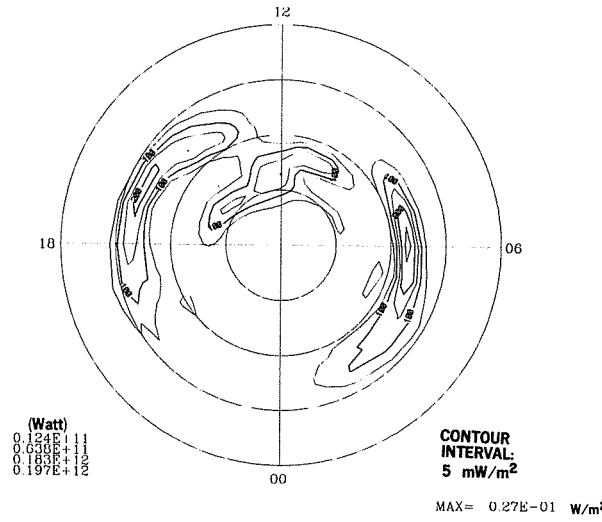

HALL CURRENT VECTORS

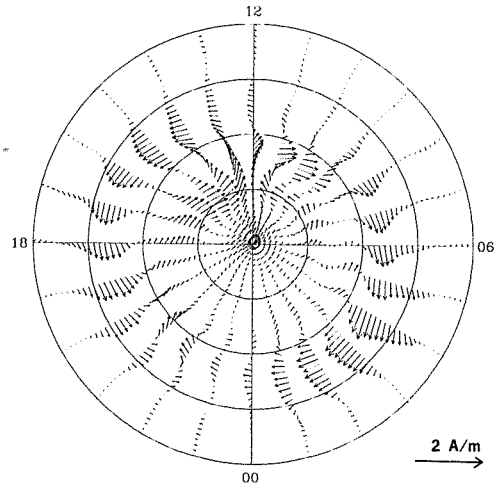

PEDERSEN CURRENT VECTORS

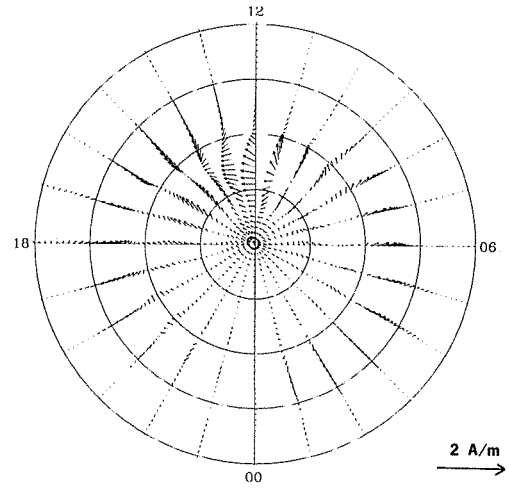

FIELD-ALIGNED HALL CURRENT

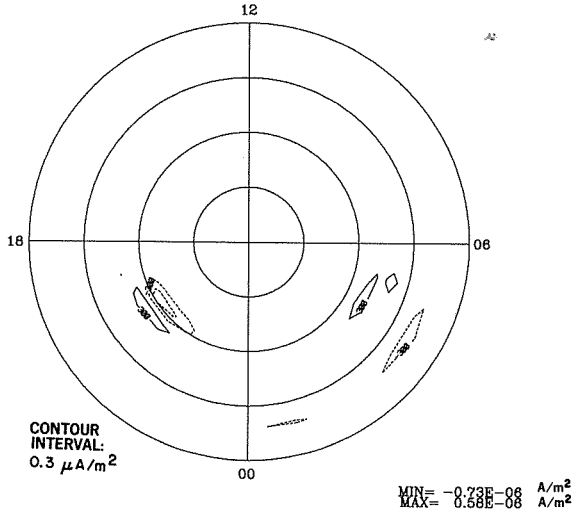

FIELD-ALIGNED PEDERSEN CURRENT

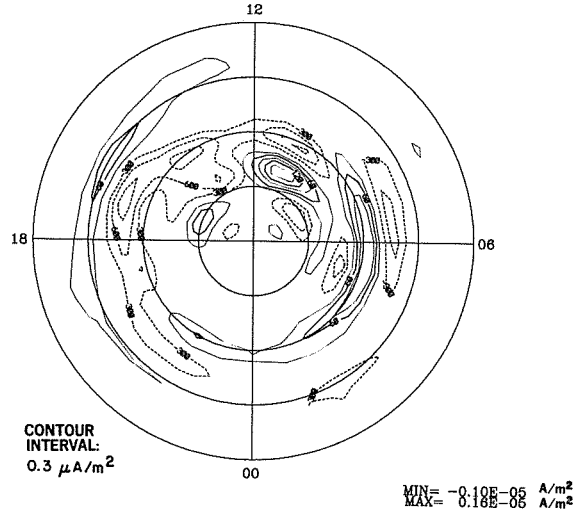

EQUIVALENT CURRENT VECTORS

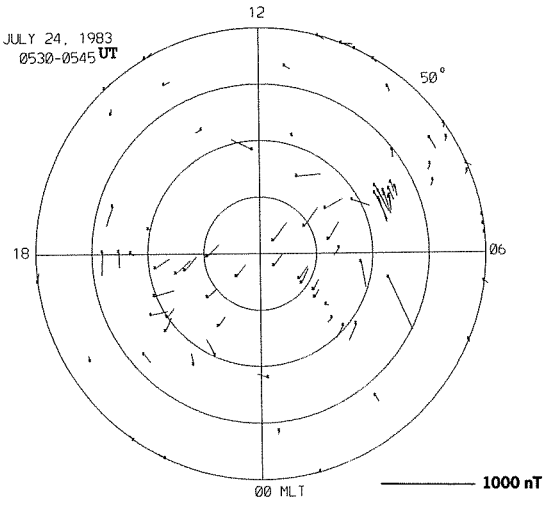

EQUIVALENT CURRENT SYSTEM

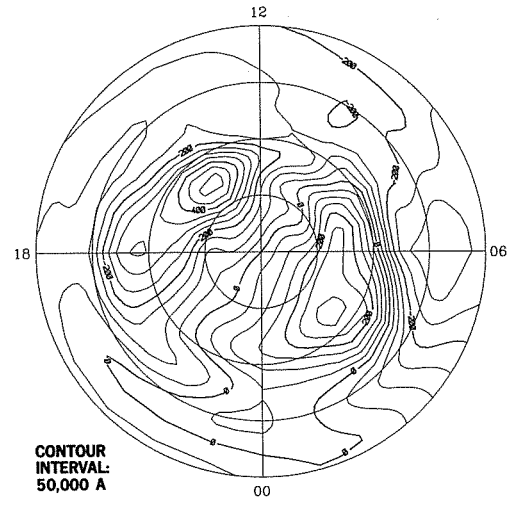

HALL CONDUCTANCE

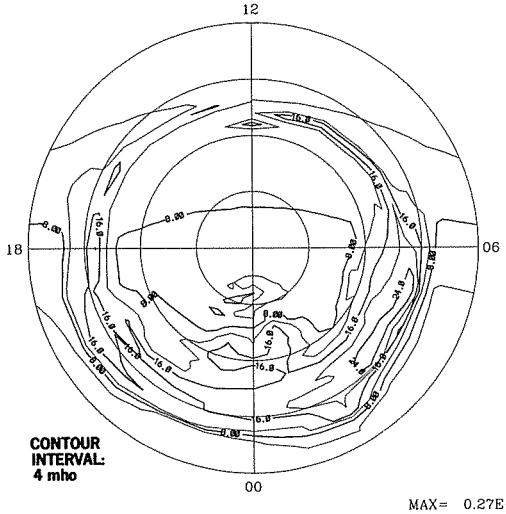

MAX= 0.27E+02 **mho**

DMSP

PEDERSEN CONDUCTANCE

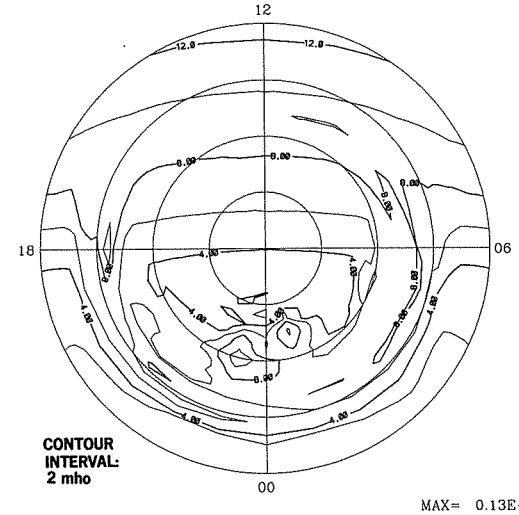

MAX= 0.13E+02 **mho**

ELECTRIC POTENTIAL

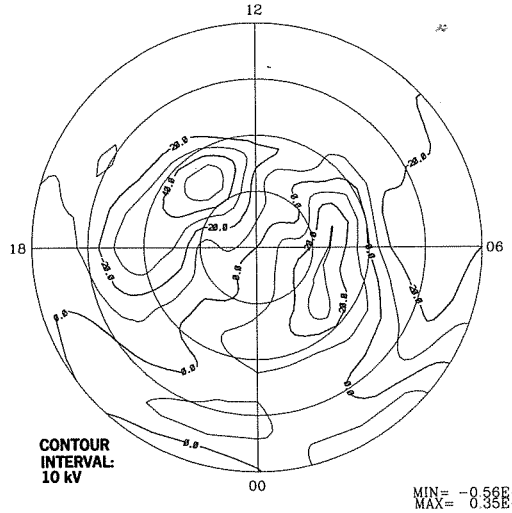

MIN= -0.56E+02 **kV**
MAX= 0.35E+02 **kV**

IONOSPHERIC CURRENT VECTORS

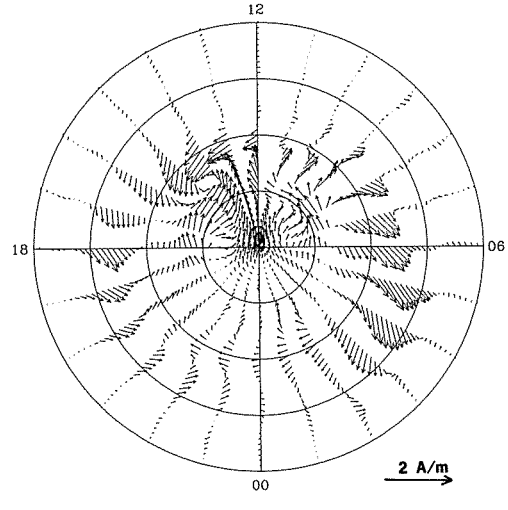

FIELD-ALIGNED CURRENT

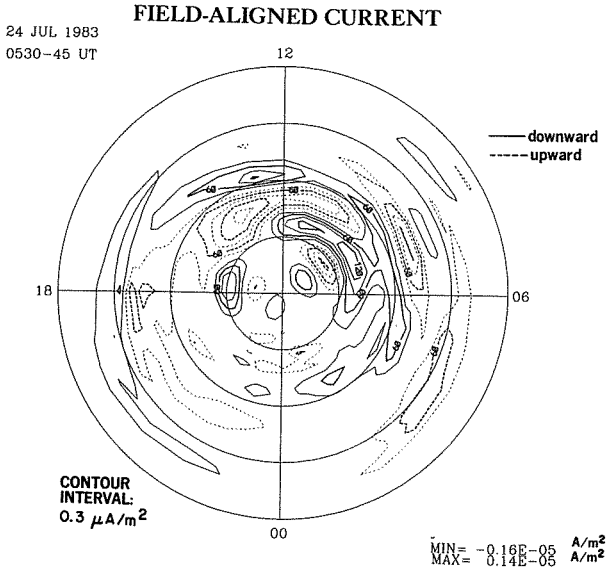

JOULE HEATING RATE

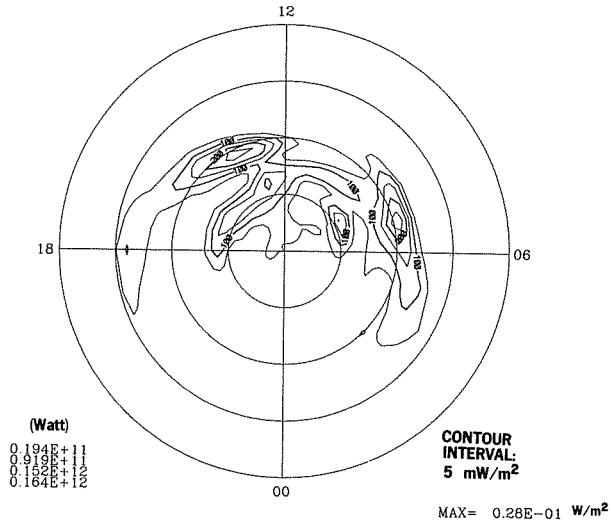

HALL CURRENT VECTORS

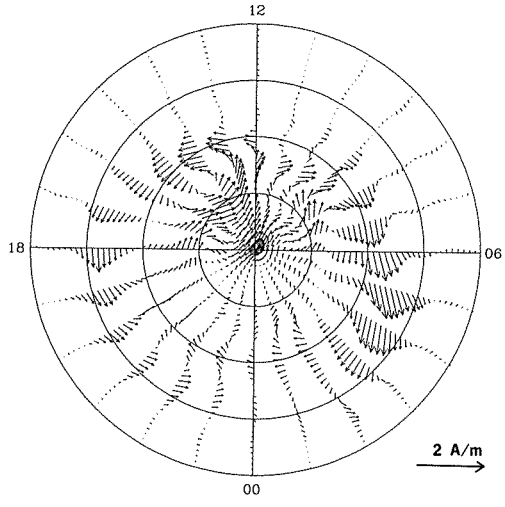

PEDERSEN CURRENT VECTORS

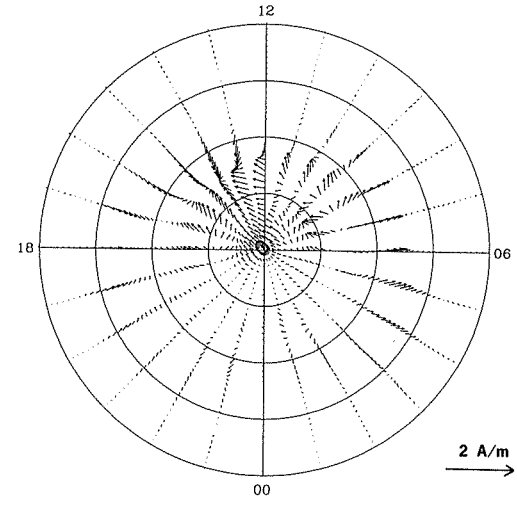

FIELD-ALIGNED HALL CURRENT

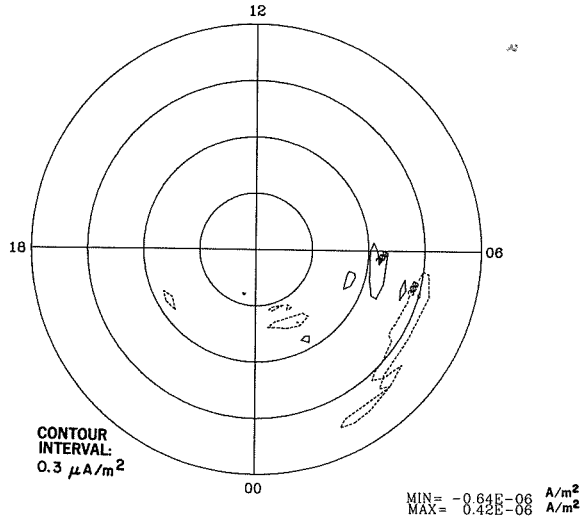

FIELD-ALIGNED PEDERSEN CURRENT

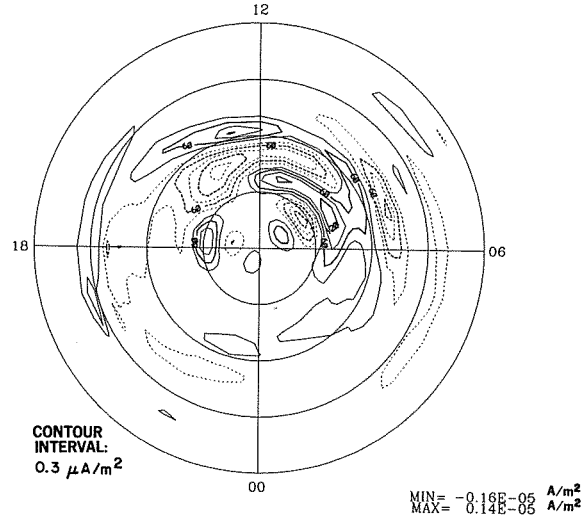

EQUIVALENT CURRENT VECTORS

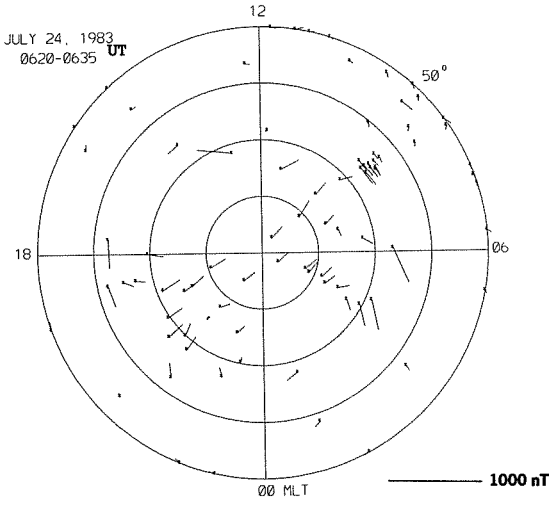

EQUIVALENT CURRENT SYSTEM

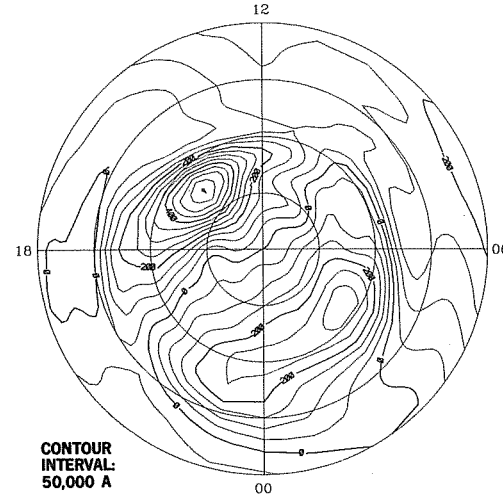

HALL CONDUCTANCE

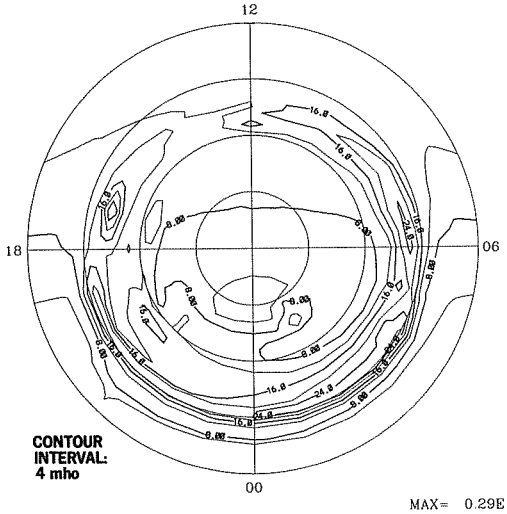

MAX= 0.29E+02 mho

DMSP

PEDERSEN CONDUCTANCE

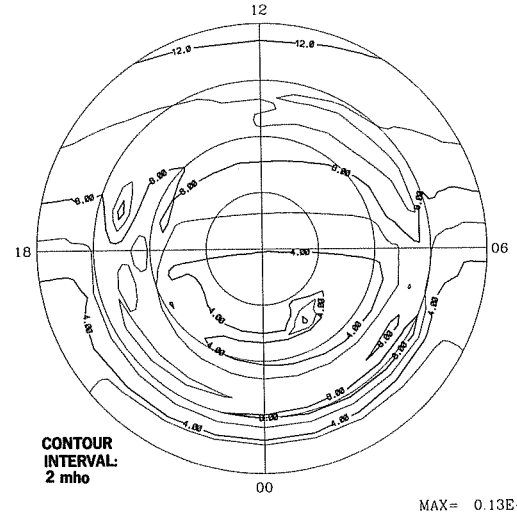

MAX= 0.13E+02 mho

ELECTRIC POTENTIAL

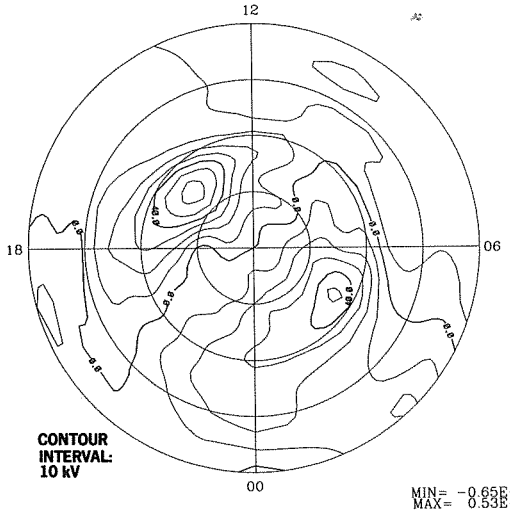

MIN= -0.65E+02 kV
MAX= 0.53E+02 kV

IONOSPHERIC CURRENT VECTORS

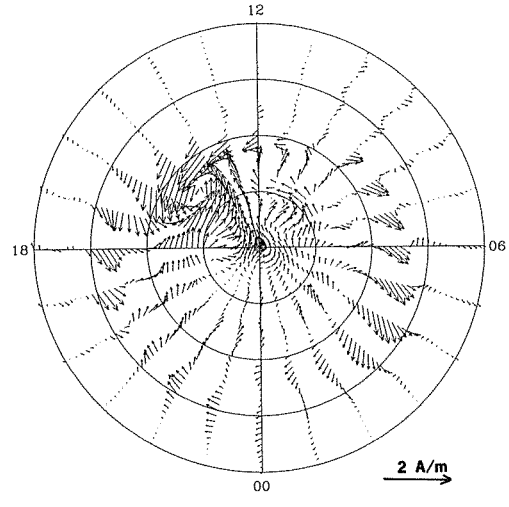

FIELD-ALIGNED CURRENT

24 JUL 1983
0620-35 UT

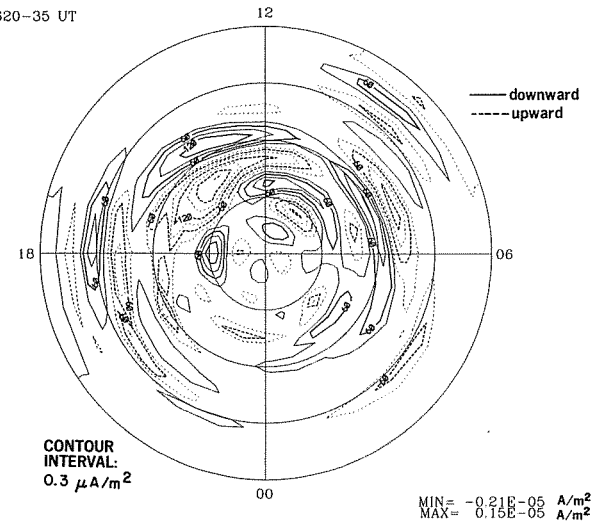

JOULE HEATING RATE

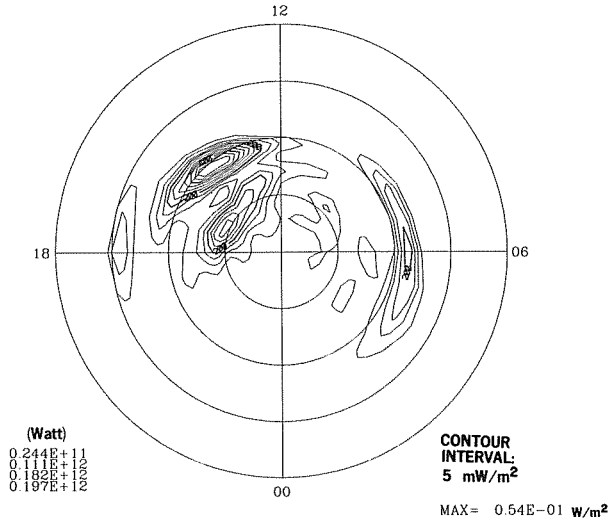

HALL CURRENT VECTORS

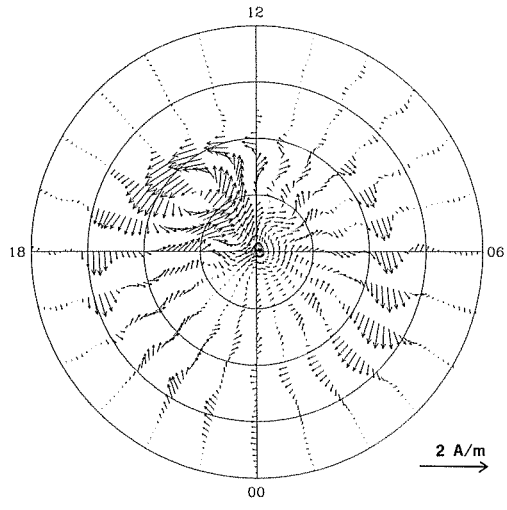

PEDERSEN CURRENT VECTORS

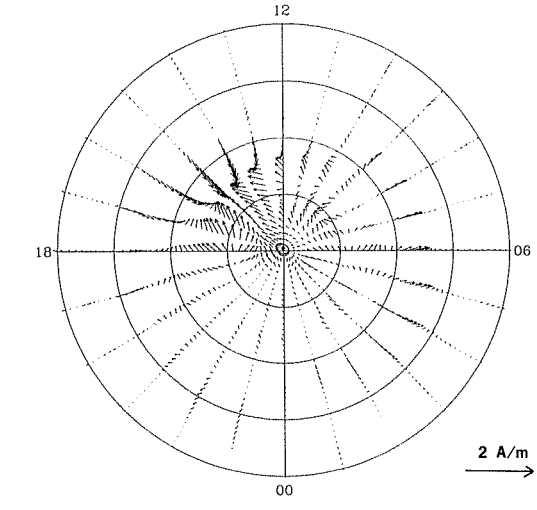

FIELD-ALIGNED HALL CURRENT

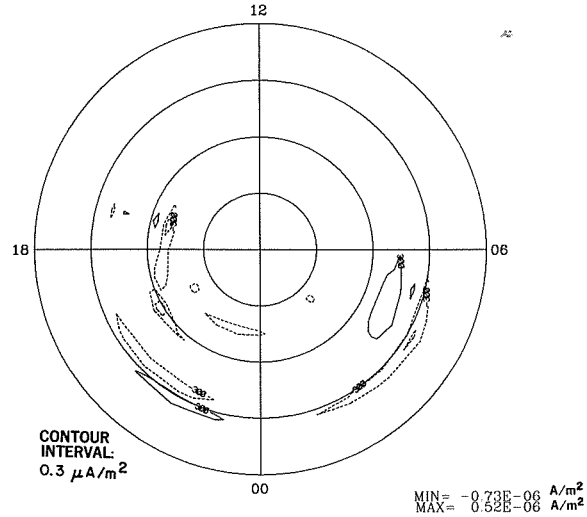

FIELD-ALIGNED PEDERSEN CURRENT

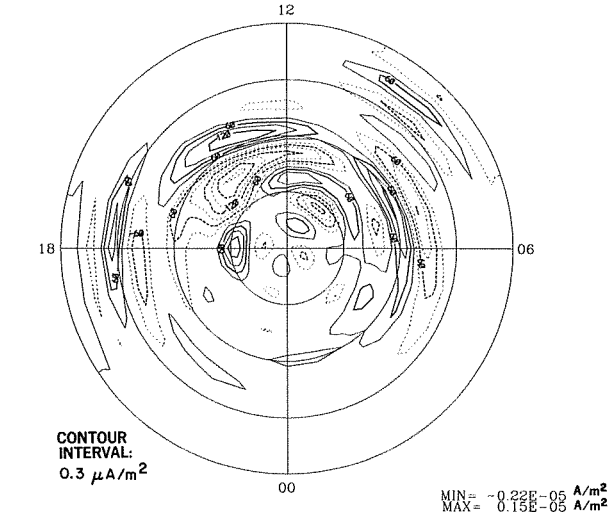

EQUIVALENT CURRENT VECTORS

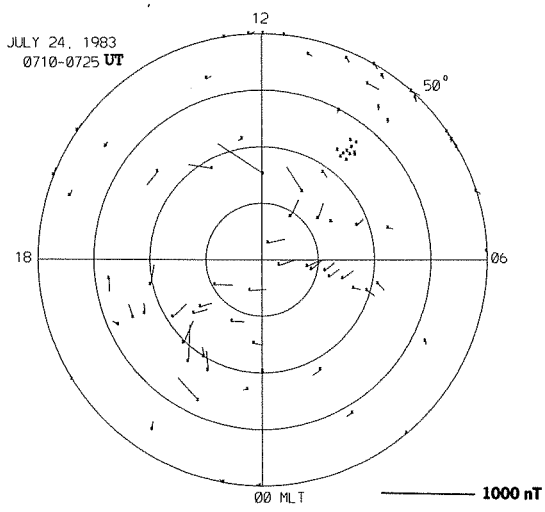

EQUIVALENT CURRENT SYSTEM

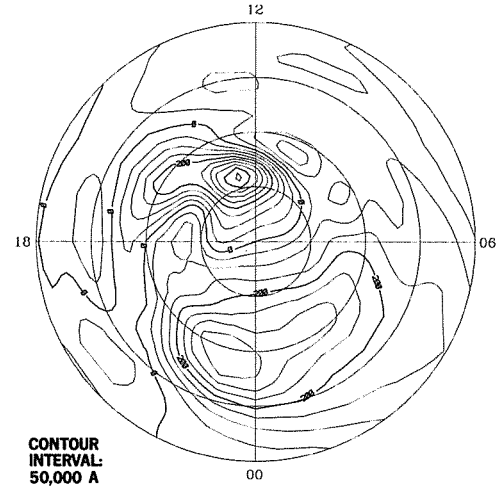

HALL CONDUCTANCE

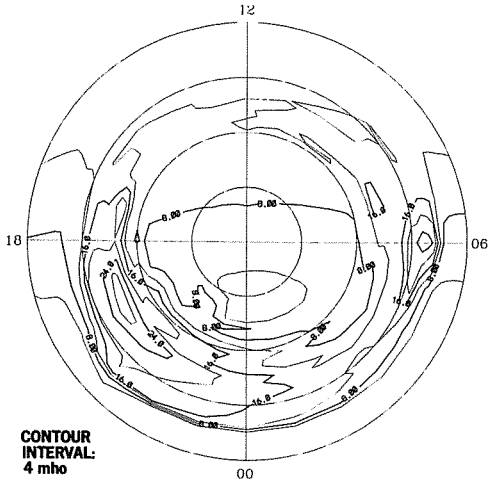

MAX= 0.29E+02 mho

DMSP

PEDERSEN CONDUCTANCE

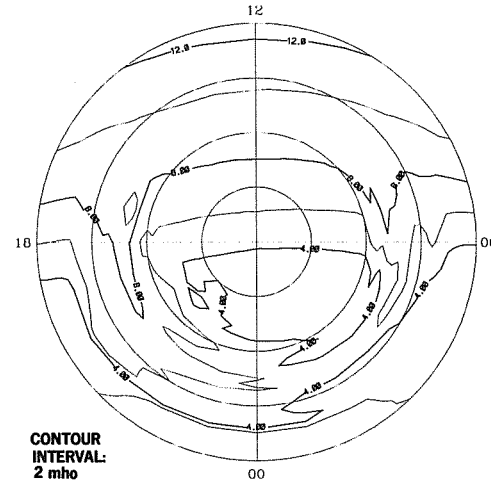

MAX= 0.13E+02 mho

ELECTRIC POTENTIAL

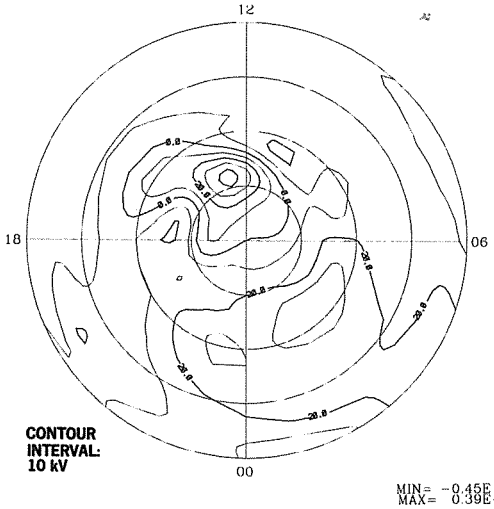

MIN= -0.45E+02 kV
MAX= 0.39E+02 kV

IONOSPHERIC CURRENT VECTORS

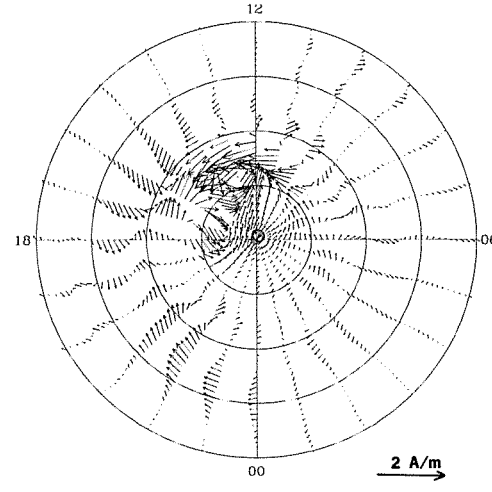

FIELD-ALIGNED CURRENT

24 JUL, 1983
0710 25 UT

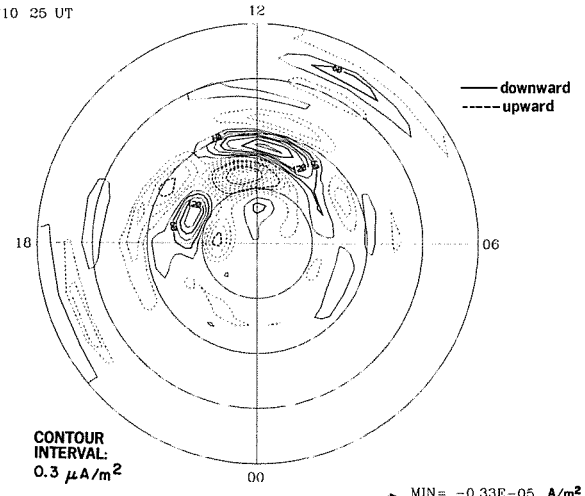

MIN= -0.33E-05 A/m²
MAX= 0.22E-05 A/m²

JOULE HEATING RATE

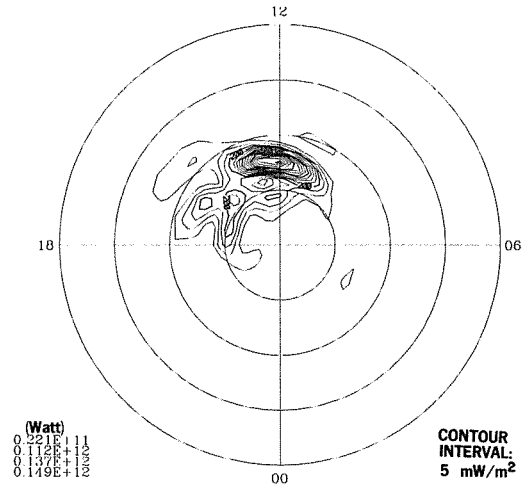

MAX= 0.83E-01 W/m²

HALL CURRENT VECTORS

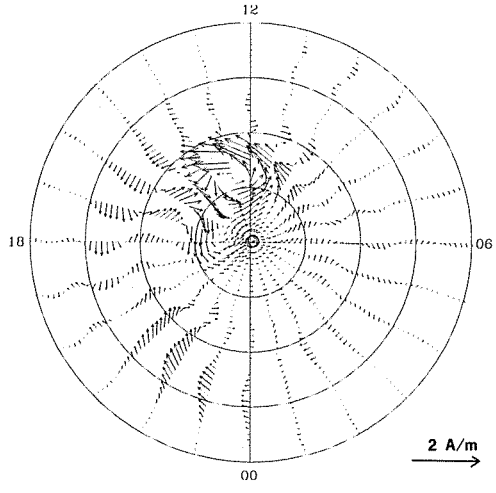

PEDERSEN CURRENT VECTORS

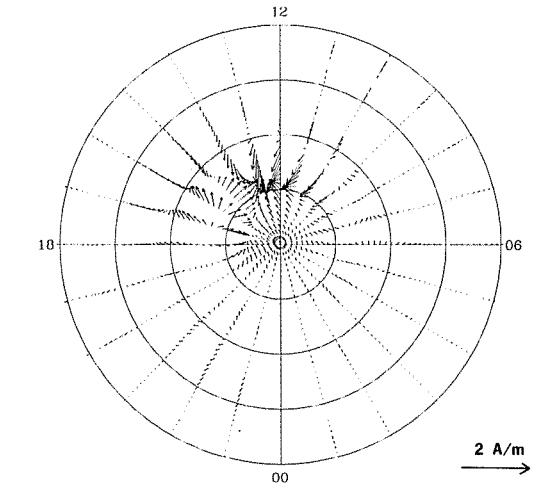

FIELD-ALIGNED HALL CURRENT

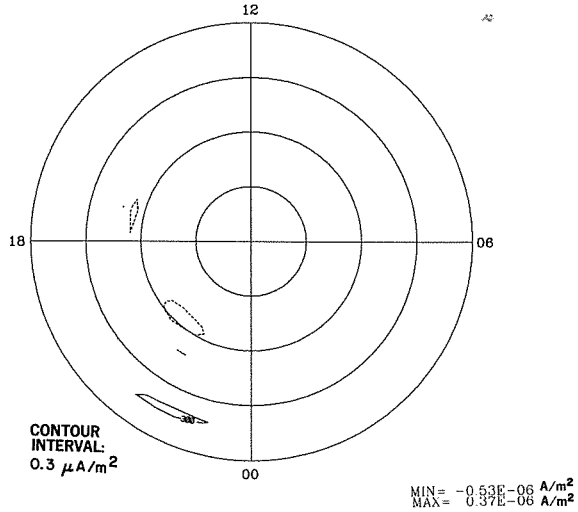

MIN= -0.53E-06 A/m²
MAX= 0.37E-06 A/m²

FIELD-ALIGNED PEDERSEN CURRENT

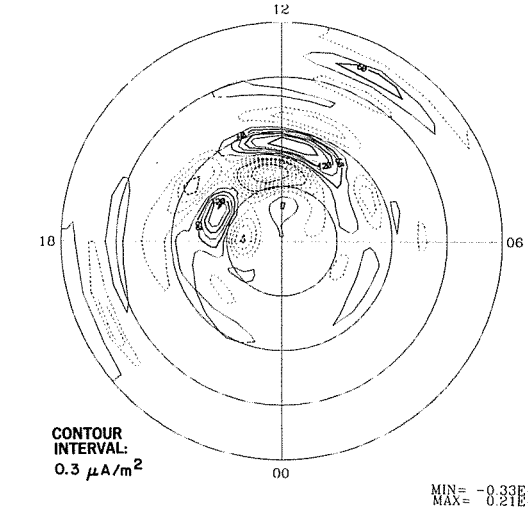

MIN= -0.33E-05 A/m²
MAX= 0.21E-05 A/m²

EQUIVALENT CURRENT VECTORS

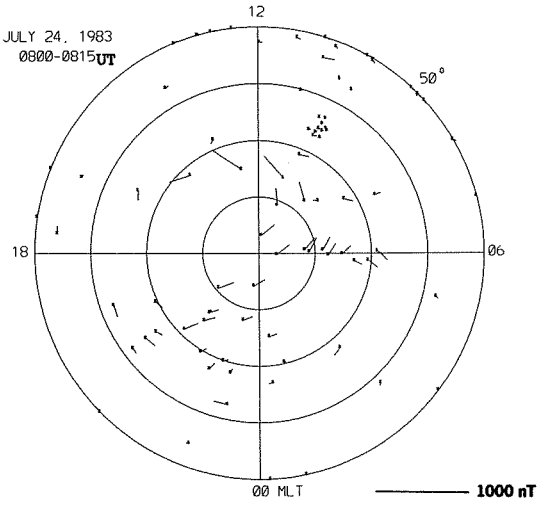

EQUIVALENT CURRENT SYSTEM

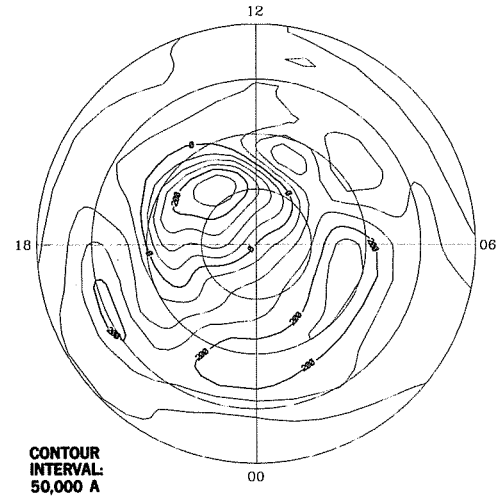

HALL CONDUCTANCE

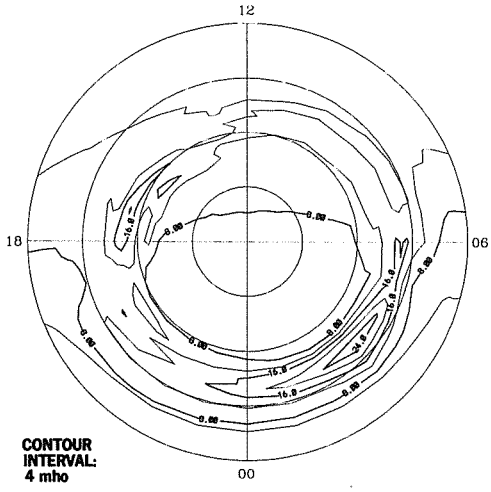

MAX= 0.27E+02 mho

DMSP

PEDERSEN CONDUCTANCE

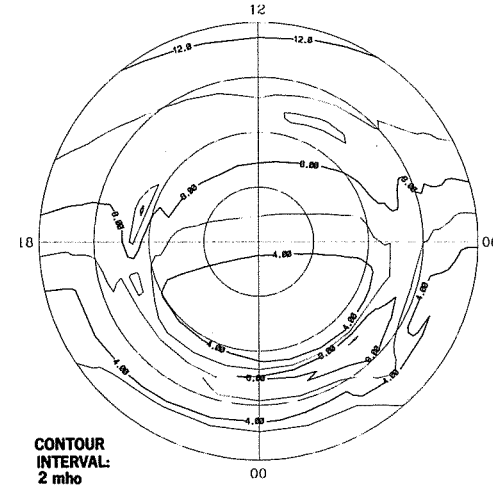

MAX= 0.13E+02 mho

ELECTRIC POTENTIAL

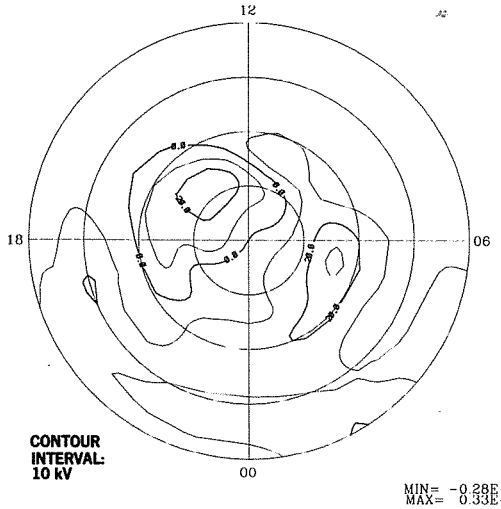

MIN= -0.28E+02 kV
MAX= 0.33E+02 kV

IONOSPHERIC CURRENT VECTORS

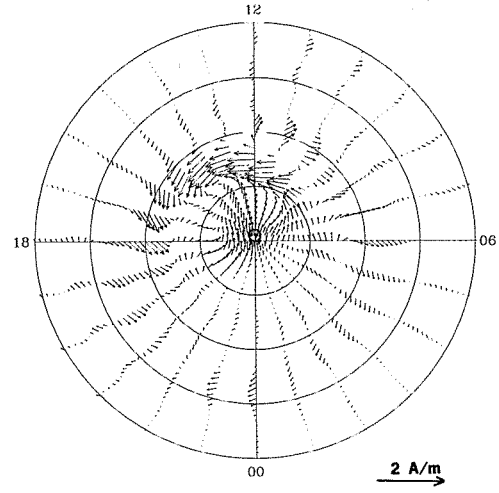

FIELD-ALIGNED CURRENT

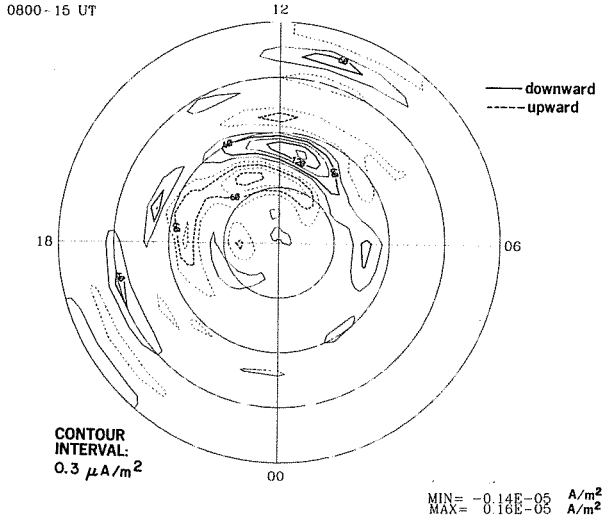

JOULE HEATING RATE

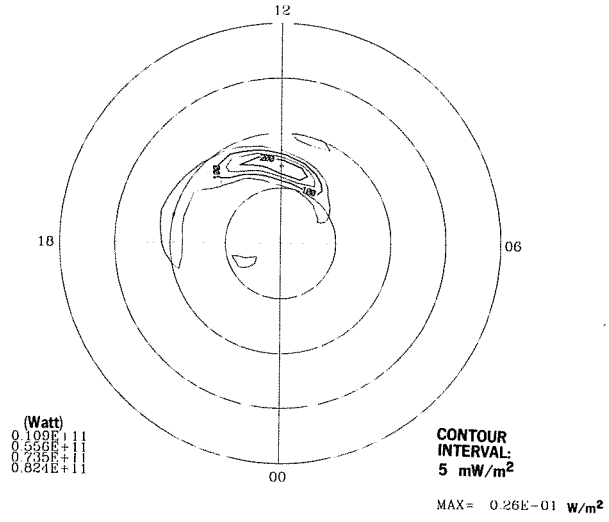

HALL CURRENT VECTORS

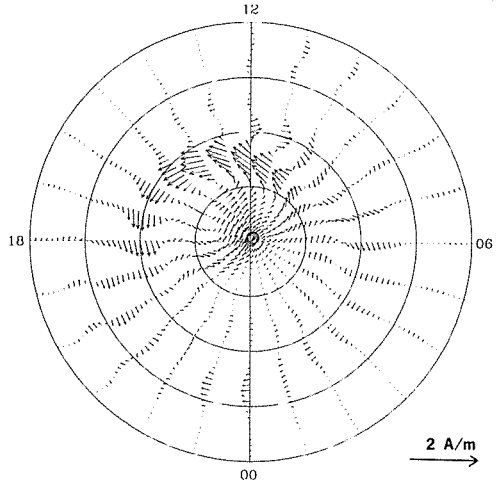

PEDERSEN CURRENT VECTORS

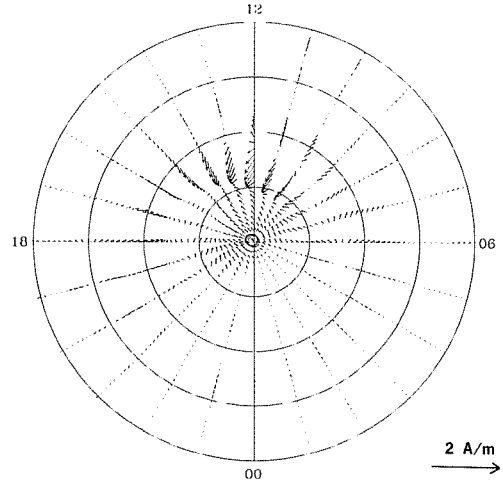

FIELD-ALIGNED HALL CURRENT

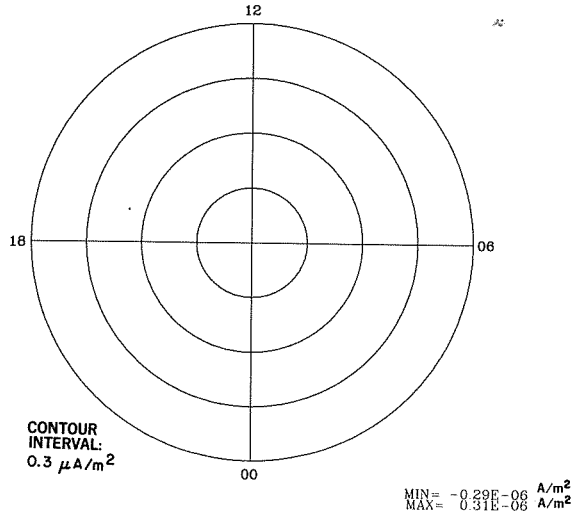

FIELD-ALIGNED PEDERSEN CURRENT

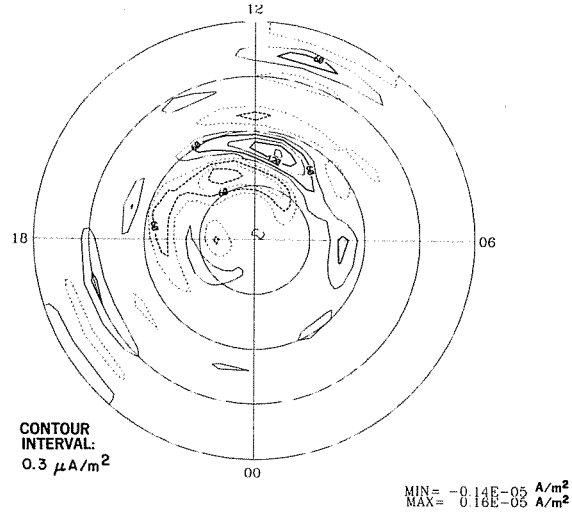

EQUIVALENT CURRENT VECTORS

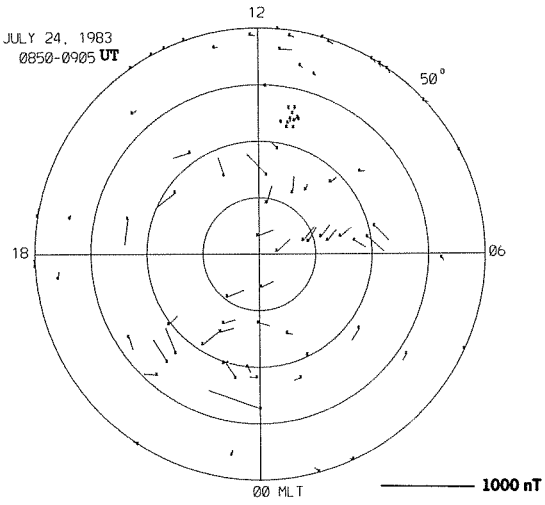

EQUIVALENT CURRENT SYSTEM

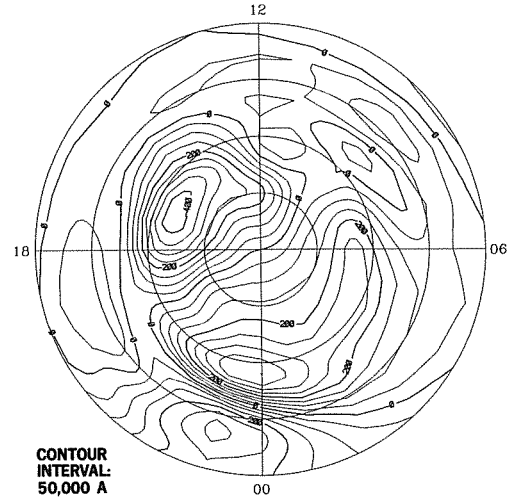

HALL CONDUCTANCE

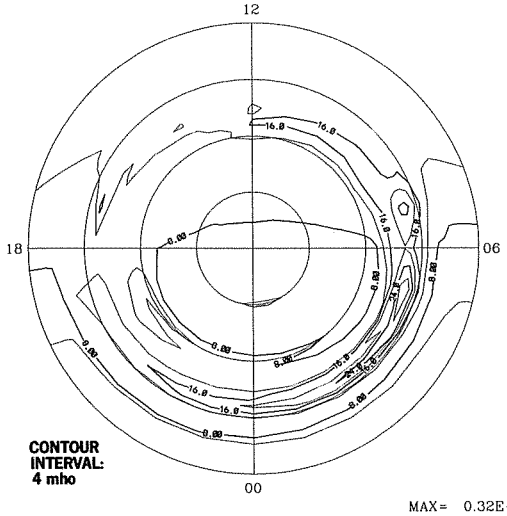

MAX= 0.32E+02 **mho**

DMSP

PEDERSEN CONDUCTANCE

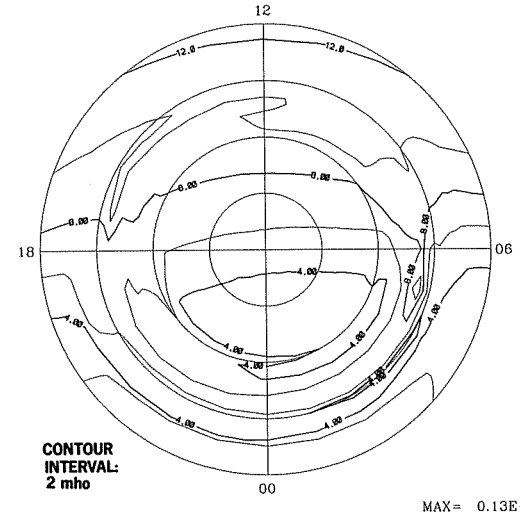

MAX= 0.13E+02 **mho**

ELECTRIC POTENTIAL

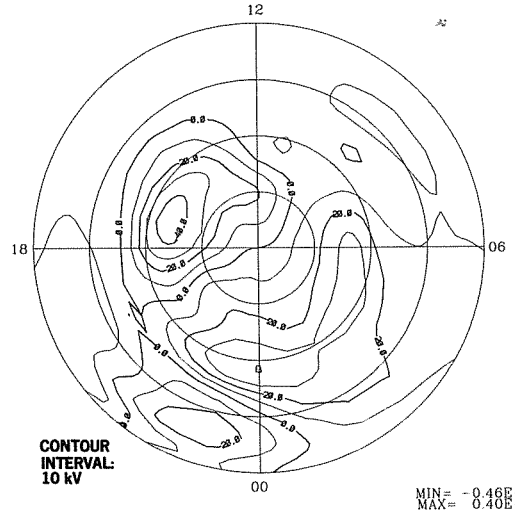

MIN= -0.46E+02 **kV**
MAX= 0.40E+02 **kV**

IONOSPHERIC CURRENT VECTORS

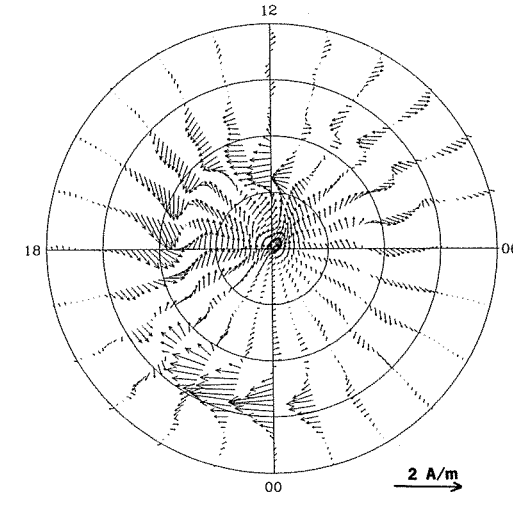

FIELD-ALIGNED CURRENT

24 JUL 1983
0850-0905 UT

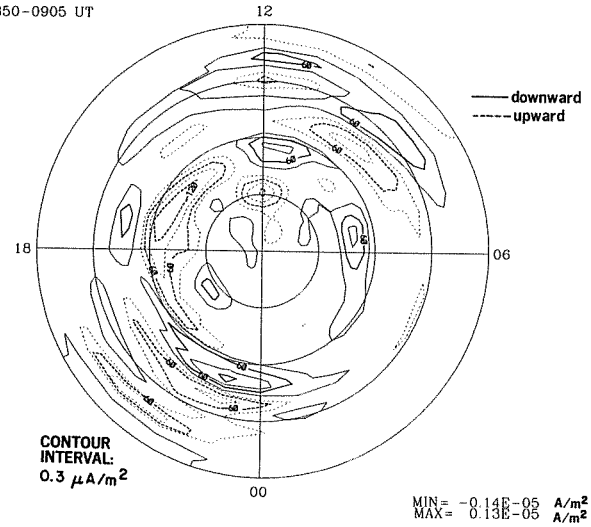

JOULE HEATING RATE

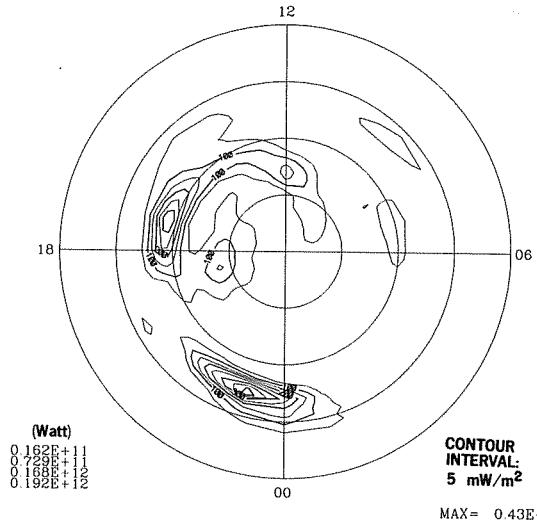

HALL CURRENT VECTORS

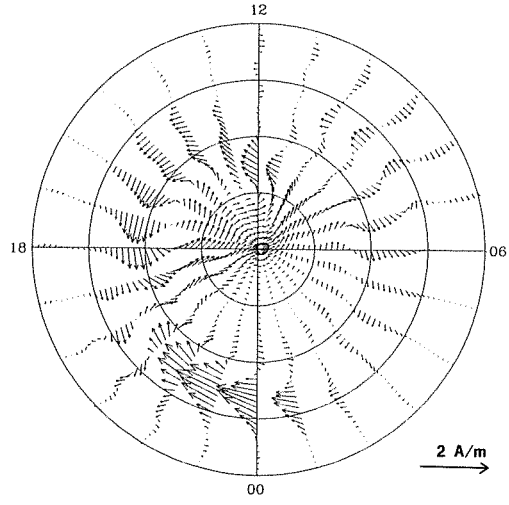

PEDERSEN CURRENT VECTORS

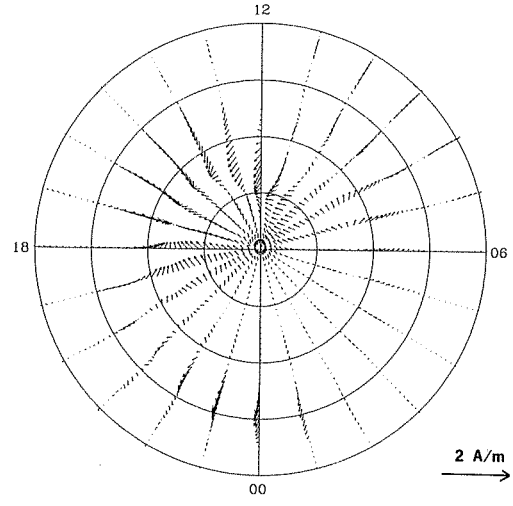

FIELD-ALIGNED HALL CURRENT

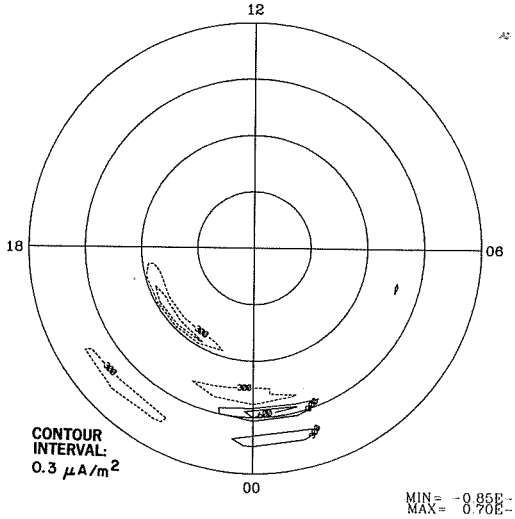

FIELD-ALIGNED PEDERSEN CURRENT

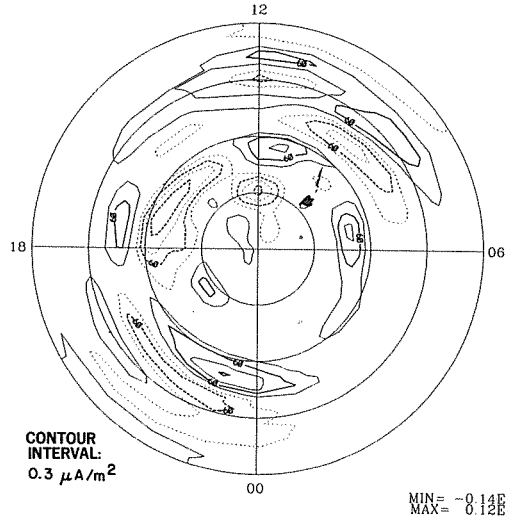

EQUIVALENT CURRENT VECTORS

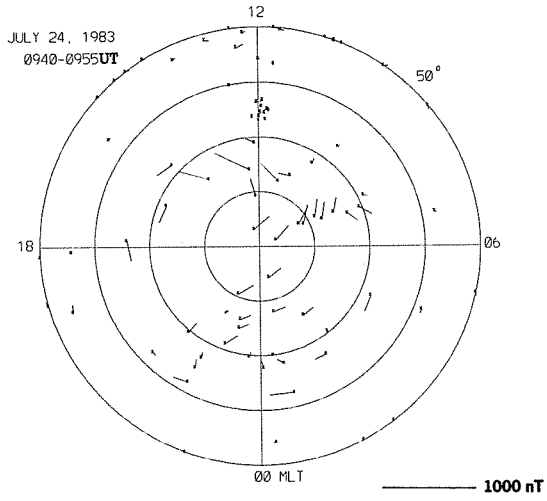

EQUIVALENT CURRENT SYSTEM

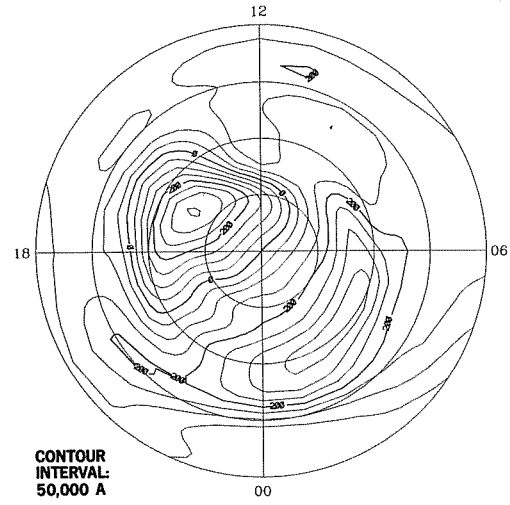

HALL CONDUCTANCE

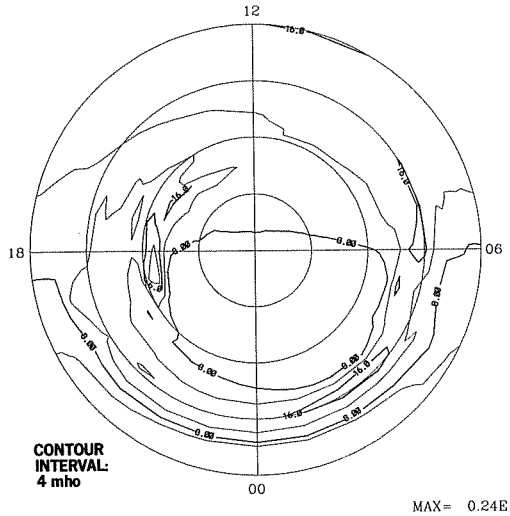

MAX= 0.24E+02 **mho**

DMSP

PEDERSEN CONDUCTANCE

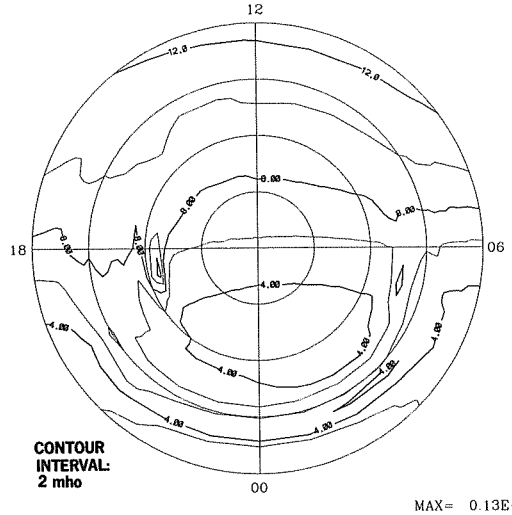

MAX= 0.13E+02 **mho**

ELECTRIC POTENTIAL

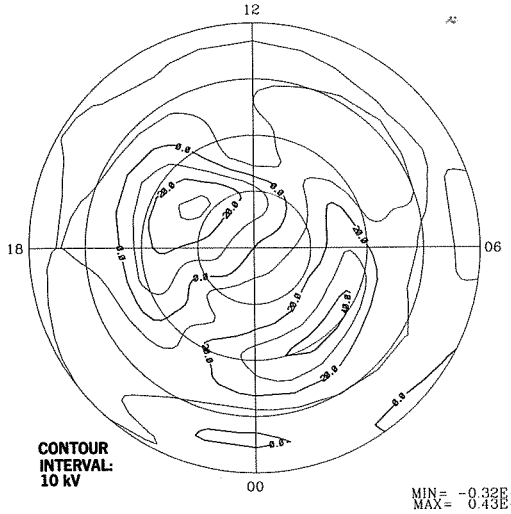

MIN= -0.32E+02 **kV**
MAX= 0.43E+02 **kV**

IONOSPHERIC CURRENT VECTORS

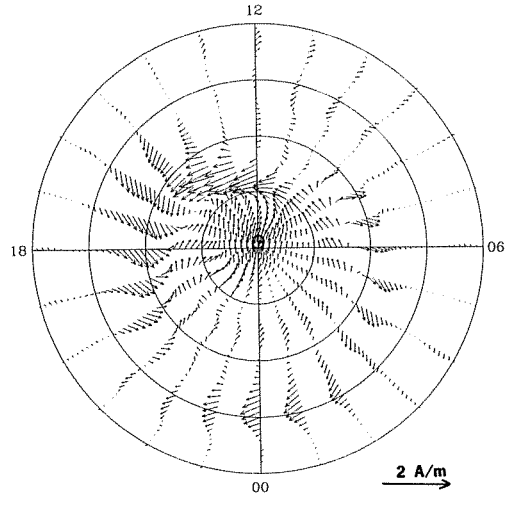

FIELD-ALIGNED CURRENT

24 JUL 1983
0940-55 UT

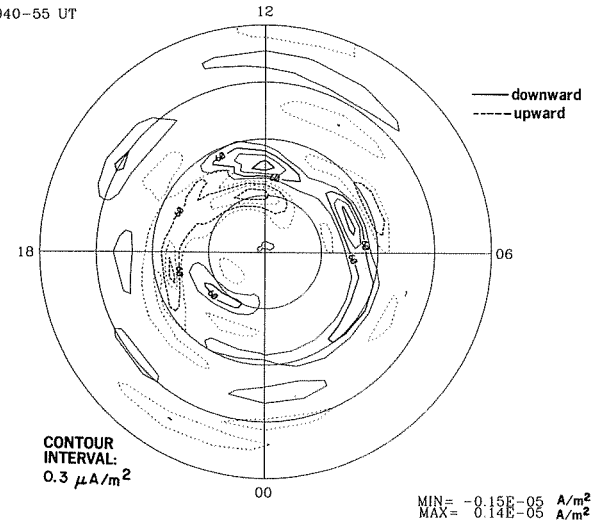

JOULE HEATING RATE

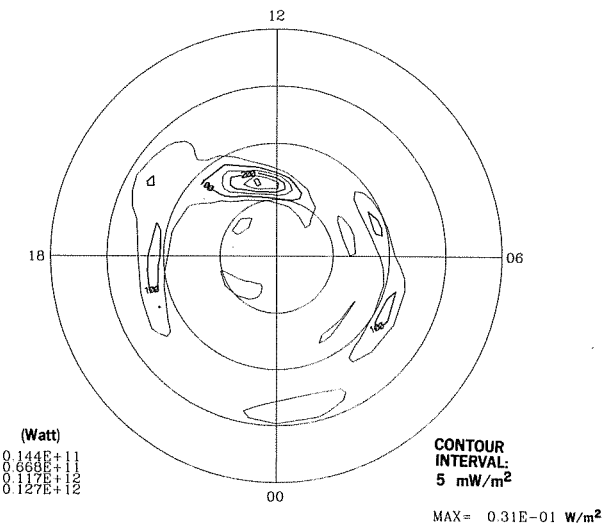

HALL CURRENT VECTORS

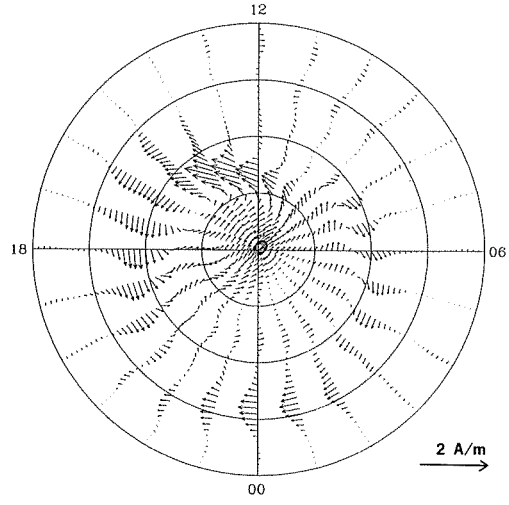

PEDERSEN CURRENT VECTORS

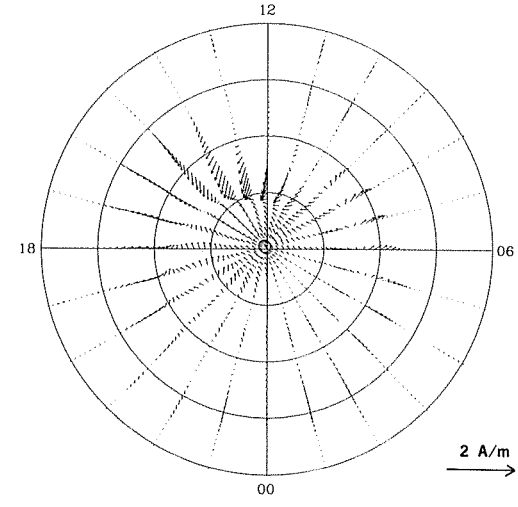

FIELD-ALIGNED HALL CURRENT

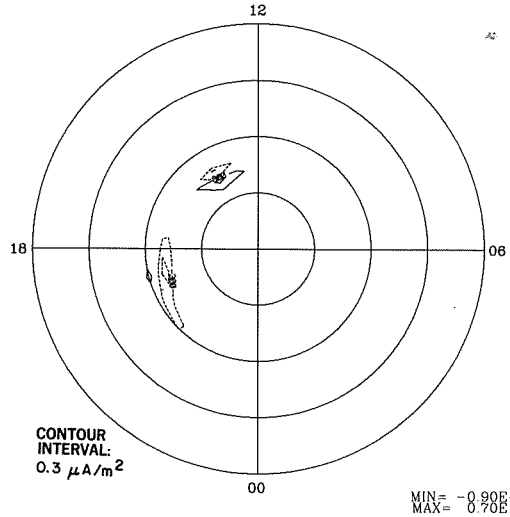

FIELD-ALIGNED PEDERSEN CURRENT

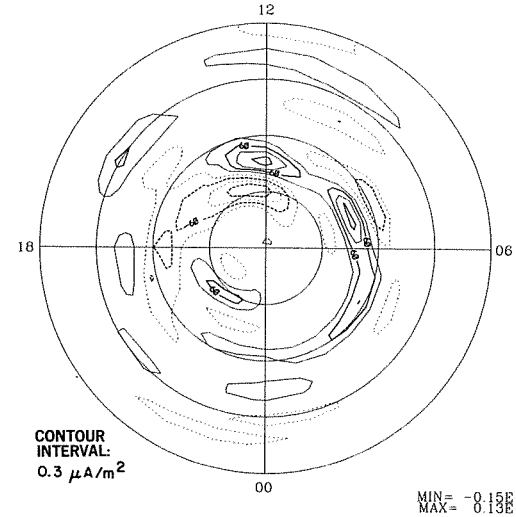

EQUIVALENT CURRENT VECTORS

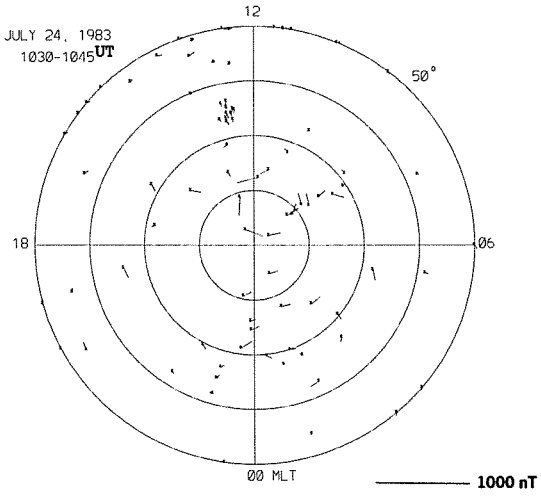

EQUIVALENT CURRENT SYSTEM

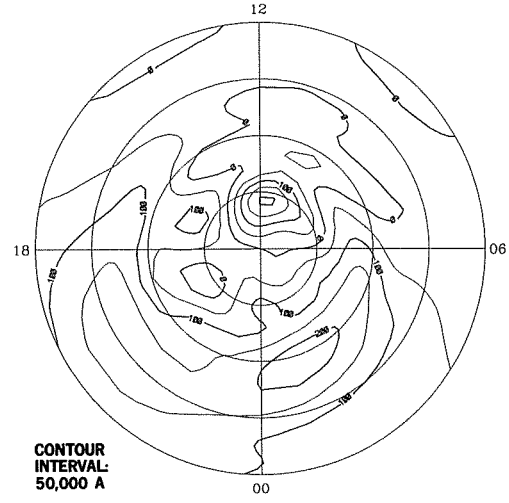

HALL CONDUCTANCE

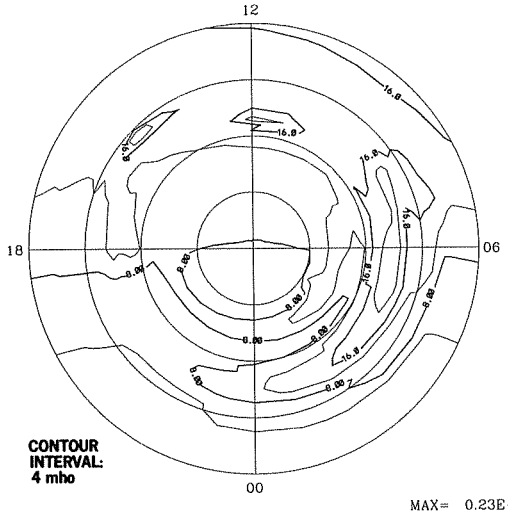

MAX= 0.23E+02 **mho**

DMSP

PEDERSEN CONDUCTANCE

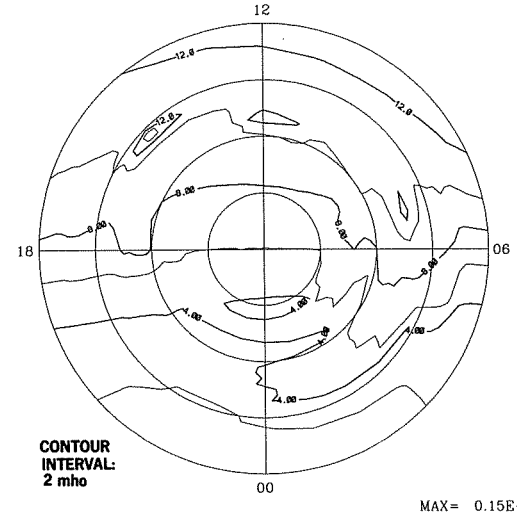

MAX= 0.15E+02 **mho**

ELECTRIC POTENTIAL

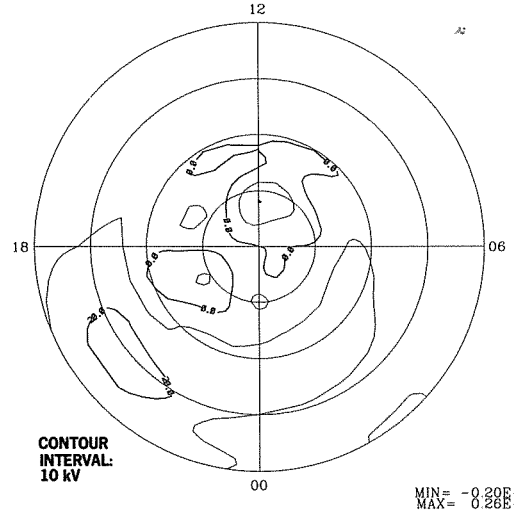

MIN= -0.20E+02 **kV**
MAX= 0.26E+02 **kV**

IONOSPHERIC CURRENT VECTORS

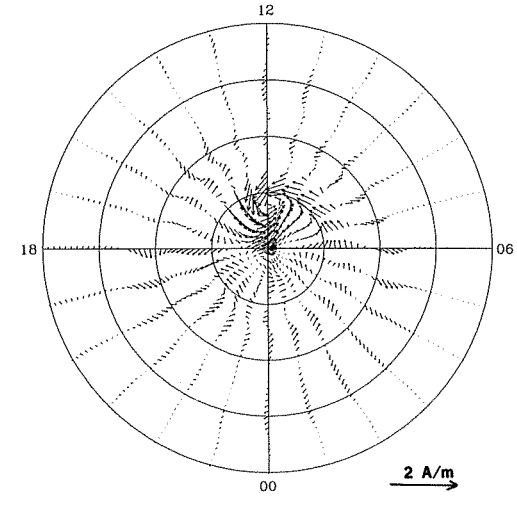

FIELD-ALIGNED CURRENT

24 JUL 1983
1030-45 UT

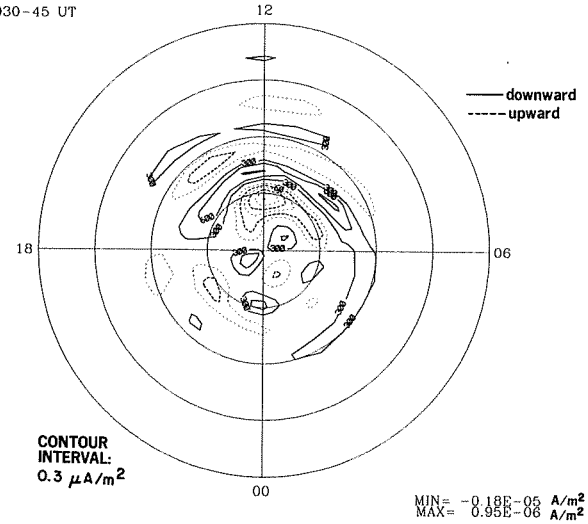

JOULE HEATING RATE

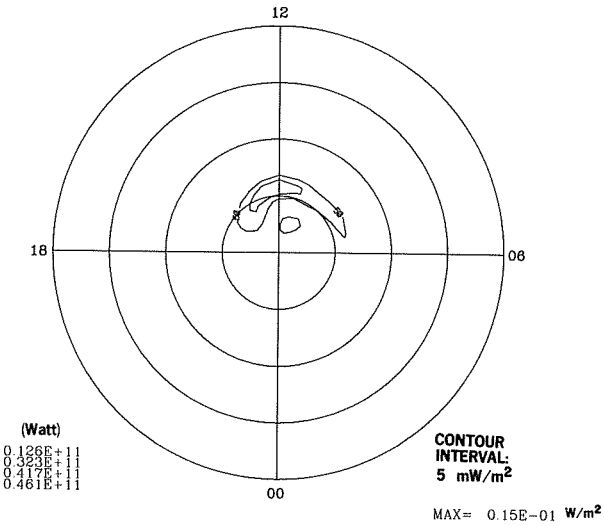

HALL CURRENT VECTORS

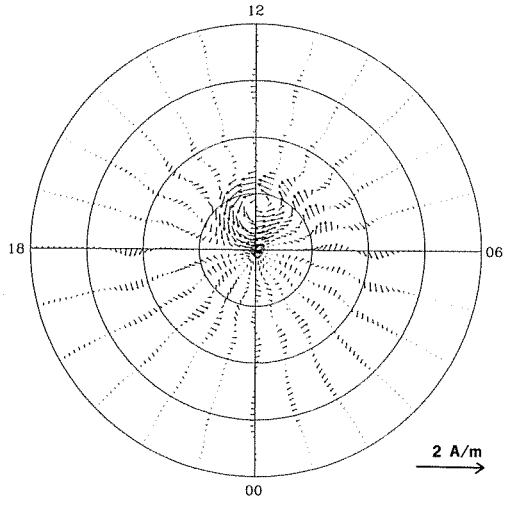

PEDERSEN CURRENT VECTORS

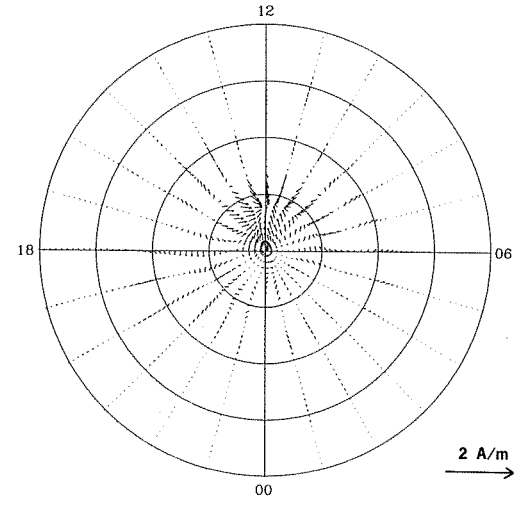

FIELD-ALIGNED HALL CURRENT

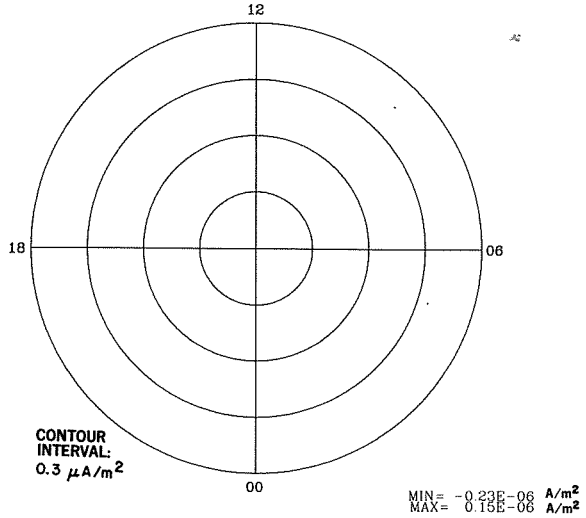

FIELD-ALIGNED PEDERSEN CURRENT

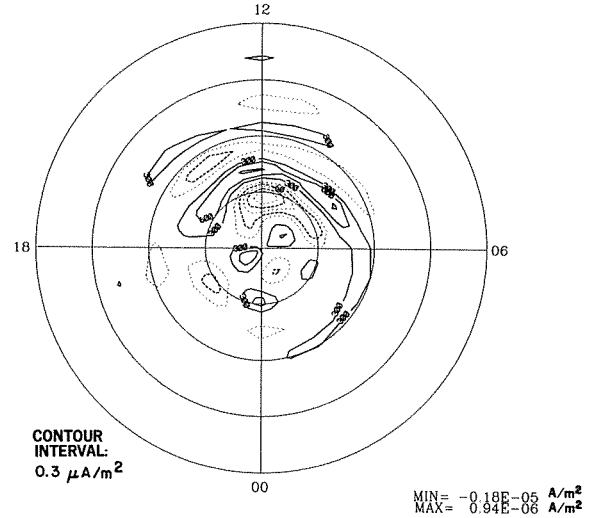

EQUIVALENT CURRENT VECTORS

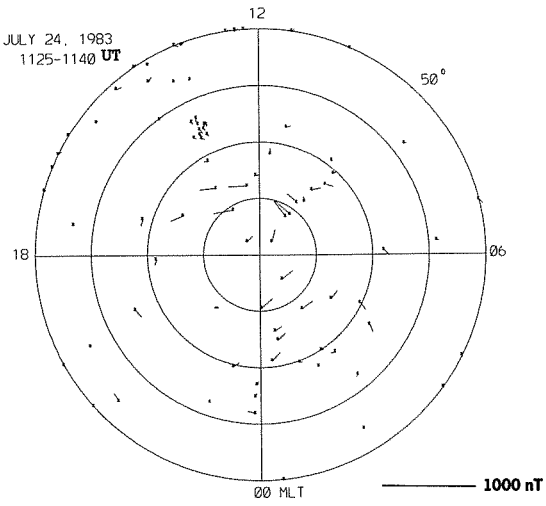

EQUIVALENT CURRENT SYSTEM

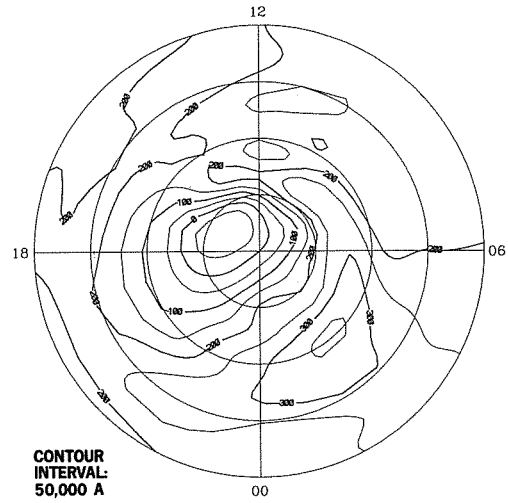

HALL CONDUCTANCE

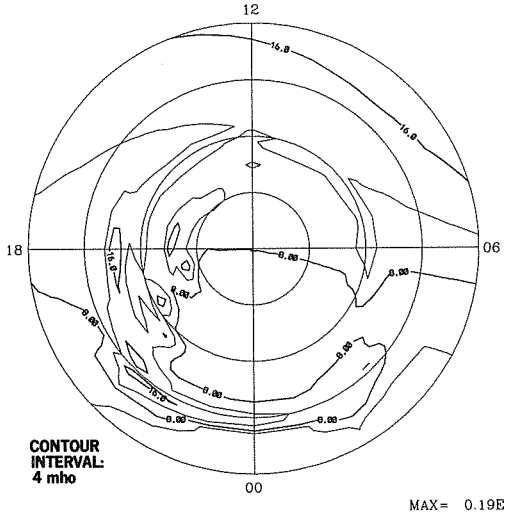

MAX= 0.19E+02 **mho**

DMSP

PEDERSEN CONDUCTANCE

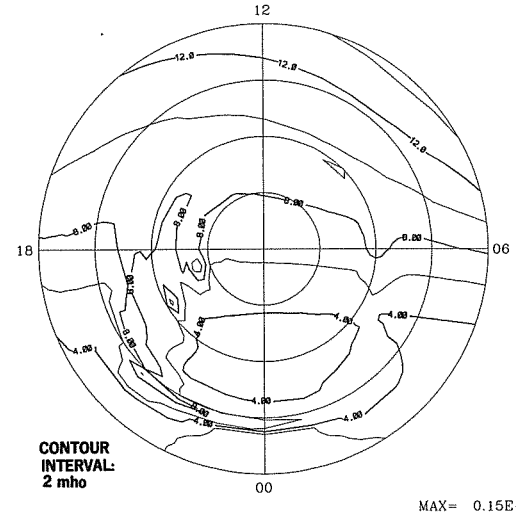

MAX= 0.15E+02 **mho**

ELECTRIC POTENTIAL

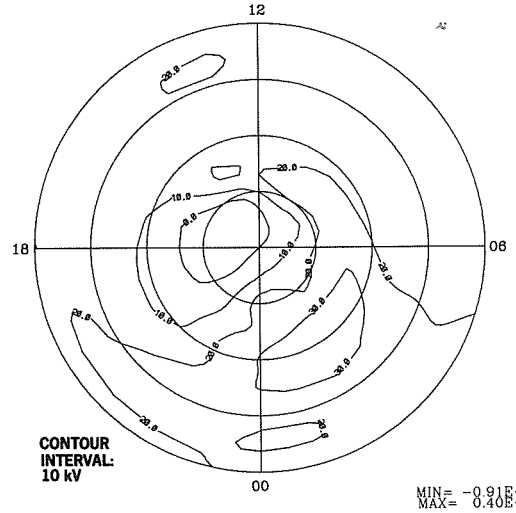

MIN= -0.91E+01 **kV**
MAX= 0.40E+02 **kV**

IONOSPHERIC CURRENT VECTORS

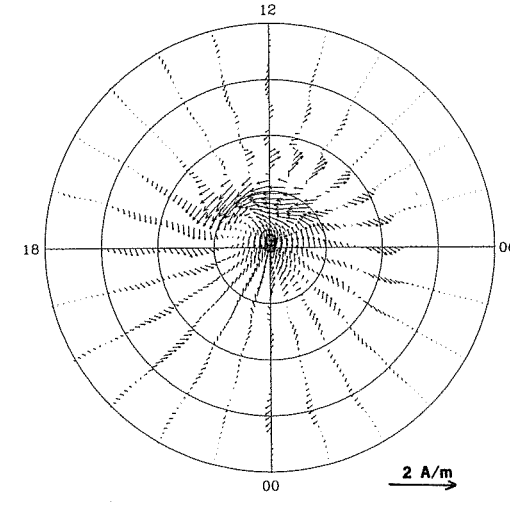

FIELD-ALIGNED CURRENT

24 JUL 1983
1125-40 UT

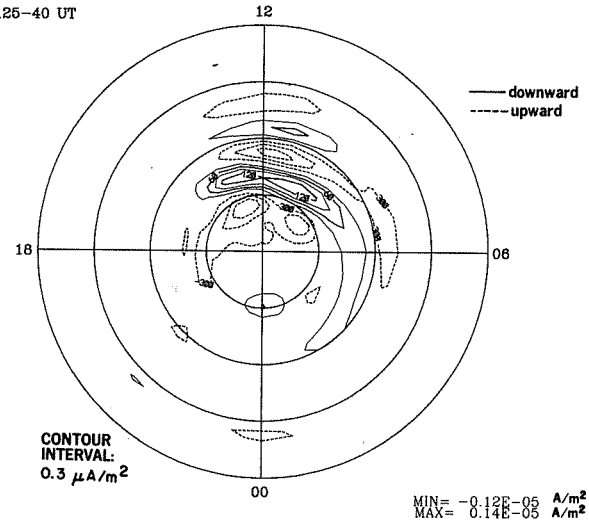

MIN= -0.12E-05 A/m²
MAX= 0.14E-05 A/m²

JOULE HEATING RATE

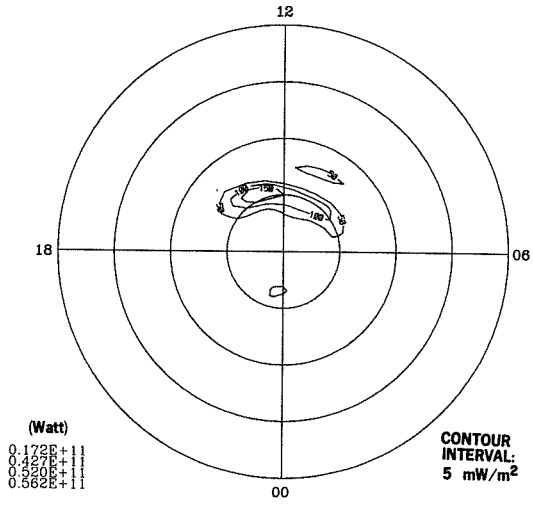

MAX= 0.20E-01 W/m²

HALL CURRENT VECTORS

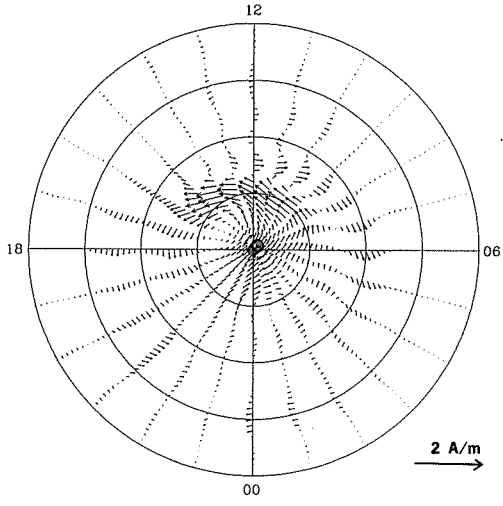

PEDERSEN CURRENT VECTORS

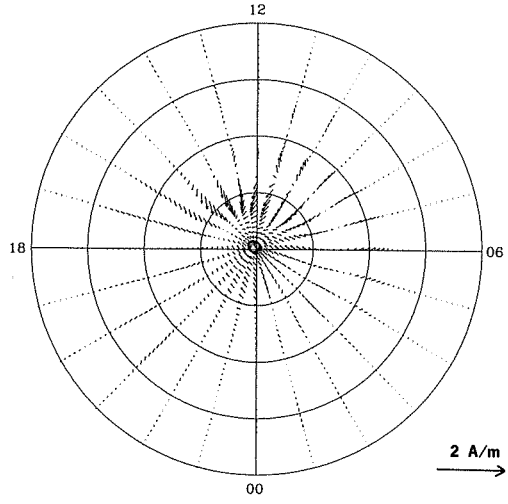

FIELD-ALIGNED HALL CURRENT

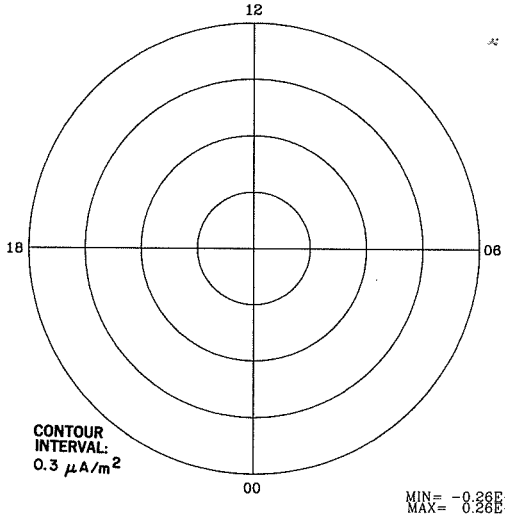

MIN= -0.26E-06 A/m²
MAX= 0.26E-06 A/m²

FIELD-ALIGNED PEDERSEN CURRENT

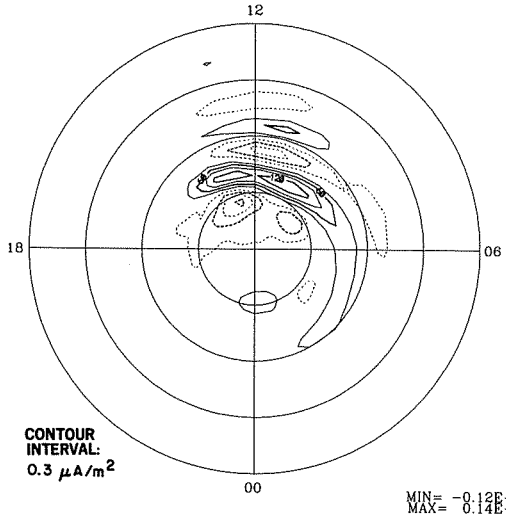

MIN= -0.12E-05 A/m²
MAX= 0.14E-05 A/m²

EQUIVALENT CURRENT VECTORS

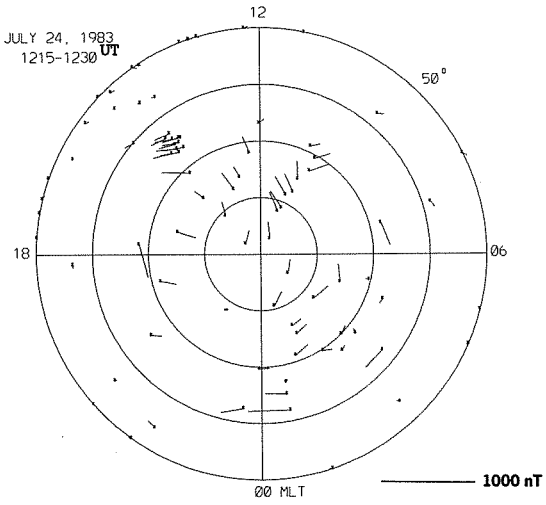

EQUIVALENT CURRENT SYSTEM

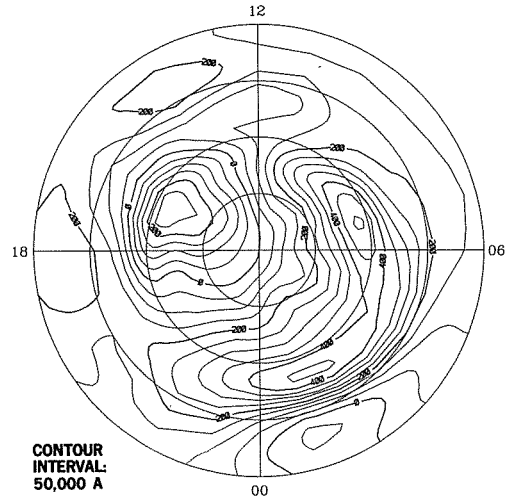

HALL CONDUCTANCE

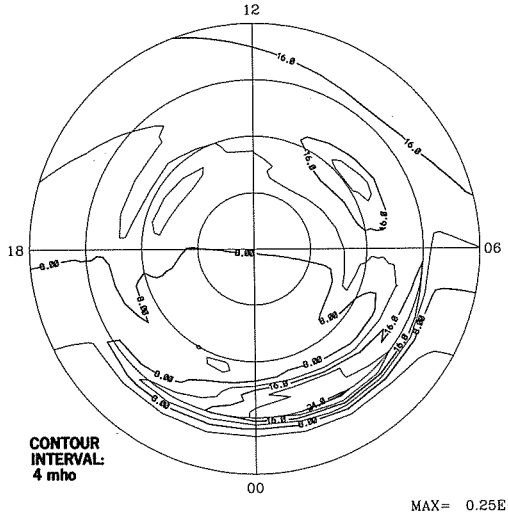

MAX= 0.25E+02 **mho**

PEDERSEN CONDUCTANCE

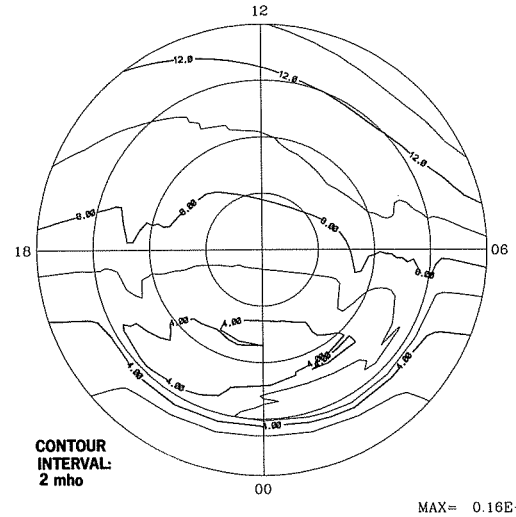

MAX= 0.16E+02 **mho**

ELECTRIC POTENTIAL

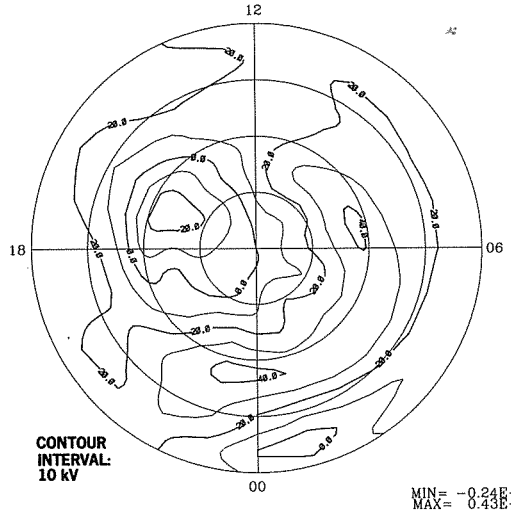

MIN= −0.24E+02 **kV**
MAX= 0.43E+02 **kV**

IONOSPHERIC CURRENT VECTORS

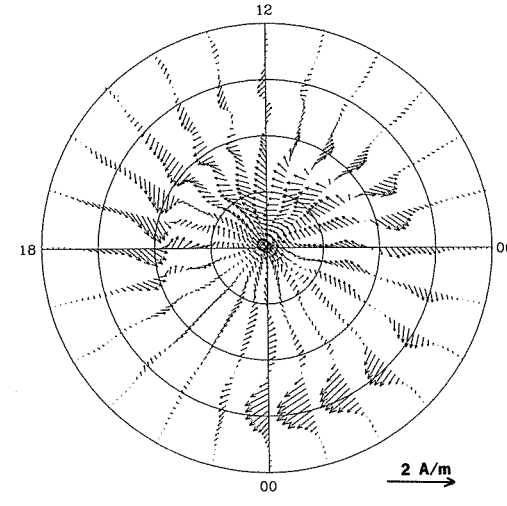

FIELD-ALIGNED CURRENT

24 JUL 1983
1215-30 UT

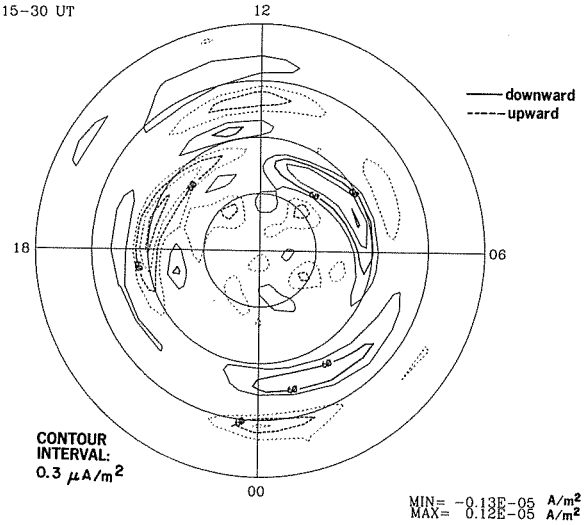

MIN= -0.13E-05 A/m²
MAX= 0.12E-05 A/m²

JOULE HEATING RATE

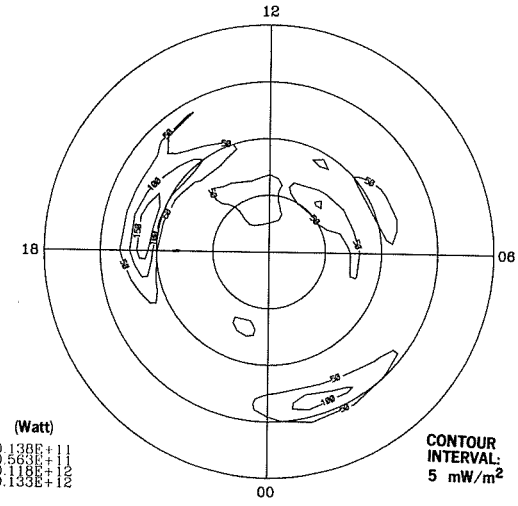

MAX= 0.20E-01 W/m²

HALL CURRENT VECTORS

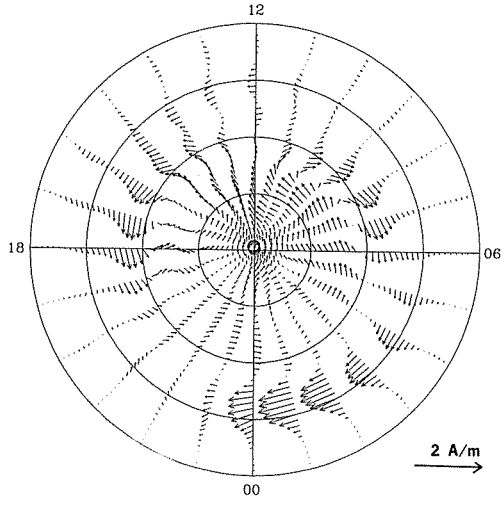

PEDERSEN CURRENT VECTORS

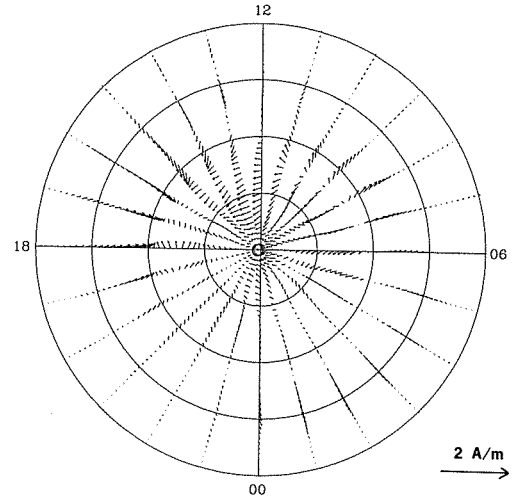

FIELD-ALIGNED HALL CURRENT

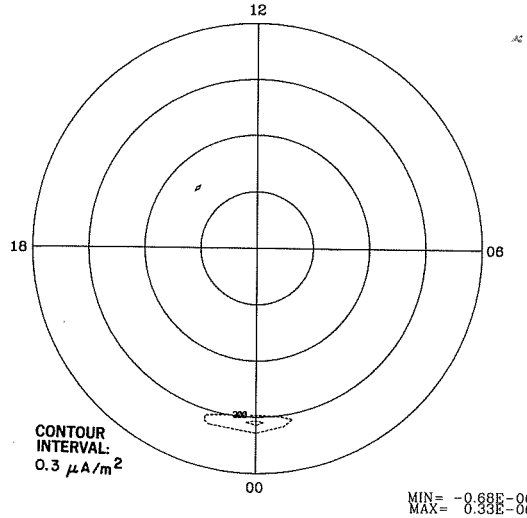

MIN= -0.68E-06 A/m²
MAX= 0.33E-06 A/m²

FIELD-ALIGNED PEDERSEN CURRENT

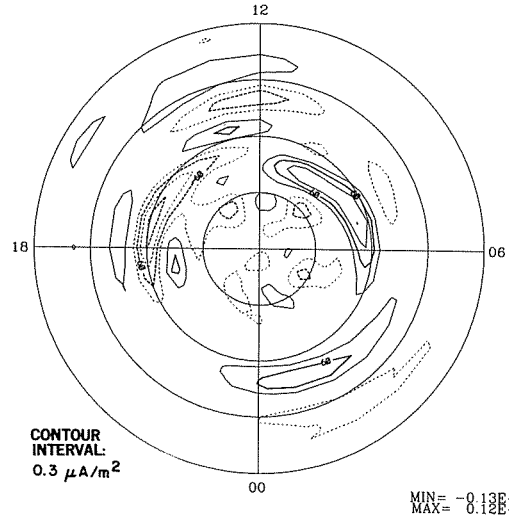

MIN= -0.13E-05 A/m²
MAX= 0.12E-05 A/m²

EQUIVALENT CURRENT VECTORS

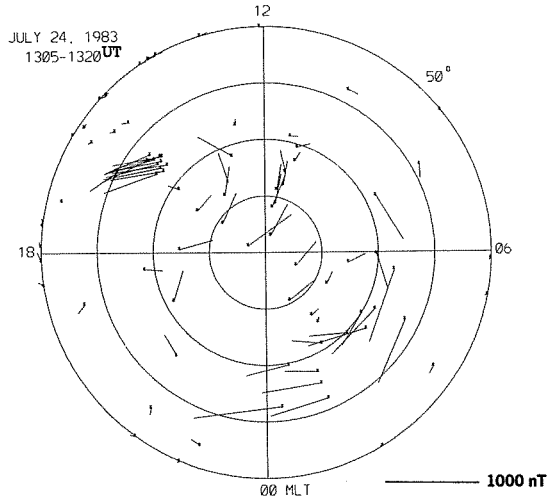

EQUIVALENT CURRENT SYSTEM

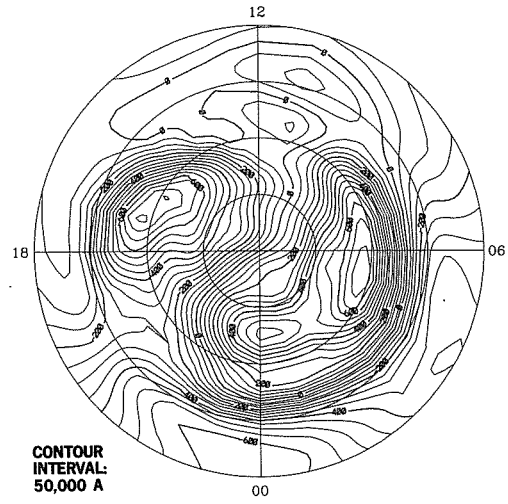

HALL CONDUCTANCE

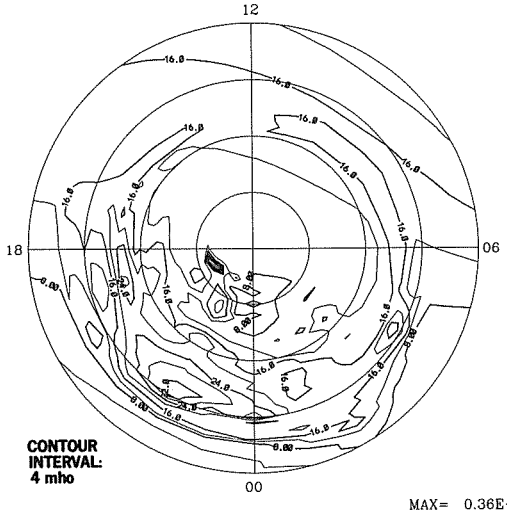

MAX= 0.36E+02 **mho**

DMSP

PEDERSEN CONDUCTANCE

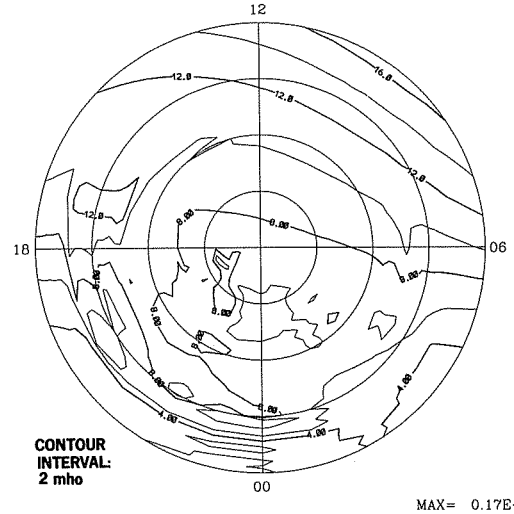

MAX= 0.17E+02 **mho**

ELECTRIC POTENTIAL

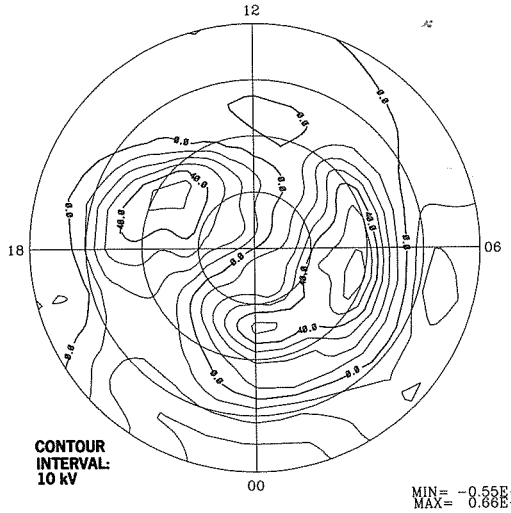

MIN= -0.55E+02 **kV**
MAX= 0.66E+02 **kV**

IONOSPHERIC CURRENT VECTORS

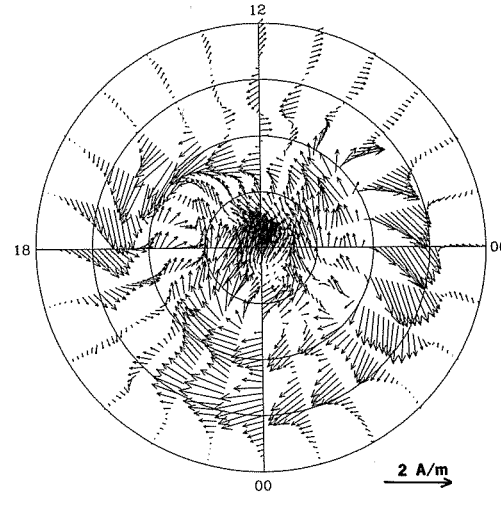

FIELD-ALIGNED CURRENT

24 JUL 1983
1305-20 UT

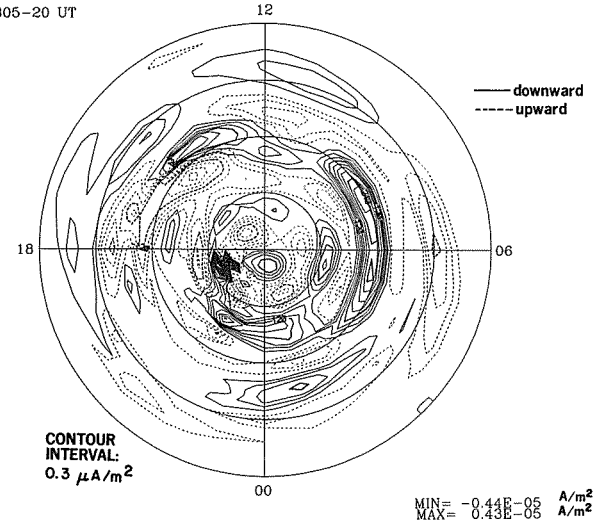

JOULE HEATING RATE

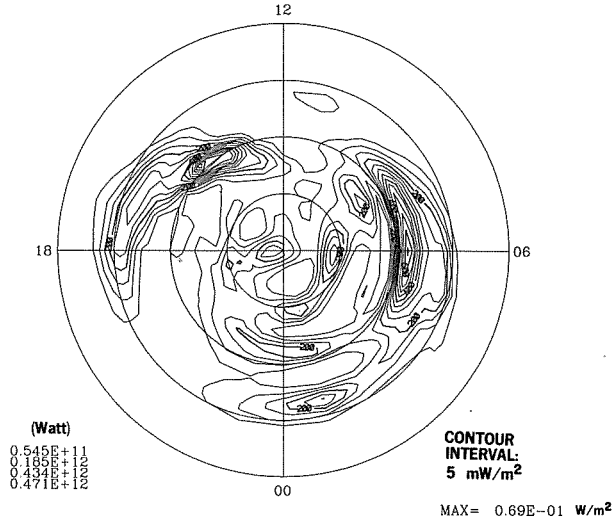

HALL CURRENT VECTORS

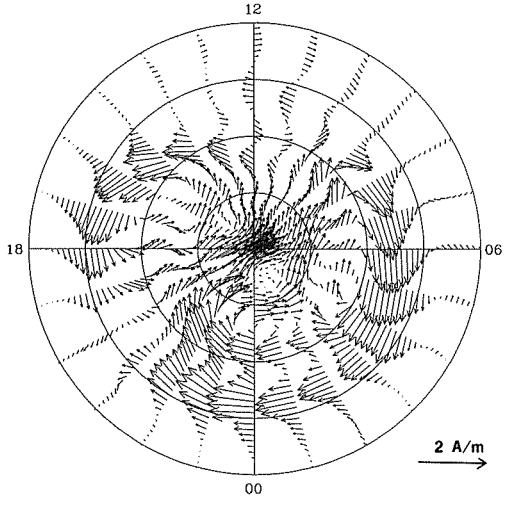

PEDERSEN CURRENT VECTORS

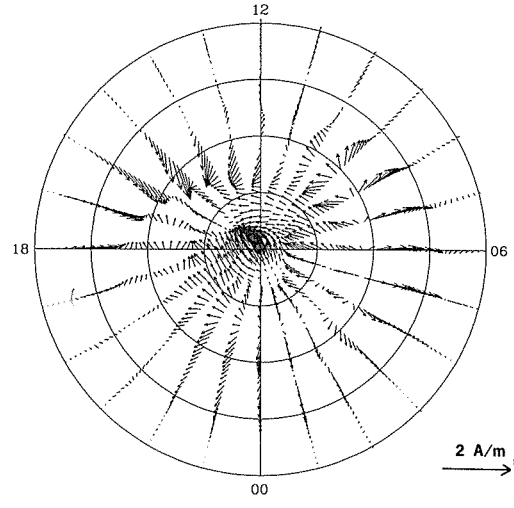

FIELD-ALIGNED HALL CURRENT

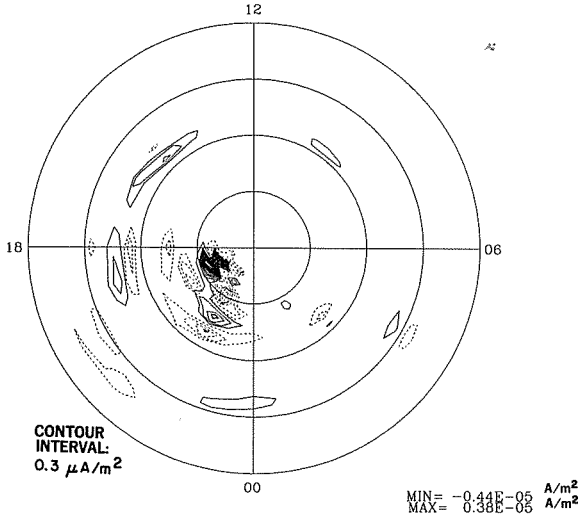

FIELD-ALIGNED PEDERSEN CURRENT

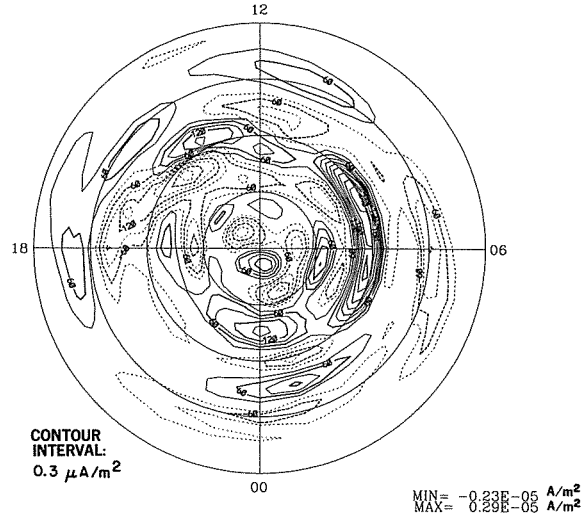

EQUIVALENT CURRENT VECTORS

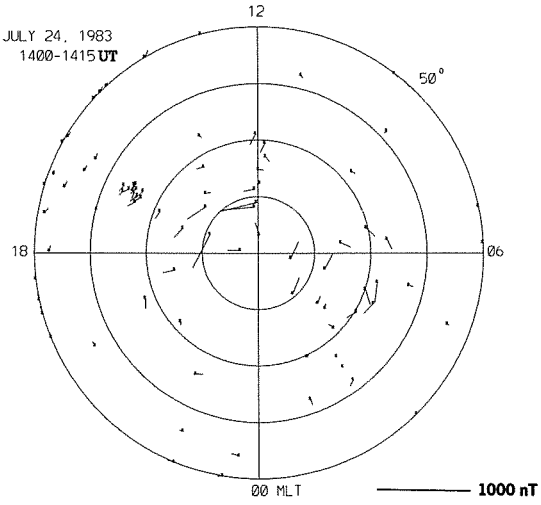

EQUIVALENT CURRENT SYSTEM

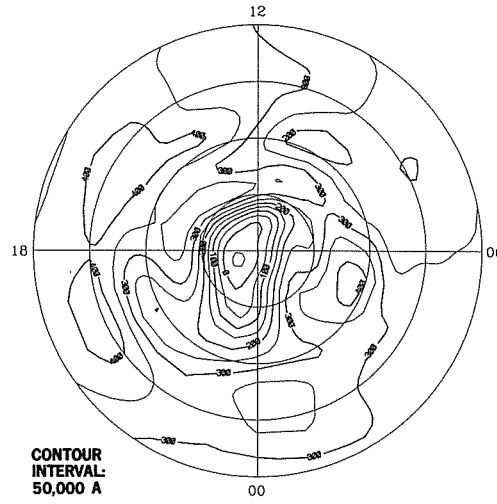

HALL CONDUCTANCE

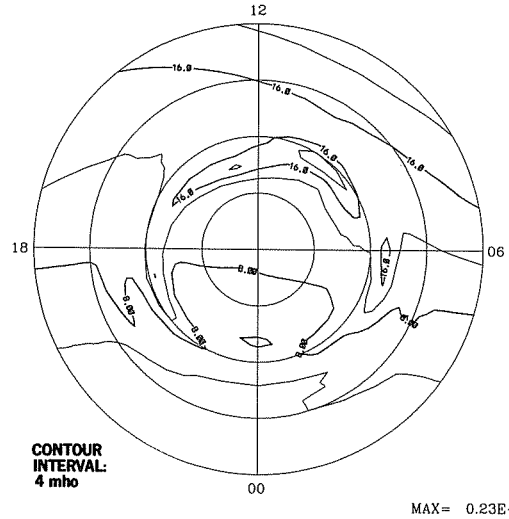

MAX= 0.23E+02 mho

PEDERSEN CONDUCTANCE

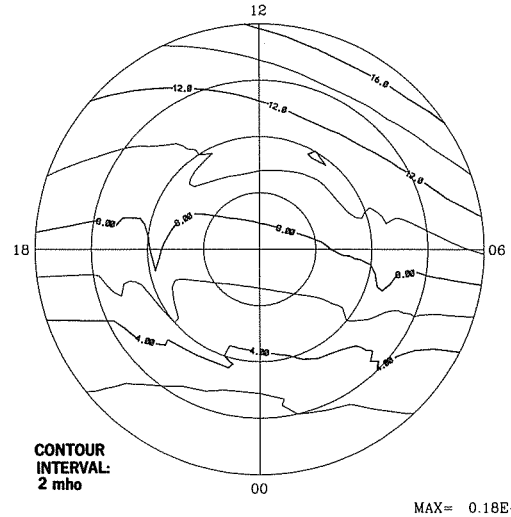

MAX= 0.18E+02 mho

ELECTRIC POTENTIAL

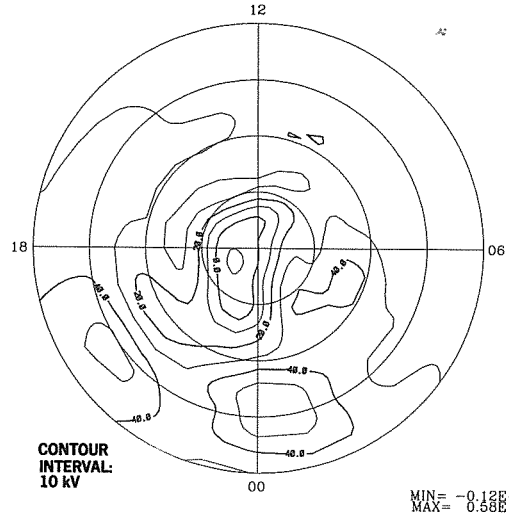

MIN= -0.12E+02 kV
MAX= 0.58E+02 kV

IONOSPHERIC CURRENT VECTORS

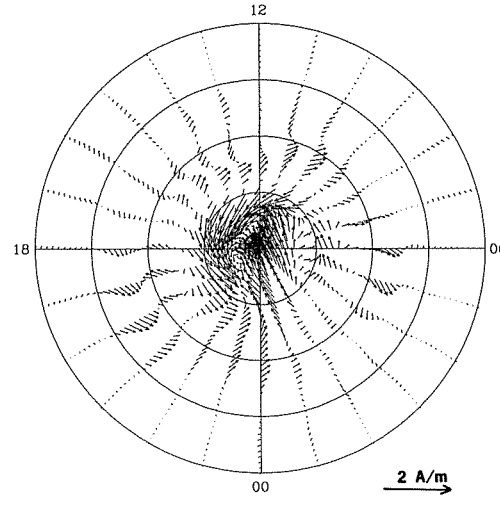

FIELD-ALIGNED CURRENT

24 JUL 1983
1400-15 UT

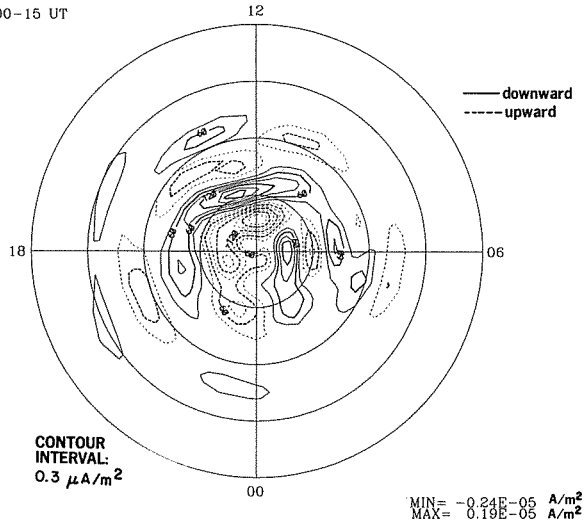

MIN= -0.24E-05 A/m²
MAX= 0.19E-05 A/m²

JOULE HEATING RATE

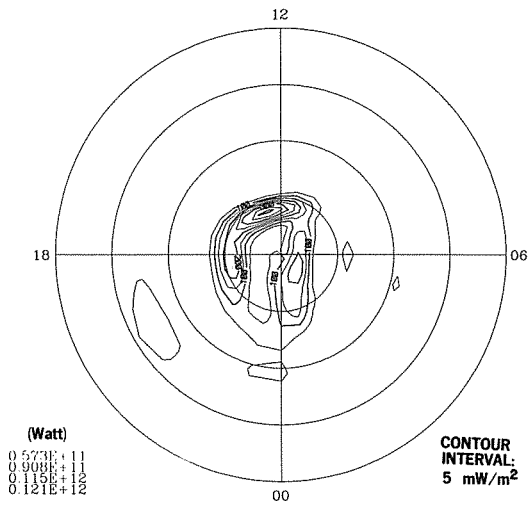

MAX= 0.42E-01 W/m²

HALL CURRENT VECTORS

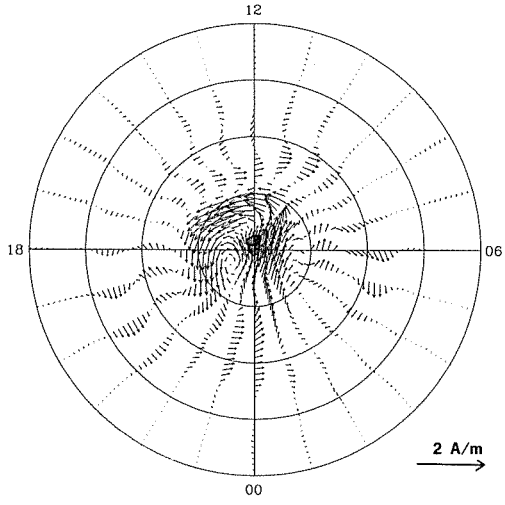

PEDERSEN CURRENT VECTORS

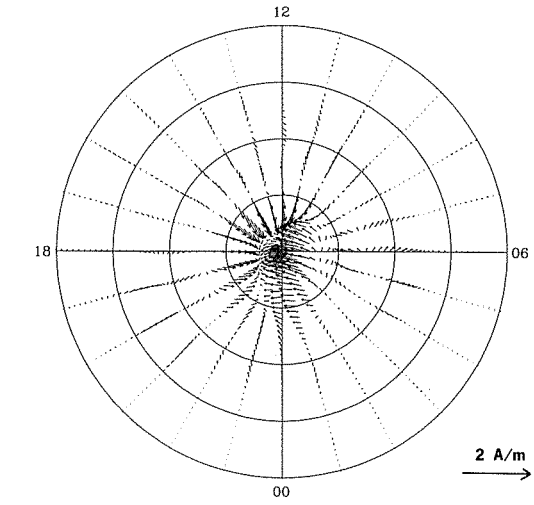

FIELD-ALIGNED HALL CURRENT

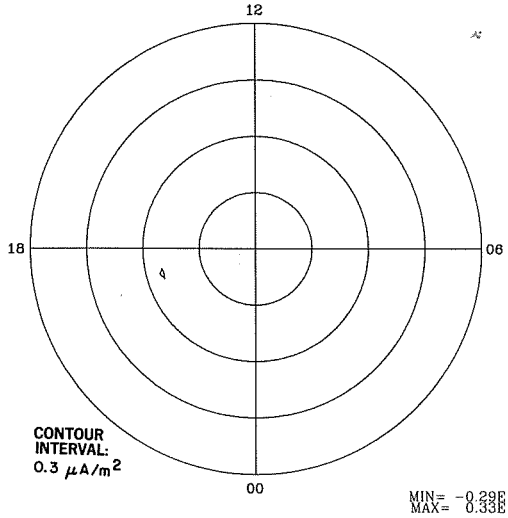

MIN= -0.29E-06 A/m²
MAX= 0.33E-06 A/m²

FIELD-ALIGNED PEDERSEN CURRENT

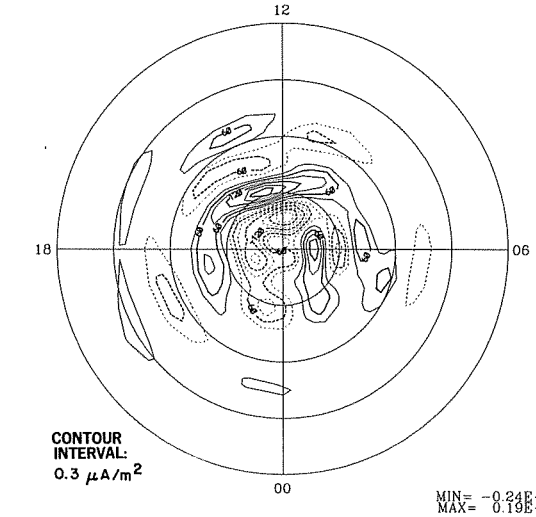

MIN= -0.24E-05 A/m²
MAX= 0.19E-05 A/m²

EQUIVALENT CURRENT VECTORS

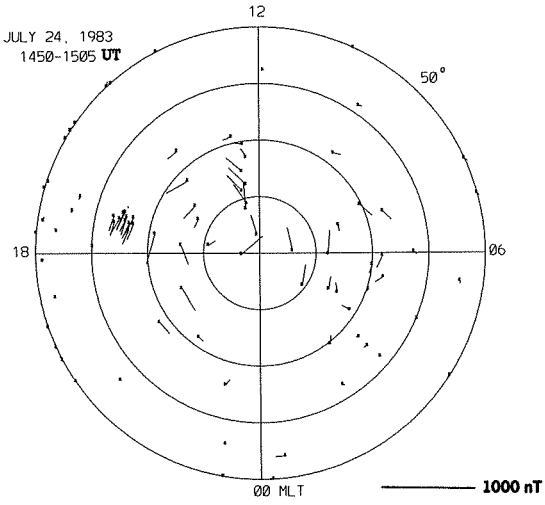

EQUIVALENT CURRENT SYSTEM

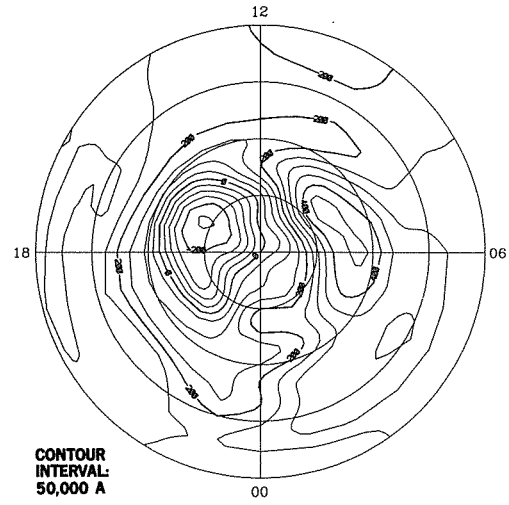

HALL CONDUCTANCE

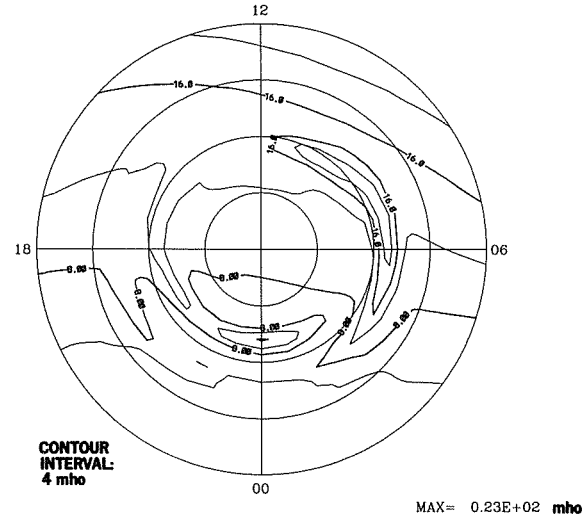

MAX= 0.23E+02 mho

PEDERSEN CONDUCTANCE

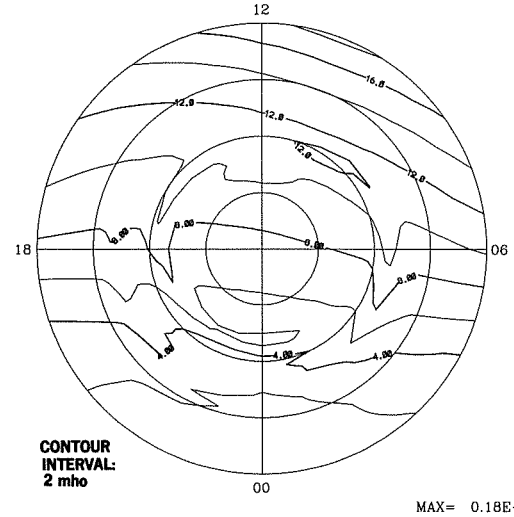

MAX= 0.18E+02 mho

ELECTRIC POTENTIAL

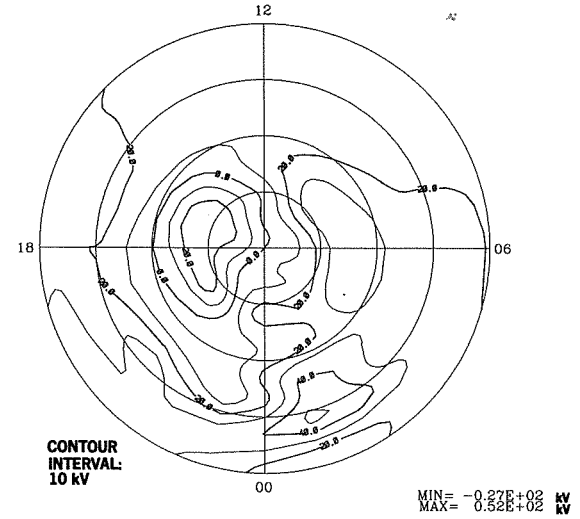

MIN= -0.27E+02 kV
MAX= 0.52E+02 kV

IONOSPHERIC CURRENT VECTORS

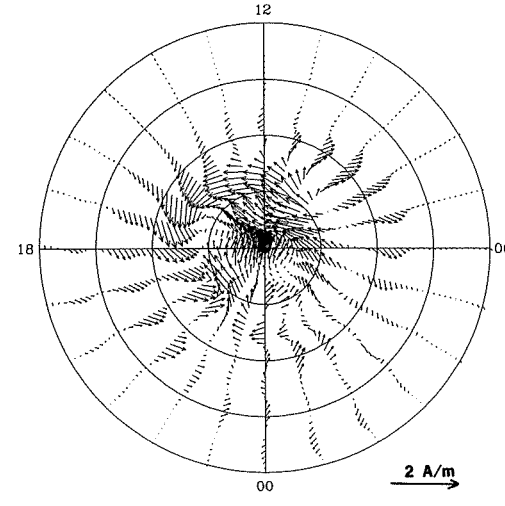

FIELD-ALIGNED CURRENT

24 JUL 1983
1450–1505 UT

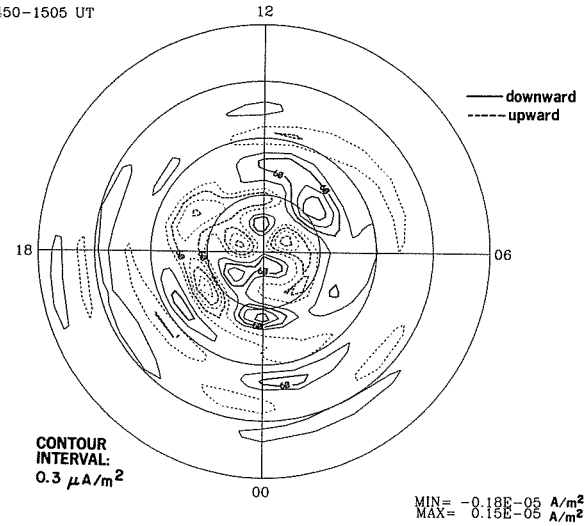

MIN= -0.18E-05 A/m²
MAX= 0.15E-05 A/m²

JOULE HEATING RATE

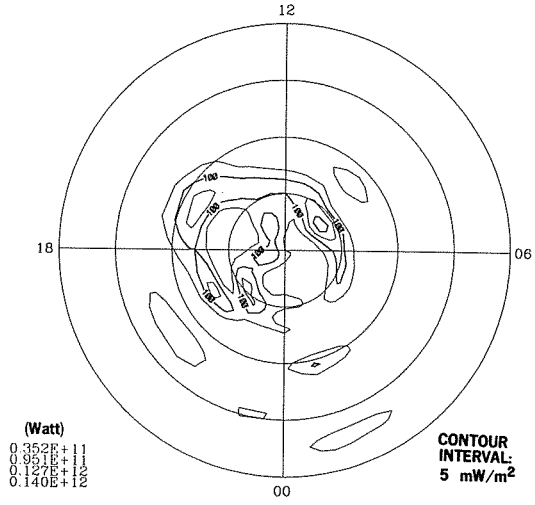

MAX= 0.22E-01 W/m²

HALL CURRENT VECTORS

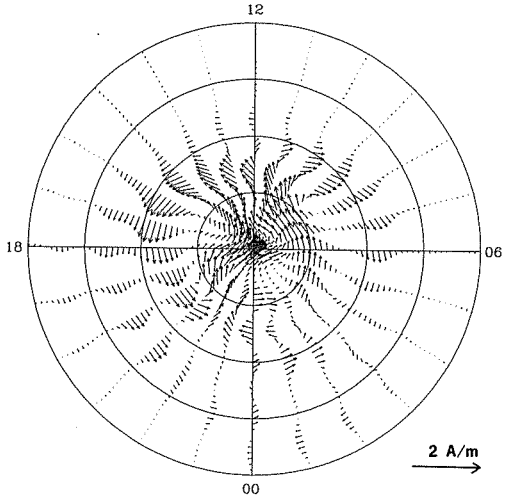

PEDERSEN CURRENT VECTORS

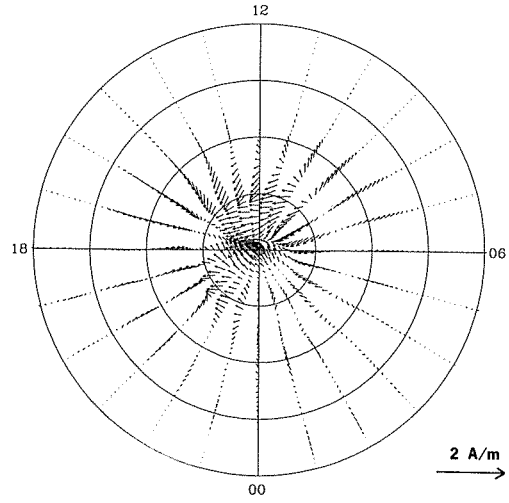

FIELD-ALIGNED HALL CURRENT

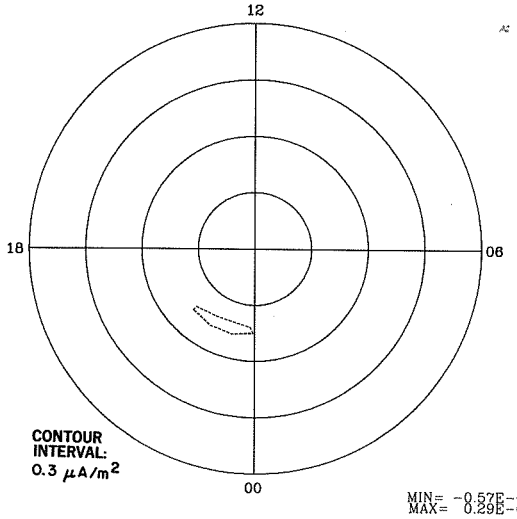

MIN= -0.57E-06 A/m²
MAX= 0.29E-06 A/m²

FIELD-ALIGNED PEDERSEN CURRENT

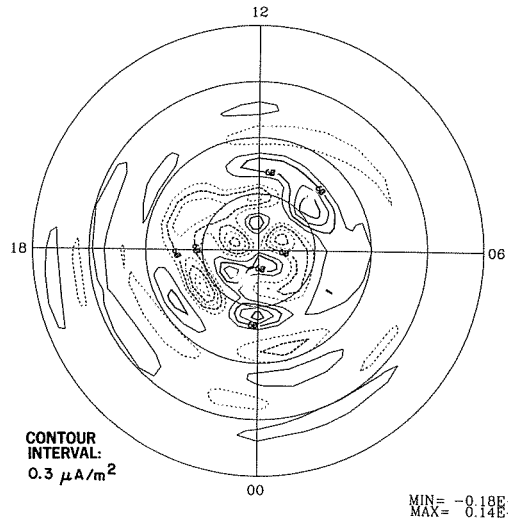

MIN= -0.18E-05 A/m²
MAX= 0.14E-05 A/m²

EQUIVALENT CURRENT VECTORS

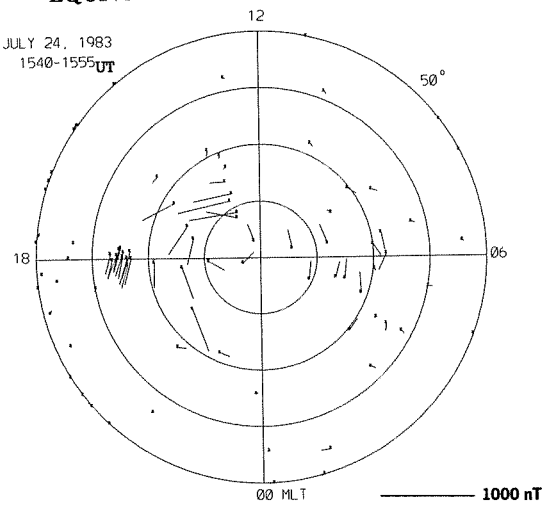

EQUIVALENT CURRENT SYSTEM

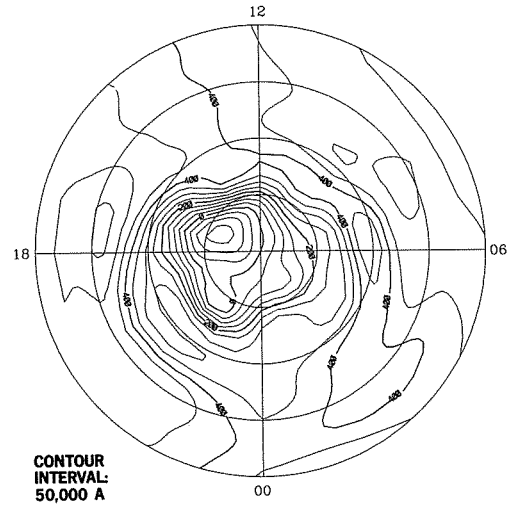

HALL CONDUCTANCE

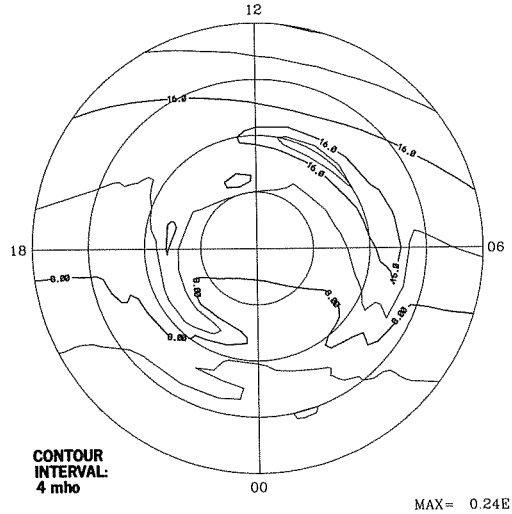

MAX= 0.24E+02 mho

PEDERSEN CONDUCTANCE

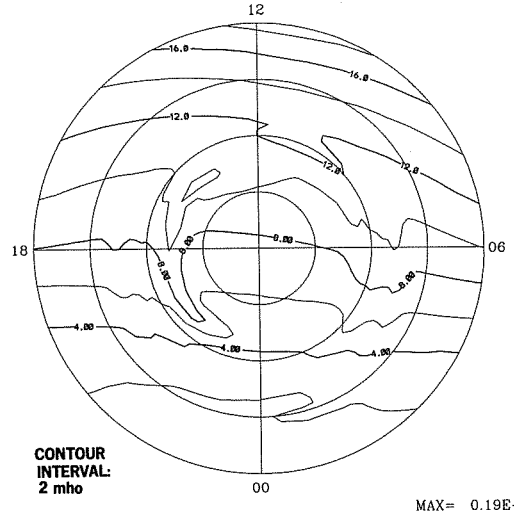

MAX= 0.19E+02 mho

ELECTRIC POTENTIAL

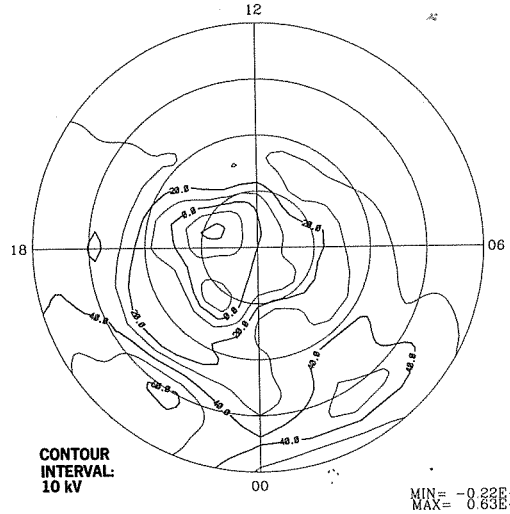

MIN= -0.22E+02 kV
MAX= 0.63E+02 kV

IONOSPHERIC CURRENT VECTORS

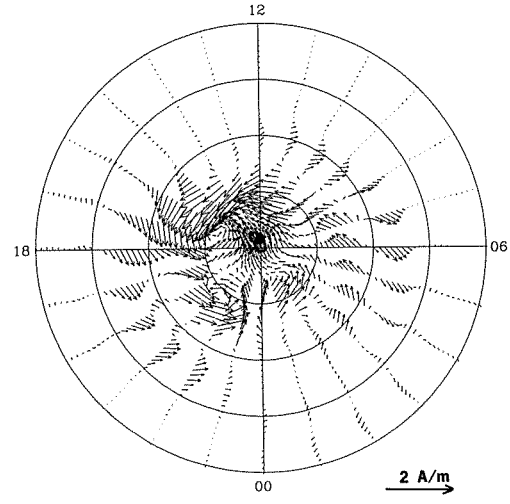

FIELD-ALIGNED CURRENT

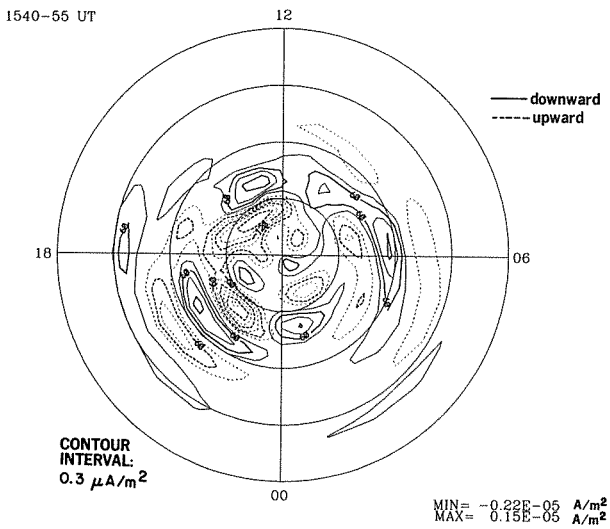

JOULE HEATING RATE

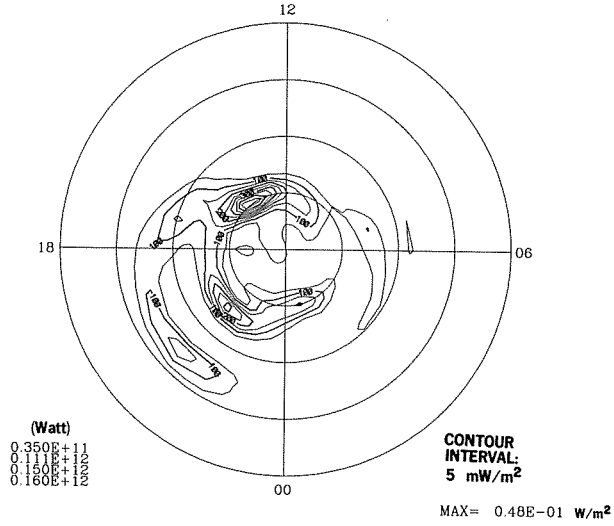

HALL CURRENT VECTORS

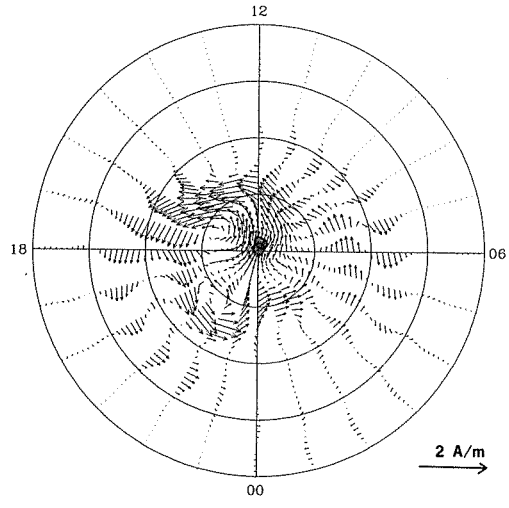

PEDERSEN CURRENT VECTORS

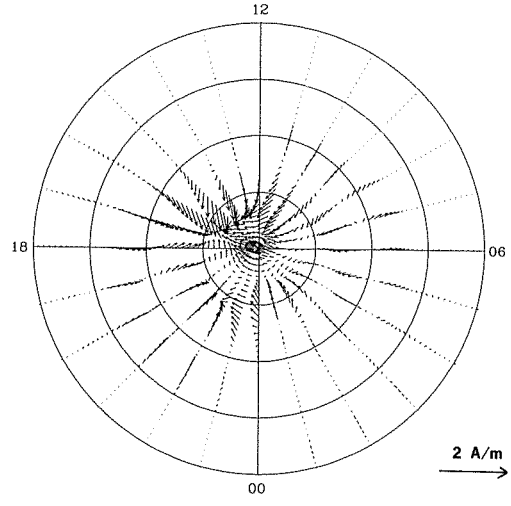

FIELD-ALIGNED HALL CURRENT

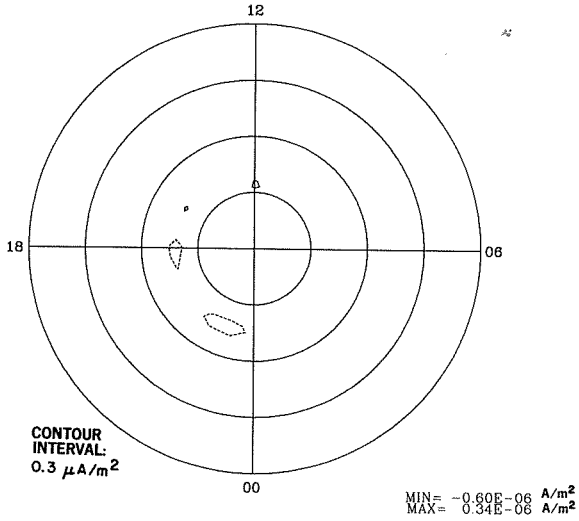

FIELD-ALIGNED PEDERSEN CURRENT

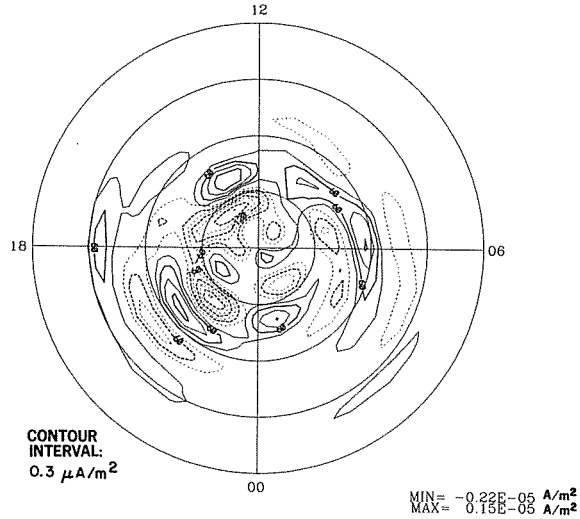

EQUIVALENT CURRENT VECTORS

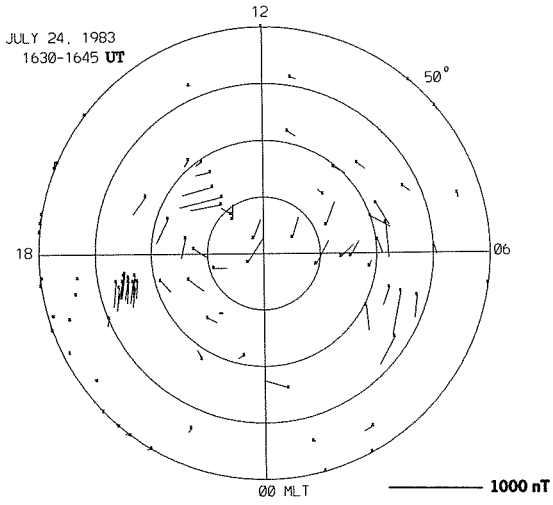

EQUIVALENT CURRENT SYSTEM

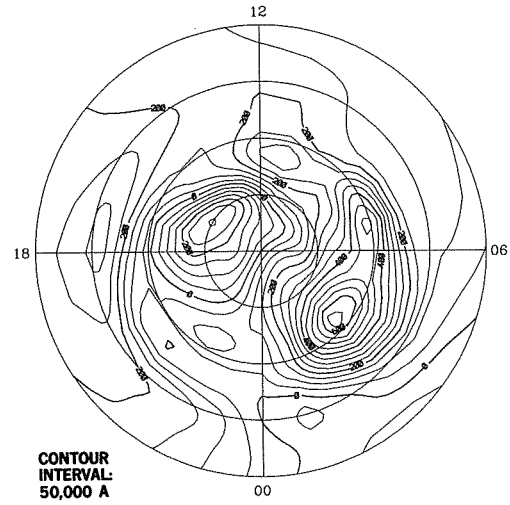

HALL CONDUCTANCE

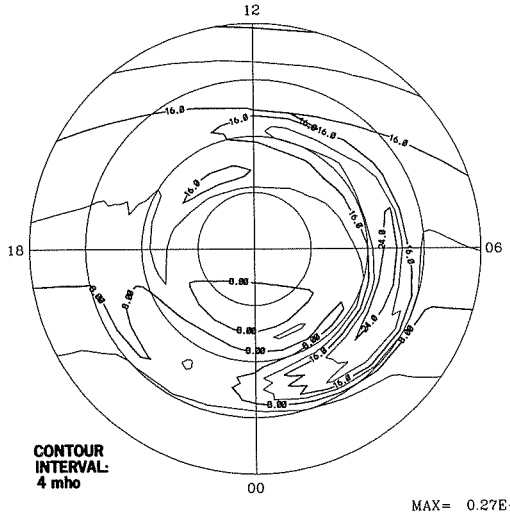

MAX= 0.27E+02 mho

PEDERSEN CONDUCTANCE

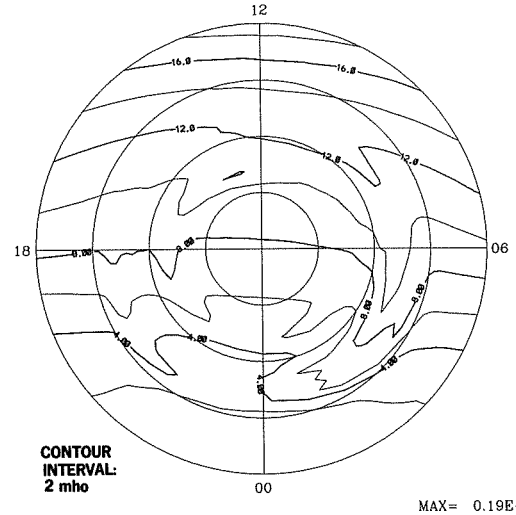

MAX= 0.19E+02 mho

ELECTRIC POTENTIAL

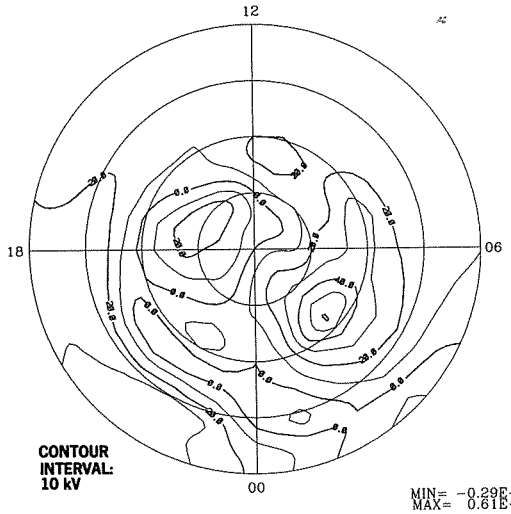

MIN= -0.29E+02 kV
MAX= 0.61E+02 kV

IONOSPHERIC CURRENT VECTORS

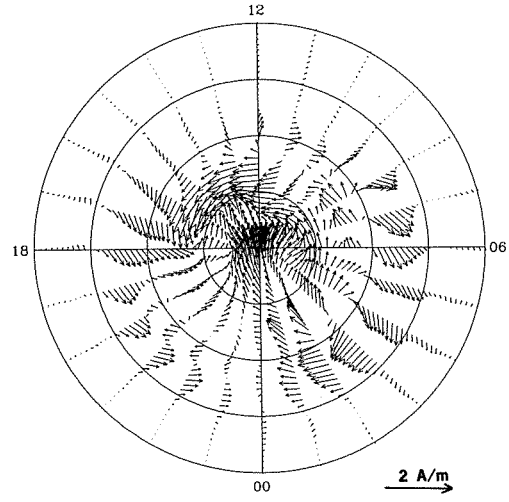

FIELD-ALIGNED CURRENT

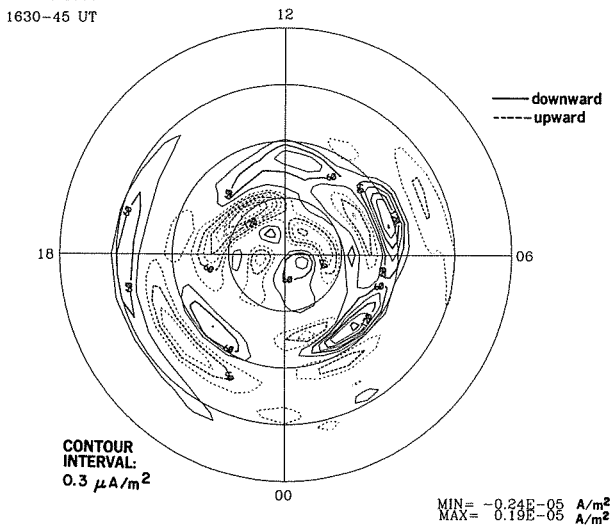

JOULE HEATING RATE

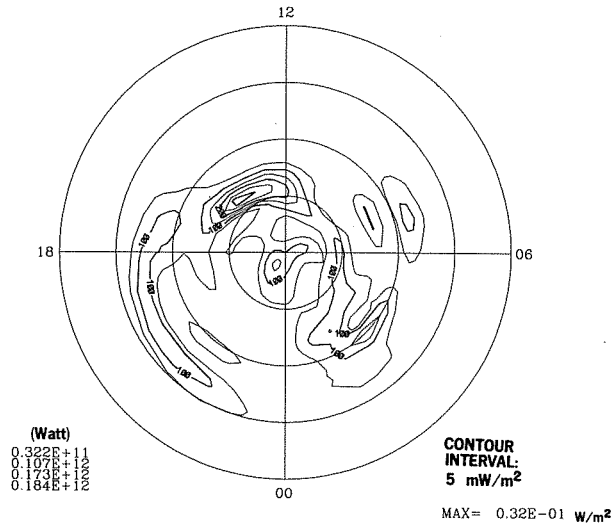

HALL CURRENT VECTORS

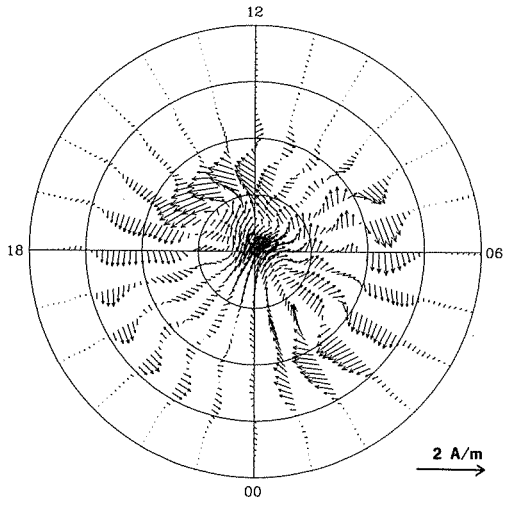

PEDERSEN CURRENT VECTORS

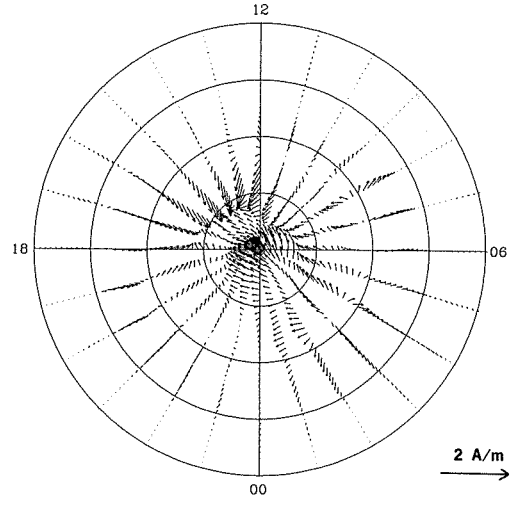

FIELD-ALIGNED HALL CURRENT

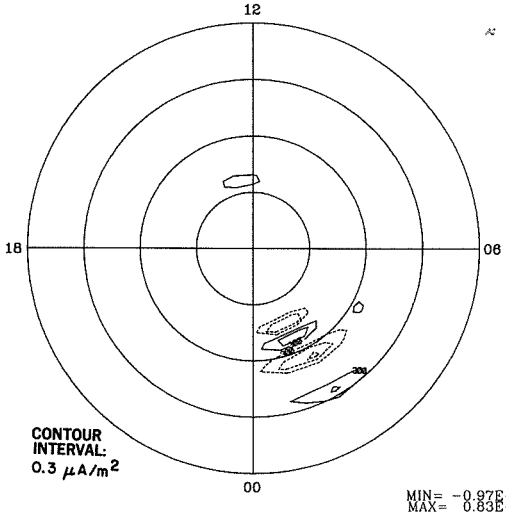

FIELD-ALIGNED PEDERSEN CURRENT

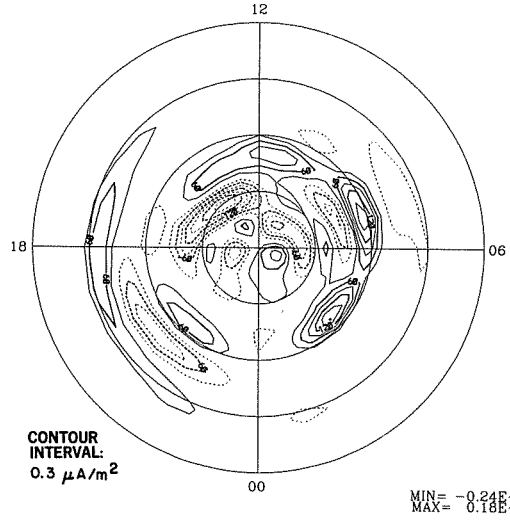

EQUIVALENT CURRENT VECTORS

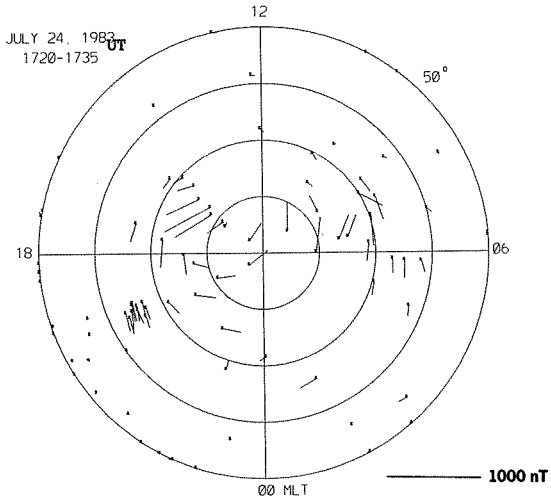

EQUIVALENT CURRENT SYSTEM

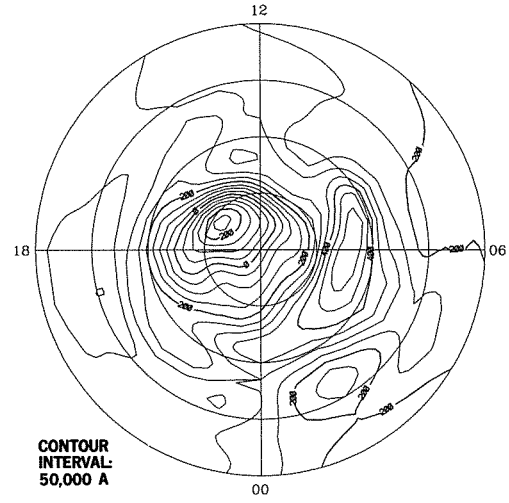

HALL CONDUCTANCE

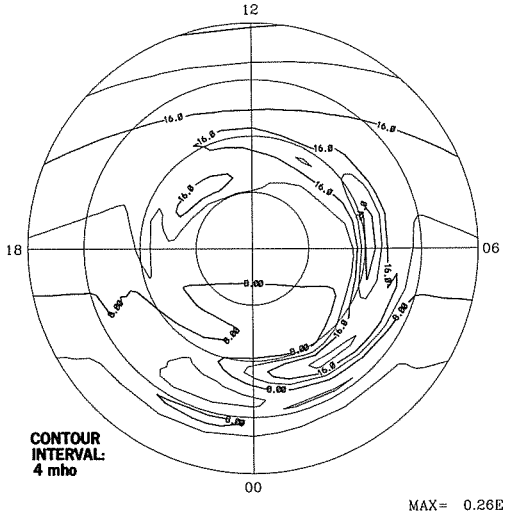

MAX= 0.26E+02 mho

PEDERSEN CONDUCTANCE

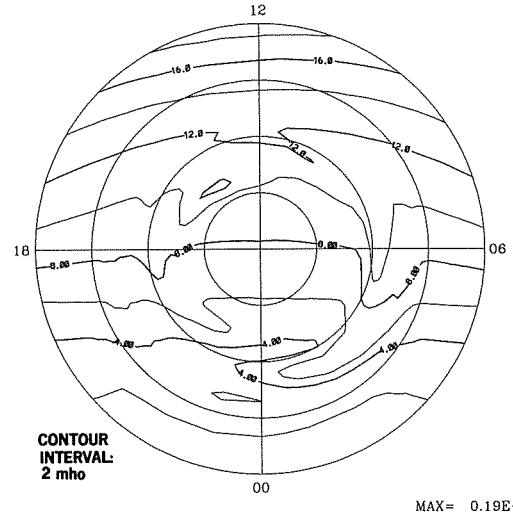

MAX= 0.19E+02 mho

ELECTRIC POTENTIAL

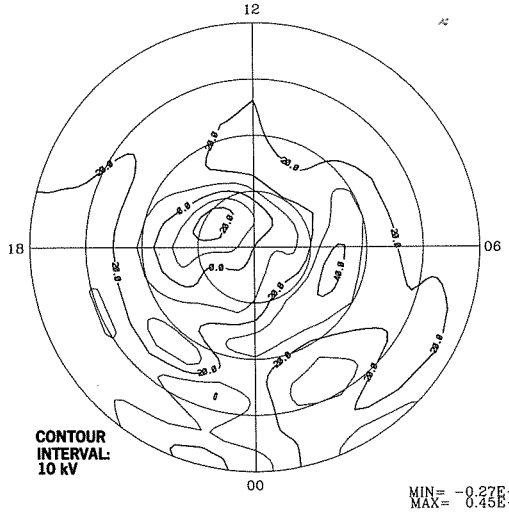

MIN= -0.27E+02 kV
MAX= 0.45E+02 kV

IONOSPHERIC CURRENT VECTORS

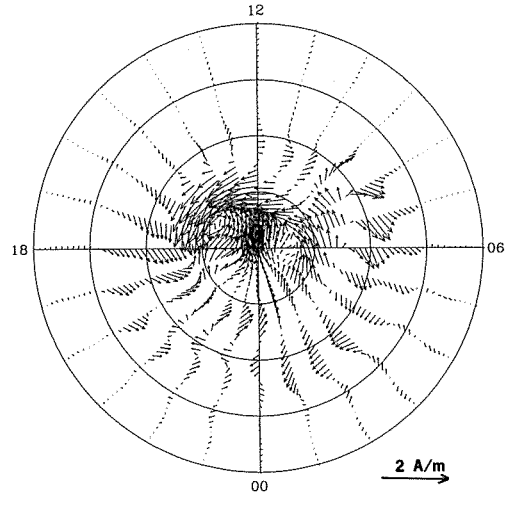

FIELD-ALIGNED CURRENT

24 JUL 1983
1720-35 UT

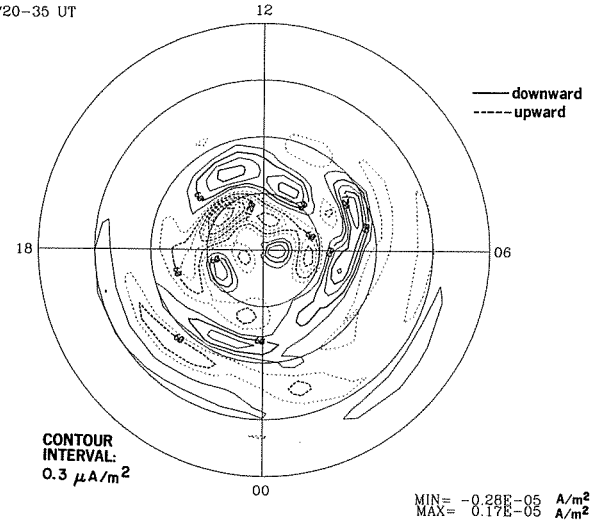

MIN= -0.28E-05 A/m²
MAX= 0.17E-05 A/m²

JOULE HEATING RATE

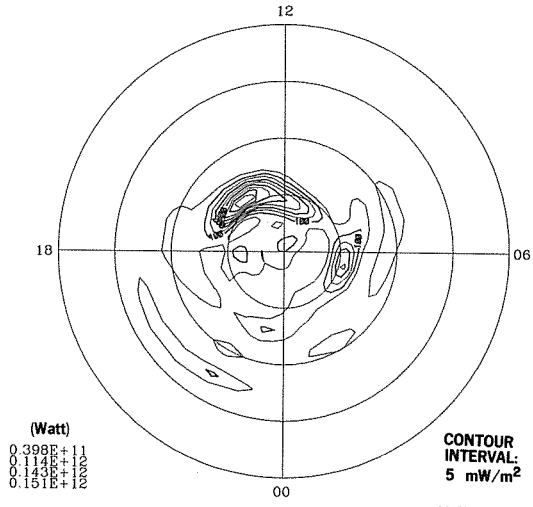

MAX= 0.47E-01 W/m²

HALL CURRENT VECTORS

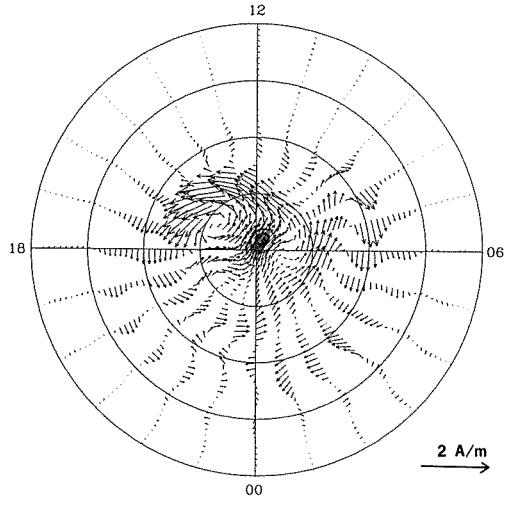

PEDERSEN CURRENT VECTORS

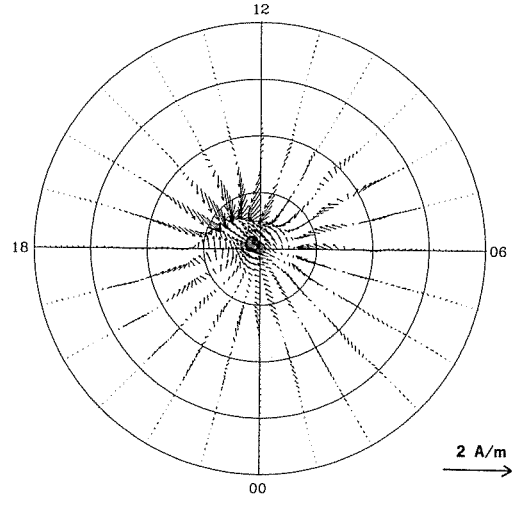

FIELD-ALIGNED HALL CURRENT

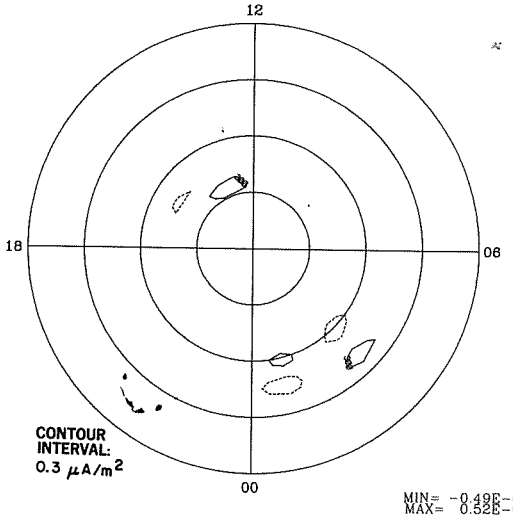

MIN= -0.49E-06 A/m²
MAX= 0.52E-06 A/m²

FIELD-ALIGNED PEDERSEN CURRENT

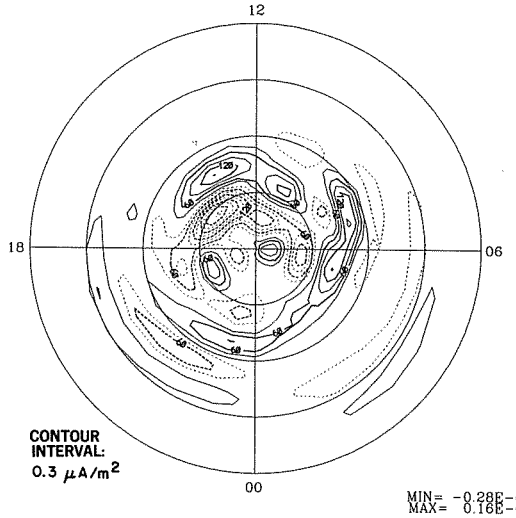

MIN= -0.28E-05 A/m²
MAX= 0.16E-05 A/m²

EQUIVALENT CURRENT VECTORS

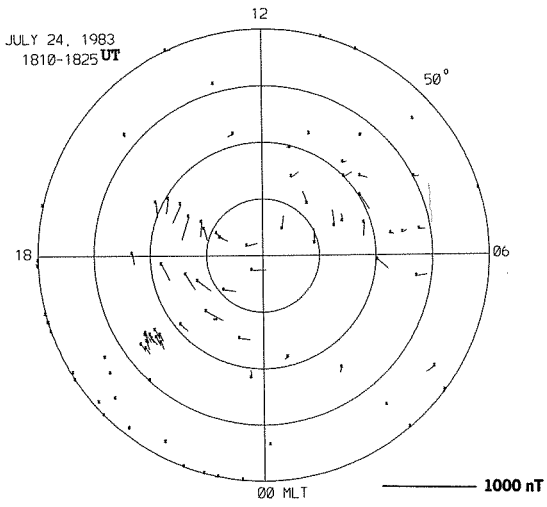

EQUIVALENT CURRENT SYSTEM

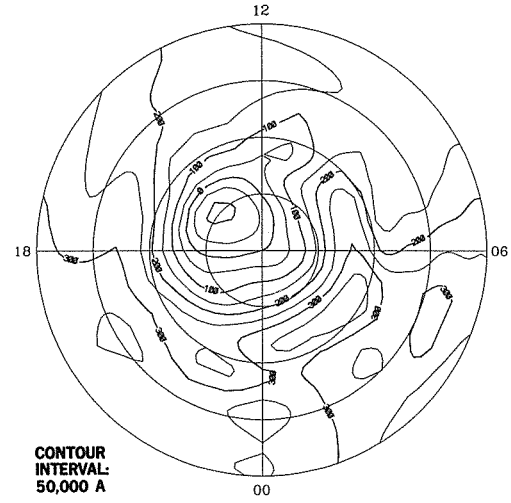

HALL CONDUCTANCE

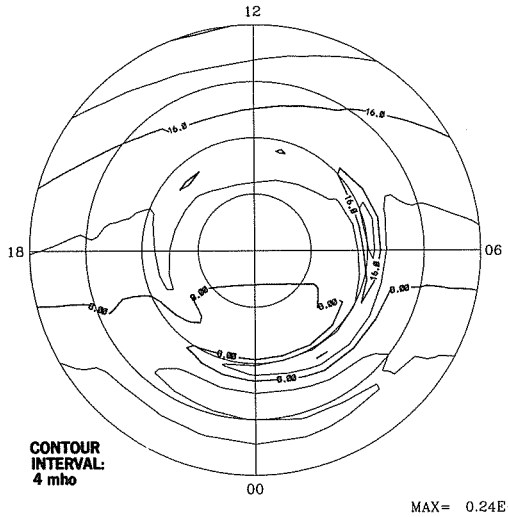

MAX= 0.24E+02 **mho**

PEDERSEN CONDUCTANCE

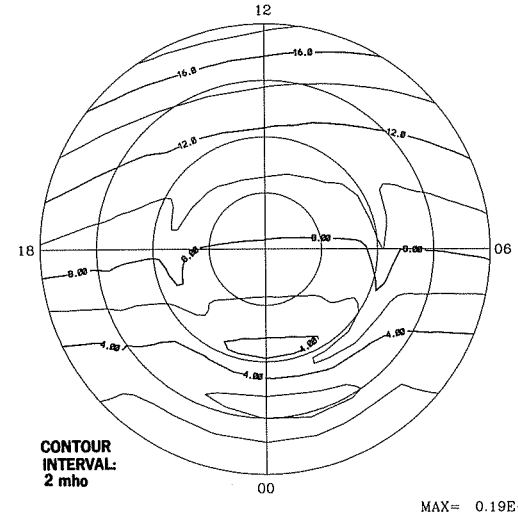

MAX= 0.19E+02 **mho**

ELECTRIC POTENTIAL

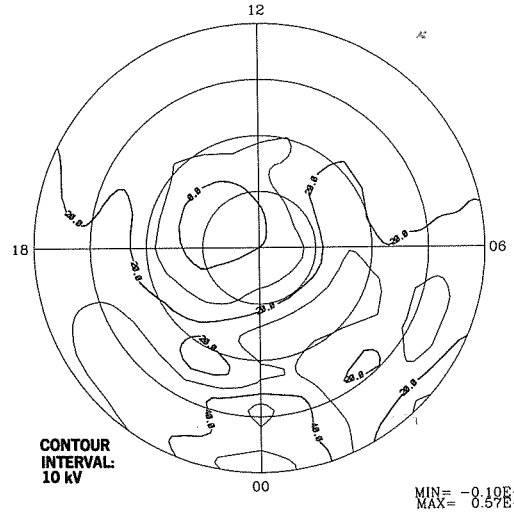

MIN= -0.10E+02 **kV**
MAX= 0.57E+02 **kV**

IONOSPHERIC CURRENT VECTORS

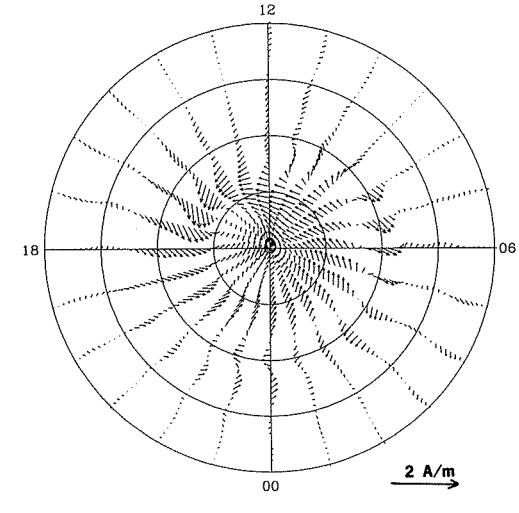

FIELD-ALIGNED CURRENT

24 JUL 1983
1810–25 UT

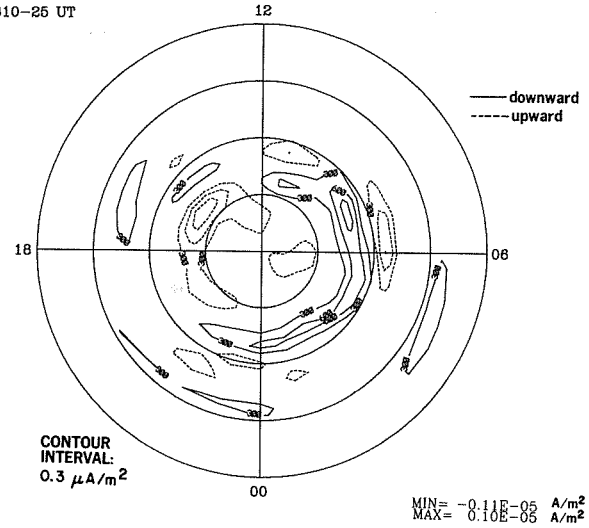

JOULE HEATING RATE

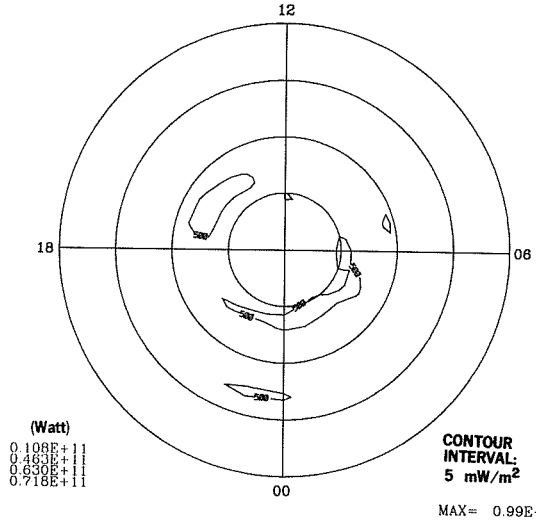

HALL CURRENT VECTORS

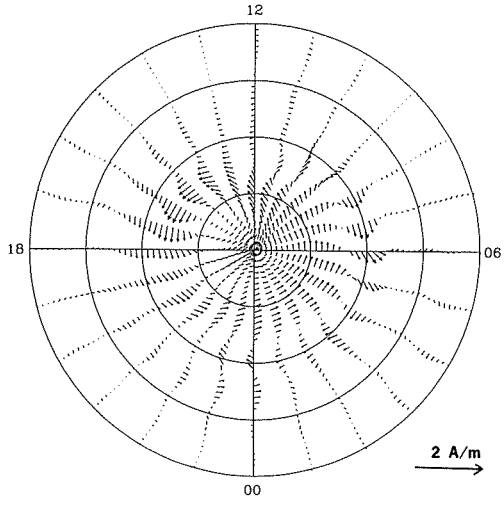

PEDERSEN CURRENT VECTORS

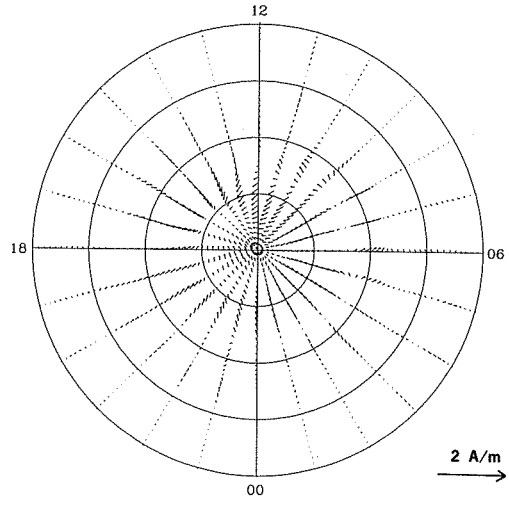

FIELD-ALIGNED HALL CURRENT

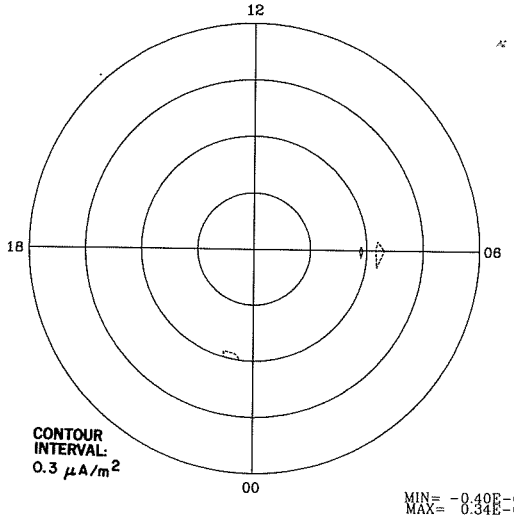

FIELD-ALIGNED PEDERSEN CURRENT

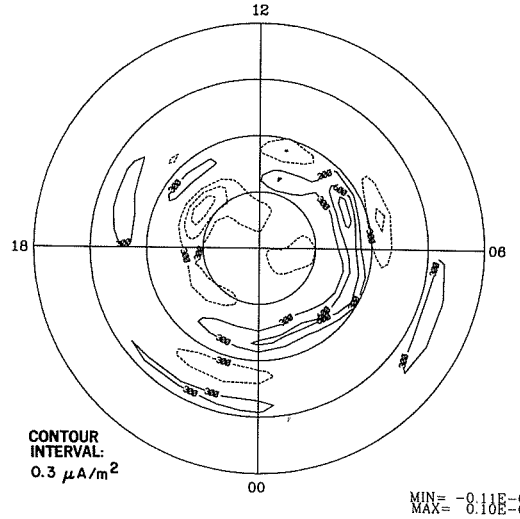

EQUIVALENT CURRENT VECTORS

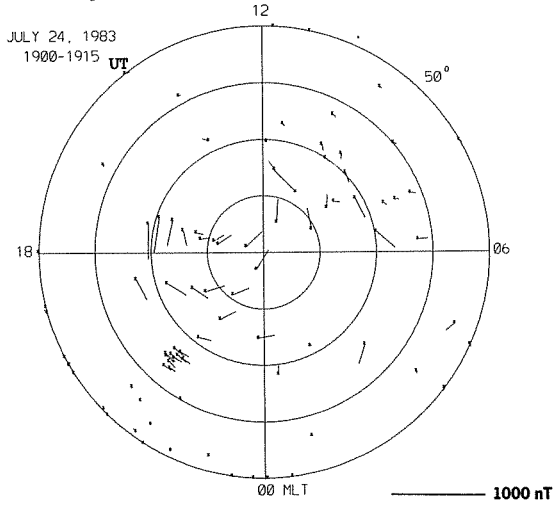

EQUIVALENT CURRENT SYSTEM

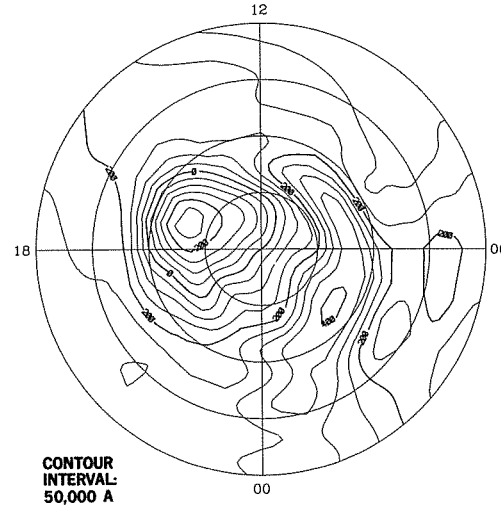

HALL CONDUCTANCE

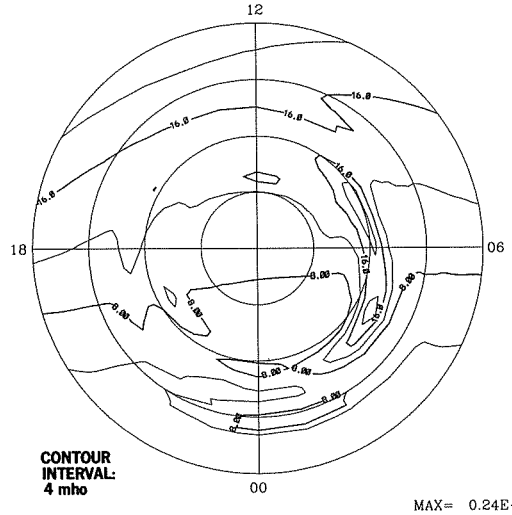

MAX= 0.24E+02 mho

PEDERSEN CONDUCTANCE

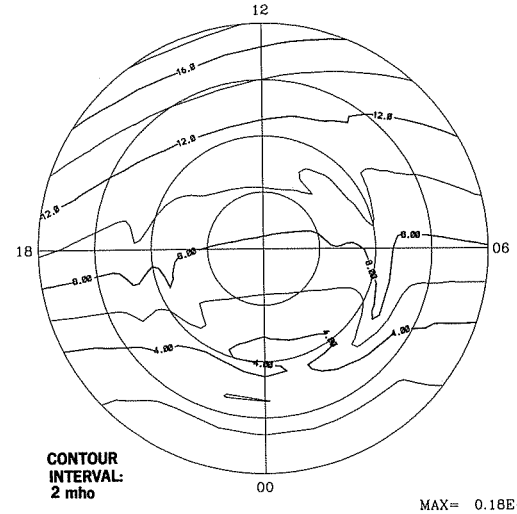

MAX= 0.18E+02 mho

ELECTRIC POTENTIAL

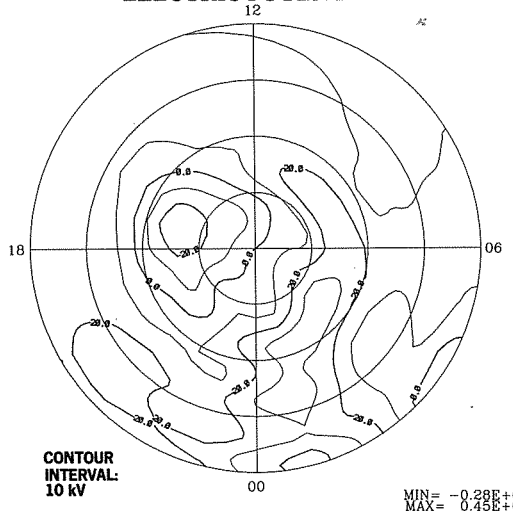

MIN= -0.28E+02 kV
MAX= 0.45E+02 kV

IONOSPHERIC CURRENT VECTORS

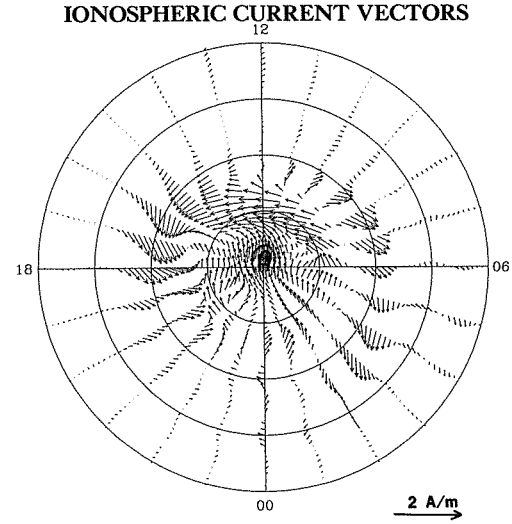

FIELD-ALIGNED CURRENT

24 JUL 1983
1900-15 UT

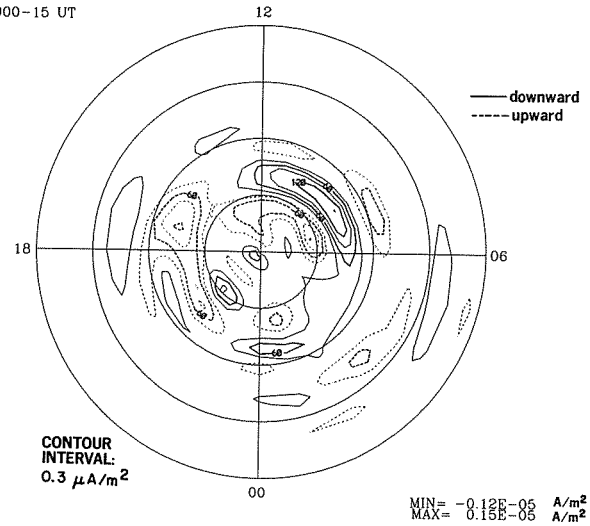

MIN= -0.12E-05 A/m²
MAX= 0.15E-05 A/m²

JOULE HEATING RATE

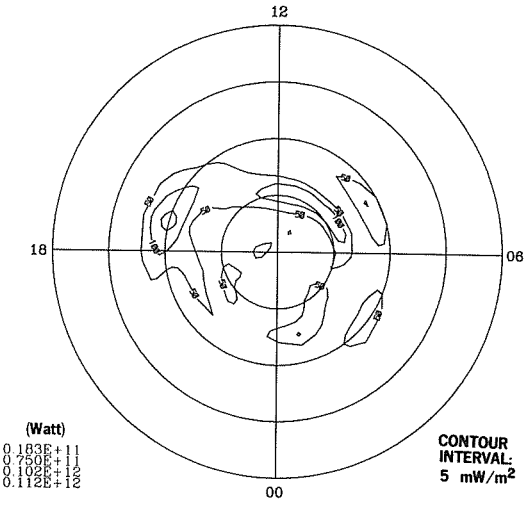

MAX= 0.17E-01 W/m²

HALL CURRENT VECTORS

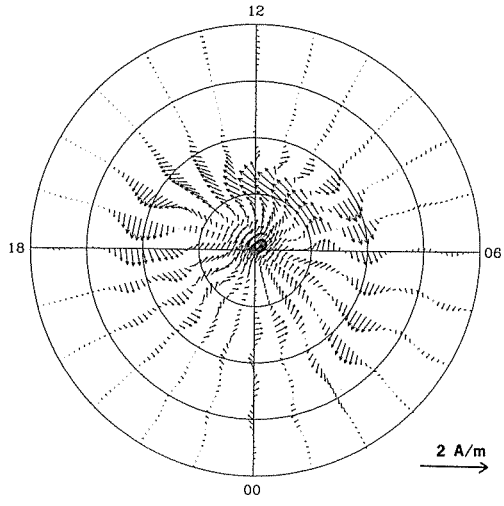

PEDERSEN CURRENT VECTORS

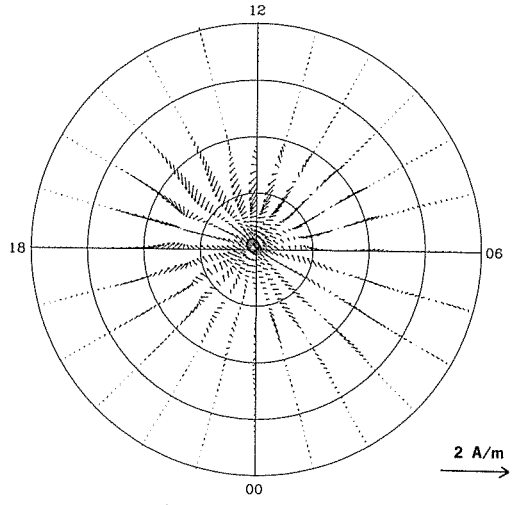

FIELD-ALIGNED HALL CURRENT

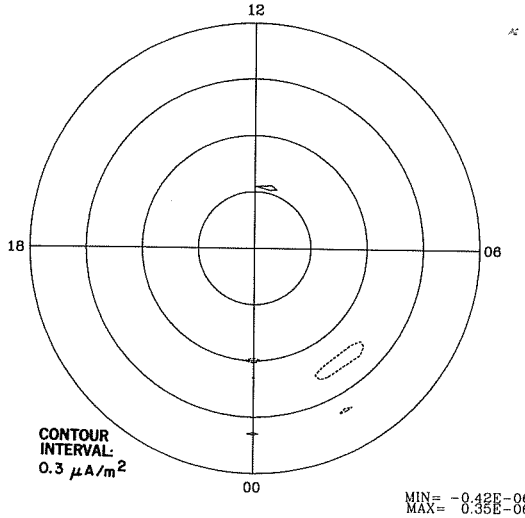

MIN= -0.42E-06 A/m²
MAX= 0.35E-06 A/m²

FIELD-ALIGNED PEDERSEN CURRENT

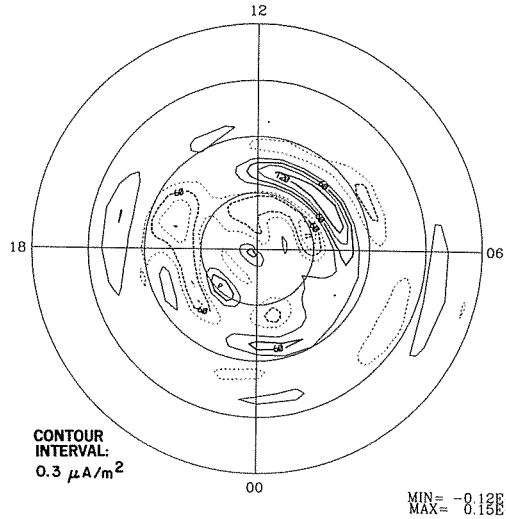

MIN= -0.12E-05 A/m²
MAX= 0.15E-05 A/m²

EQUIVALENT CURRENT VECTORS

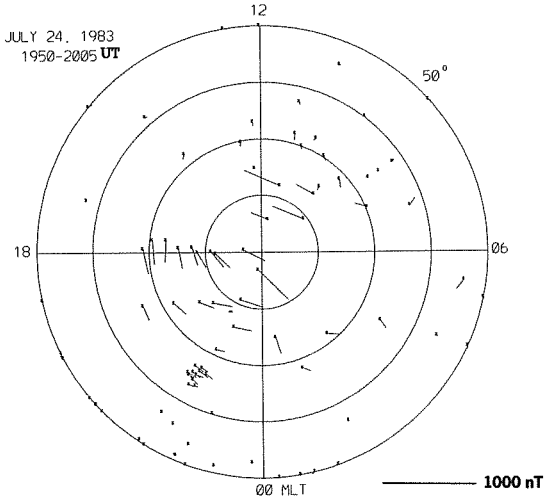

EQUIVALENT CURRENT SYSTEM

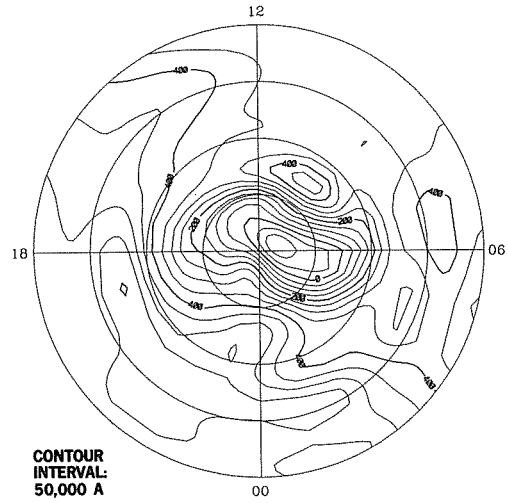

HALL CONDUCTANCE

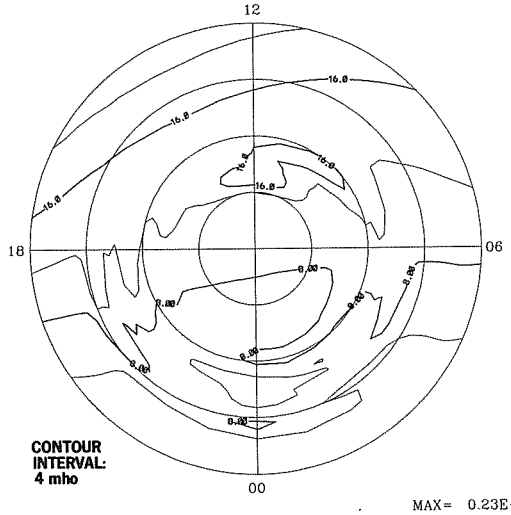

MAX= 0.23E+02 **mho**

PEDERSEN CONDUCTANCE

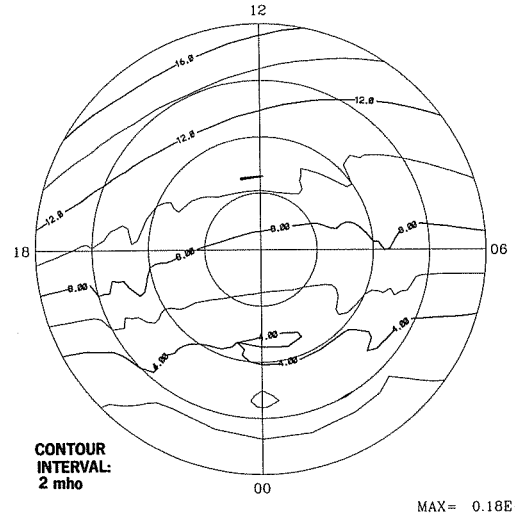

MAX= 0.18E+02 **mho**

ELECTRIC POTENTIAL

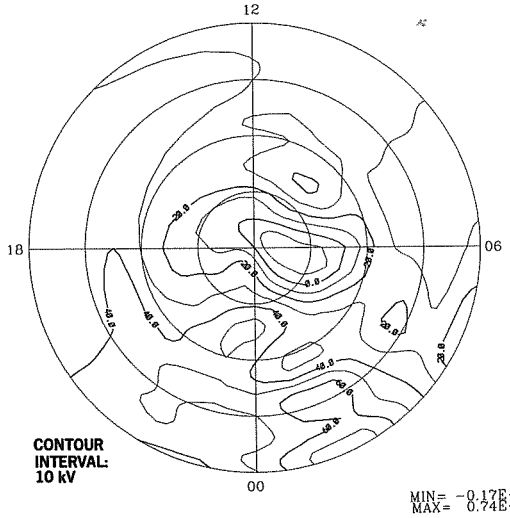

MIN= -0.17E+02 **kV**
MAX= 0.74E+02 **kV**

IONOSPHERIC CURRENT VECTORS

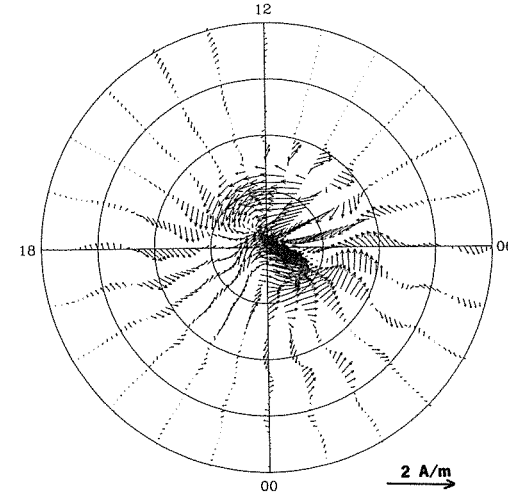

FIELD-ALIGNED CURRENT

24 JUL 1983
1950-2005 UT

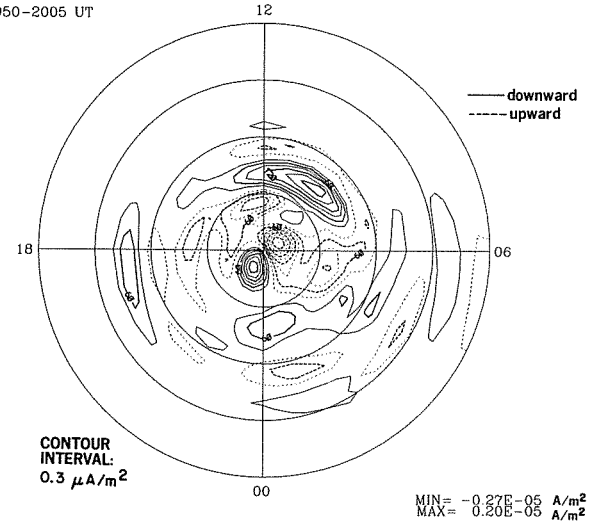

MIN= -0.27E-05 A/m²
MAX= 0.20E-05 A/m²

JOULE HEATING RATE

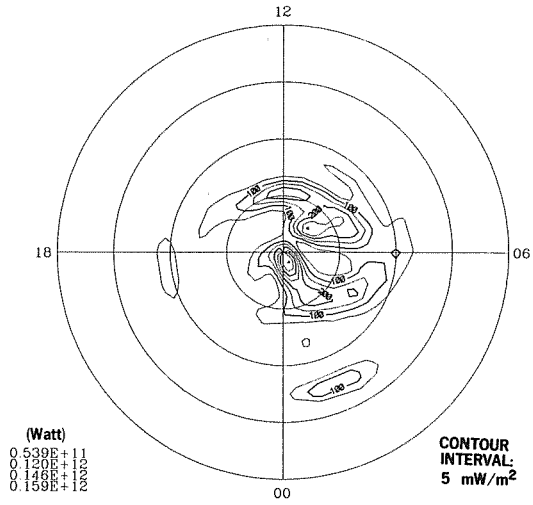

MAX= 0.40E-01 W/m²

HALL CURRENT VECTORS

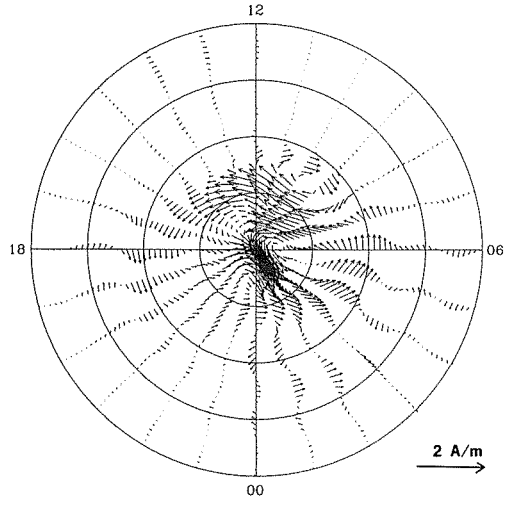

PEDERSEN CURRENT VECTORS

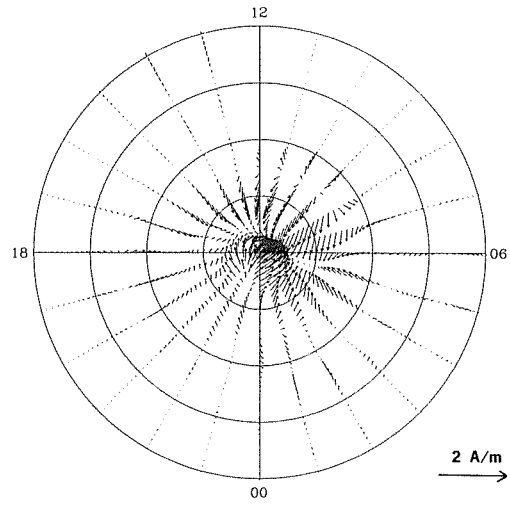

FIELD-ALIGNED HALL CURRENT

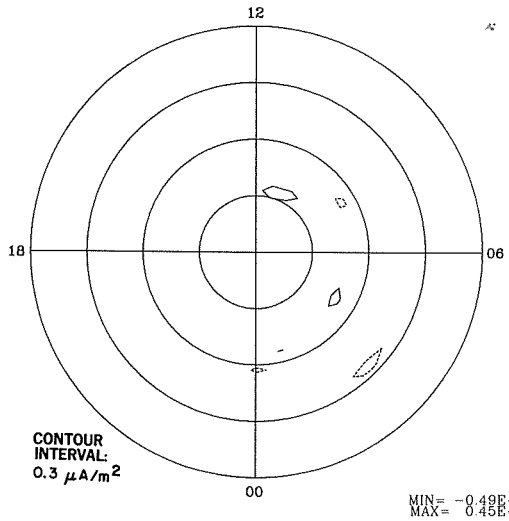

MIN= -0.49E-06 A/m²
MAX= 0.45E-06 A/m²

FIELD-ALIGNED PEDERSEN CURRENT

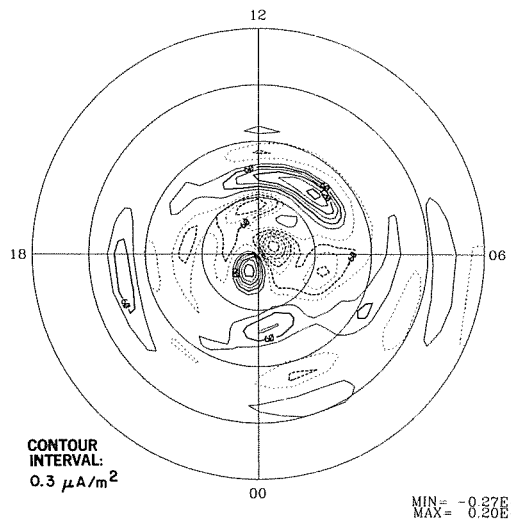

MIN= -0.27E-05 A/m²
MAX= 0.20E-05 A/m²

EQUIVALENT CURRENT VECTORS

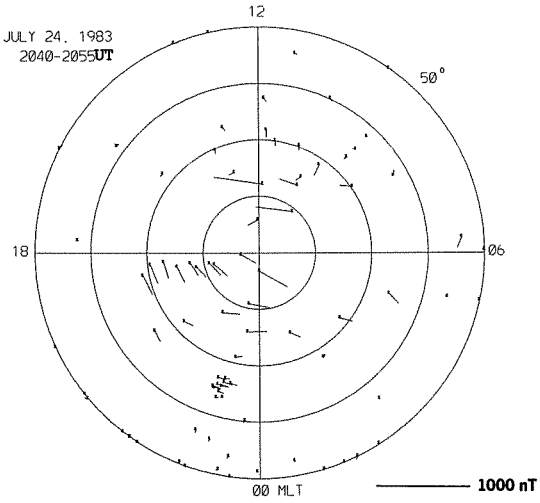

EQUIVALENT CURRENT SYSTEM

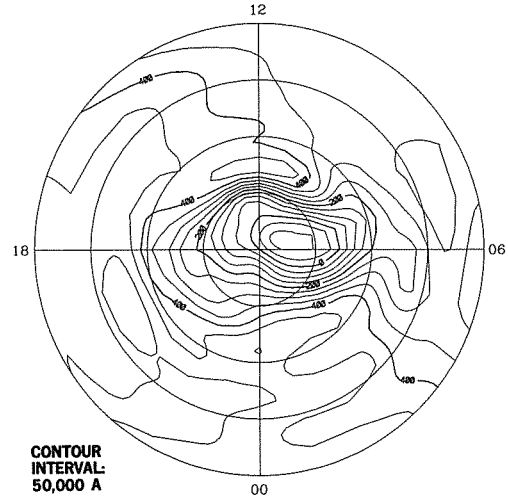

HALL CONDUCTANCE

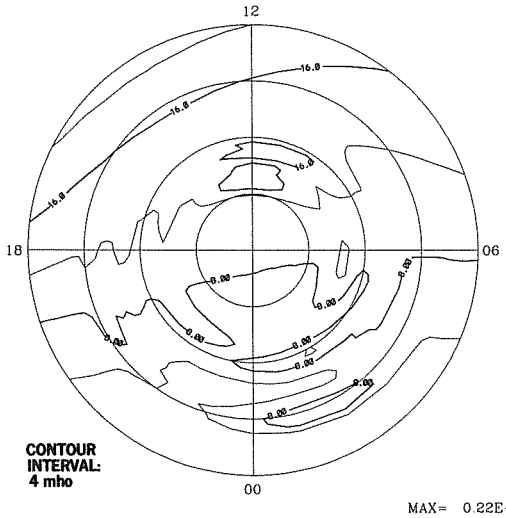

MAX= 0.22E+02 **mho**

PEDERSEN CONDUCTANCE

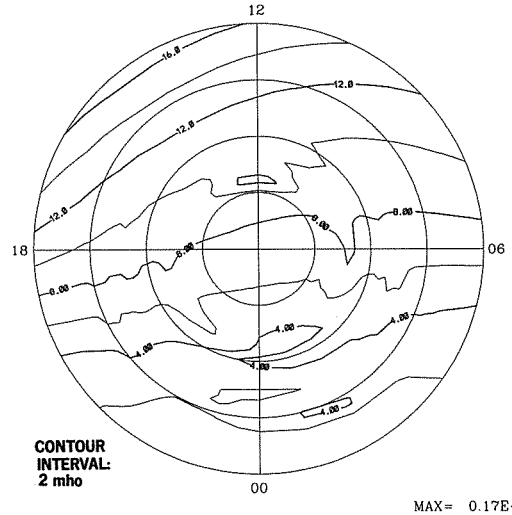

MAX= 0.17E+02 **mho**

ELECTRIC POTENTIAL

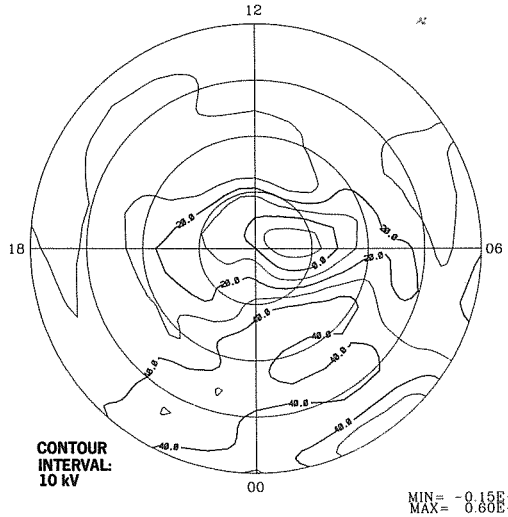

MIN= -0.15E+02 **kV**
MAX= 0.60E+02 **kV**

IONOSPHERIC CURRENT VECTORS

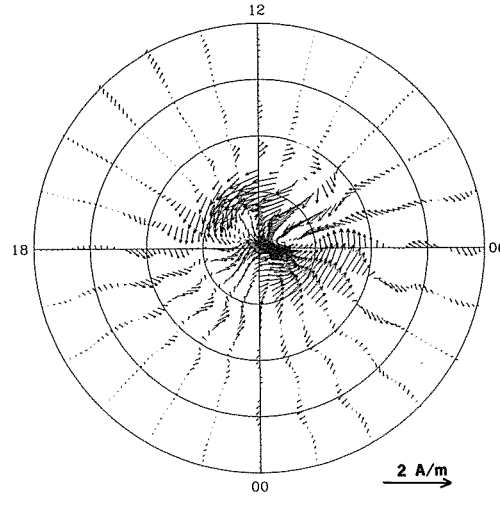

FIELD-ALIGNED CURRENT

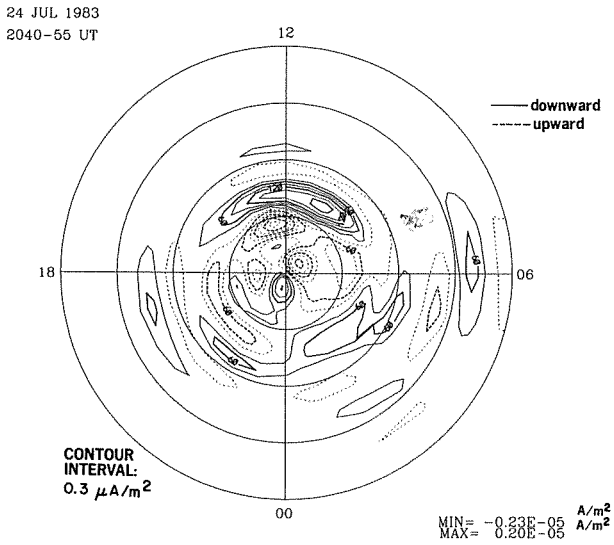

JOULE HEATING RATE

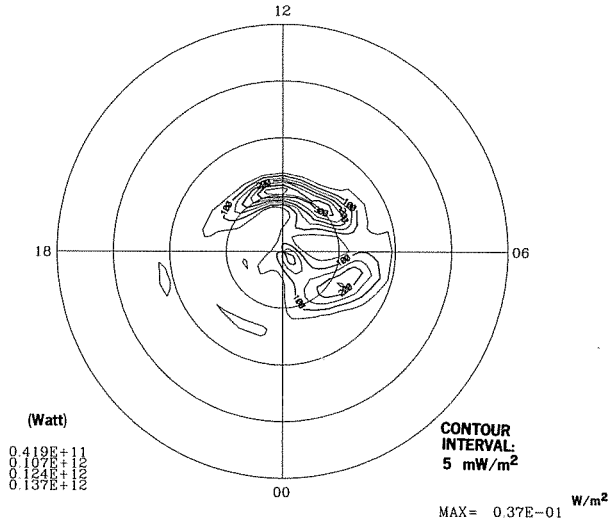

HALL CURRENT VECTORS

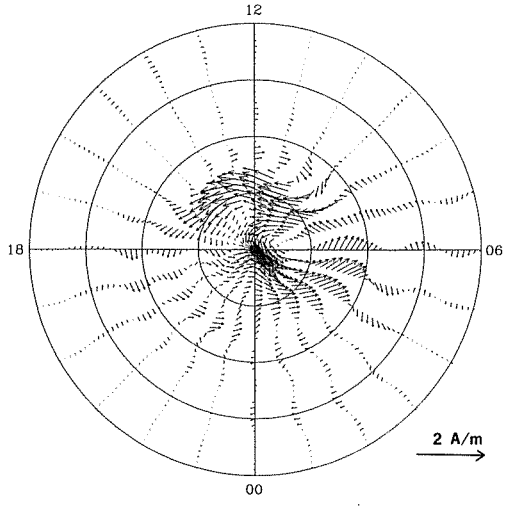

PEDERSEN CURRENT VECTORS

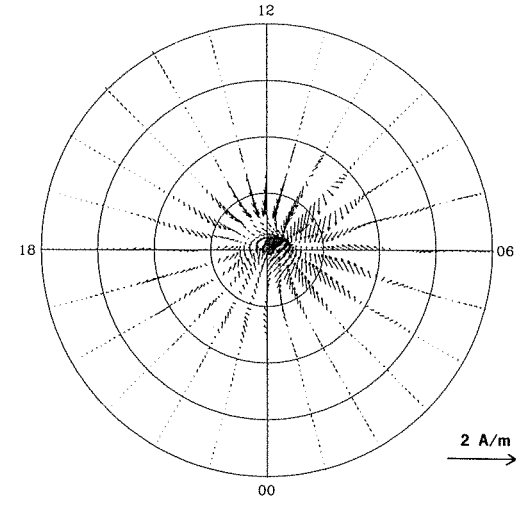

FIELD-ALIGNED HALL CURRENT

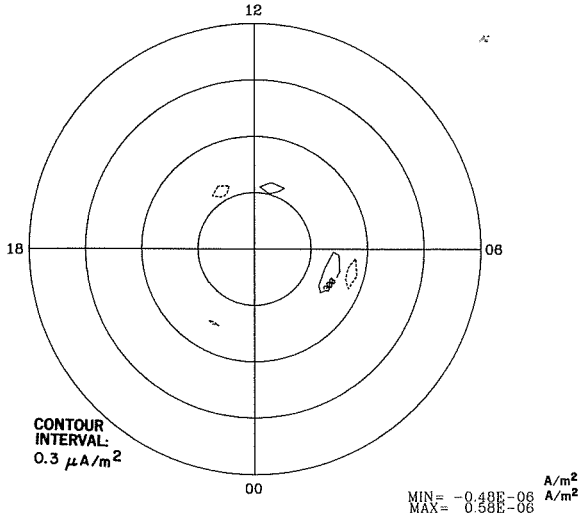

FIELD-ALIGNED PEDERSEN CURRENT

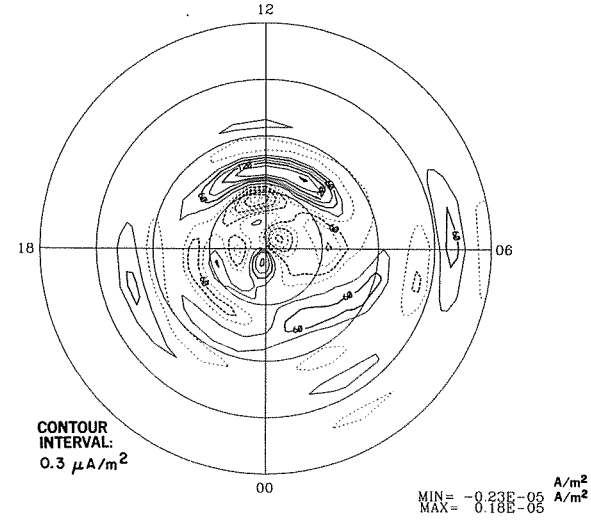

EQUIVALENT CURRENT VECTORS

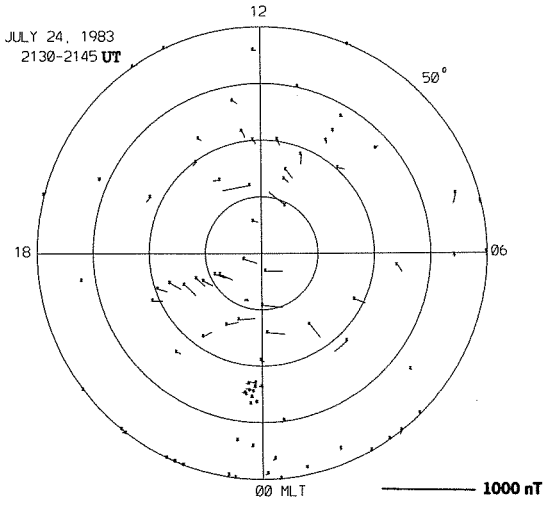

EQUIVALENT CURRENT SYSTEM

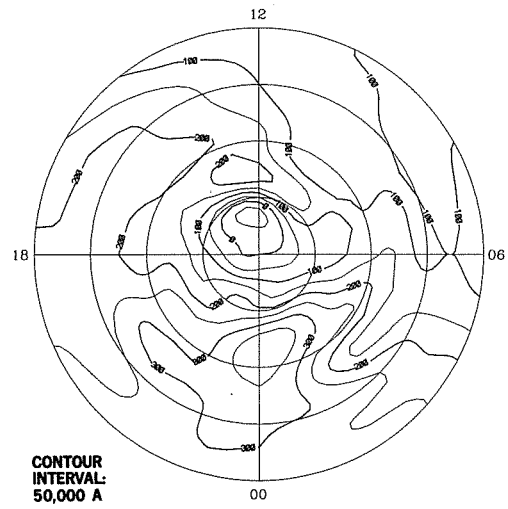

HALL CONDUCTANCE

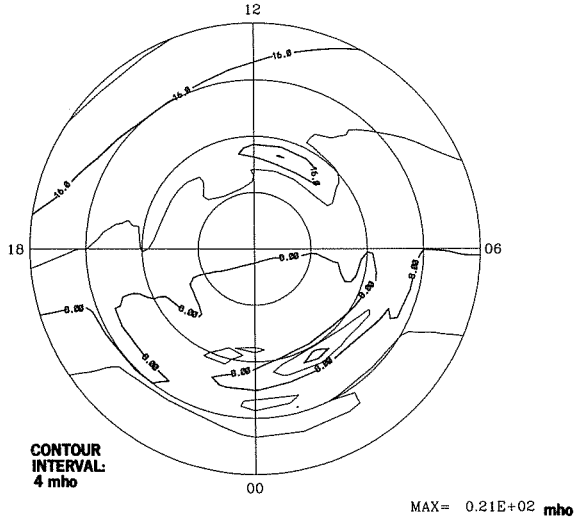

MAX= 0.21E+02 mho

PEDERSEN CONDUCTANCE

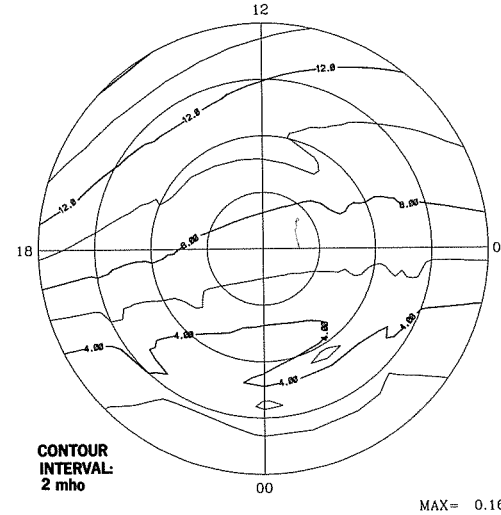

MAX= 0.16E+02 mho

ELECTRIC POTENTIAL

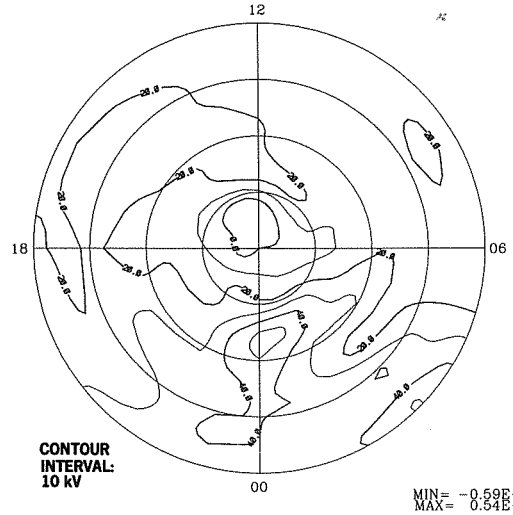

MIN= -0.59E+01 kV
MAX= 0.54E+02 kV

IONOSPHERIC CURRENT VECTORS

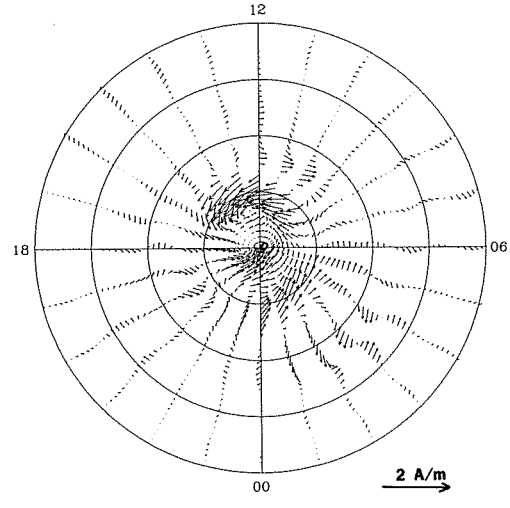

FIELD-ALIGNED CURRENT

24 JUL 1983
2130-45 UT

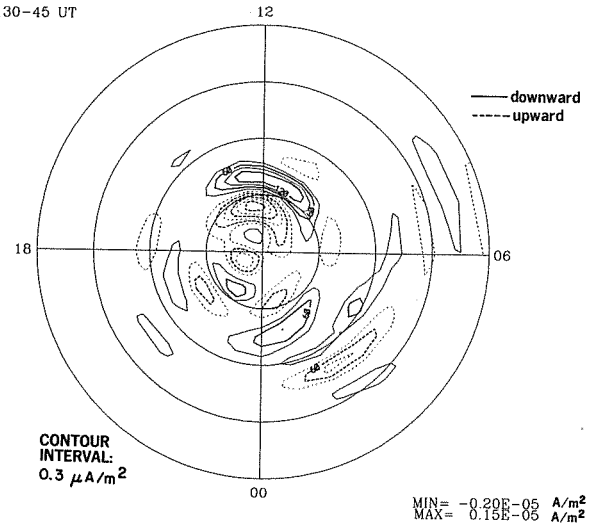

MIN= -0.20E-05 A/m²
MAX= 0.15E-05 A/m²

JOULE HEATING RATE

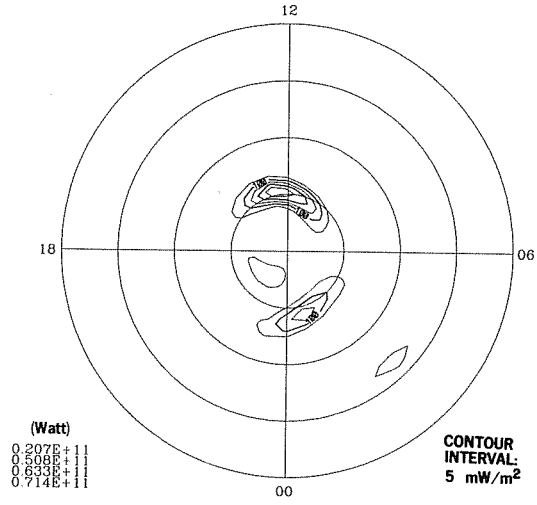

MAX= 0.29E-01 W/m²

HALL CURRENT VECTORS

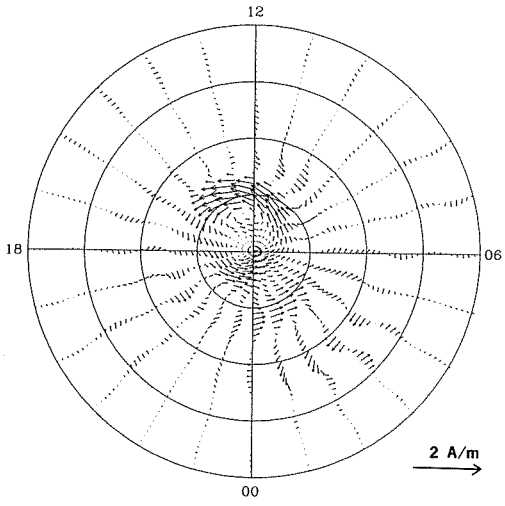

PEDERSEN CURRENT VECTORS

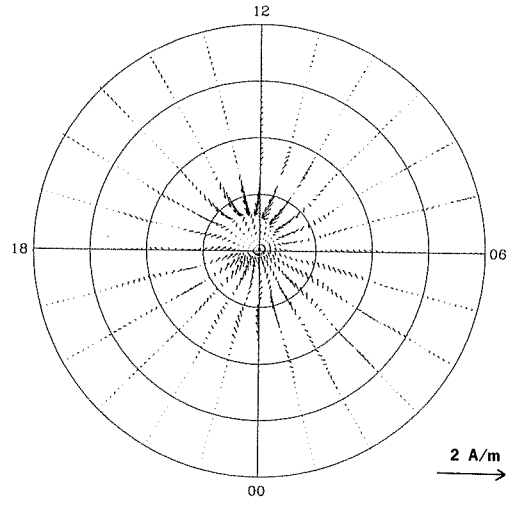

FIELD-ALIGNED HALL CURRENT

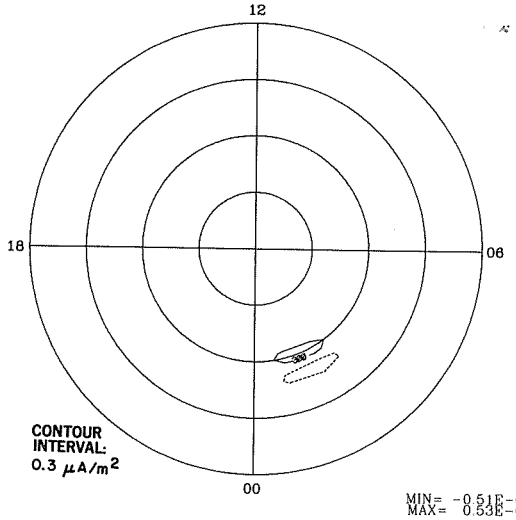

MIN= -0.51E-06 A/m²
MAX= 0.53E-06 A/m²

FIELD-ALIGNED PEDERSEN CURRENT

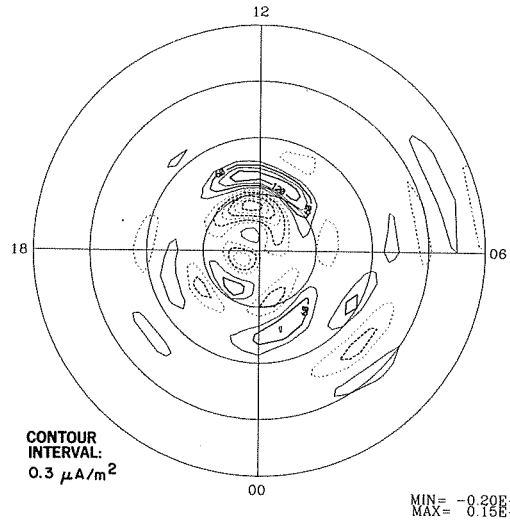

MIN= -0.20E-05 A/m²
MAX= 0.15E-05 A/m²

EQUIVALENT CURRENT VECTORS

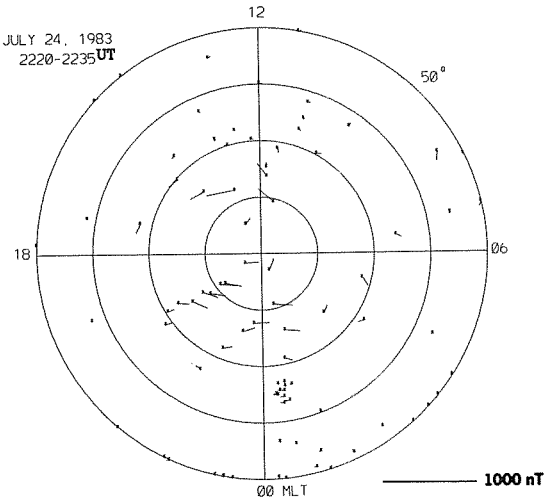

EQUIVALENT CURRENT SYSTEM

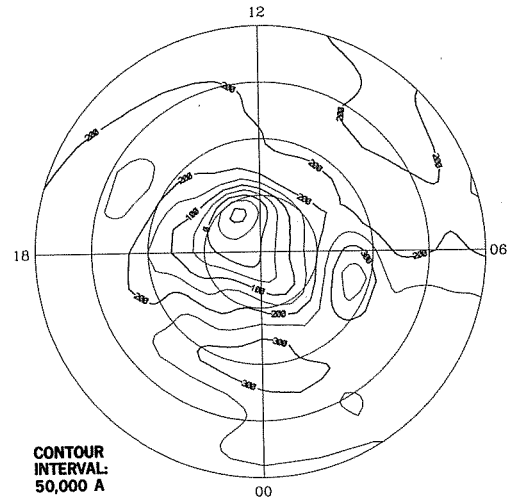

HALL CONDUCTANCE

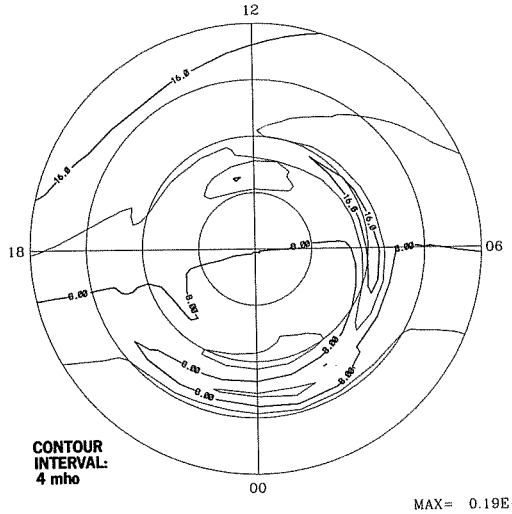

MAX= 0.19E+02 mho

PEDERSEN CONDUCTANCE

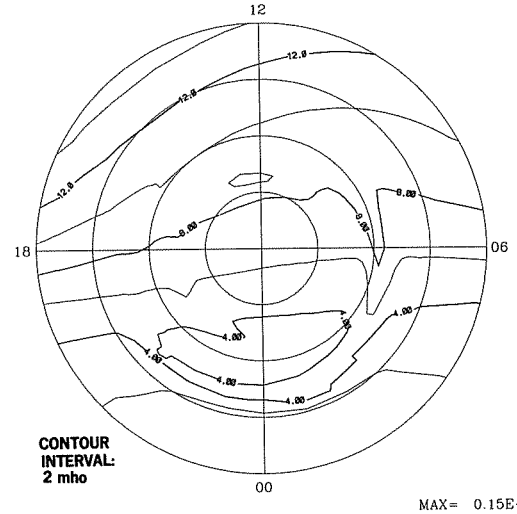

MAX= 0.15E+02 mho

ELECTRIC POTENTIAL

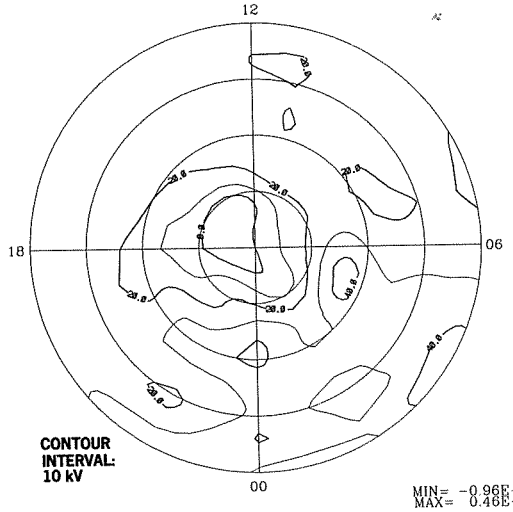

MIN= -0.96E+01 kV
MAX= 0.46E+02 kV

IONOSPHERIC CURRENT VECTORS

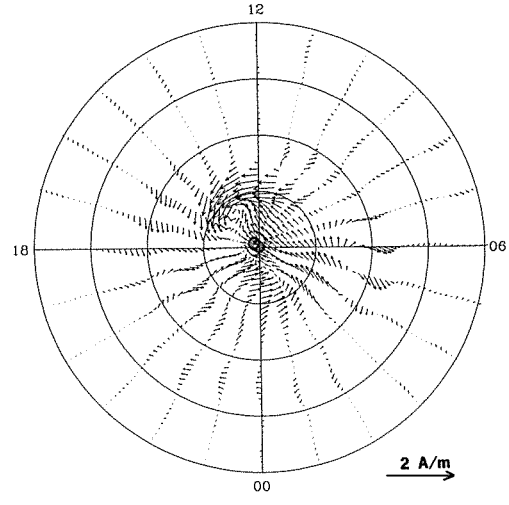

FIELD-ALIGNED CURRENT

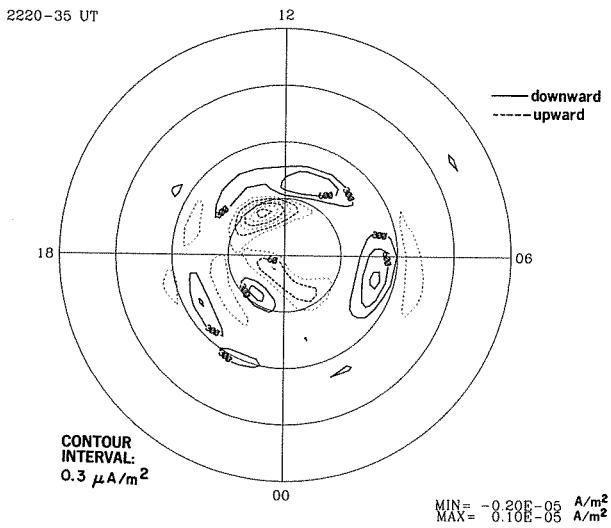

JOULE HEATING RATE

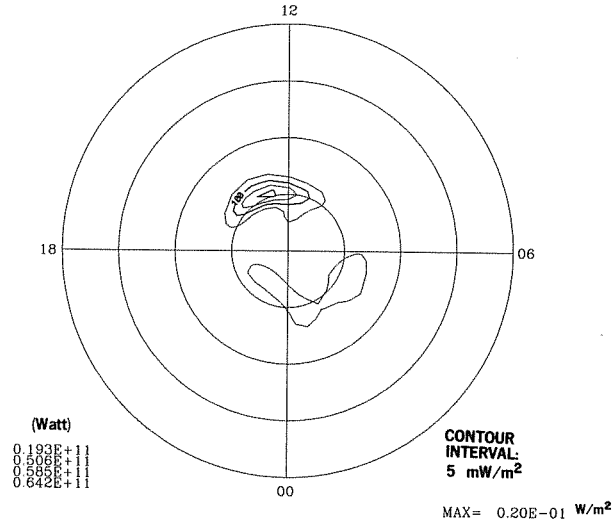

HALL CURRENT VECTORS

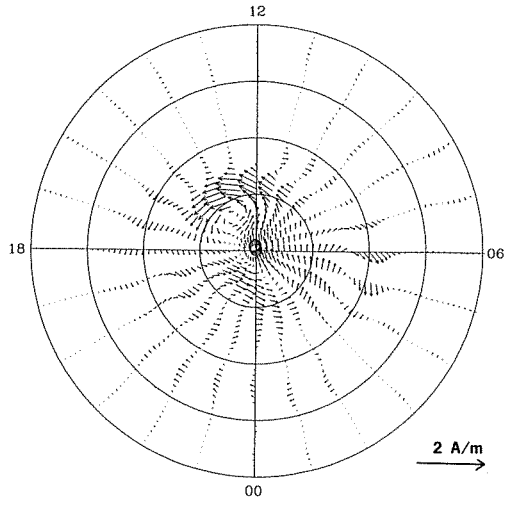

PEDERSEN CURRENT VECTORS

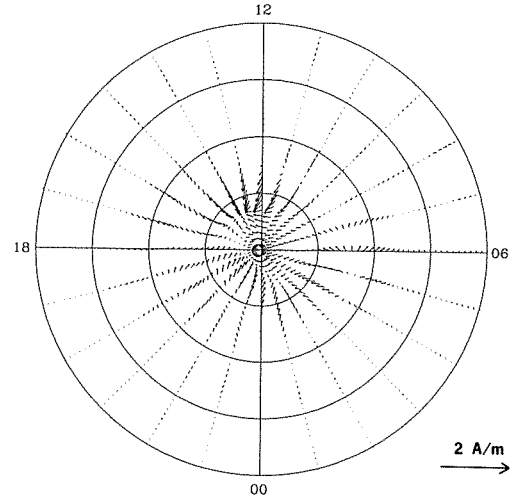

FIELD-ALIGNED HALL CURRENT

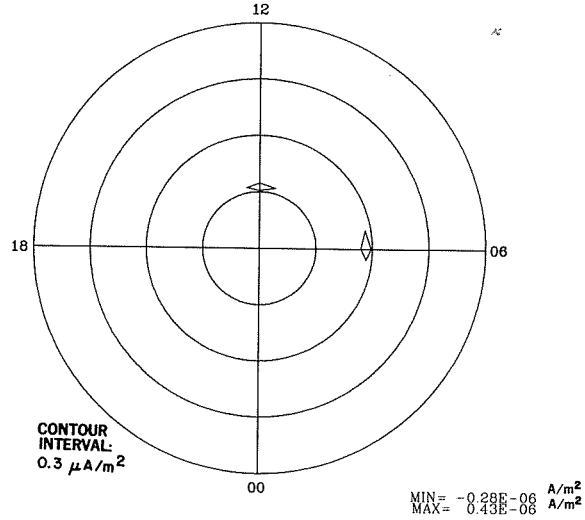

FIELD-ALIGNED PEDERSEN CURRENT

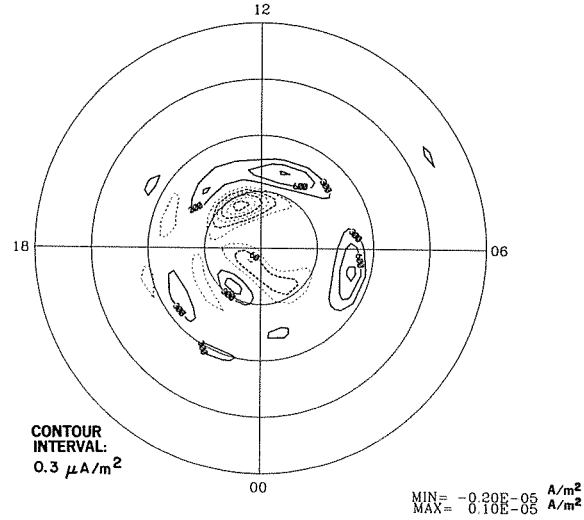

EQUIVALENT CURRENT VECTORS

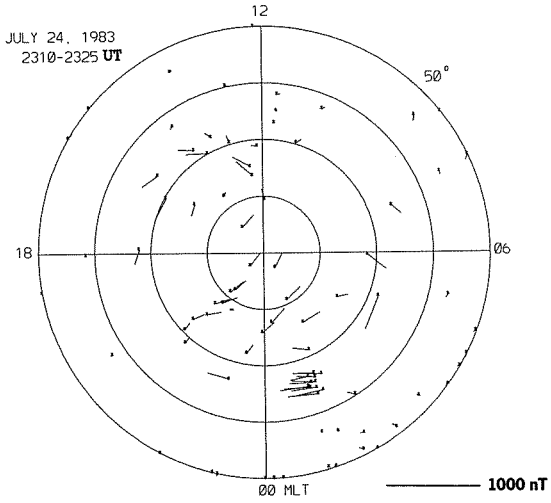

EQUIVALENT CURRENT SYSTEM

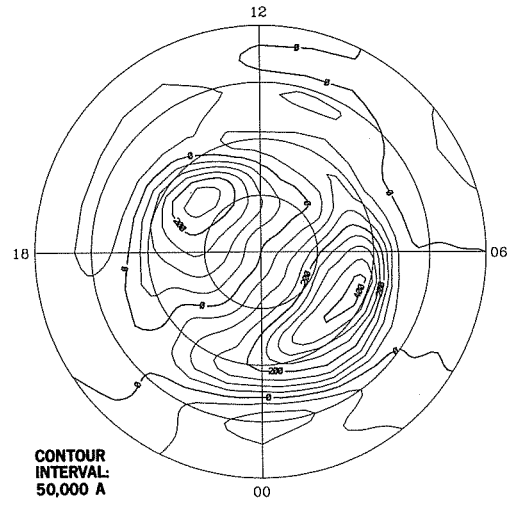

HALL CONDUCTANCE

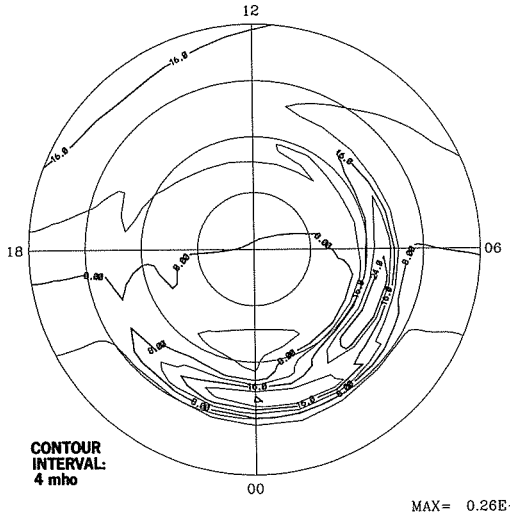

MAX= 0.26E+02 **mho**

PEDERSEN CONDUCTANCE

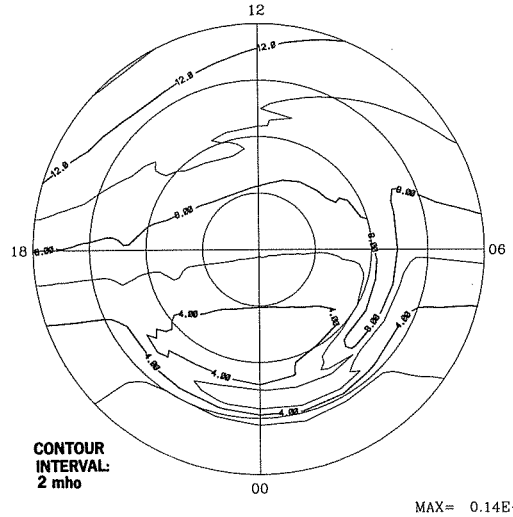

MAX= 0.14E+02 **mho**

ELECTRIC POTENTIAL

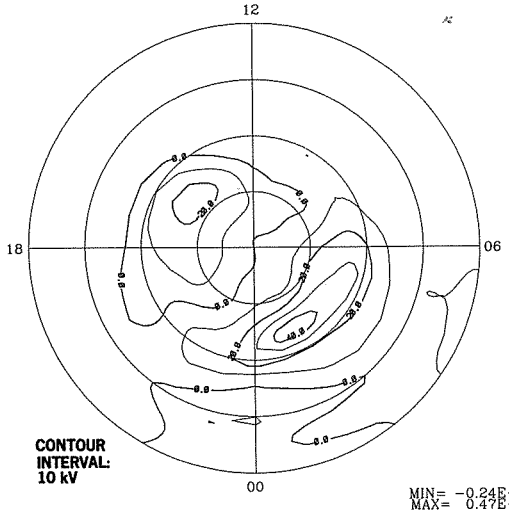

MIN= -0.24E+02 **kV**
MAX= 0.47E+02 **kV**

IONOSPHERIC CURRENT VECTORS

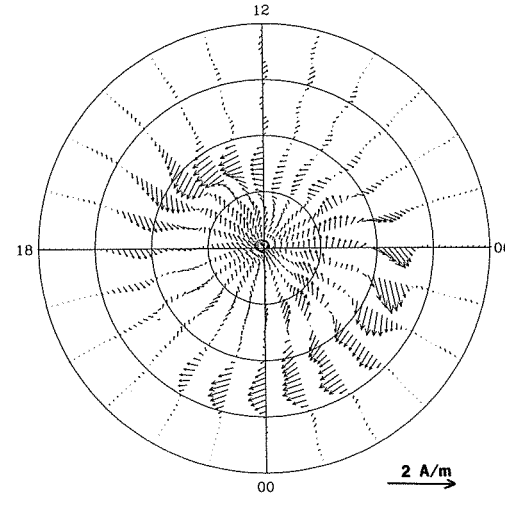

FIELD-ALIGNED CURRENT

24 JUL 1983
2310–25 UT

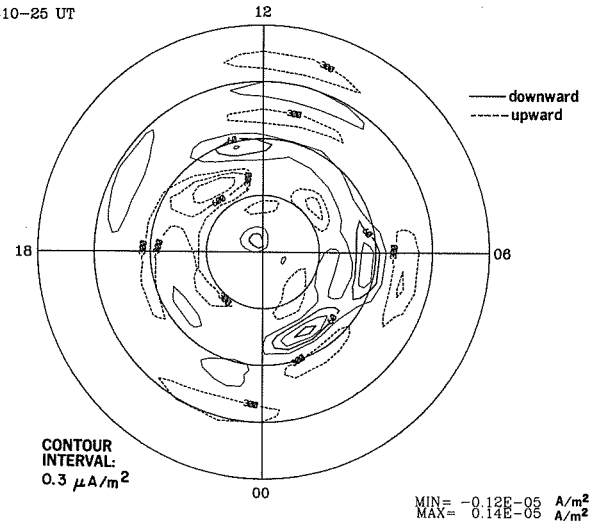

MIN= −0.12E−05 A/m²
MAX= 0.14E−05 A/m²

JOULE HEATING RATE

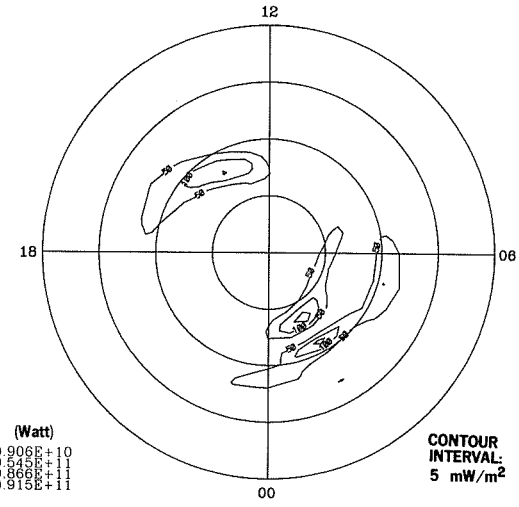

MAX= 0.18E−01 W/m²

HALL CURRENT VECTORS

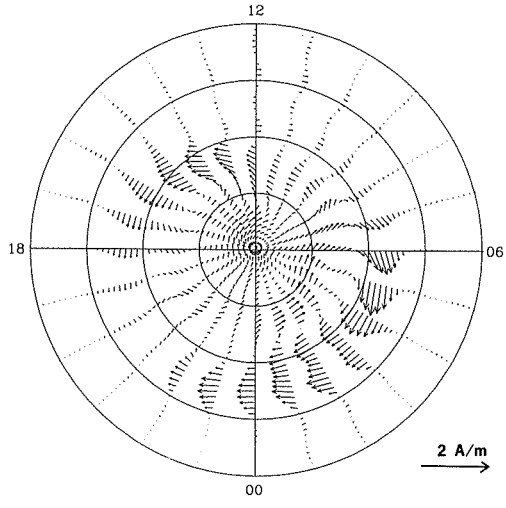

PEDERSEN CURRENT VECTORS

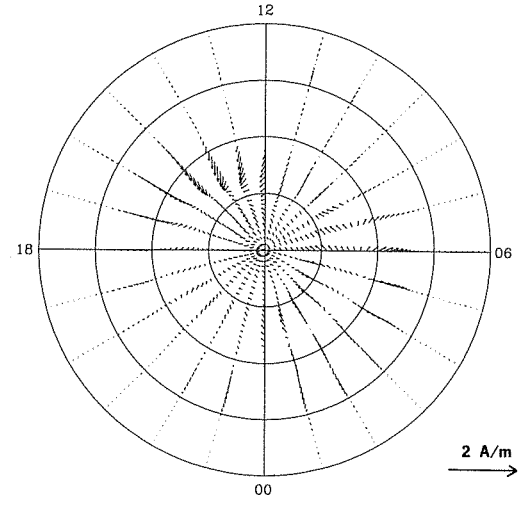

FIELD-ALIGNED HALL CURRENT

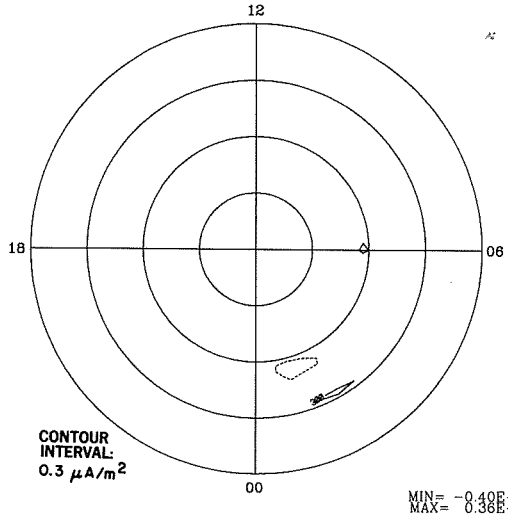

MIN= −0.40E−06 A/m²
MAX= 0.36E−06 A/m²

FIELD-ALIGNED PEDERSEN CURRENT

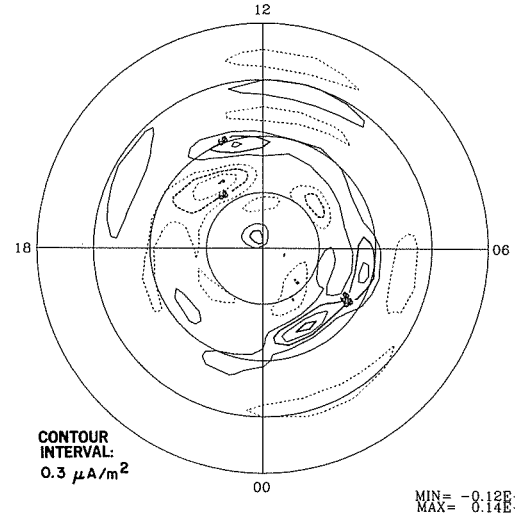

MIN= −0.12E−05 A/m²
MAX= 0.14E−05 A/m²

UAG SERIES OF REPORTS (Most Recent Issues)

Fewer than four UAG Reports are published at irregular intervals each year. Copies of these publications may be purchased through the NATIONAL GEOPHYSICAL DATA CENTER, Solar-Terrestrial Physics Division (E/GC2) 325 Broadway, Boulder, Colorado 80303, USA. A $10.00 handling charge per order will be added to single-copy price, if any, listed below. Please note, too, that some reports are available on microfiche only. Orders must include check or money order payable in U.S. currency to Commerce, NOAA/NGDC.

UAG-45 AURORAL ELECTROJET MAGNETIC ACTIVITY INDICES AE(11) FOR 1972, by Joe Haskell Allen, Carl C. Abston and Leslie D. Morris, National Geophysical and Solar-Terrestrial Data Center, Boulder, CO, May 1975, 144 pp, $1.50 (microfiche only).

UAG-46 INTERPLANETARY MAGNETIC FIELD DATA 1963-1964, by Joseph H. King, National Space Science Data Center, NASA Goddard Space Flight Center, Greenbelt, MD, June 1975, 382 pp, $2.95.

UAG-47 AURORAL ELECTROJET MAGNETIC ACTIVITY INDICES AE(11) FOR 1973, by Joe Haskell Allen, Carl C. Abston and Leslie D. Morris, National Geophysical and Solar-Terrestrial Data Center, Boulder, CO, June 1975, 144 pp, $1.50 (microfiche only).

UAG-48 [Superseded by UAG-48A]

UAG-48A SYNOPTIC OBSERVATIONS OF THE SOLAR CORONA DURING CARRINGTON ROTATIONS 1580-1596 (11 OCTOBER 1971 - 15 JANUARY 1973), [Re-issue of UAG-48 with quality images], by R.A. Howard, M.J. Koomen, D.J. Michels, R. Tousey, C.R. Detwiler, D.E. Roberts, R.T. Seal, and J.D. Whitney, U.S. Naval Research Laboratory, Washington, DC; and R.T. Hansen and S.F. Hansen, C.J. Garcia and E. Yasukawa, High Altitude Observatory, NCAR, Boulder, CO, February 1976, 200 pp, $4.27. Supersedes UAG-48.

UAG-49 [Superseded by UAG-92]

UAG-50 HIGH-LATITUDE SUPPLEMENT TO THE URSI HANDBOOK ON IONOGRAM INTERPRETATION AND REDUCTION, edited by W.R. Piggott, British Antarctic Survey, c/o Appleton Laboratory, Slough, UK, October 1975, 294 pp, $4.00.

UAG-51 SYNOPTIC MAPS OF SOLAR CORONAL HOLE BOUNDARIES DERIVED FROM HE II 304A SPECTROHELIOGRAMS FROM THE MANNED SKYLAB MISSIONS, by J.D. Bohlin and D.M. Rubenstein, U.S. Naval Research Laboratory, Washington, DC, November 1975, 30 pp.

UAG-52 EXPERIMENTAL COMPREHENSIVE SOLAR FLARE INDICES FOR CERTAIN FLARES, 1970-1974, by Helen W. Dodson and E. Ruth Hedeman, McMath-Hulbert Observatory, University of Michigan, Pontiac, MI, November 1975, 27 pp.

UAG-53 DESCRIPTION AND CATALOG OF IONOSPHERIC F-REGION DATA, JICAMARCA RADIO OBSERVATORY (NOVEMBER 1966 - APRIL 1969), by W.L. Clark and T.E. Van Zandt, NOAA Aeronomy Laboratory, Boulder, CO, and J.P. McClure, University of Texas at Dallas, Dallas, TX, April 1976, 10 pp.

UAG-54 [Superseded by UAG-85]

UAG-55 EQUIVALENT IONOSPHERIC CURRENT REPRESENTATIONS BY A NEW METHOD, ILLUSTRATED FOR 8-9 NOVEMBER 1969 MAGNETIC DISTURBANCES, by Y. Kamide, Cooperative Institute for Research in Environmental Sciences, University of Colorado, Boulder, CO; H.W. Kroehl, Data Studies Division, National Geophysical and Solar-Terrestrial Data Center, Boulder, CO; M. Kanamitsu, Advanced Study Program, National Center for Atmospheric Research, Boulder, CO; Joe Haskell Allen, Data Studies Division, National Geophysical and Solar-Terrestrial Data Center, Boulder, CO; and S.-I. Akasofu, Geophysical Institute, University of Alaska, Fairbanks, AK, April 1976, 91 pp, $1.50 (microfiche only).

UAG-56 ISO-INTENSITY CONTOURS OF GROUND MAGNETIC H PERTURBATIONS FOR THE DECEMBER 16-18, 1971, GEOMAGNETIC STORM, Y. Kamide, Cooperative Institute for Research in Environmental Sciences, University of Colorado, Boulder, CO, April 1976, 37 pp.

UAG-57 MANUAL ON IONOSPHERIC ABSORPTION MEASUREMENTS, edited by K. Rawer, Institut fur Physikalische Weltraumforschung, Freiburg, GFR, June 1976, 302 pp, $4.27.

UAG-58 ATS-6 RADIO BEACON ELECTRON CONTENT MEASUREMENTS AT BOULDER, JULY 1974 - MAY 1975, by R.B. Fritz, NOAA Space Environment Laboratory, Boulder, CO, September 1976, 61 pp.

UAG-59 AURORAL ELECTROJET MAGNETIC ACTIVITY INDICES AE(11) FOR 1974, by Joe Haskell Allen, Carl C. Abston and Leslie D. Morris, National Geophysical and Solar-Terrestrial Data Center, Boulder, CO, December 1976, 144 pp, $2.16.

UAG-60 GEOMAGNETIC DATA FOR JANUARY 1976 [AE(7) INDICES AND STACKED MAGNETOGRAMS], by Joe Haskell Allen, Carl C. Abston and Leslie D. Morris, National Geophysical and Solar-Terrestrial Data Center, Boulder, CO, July 1977, 57 pp.

UAG-61 COLLECTED DATA REPORTS FOR STIP INTERVAL II 20 MARCH - 5 MAY 1976, edited by Helen E. Coffey and John A. McKinnon, World Data Center A for Solar-Terrestrial Physics, Boulder, CO, August 1977, 313 pp, $2.95.

UAG-62 GEOMAGNETIC DATA FOR FEBRUARY 1976 [AE(7) INDICES AND STACKED MAGNETOGRAMS], by Joe Haskell Allen, Carl C. Abston and Leslie D. Morris, National Geophysical and Solar-Terrestrial Data Center, Boulder, CO, September 1977, 55 pp.

UAG-63 GEOMAGNETIC DATA FOR MARCH 1976 [AE(7) INDICES AND STACKED MAGNETOGRAMS], by Joe Haskell Allen, Carl C. Abston and Leslie D. Morris, National Geophysical and Solar-Terrestrial Data Center, Boulder, CO, September 1977, 57 pp.

UAG-64 GEOMAGNETIC DATA FOR APRIL 1976 [AE(8) INDICES AND STACKED MAGNETOGRAMS], by Joe Haskell Allen, Carl C. Abston and Leslie D. Morris, National Geophysical and Solar-Terrestrial Data Center, Boulder, CO, February 1978, 55 pp.

UAG-65 THE INFORMATION EXPLOSION AND ITS CONSEQUENCES FOR DATA ACQUISITION, DOCUMENTATION, PROCESSING, by G.K. Hartmann, Max-Planck-Institut fur Aeronomie, Lindau, GFR, May 1978, 36 pp.

UAG-66 SYNOPTIC RADIO MAPS OF THE SUN AT 3.3 MM 1970-1973, by Earle B. Mayfield and Fred I. Shimabukuro, Aerospace Corp., El Segundo, CA, May 1978, 30 pp.

UAG-67 IONOSPHERIC D-REGION PROFILE DATA BASE, A COLLECTION OF COMPUTER-ACCESSIBLE EXPERIMENTAL PROFILES OF THE D AND LOWER E REGIONS, by L.F. McNamara, Ionospheric Prediction Service, Sydney, Australia, August 1978, 30 pp, $1.50 (microfiche only).

UAG-68 A COMPARATIVE STUDY OF METHODS OF ELECTRON DENSITY PROFILE ANALYSIS, by L.F. McNamara, Ionospheric Prediction Service, Sydney, Australia, August 1978, 30 pp, $1.50 (microfiche only).

UAG-69 SELECTED DISTURBED D-REGION ELECTRON DENSITY PROFILES. THEIR RELATION TO THE UNDISTURBED D REGION, by L.F. McNamara, Ionospheric Prediction Service, Sydney, Australia, October 1978, 50 pp, $1.50 (microfice only).

UAG-70 ANNOTATED ATLAS OF H-ALPHA SYNOPTIC CHARTS FOR SOLAR CYCLE 20 (1964-1974) CARRINGTON SOLAR ROTATIONS 1487-1616, by Patrick S. McIntosh, NOAA Space Environment Laboratory, Boulder, CO, February 1979, 327 pp, $3.50.

UAG-71 MAGNETIC POTENTIAL PLOTS OVER THE NORTHERN HEMISPHERE FOR 26-28 MARCH 1976, A.D. Richmond, NOAA Space Environment Laboratory, Boulder, CO; H.W. Kroehl, National Geophysical and Solar-Terrestrial Data Center, Boulder, CO; M.A. Henning, Lockheed Missiles and Space Co., Aurora, CO; and Y. Kamide, Kyoto Sangyo University, Kyoto, Japan, April 1979, 118 pp, $1.50.

UAG-72 ENERGY RELEASE IN SOLAR FLARES, PROCEEDINGS OF THE WORKSHOP ON ENERGY RELEASE IN FLARES, 26 FEBRUARY - 1 MARCH 1979, CAMBRIDGE, MASSACHUSETTS, U.S.A., edited by David M. Rust, American Science and Engineering, Inc., Cambridge, MA; and A. Gordon Emslie, Harvard-Smithsonian Center for Astrophysics, Cambridge, MA, July 1979, 68 pp, $1.50 (micro-fiche only).

UAG-73 AURORAL ELECTROJET MAGNETIC ACTIVITY INDICES AE(11-12) FOR JANUARY - JUNE 1975, by Joe Haskell Allen, Carl C. Abston, J.E. Salazar and J.A. McKinnon, National Geophysical and Solar-Terrestrial Data Center, NOAA, Boulder, CO, August 1979, 114 pp, $1.75 (microfiche only).

UAG-74 ATS-6 RADIO BEACON ELECTRON CONTENT MEASUREMENTS AT OOTACAMUND, INDIA, OCTOBER - JULY 1976, by S.D. Bouwer, K. Davies, R.F. Donnelly, R.N. Grubb, J.E. Jones and J.H. Taylor, NOAA Space Environment Laboratory, Boulder, CO; and R.G. Rastogi, M.R. Deshpande, H. Chandra and G. Sethia, Physical Research Laboratory, Ahmedabad, India, March 1980, 58 pp, $2.50.

UAG-75 THE ALASKA IMS MERIDIAN CHAIN: MAGNETIC VARIATIONS FOR 9 MARCH - 27 APRIL 1978, by H.W. Kroehl and G.P. Kosinski, National Geophysical and Solar-Terrestrial Data Center, Boulder, CO; S.-I. Akasofu, G.J. Romick, C.E. Campbell and G.K. Corrick, University of Alaska, Fairbanks, AK; and C.E. Hornback and A.M. Gray, NOAA Space Environment Laboratory, Boulder, CO, June 1980, 107 pp, $3.00.

UAG-76 AURORAL ELECTROJET MAGNETIC ACTIVITY INDICES AE(12) FOR JULY - DECEMBER 1975, by Joe Haskell Allen, Carl C. Abston, J.E. Salazar and J.A. McKinnon, National Geophysical and Solar-Terrestrial Data Center, NOAA, Boulder, CO, August 1980, 116 pp, $2.50.

UAG-77 SYNOPTIC SOLAR MAGNETIC FIELD MAPS FOR THE INTERVAL INCLUDING CARRINGTON ROTATIONS 1601-1680, MAY5, 1973 - APRIL 26, 1979, by J. Harvey, B. Gillespie, P. Miedaner and C. Slaughter, Kitt PeakNational Observatory, Tucson, AZ, August 1980, 66 pp, $2.50.

UAG-78 THE EQUATORIAL LATITUDE OF AURORAL ACTIVITY DURING 1972-1977, by N.R. Sheeley, Jr. and R.A. Howard, E.O. Hulbert Center for Space Research, U.S. Naval Research Laboratory, Washington, DC and B.S. Dandekar, Air Force Geophysics Laboratory, Hanscom AFB, MA, October 1980, 61 pp, $3.00.

UAG-79 SOLAR OBSERVATIONS DURING SKYLAB, APRIL 1973 - FEBRUARY 1974, I. CORONAL X-RAY STRUCTURE, II. SOLAR FLARE ACTIVITY, by J.M. Hanson, University of Michigan, Ann Arbor, MI; and E.C. Roelof and and R.E. Gold, The Johns Hopkins University, Laurel, MD, December 1980, 43 pp, $2.50.

UAG-80 EXPERIMENTAL COMPREHENSIVE SOLAR FLARE INDICES FOR 'MAJOR' AND CERTAIN LESSER FLARES, 1975-1979, compiled by Helen W. Dodson and E. Ruth Hedeman, The Johns Hopkins University, Laurel, MD, July 1981, 33 pp, $2.00.

UAG-81 EVOLUTIONARY CHARTS OF SOLAR ACTIVITY (CALCIUM PLAGES) AS FUNCTIONS OF HELIOGRAPHIC LONGITUDE AND TIME, 1964-1979, by E. Ruth Hedeman, Helen W. Dodson and Edmond C. Roelof, The Johns Hopkins University, Laurel, MD, August 1981, 103 pp, $4.00.

UAG-82 INTERNATIONAL REFERENCE IONOSPHERE - IRI 79, edited by J. Virginia Lincoln and Raymond O. Conkright, National Geophysical and Solar-Terrestrial Data Center, NOAA, Boulder, CO, November 1981, 243 pp, $4.50.

UAG-83 SOLAR-GEOPHYSICAL ACTIVITY REPORTS FOR SEPTEMBER 7-24, 1977 AND NOVEMBER 22, 1977, Parts 1 and 2, compiled by John A. McKinnon and J. Virginia Lincoln, World Data Center A for Solar-Terrestrial Physics, NOAA, Boulder, CO, February 1982, 553 pp, $10.00.

UAG-84 CATALOG OF AURORAL RADIO ABSORPTION DURING 1976-1979 AT ABISKO, SWEDEN, by J.K. Hargreaves, C.M. Taylor and J.M. Penman, Environmental Sciences Department, University of Lancaster, Lancaster, UK, July 1982, 69 pp, $3.00.

UAG-85 [Superseded by UAG-91]

UAG-86 [Superseded by UAG-92]

UAG-87 CHANGES IN THE GLOBAL ELECTRIC FIELDS AND CURRENTS FOR MARCH 17-19, 1978, FROM SIX IMS MERIDIAN CHAINS OF MAGNETOMETERS, by Y. Kamide, Kyoto Sangyo University, Kyoto, Japan; H.W. Kroehl, National Geophysical Data Center, NOAA, Boulder, CO; and A.D. Richmond, NOAA Space Environment Laboratory, Boulder, CO, November 1982, 102 pp, $3.50.

UAG-88 NUMERICAL MODELING OF IONOSPHERIC PARAMETERS FROM GLOBAL IMS MAGNETOMETER DATA FOR THE CDAW-6 INTERVALS, by Y. Kamide, Kyoto Sangyo University, Kyoto, Japan; H.W. Kroehl, National Geophysical Data Center, NOAA, Boulder, CO; and B.A. Hausman, National Geophysical Data Center, NOAA, Boulder, CO, November 1983, 197 pp, $4.00.

UAG-89 ATMOSPHERIC HANDBOOK: ATMOSPHERIC DATA TABLES AVAILABLE ON COMPUTER TAPE, by V.E. Derr, NOAA Environmental Research Laboratories, Boulder, CO, July 1984, 56 pp.

UAG-90 EXPERIENCE WITH PROPOSED IMPROVEMENTS OF THE INTERNATIONAL REFERENCE IONOSPHERE (IRI): CONTRIBUTED PAPERS, MAINLY FROM THE URSI-COSPAR WORKSHOP HELD IN BUDAPEST IN 1980, edited by K. Rawer, University of Freiburg, Federal Republic of Germany, and C.M. Minnis, International Union of Radio Science (URSI), Brussels, Belgium, May 1984, 233 pp, $6.00.

UAG-91 COMBINED CATALOG OF IONOSPHERE VERTICAL SOUNDINGS DATA, compiled by Raymond O. Conkright and Marcus O. Ertle, National Geophysical Data Center, NOAA, Boulder, CO, December 1984, 174 pp.

UAG-92 INTERNATIONAL CATALOG OF GEOMAGNETIC DATA, compiled by C.C. Abston, National Geophysical Data Center, NOAA, Boulder, CO; N.E. Papitashvili, Academy of Sciences of the USSR, World Data Center B2, Moscow, USSR; and V.O. Papitashvili, IZMIRAN, Moscow Region, USSR, August 1985, 291 pp. Supersedes UAG-35, 49, and 86.

UAG-93 IONOGRAM ANALYSIS WITH THE GENERALIZED PROGRAM POLAN, by J.E. Titheridge, University of Auckland, New Zealand, December 1985, 194 pp.

UAG-94 THE SOLAR MAGNETIC FIELD--1976 THROUGH 1985: AN ATLAS OF PHOTOSPHERIC MAGNETIC FIELD OBSERVATIONS AND COMPUTED CORONAL MAGNETIC FIELDS FROM THE JOHN M. WILCOX SOLAR OBSERVATORY AT STANFORD, by J. Todd Hoeksema and Philip H. Scherrer, Center for Space Science and Astrophysics, Stanford University, Stanford, CA, January 1986, 370 pp, $9.00.

UAG-95 SUNSPOT NUMBERS: 1610-1985, (based on THE SUNSPOT-ACTIVITY IN THE YEARS 1610-1960, by Prof. M. Waldmeier, Copyright 1961, Swiss Federal Observatory, Zurich, Switzerland), revised by John A. McKinnon, National Geophysical Data Center, NOAA, Boulder, CO, January 1987, 112 pp, $10.00.

UAG-96 SOLAR-GEOPHYSICAL ACTIVITY REPORTS FOR STIP INTERVAL XV, 12-21 February 1984 Ground Level Event, AND STIP INTERVAL XVI, 20 April - 4 May 1984 Forbush Decrease, compiled by Helen E. Coffey and Joe H. Allen, National Geophysical Data Center, NOAA, Boulder, CO, July 1987, 418 pp, $15.00.

UAG-97 NUMERICAL MODELING OF POLAR IONOSPHERIC ELECTRODYNAMICS FOR JULY 23-24, 1983, UTILIZING IONOSPHERIC CONDUCTANCES DEDUCED FROM DMSP X-RAY IMAGES, by B.-H. Ahn, Kyungpook National University, Taegu, Korea; E. Friis-Christensen, Division of Geophysics, Danish Meteorological Institute, Copenhagen, Denmark; D.J. Gorney, Space Sciences Laboratory, The Aerospace Corporation, Los Angeles, CA; Y. Kamide, Kyoto Sangyo University, Kyoto, Japan; and H.W. Kroehl, National Geophysical Data Center, NOAA, Boulder, CO, April 1988, 133 pp, $12.00.

☆ U.S. GOVERNMENT PRINTING OFFICE:1988-575-414/85144